UNIMORE
UNIVERSITÀ DEGLI STUDI DI
MODENA E REGGIO EMILIA

# UNIVERSITY OF MODENA AND REGGIO EMILIA

## Phd School of Food and Agricultural Science, Technology and Biotechnology

---

XXXVIII Cycle

*Smart sensing and data-driven approaches for food quality and safety in the agri-food chain.*


PhD Student: **Elisabetta Poeta**

Supervisor: **Prof. Andrea Pulvirenti**
Co-Supervisor: **Dr. Veronica Sberveglieri**

Dean of PhD School: **Prof. Fabio Licciardello**

# INDEX

# ABSTRACT

The agri-food sector plays a strategic role at the global level, not only for its primary function of nutrition and public health protection, but also for its economic, environmental, and social implications. Population growth, supply chain complexity, and the increasing demand for efficiency and sustainability pose new challenges to ensuring food quality, safety, and traceability.

Traditional analytical methodologies of chemical, physical, and microbiological nature remain fundamental tools due to their high accuracy and regulatory validation. However, their high cost, long analysis times, and limited applicability for rapid and real-time monitoring reduce their effectiveness in modern production environments.

In this context, *smart sensing* technologies — in particular, devices based on metal oxide (MOX) sensors — represent an innovative and sustainable solution for rapid and non-destructive food quality assessment. Owing to their chemoresistive response and the possibility of integration with IoT platforms, MOX sensors enable the analysis of volatile organic compound (VOC) profiles and the development of predictive shelf-life models, thereby contributing to waste reduction and greater transparency across the food supply chain.

This PhD thesis presents several research projects that integrate traditional analytical methodologies with innovative approaches based on MOX sensors. The case studies involve different matrices and objectives, ranging from the assessment of freshness in fruit and meat products to the production of baked goods and fermented derivatives designed to meet consumer preferences.

The obtained results show a remarkable correlation between reference techniques (GC–MS, microbiological, and sensory analyses) and the responses provided by nanostructured sensor devices, confirming the reliability, sensitivity, and robustness of MOX-based systems. These findings highlight that electronic noses and MOX sensors can serve as effective tools for the evaluation of food quality and safety.

Overall, MOX sensor technologies represent one of the most promising frontiers for the future of agri-food monitoring. Their integration with machine learning algorithms and IoT systems paves the way for intelligent and adaptive devices capable of operating in real time and supporting quality management and sustainability throughout the entire production and distribution chain.

# 1

# INTRODUCTION

Access to safe and nutritionally adequate food is recognized as a fundamental right of every individual, as already established in 1992 by the *World Declaration on Nutrition* promoted by FAO and WHO.

Today, the agri-food sector is not only a source of nourishment but also a strategic pillar that directly affects public health, economic development, environmental protection, and social cohesion. However, global population growth, the lengthening of supply chains, and the constant pursuit of efficiency and sustainability make it increasingly complex to guarantee food that is safe, high-quality, and traceable.

These challenges are further compounded by changes related to market globalization, migration and tourism flows, population aging, and evolving consumption habits. Moreover, new critical issues have emerged due to climate change and extreme weather events, which increasingly affect food production and safety. In such a dynamic context, the risk of contamination and the spread of foodborne diseases are amplified, making food safety an indispensable priority for collective health [1].

Within this framework, the Codex Alimentarius plays a pivotal role. It represents a comprehensive collection of internationally recognized standards, guidelines, and codes of practice, whose primary objectives are the protection of consumer health and the promotion of fair practices in the food trade. The governance of the Codex is entrusted to the Codex Alimentarius Commission (CAC), a joint intergovernmental body established by the Food and Agriculture Organization of the United Nations (FAO) and the World Health Organization (WHO), comprising 186 Member States, one Member Organization, and more than 200 observers from civil society. Almost all food products traded worldwide fall within the scope of Codex standards, which contribute not only to ensuring the safety of the global food supply but also to facilitating international trade. At the same time, these standards serve as a fundamental reference for the development of national food policies, reinforcing food safety as a core pillar of global food security.

The Codex Alimentarius is subject to a continuous updating process coordinated by FAO and WHO, aimed at incorporating the latest scientific evidence, addressing emerging risks to consumer health, and ensuring regulatory harmonization in an increasingly globalized food market. The most recent

update was adopted on 14 November 2025, reflecting the need to align existing standards with advances in scientific knowledge, technological innovations in food production, and evolving international trade dynamics, while maintaining a high level of consumer protection and regulatory coherence worldwide.

The process that brings food "from farm to fork" has undergone radical transformations over the past half-century: a localized food contamination event can now impact consumer health on the other side of the planet. This implies that all actors in the food chain—from producers to final consumers—must adopt safe food-handling practices.

Beyond FAO and WHO, several other international agencies are dedicated to food safety. In the United States, the *Centers for Disease Control and Prevention* (CDC), based in Atlanta, collect and analyze data on foodborne outbreaks, making them publicly available online. Within the CDC, the *Food Net* division is exclusively dedicated to monitoring issues related to foodborne diseases. At the European level, the *European Centre for Disease Prevention and Control* (ECDC) conducts surveillance activities, while a central role is played by the *European Food Safety Authority* (EFSA), which provides scientific advice to the European Commission, the European Parliament, and EU Member States. Another key institution is the *Food and Drug Administration* (FDA), a U.S. agency based in Maryland, which plays a crucial role in regulating and monitoring food safety both nationally and internationally.

## 1.1 Food Safety and Food Security

### 1.1.1 Food Safety

Food safety is a broad concept that primarily concerns the prevention of harm and disease in consumers during the preparation, handling, and storage of food. It encompasses the assessment and management of chemical, physical, and microbiological risks associated with food consumption.

Traditionally, animals intended for human consumption have been considered the main vectors of pathogens responsible for foodborne diseases, due to the microorganisms present in their gastrointestinal tract. However, in recent decades, the largest and most frequent outbreaks of microbial diseases have been associated with the consumption of leafy vegetables and fruits [2].

A notable example is the outbreak of hemolytic uremic syndrome that occurred between Germany and Spain in 2011. The epidemic, caused by Shiga toxin-producing *Escherichia coli* O104:H4 (belonging to the enterohemorrhagic *E. coli* group, EHEC), led to at least 32 deaths in Germany and over one thousand confirmed infections. Initially, German authorities mistakenly identified Spanish

cucumbers as the source of contamination, triggering what was referred to as the "cucumber crisis." Subsequent analyses, commissioned by the European Commission, confirmed the absence of *E. coli* contamination in cucumbers from Almería, Granada, and Málaga, also revealing that the bacteria detected in some imported samples belonged to a different, non-epidemic strain. Eventually, German authorities attributed the outbreak to organic fenugreek sprouts (*Trigonella foenum-graecum*) imported from Egypt, likely because of cross-contamination [3].

Food contamination can occur at any stage of the production and distribution chain. To mitigate such risks, control programs such as Hazard Analysis and Critical Control Points (HACCP) have been developed and widely implemented in the food sector. Since most foodborne diseases are caused by microorganisms rather than foreign bodies or allergens, HACCP protocols primarily focus on reducing and preventing pathogen contamination [4]. However, due to the severity of certain infections, a zero-tolerance policy is applied to specific pathogens, such as *Listeria monocytogenes* and Shiga toxin-producing *Escherichia coli* (STEC), including O157:H7. [5]. Similar guidelines have also been developed for allergens and gluten content in food [6].

### 1.1.2 Food Security

The Food and Agriculture Organization (FAO) of the United Nations defines food security as follows: *"Food security exists when all people, at all times, have physical, social and economic access to sufficient, safe and nutritious food that meets their dietary needs and food preferences for an active and healthy life. Household food security is the application of this concept to the family level, with individuals as the focus of concern"* [7].

Most undernourished people in the world live in developing countries; two-thirds are concentrated in just seven states (Bangladesh, China, Congo, Ethiopia, India, Indonesia, and Pakistan), and over 40% reside in China and India. Sub-Saharan Africa, however, has the highest proportion of undernutrition, with about 30% of the population affected.

Food security is influenced by multiple factors, including climate change, biodiversity loss, dependence on fossil fuels, and the use of food crops for biofuel production. There is a close relationship between food security and anthropogenic climate change. Numerous studies have analyzed the impact of global warming on agricultural productivity, showing, for instance, a reduction in wheat and rice yields of about 5% for each degree increase in temperature beyond 32 °C [8].

The stability of food supply can also be compromised by the increasing frequency and intensity of extreme weather events such as cyclones, floods, hailstorms, or droughts. However, food security

depends not only on resource availability but also on households' capacity to access, store, and process available food.

Furthermore, climate change affects people's ability to safely utilize food, increasing the risk of waterborne and foodborne diseases. It has been demonstrated, for example, that common illnesses such as salmonellosis exhibit an almost linear increase in reported cases for every degree rise in weekly average temperature [9].

Thus, the challenge of food security lies not only in ensuring sufficient access to food for all to lead a productive life but also in guaranteeing that such food is safe, i.e., free from chemical, physical, or biological hazards.

## 1.2 Food Risk

It is first important to distinguish between *hazard* and *risk*:

- A *hazard* is defined as a chemical, physical, or biological agent—or a practice—that has the potential to cause a proven adverse health effect. The application of safety measures reduces the likelihood of such a hazard causing harm, allowing us to state that the risk has been managed or reduced.
- *Risk*, on the other hand, refers to the probability that an adverse effect will occur. The level of risk is determined by the combination of probability and the severity of the consequences (type of harm, number of people affected, etc.). The concept of risk is therefore closely linked to exposure to a hazard, such as the consumption of contaminated food, and depends on the quantity and frequency of consumption. Risk management aims to decrease either the probability of damage occurring or its severity.

For this reason, it is essential that producers have in-depth knowledge of the characteristics of their products and processes to identify hazards and effectively manage risks. Consumer and buyer trust requires that all actors in the food chain adopt risk analysis tools and control systems along the entire production and distribution chain, from farm to fork [10].

On the demand side, consumer behavior is strongly influenced by risk perception. Risk-averse individuals, for example, will tend to avoid a product even when the probability of harm is very low. Schroeder et al. [11] distinguish between *risk perception* and *risk attitude*: the former reflects an individual's subjective assessment of the risk associated with a specific situation (e.g., health risk from consuming a food product), while the latter indicates an individual's general propensity to accept or reject risk. This leads to three typical profiles: *risk-averse* individuals, who favor choices

perceived as safe; *risk-neutral* individuals, who are indifferent to different levels of risk; and *risk-seeking* individuals, who tend to pursue risky situations.

According to a survey conducted by the European Food Information Council (EUFIC), in collaboration with EFSA and the European Commission, European citizens consider their health more threatened by factors such as environmental pollution, traffic accidents, or serious diseases than by the foods they consume daily. The study, conducted in 25 EU countries on a middle-aged population sample, highlights that although food retains a positive meaning related to taste and pleasure, awareness of the link between diet and health is growing, summarized in the concept "we are what we eat." Three out of five consumers spontaneously associate food with well-being. Moreover, past events such as the BSE (bovine spongiform encephalopathy) crisis or dioxin contamination today have less emotional impact compared to issues such as foodborne infections, chemical residues, or obesity.

When presented with a list of food-related risks, consumers tend to worry more about external factors perceived as beyond their control (e.g., accidental contamination) than about risks related to their own personal behavior, such as food allergies, poor domestic hygiene in food preparation, or weight gain. In general, women are more aware of and sensitive to food safety issues than men.

The level of trust in public authorities is overall high: 54% of respondents believe that institutions take health issues seriously and act promptly; however, 47% think that producers' economic interests sometimes prevail over consumer protection. Finally, more than 60% of respondents believe that political decisions are based on the most recent scientific evidence available.

Overall, as illustrated in Figure 1, risks in the food sector are commonly classified into three main categories, namely physical, chemical, and biological risks [12].

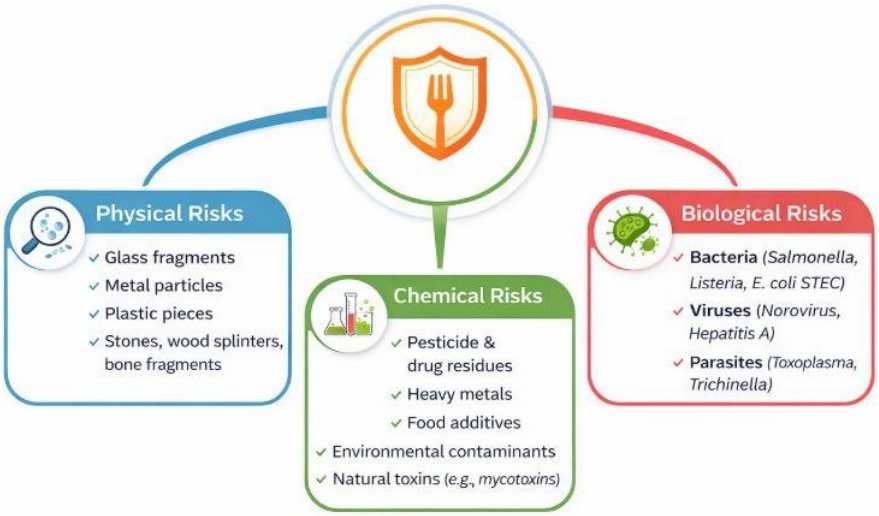


**Figure 1.** Classification of risk in the Agri-Food Sector.

### 1.2.1 Physical Risk

Although physical risks are generally considered less critical than chemical and biological risks, they can still pose significant hazards and have serious impacts on consumer food safety. Foreign objects found in foods may include bone fragments, metal splinters, hypodermic needles, shotgun pellets, residues of packaging materials, stones, glass, wood splinters, insects or other contaminants, as well as personal items or any material that should not normally be present in a food product [13].

A review of the medical literature reported approximately 437 cases of injuries caused by foreign bodies in food over a 21-year period (about 21 cases per year), with glass identified as the leading cause of injury [4].

Physical contamination can occur at any stage of the food supply chain. Such contaminants are defined as additional materials or foreign objects, not normally present in foods, capable of causing injury, illness, or even psychological trauma to the consumer. Unsurprisingly, the presence of foreign bodies is among the principal causes of consumer complaints in the agri-food industry and accounts for a significant number of market withdrawals and product recalls.

Foreign bodies may be intrinsic to the product, originate in the field, derive from raw materials or packaging materials. Sources of contamination are manifold and may include processing facilities, equipment, or even personnel involved at various stages of the chain. The presence of such materials may be accidental or, in rare cases, the result of deliberate introduction into foods (tampering).

The types of foreign material found in food products are numerous. In animal-derived products, for example, bone fragments, hair, or feathers may occur; in plant products grown in contact with soil, such as fruits and vegetables, residues of stones, dirt, or sand are common. Metal is one of the most frequent physical contaminants and may be introduced at any stage of the food chain, from the field to the final consumer. However, the greatest risk is often associated with industrial processing, particularly cutting, slicing, or grinding operations.

The presence of foreign materials may derive from any element that comes into contact with food, whether during handling by personnel or during transport or storage. Jewellery and personal items are common physical contaminants, generally attributable to poor food-handling practices. Packaging materials and containers represent another source of risk: glass, for instance, is among the most critical contaminants associated with this category [14].

Factors determining the potential risk of physical injury to consumers include, among others:

- the type of food;

- the mode of consumption;
- the size of the foreign body;
- the hardness, shape, and sharpness of the foreign body;
- its nature and the ease with which it can be detected.

Radionuclides are also considered physical contaminants. Invisible to the naked eye and detectable only with specific instruments, they can pose severe health risks, including the onset of chronic and potentially fatal diseases.

The prevention of physical risks has become a mandatory requirement. It can be implemented through control of raw materials and ingredients, the adoption of Good Manufacturing Practices (GMPs), the elimination of potential sources of contamination in production and storage areas, the establishment of appropriate equipment maintenance programs, and the installation of effective systems for detecting and removing foreign bodies. In particular, the use of metal detectors or magnets enables detection of metal fragments along the production line, while filters and sieves can retain and remove unwanted materials [15].

### 1.2.2 Chemical Risk

Adverse reactions to chemical compounds present in foods represent one of the most significant issues in food safety and can be divided into two main categories: food intoxications and food hypersensitivities, commonly known as allergies.

Intoxication is caused by ingestion of toxic substances, either naturally occurring or introduced accidentally or deliberately during food production and processing. Hypersensitivities, by contrast, result from an abnormal immune response to specific molecules—often proteins—that act as allergens in predisposed individuals.

A critical concern is the presence of chemical residues in food. Such residues may result from the use of substances required at certain production stages, even if their presence in the final product is unintended. This category includes, for example, pesticide residues, heavy metals, and veterinary drugs which, if not adequately controlled, may pose a concrete risk to consumer health [16].

According to the U.S. National Institute of Allergy and Infectious Diseases (NIAID), approximately 5% of children and 4% of adults in the United States suffer from food allergies. These figures reflect not only the considerable prevalence of the problem but also its social and economic impact: food allergies affect quality of life, require specific preventive and therapeutic strategies, and pose significant challenges to healthcare systems. Moreover, accidental exposure to allergens may have serious consequences, up to potentially fatal reactions such as anaphylaxis.

Globally, growing consumer awareness and increased regulatory attention have led to progressively stricter legislation. In the European Union, for example, the European Food Safety Authority (EFSA) plays a central role in risk assessment related to chemical residues and allergens, providing scientific opinions to the European Commission and Member States. In parallel, EU food information legislation (Regulation (EU) No 1169/2011) mandates clear indication of allergens in both prepacked and non-prepacked foods to protect consumers.

#### 1.2.2.1 Allergens

All individuals can experience food intoxication if exposure to certain compounds is sufficiently high. Among the most common forms of hypersensitivity are food allergies, due to an abnormal immune response. Substances capable of causing adverse reactions include food additives, residues of chemicals used in production processes, environmental contaminants, and endogenous compounds naturally present in foods.

It is estimated that about 2% of the population exhibits adverse reactions to specific foods, with clinical manifestations ranging from mild symptoms—such as rhinitis, cough, sneezing, or pruritus—to severe conditions such as anaphylactic shock, characterized by glottic edema, hypotension, and potentially fatal respiratory distress.

Given the public health relevance of food allergies, authorities have introduced consumer protection measures. European legislation requires the mandatory labelling of allergens, even when present only in trace amounts. These substances must be clearly listed among the ingredients with explicit mention of the allergen. European regulations also set maximum limits for chemical contaminants in foods, establishing threshold values for various substances considered potentially harmful to health [17].

#### 1.2.2.2 Pesticides

The term “pesticides” encompasses a wide range of products used to control harmful organisms in agricultural crops. This category includes insecticides, fungicides, herbicides, molluscicides, plant growth regulators, animal repellents, and rodenticides. Many pesticides are synthetic chemicals, but some derive from natural sources, such as pyrethrins extracted from chrysanthemum.

Trace residues of pesticides may be present in foods placed on the market. To protect consumer health, legislation establishes Maximum Residue Levels (MRLs), expressed in mg/kg or parts per million (ppm). These values, defined at the international level, do not represent toxicological safety thresholds but indicators of compliance with Good Agricultural Practices (GAP). Exceeding an MRL signals non-compliant use of a plant protection product, for example in dosage or application method.

MRLs may be set by various reference authorities, including the European Union, the Codex Alimentarius Commission, and, in some cases, the U.S. Environmental Protection Agency (EPA). Their harmonization is essential to facilitate international trade and ensure uniform food safety standards [18].

#### 1.2.2.3 Heavy Metals

Heavy metal, characterized by high density and potential toxicity, represent one of the main categories of environmental and food contaminants. Those of greatest toxicological concern include cadmium (Cd), mercury (Hg), lead (Pb), and arsenic (As), all listed among the World Health Organization's ten chemicals of major public health concern. Other elements, such as selenium (Se), antimony (Sb), and cobalt (Co), can also negatively affect human health upon exposure [19].

Although naturally present in the Earth's crust, these elements tend to accumulate due to anthropogenic activities, entering the food chain through contaminated air, water, and soil. Once absorbed by plants and animals, they can reach humans via inhalation, ingestion, or dermal exposure, interacting with vital cellular components and impairing biological functions.

The toxic effects of lead, arsenic, and mercury were known in ancient times; however, systematic studies on metal toxicity date back to the nineteenth century. In cases of acute or chronic poisoning, the most common treatment involves administration of chelating agents capable of binding the metal and promoting its elimination [20].

It is important to note that certain trace metals—such as copper (Cu), nickel (Ni), and chromium (Cr)—play essential physiological roles when ingested in limited amounts but become toxic above specific thresholds. For this reason, European legislation (Regulation (EC) No 1881/2006) sets maximum permissible levels for these elements in foods, with the aim of reducing risks to public health.

#### 1.2.2.4 Veterinary Drugs

With the intensification of animal production, the use of veterinary drugs has become increasingly important. Farmed animals may be treated for various purposes, particularly for controlling infectious diseases caused by microorganisms, parasites, or fungi, both in intensive farming systems and in companion animals. Treatment may target the individual animal, but in large groups it is often administered through feed.

Alongside increasing production intensification, the prophylactic use of drugs has also become widespread as a preventive measure against disease onset. Some antibiotics, added to feed at sub-

therapeutic concentrations can modify the intestinal microbiota, thereby improving feed conversion efficiency. In addition, growth promoters with anabolic action exert their effects through modulation of animal metabolism. Finally, hormonal drugs are used in animal husbandry—for example, to regulate reproduction and facilitate the management of herds and poultry flocks [21].

#### 1.2.2.5 Fertilizers

The use of fertilizers must be carefully regulated, both to prevent excessive quantities from entering the food chain and to avoid damage to aquatic ecosystems and soils. Certain products—particularly those originating outside Europe—have been found to contain contaminant levels, such as heavy metals, exceeding internationally established limits, with the risk of accumulation in food crops. For this reason, it is essential that farmers use only fertilizers tested and approved by the competent official control authorities, thereby ensuring the safety of agricultural production and the protection of the environment [22].

#### 1.2.2.6 Lubricants and Detergents

Lubricants are used to reduce friction between mechanical surfaces, decrease wear and ensure smoother and quieter operation of equipment. Detergents, by contrast, are intended to remove organic and inorganic residues—such as food particles, fats, and dirt—and to keep surfaces visibly clean. It is important to distinguish detergents from sanitizers: the latter do not remove soil but reduce the microbial load to acceptable levels, acting only on already clean surfaces; they do not sterilize nor guarantee the total absence of microorganisms.

All these products are widely used in the food industry and, if improperly applied, may constitute a source of accidental contamination. For this reason, lubricants and detergents must be used strictly according to the manufacturer's instructions, in appropriate quantities (neither excessive nor insufficient), and, where necessary, be of food-grade quality [23].

Control and prevention of chemical risk in foods require complex procedures, which include:

- Separation of production lines to reduce the risk of cross-contamination, particularly from allergens;
- Careful monitoring of raw materials to avoid the presence of pesticides, fertilizers, or heavy metal substances that can accumulate in plant matrices;
- Regular cleaning and disinfection of equipment, indispensable for consumer safety. In this context, maintenance operations—such as lubrication of mechanical parts—and sanitation

activities must be carried out when there is no direct exposure to food and in full compliance with the manufacturer's instructions.

### 1.2.3 Biological Risk

Among the various factors that can compromise food safety, biological hazards are undoubtedly those that most capture public attention. Unlike chemical or physical hazards, which are often less immediately perceptible, microbial contamination tends to involve large numbers of consumers and presents with acute, recognizable symptoms such as nausea, fever, or abdominal pain. These features make such episodes particularly visible and concerning, not only for individuals but for the broader community, with a direct socio-economic and public health impact.

From a definitional standpoint, any living organism capable of colonizing a food, surviving or multiplying within it, can be considered a potential biological hazard. According to estimates by the Centers for Disease Control and Prevention (CDC), approximately 9.4 million cases of foodborne illness and over 1,300 deaths occur each year in the United States, attributable to 31 major foodborne pathogens. These figures underscore that the microbiological quality of foods is a priority aspect of food safety, placing the prevention of microbial contamination at the center of control strategies along the entire production chain.

The microorganisms most frequently responsible for foodborne illness include noroviruses, *Salmonella* spp., *Clostridium* spp., and *Campylobacter* spp., which account for most reported cases. The most severe clinical forms, with potential fatal outcomes, are mainly associated with *Listeria monocytogenes* and *Escherichia coli* O157:H7—pathogens particularly insidious for vulnerable populations such as children, the elderly, or immunocompromised individuals [24].

Beyond pathogenic microorganisms, the concept of biological risk also encompasses other categories:

- Macrobiological hazards, such as the accidental presence of insects or small rodents in foods. Although undesirable and repellent to consumers, these are unlikely to pose a concrete health risk, as they can generally be detected and removed with relative ease.
- Parasites are often underestimated or excluded from HACCP assessments, partly due to the belief that they represent a problem confined to specific geographic areas, particularly in developing countries. However, even in industrialized contexts, certain parasitic species can pose significant threats, especially in raw or insufficiently heat-treated foods.

In sum, biological risks represent one of the most significant challenges in food safety, combining high frequency with potentially severe public health consequences. Their management requires a

systematic approach, ranging from strict adherence to hygienic standards during production and processing, to epidemiological surveillance and consumer education.

### 1.2.3.1 Food Poisoning vs. Food Infection

It is essential to distinguish between food poisoning and food infection, as the pathogenic mechanisms and health consequences differ markedly.

Food poisoning is caused by ingestion of foods contaminated with toxins, produced by microorganisms or naturally present in certain foods (e.g., specific mushroom species). These substances directly interfere with biological processes and, once they reach high concentrations, provoke acute effects within a few hours of consumption. Typical symptoms include nausea, vomiting, and general malaise. Some bacterial toxins—such as those produced by *Staphylococcus aureus* and *Clostridium botulinum*—are particularly dangerous, whereas others, such as mycotoxins, may exert chronic effects even at low doses, with carcinogenic, immunotoxin, or teratogenic properties. A critical feature is their heat resistance: common thermal treatments, including cooking, cannot completely inactivate them.

Food infections, by contrast, result from ingestion of viable microorganisms that colonize the intestine, where they multiply and—in some cases—release toxins capable of damaging epithelial cells. Symptoms—abdominal pain and fever—may appear within hours or days after ingestion of the contaminated food. In many cases, symptoms resolve spontaneously, but the infected individual may continue to shed the microorganism in feces, becoming an asymptomatic carrier able to transmit the pathogen to others through poor hygiene or cross-contamination. Frequently implicated bacteria include *Salmonella* spp., *Campylobacter jejuni*, and *Escherichia coli*; enteric viruses are also an important cause of foodborne infection. Adequate cooking (temperatures above 70 °C) is sufficient to inactivate the vast majority of non-spore-forming bacteria.

Effective management of microbiological risk therefore requires thorough knowledge of pathogen biology, contamination mechanisms, and critical control points (CCPs) along the food chain [25].

### 1.2.3.2 Bacteria

Bacteria are the most well-known agents of microbiological risk and represent the leading cause of foodborne diseases. Their proliferation is favored by poor hygiene, inadequate control of temperature and humidity, and improper handling practices.

Clinical manifestations associated with bacterial foodborne illness vary according to the responsible species and the ingested microbial load. Under favorable conditions, bacterial populations can

double approximately every 20–30 minutes, making the risk of contamination and cross-contamination particularly high.

The species most relevant to food safety include:

- *Salmonella* spp., among the principal agents of foodborne illness worldwide;
- *Campylobacter* spp., a common cause of enteritis;
- *Listeria monocytogenes*, associated with severe forms such as listeriosis, particularly dangerous for pregnant women and immunocompromised individuals;
- *Escherichia coli* (especially serotype O157:H7), capable of causing hemolytic–uremic syndromes;
- *Staphylococcus aureus*, known for producing heat-stable enterotoxins;
- *Clostridium botulinum*, responsible for botulism, one of the most severe food intoxications.

#### 1.2.3.3 Molds

Fungi may occur as yeasts or molds, with distinct roles in the food domain. Yeasts are frequently present on the surface of fruits and may reduce shelf-life, although they generally do not pose a health risk. Molds, by contrast, have a dual nature: on the one hand, they are indispensable in certain technological processes (e.g., soy fermentation; ripening of blue and bloomy-rind cheeses); on the other, they can produce toxic secondary metabolites—mycotoxins.

Mycotoxins—including aflatoxins, fumonisins, and ochratoxins—are highly toxic, carcinogenic, and immunotoxin compounds, resistant to thermal treatments and digestive processes. A historical example of contamination is ergotism, caused by ergot (*Claviceps purpurea*) in rye, whose alkaloids led to severe mass intoxication episodes.

To reduce the risk of mycotoxin contamination, controlled use of fungicides can be beneficial, though it must be balanced against broader plant protection considerations. Since the discovery of aflatoxins in the 1960s, many countries have adopted specific regulations.

#### 1.2.3.4 Protozoa

Foodborne protozoan infections are relatively rare in industrialized countries but represent a significant issue in developing regions. Notable protozoa include:

- *Toxoplasma gondii*, the agent of toxoplasmosis, transmitted through contact with cat feces, raw milk, or undercooked meat;
- *Cryptosporidium* spp., responsible for gastroenteritis characterized by watery diarrhea; it is resistant to chlorination and can contaminate water and foods irrigated with wastewater;

- *Giardia lamblia*, widespread in humans and animals, causing giardiasis with persistent intestinal symptoms; it has been isolated in crops irrigated with contaminated water (root vegetables, lettuces, strawberries).

#### 1.2.3.5 Viruses and Prions

In recent decades, foodborne viral infections have gained increasing importance, also due to changes in dietary habits and production systems. Viruses—particularly noroviruses and hepatitis A—are transmitted primarily via the fecal–oral route through contaminated foods or water.

An additional group of biological hazards is represented by prions, unconventional infectious agents responsible for transmissible spongiform encephalopathies (TSEs), such as bovine spongiform encephalopathy (BSE) and Creutzfeldt–Jakob disease (CJD). These diseases, characterized by long incubation periods and irreversible neurodegenerative progression, raised significant public health concern in the 1990s [26].

#### 1.2.3.6 Conventional Techniques for Detecting Biological Hazards

Identifying biological contaminants in foods is a complex challenge. The difficulty stems not only from the need to distinguish pathogenic microorganisms from harmless ones, but also from the requirement to employ analytical methodologies that are sensitive, specific, and internationally validated.

The principal methods include:

- Traditional culture-based methods, both quantitative (e.g., MPN, plate count) and qualitative (presence/absence);
- Rapid automated methods, such as ATP bioluminescence;
- Microscopic techniques, including DEFT (Direct Epifluorescence Filter Technique), flow cytometry (FC), and solid-phase cytometry (SPC);
- Immunological methods, such as ELISA, ELFA, and lateral-flow devices;
- Molecular methods, including FISH and PCR.

Method selection depends on criteria such as accuracy, sensitivity, turnaround time, degree of automation, costs, and ease of use [27].

Within the context of this thesis, particular attention will be devoted to the development and application of electronic devices based on arrays of metal oxide (MOX) gas sensors. These systems enable analysis of the sampled headspace composition, offering a rapid and non-destructive solution

for food quality monitoring. The potential and applications of this technology will be explored in subsequent chapters.

In particular, the following topics will be addressed:

- The electronic nose, including a description of operating principles, architectures, and signal processing strategies.
- Application case studies, comprising:
    - Analysis of the volatilome of table grapes using traditional (GC–MS) and innovative approaches (S3+ electronic nose), with the aim of assessing grape freshness and identifying the most suitable storage atmosphere to extend shelf-life;
    - Characterization of chicken meat from animals fed different diets (traditional and sustainable), to verify whether a sustainable diet based on insect meal can complement or replace conventional feed;
    - Study of sourdough using an electronic nose different from the S3+ system, with the goal of identifying the optimal sourdough stage for artisanal bread production;
    - Analysis of doughs for baked products to determine the optimal proofing point and ensure final product quality.
    - The study of extra virgin olive oil adulteration with lower-quality oils through the combined use of traditional and innovative analytical techniques.

Although each case has been developed with specific purposes, they share a common thread: the use of innovative techniques to support and improve quality, traceability, and sustainability in the agri-food sector.

## 1.3 BIBLIOGRAPHY


1. Agriculture Institute. *Good Manufacturing Practices (GMP) for Ensuring Food Quality.* Food Fundamentals, 2024, February 12.

2. Bahrulolum, H.; Nooraei, S.; Javanshir, N.; Tarrahimofrad, H.; Mirbagheri, V.S.; Easton, A.J.; Ahmadian, G. *Green Synthesis of Metal Nanoparticles Using Microorganisms and Their Application in the Agrifood Sector.* J. Nanobiotechnol. 2021, *19*(1), 86. https://doi.org/10.1186/s12951-021-00834-3.

3. Bártíková, H.; Podlipná, R.; Skálová, L. *Veterinary Drugs in the Environment and Their Toxicity to Plants.* Chemosphere 2016, *144*, 2290–2301. https://doi.org/10.1016/j.chemosphere.2015.10.137.

4. Donno, D.; Mellano, M.G.; Gamba, G.; Riondato, I.; Beccaro, G.L. *Analytical Strategies for Fingerprinting of Antioxidants, Nutritional Substances, and Bioactive Compounds in Foodstuffs Based on High Performance Liquid Chromatography-Mass Spectrometry: An Overview.* Foods 2020, *9*(12), 1734. https://doi.org/10.3390/foods9121734.

5. Duchenne-Moutien, R.A.; Neetoo, H. *Climate Change and Emerging Food Safety Issues: A Review.* J. Food Prot. 2021, *84*(11), 1884–1897. https://doi.org/10.4315/JFP-21-141.

6. European Center of Disease Control (ECDC). *Outbreak of Shiga Toxin-Producing E. coli O104 (STEC O104:H4) Infections Associated with Travel to Germany (Final Update).* E. coli Microbial Outbreaks 2011.

7. European Commission. *Protecting the Food Chain from Prions: Shaping European Priorities through Basic and Applied Research.* Seventh Framework Programme, 2024.

8. Ezzatpanah, H.; Gómez-López, V.M.; Koutchma, T.; Lavafpour, F.; Moerman, F.; Mohammadi, M.; Raheem, D. *Risks and New Challenges in the Food Chain: Viral Contamination and Decontamination from a Global Perspective, Guidelines, and Cleaning.* Compr. Rev. Food Sci. Food Saf. 2022, *21*(2), 868–903. https://doi.org/10.1111/1541-4337.12899.

9. Food and Agriculture Organization of the United Nations (FAO). *Trade Reforms and Food Security: Conceptualizing the Linkages.* FAO: Rome, Italy, 2003.

10. Food and Drug Administration (FDA). *Approaches to Establish Thresholds for Major Food Allergens and for Gluten in Food.* FDA Department: Washington, DC, USA, 2006.

11. Food and Drug Administration (FDA). *Reducing Foodborne Illness Risk Factors in Food Service and Retail Establishments.* FDA Department: Washington, DC, USA, 2014.

12. Gorham, J.R.; Zurek, L. *Filth and Other Foreign Objects in Foods: A Review of Analytical Methods and Health Significance.* In *Handbook of Food Science, Technology and Engineering*; Taylor and Francis, CRC Press: Boca Raton, FL, USA, 2006.

13. Hanning, I.B.; Nutt, J.D.; Ricke, S.C. *Salmonellosis Outbreaks in the United States Due to Fresh Produce: Sources and Potential Intervention Measures.* Foodborne Pathog. Dis. 2009, *6*, 635–648.

14. Hanning, I.B.; O'Bryan, C.A.; Crandall, P.G.; Ricke, S.C. *Food Safety and Food Security.* Nature Educ. Knowl. 2012, *3*(9).

15. Jyothi, N.R. *Heavy Metal Sources and Their Effects on Human Health.* IntechOpen: London, UK, 2020. ISBN 978-1-83968-122-6.

16. L'Abbate, N.; Lorusso, A.; Lasalvia, M. *Production Cycles and Risk Agents in the Agri-Food Sector.* G. Ital. Med. Lav. Ergon. 2010, *32*(4 Suppl), 408–412.

17. Lawrence, D.T.; Dobmeier, S.G.; Bechtel, L.K.; Holstege, C.P. *Food Poisoning.* Emerg. Med. Clin. N. Am. 2007, *25*(2), 357–373. https://doi.org/10.1016/j.emc.2007.02.014.

18. Liu, R.; Liu, H.-C.; Shi, H.; Gu, X. *Occupational Health and Safety Risk Assessment: A Systematic Literature Review of Models, Methods, and Applications.* Saf. Sci. 2023, *160*, 106050. https://doi.org/10.1016/j.ssci.2022.106050.

19. Lykogianni, M.; Bempelou, E.; Karamaouna, F.; Aliferis, K.A. *Do Pesticides Promote or Hinder Sustainability in Agriculture? The Challenge of Sustainable Use of Pesticides in Modern Agriculture.* Sci. Total Environ. 2021, *795*, 148625. https://doi.org/10.1016/j.scitotenv.2021.148625.

20. Mills, E.N.C.; Adel-Patient, K.; Bernard, H.; De Loose, M.; Gillard, N.; Huet, A.C.; Larré, C.; Nitride, C.; Pilolli, R.; Tranquet, O.; Pouke, C.V.; Monaci, L. *Detection and Quantification of Allergens in Foods and Minimum Eliciting Doses in Food-Allergic Individuals (ThRAll).* J. AOAC Int. 2019, *102*(5), 1346–1353. https://doi.org/10.5740/jaoacint.19-0063.

21. Pablos, C.; Romero, A.; de Diego, A.; Vargas, C.; Bascón, I.; Pérez-Rodríguez, F.; Marugán, J. *Novel Antimicrobial Agents as Alternatives to Chlorine with Potential Applications in the Fruit and Vegetable Processing Industry.* Int. J. Food Microbiol. 2018, *285*, 92–97. https://doi.org/10.1016/j.ijfoodmicro.2018.07.029.

22. Perez-Sepulveda, B.M.; Hinton, J.C.D. *Microbe Profile: Salmonella Typhimurium—The Master of the Art of Adaptation.* Microbiology (Reading) 2025, *171*(1), 001521. https://doi.org/10.1099/mic.0.001521.

23. Raposo, A.; Ramos, F.; Raheem, D.; Saraiva, A.; Carrascosa, C. *Food Safety, Security, Sustainability and Nutrition as Priority Objectives of the Food Sector.* Int. J. Environ. Res. Public Health 2021, *18*(15), 8073. https://doi.org/10.3390/ijerph18158073.

24. Sannolo, N.; Simonelli, A.; Basilicata, P.; Miraglia, N. *Production Cycles and Risk Agents.* G. Ital. Med. Lav. Ergon. 2010, *32*(4 Suppl), 404–407.

25. Schroeder, T.C.; Tonsor, G.T.; Pennings, J.M.E.; Mintert, J. *Consumer Food Safety Risk Perceptions and Attitudes: Impacts on Beef Consumption Across Countries.* B.E. J. Econ. Anal. Policy 2007, *7*(1), 1–29.

26. Tchounwou, P.B.; Yedjou, C.G.; Patlolla, A.K. *Heavy Metals Toxicity and the Environment.* In EXS; Volume 101; Springer: Basel, Switzerland, 2012; pp. 133–164. https://doi.org/10.1007/978-3-7643-8340-4_6.

27. Vicién, C.; Rubinstein, C. *Graduate Certificate on Risk Analysis for the Agrifood Sector at the University of Buenos Aires.* Front. Bioeng. Biotechnol. 2024, *12*, 1378538. https://doi.org/10.3389/fbioe.2024.1378538.

# 2

# DEVICE EQUIPPED WITH TAILORED METAL OXIDE SENSORS

## 2.1 Smart sensing for agri-food supply chain control

Quality control has traditionally relied on well-established analytical techniques of chemical, physical, and microbiological nature, which represent the reference standard for accuracy and sensitivity and are essential for regulatory validation. However, they present structural constraints: they often require destructive sampling, well-equipped laboratories, highly trained personnel, and analysis times that are incompatible with in-line or large-scale monitoring. These limitations hinder the adoption of continuous and pervasive control strategies, which are particularly necessary at critical stages of the supply chain (storage, processing, distribution) [1].

To address these challenges, in recent years smart sensing technologies have emerged as complementary tools to conventional analytical methods. Three families are particularly relevant: the electronic nose (e-nose), the electronic tongue (e-tongue), and visual systems (VSs) [2]. E-noses analyze the volatile fraction (VOCs) emitted by products, e-tongues operate in the liquid phase to discriminate between tastes and dissolved species, while VSs quantify optical and morphological parameters—such as color, texture, and surface homogeneity—through advanced imaging and photometric systems. These instruments are rapid, non- or minimally destructive, easily automated, and suitable for real-time monitoring [3].

Within this landscape, semiconductor metal oxides (MOX) play a central role, especially in electronic-nose architecture. Their response is based on changes in electrical resistance as the gas composition varies, yielding signals that are easily acquired by low-power electronics and integrable on miniaturized platforms. Although they do not achieve the molecular specificity of GC-MS, MOX sensors enable rapid, wide-coverage, low-cost screening—ideal for frequent checks and broad deployment [4].

This chapter provides: (i) a treatment of the physical and technological principles of MOX sensors; (ii) their use in multisensor arrays for e-nose implementation; (iii) major applications; and (iv) development prospects in terms of materials, algorithms, and integration with the Internet of Things (IoT). This framework underpins the subsequent experimental chapters, which present protocols, analysis pipelines, and results on real-world use cases.

## 2.2 Metal Oxide (MOX) Sensors and operating principles

MOX sensors belong to the category of chemoresistive devices, as their output signal is the electrical resistance, which varies in response to interactions between the sensing material and the gas molecules present in the environment [4]. Under ambient conditions (air), oxygen molecules are adsorbed onto the semiconductor surface, capturing electrons from the conduction band in n-type semiconductors, or interacting with holes in p-type semiconductors. This process leads to the formation of oxygen species ($O_2^-$, $O^-$, $O^{2-}$), whose distribution depends on the temperature and surface state of the material (Figure 1). These interactions create depletion or accumulation regions of charge carriers within a few nanometers of the surface, thereby altering the potential barrier at the grain boundaries and consequently the overall resistance of the sensing film [5].

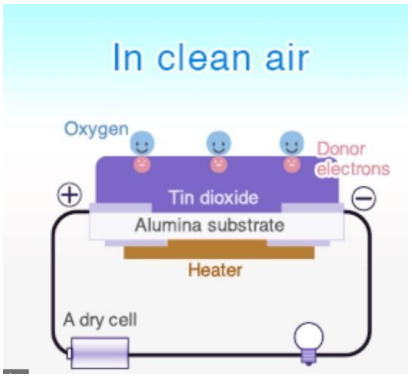


**Figure 1.** Behavior of the sensitive materials under standard conditions during exposure to air.

When the sensor is exposed to a reducing gas (e.g., CO, $H_2$, $CH_4$, or $C_2H_5OH$), the reaction with adsorbed oxygen releases electrons that repopulate the conduction band in n-type materials, resulting in a decrease in resistance (Figure 2). Conversely, exposure to oxidizing gases (such as $NO_2$, $O_3$, or $Cl_2$) causes an increase in resistance. In p-type semiconductors (e.g., NiO or $Co_3O_4$), the effect is reversed: reducing gases increase resistance, while oxidizing gases lead to its reduction [6].

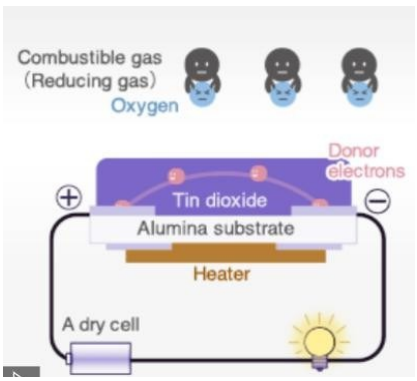


**Figure 2.** Behavior of the sensitive materials upon exposure to analytes in air

To characterize a MOX sensor, the following parameters are typically considered: sensitivity (ratio or difference between R_air and R_gas), limit of detection (LOD), response time ($t_{90}$) and recovery time, selectivity, stability (long-term drift), repeatability, and robustness against environmental variables (temperature, humidity). Relative humidity competes with VOCs for adsorption sites and may either block active sites or generate hydroxyl species; thus, humidity compensation—through auxiliary sensors and multivariate models—is crucial to reduce systematic errors. The operating temperature (200–500 °C) governs adsorption/desorption kinetics and the speciation of adsorbed oxygen; the optimal set-point is specific to each material–analyte pair (e.g., in $SnO_2$, maximum response to $CH_4$ is typically observed at higher temperatures than for CO).

The most employed oxides include $SnO_2$, ZnO, $WO_3$, $In_2O_3$ (n-type) and NiO, $Co_3O_4$, CuO (p-type). Performance depends on morphology (thin films, nanowires, nanorods, aerogels, porous layers), grain size, and catalytic doping with metals (Pt, Pd, Au, Ag) or mixed oxides to selectively activate surface reactions. Functional layers with MOFs or zeolites can act as selective filters or pre-concentrators, modulating VOC access to active sites [1].

A typical MOX device comprises: a dielectric substrate (often $Si/SiO_2$ or alumina), interdigitated electrodes, the sensitive film, and an integrated micro-heater. The front-end electronics employ voltage dividers or Wheatstone bridge configurations to linearize the response and improve the signal-to-noise ratio. Signal digitization (ADC) is followed by digital filtering (low-pass, median) and by normalization and drift correction procedures (baseline tracking, detrending, T/RH-related compensation) [7].

Since the response of a single MOX sensor is not uniquely selective, several strategies are pursued: (i) thermal modulation to extract dynamic signatures sensitive to reaction kinetics; (ii) targeted catalytic functionalization; (iii) arrays with diverse materials and operating conditions; (iv) sample pre-treatment (filters, pre-concentrators, humidity control); and (v) multivariate models capable of separating variability sources and compensating for interferences [8].

## 2.3 Architecture and data pipeline

A sensor-based analytical system consists of a sampling module, a sensor array, a signal conditioning unit (including filters and amplifiers), a data acquisition system, and analysis software. The operation alternates between measurement phases, during which the device is exposed to the sample, and recovery phases, in which filtered air or a reference gas is used. Exposure times and flow rates are optimized to ensure an appropriate balance between adsorption kinetics and analytical throughput.

In the food sector, headspace analysis is common. Pump flow rate, conditioning, exposure, and flushing times determine reproducibility and cycle speed. For humid or fatty matrices, moisture traps or heated sampling lines are employed to avoid condensation. For VOCs at low concentration, thermal pre-concentrators or selective adsorbent materials are often used.

Beyond steady-state measures (resistance plateau), dynamic features are highly informative, including temporal derivatives, areas under the curve, overshoot, rise and decay times, and frequency-domain parameters extracted from modulated signals. Features are normalized, scaled, and subsequently subjected to dimensionality reduction techniques—such as Principal Component Analysis (PCA), t-distributed Stochastic Neighbor Embedding (t-SNE), and Uniform Manifold Approximation and Projection (UMAP)—to reduce collinearity and improve class separability.

For classification tasks (e.g., discrimination between fresh and spoiled samples, geographical origin, or species/variety identification), commonly adopted models include Linear Discriminant Analysis (LDA), Quadratic Discriminant Analysis (QDA), Support Vector Machines (SVM), Random Forest classifiers, k-Nearest Neighbors (k-NN), and lightweight Artificial Neural Networks (ANNs). For regression tasks (e.g., freshness indices, estimated microbial load, or surrogate concentration prediction), methods such as Partial Least Squares regression (PLS), Ridge and Least Absolute Shrinkage and Selection Operator (Lasso) regression, Support Vector Regression (SVR), and Gradient Boosting algorithms are commonly employed.

Model validation strategies include stratified k-fold cross-validation, bootstrapping, or temporal hold-out validation, depending on the data structure and experimental design. Typical performance metrics include accuracy, F1-score, and Area Under the Receiver Operating Characteristic Curve (AUC) for classification tasks, and Root Mean Square Error (RMSE), Mean Absolute Error (MAE), and the coefficient of determination ($R^2$) for regression tasks. Probabilistic calibration methods, such as Platt scaling and isotonic regression, enable the definition of interpretable decision thresholds in operational systems [9].

MOX sensors are subject to drift due to aging, surface contamination, or environmental variations. Mitigation strategies include periodic calibration, quality control with reference gases, drift compensation techniques (detrending, filtered-air anchoring, domain adaptation), and transfer learning to enable model portability across devices or sensor batches. In-service monitoring logics (control charts, novelty indices) help identify out-of-domain conditions and prevent incorrect decisions [10].

## 2.4 MOX sensors in the agri-food sector

### 2.4.1 Freshness and shelf-life monitoring

In the agri-food sector, MOX sensors play a strategic role in monitoring food freshness. During the degradation of meat, fish, and dairy products, characteristic volatile organic compounds are formed—such as biogenic amines, aldehydes, and organic acids—whose presence and concentration vary depending on storage time and cold chain conditions [11]. Devices equipped with MOX sensors can recognize specific patterns associated with refrigeration or freezing processes, storage duration, and potential operational anomalies. Their integration with predictive shelf-life models enables the estimation of the remaining consumption time, thereby contributing to waste reduction and a more efficient inventory management [12].

From a chemical standpoint, specific volatile markers are highly informative: in fish, trimethylamine (TMA), derived from TMAO degradation, increases with spoilage; $MoO_3$-based MOX sensors—sometimes in composites with MXene $Ti_3C_2Tx$—have demonstrated high sensitivity to TMA and rapid response times, in some cases already at room temperature [13]. In animal products, $H_2S$ increases with protein degradation; nanostructured architectures (e.g., nanorods, decorated nanofibers) and catalytic functionalization enhance selectivity and detection limits [14]. In fruits and vegetables, ethylene ($C_2H_4$), the ripening hormone, drives senescence: MOX sensors based on $SnO_2$, $WO_3$, or CuO, sometimes combined with oxidative filters to reduce interferences, enable ripening monitoring and cold-chain optimization [15].

### 2.4.2 Rapid screening of microbiological and chemical contamination

Microbiological or chemical contamination produces volatile fingerprints before reaching human sensory thresholds. E-noses enable rapid screening at raw material intake and process control, with response times shorter than culture-based methods [16]. Typical microbial growth markers include $NH_3$, alcohols (e.g., ethanol), aldehydes (e.g., hexanal), ketones (e.g., acetone), organic acids (e.g., acetic acid), and $H_2S$ [17]. Studies combining GC-MS, microbiological analyses, and MOX-based e-noses (pure $SnO_2$ and Pd/Au-doped, 350–500 °C) have demonstrated: (i) early discrimination between contaminated and healthy samples via PCA; (ii) tracking of microbial growth phases (e.g., coliform log-phase); (iii) applicability in real matrices (e.g., maize contaminated with *Fusarium verticillioides*, with toxigenic strain recognition within 48 h). In high-water-activity products such as jams and jellies, differentiated sensor configurations combined with multivariate analysis allow mold detection from the first day, though discrimination is reduced in the presence of antimicrobial ingredients (e.g., ginger) [18].

### 2.4.3 Traceability and protection of quality labels

Regarding authenticity verification and fraud prevention, a significant contribution arises from the integration of MOX sensor arrays with classification and regression models. The VOC fingerprints generated by products make it possible to discriminate among different animal species (e.g., in meat), varieties and processing types (such as in cheese), as well as geographical origins and farming or cultivation practices. The use of these tools during raw material acceptance or pre-labelling phases provides valuable support for strengthening traceability along the production chain and protecting quality labels [19].

During processing stages, such as fermentation, ripening, roasting, or cooking, the chemical changes occurring within the product are reflected in the profiles of volatile compounds. In this context, MOX-based systems enable in-line monitoring, ensuring uniformity and sensory quality of the final product while promoting the implementation of statistical process control and production optimization strategies.

In modified atmosphere packaging (MAP), miniaturized MOX platforms can detect micro-leaks or variations in internal gas composition, estimate film permeability, and predict product evolution. Their integration with smart labels and temperature/humidity data loggers enables the development of quality monitoring dashboards throughout the supply chain.

Compared with reference methods alone, devices equipped with MOX sensors provide broader analytical coverage and faster response times across multiple samples, making them ideal for high-frequency screening. While targeted analytical confirmations remain essential for quantification and speciation-level identification, the combination of MOX arrays, chemometric or machine learning models, and IoT integration represents a practical and scalable solution for freshness monitoring, early contamination detection, and authenticity protection at the industrial scale.

Figure 3 provides a graphical summary of the concepts discussed in this section, highlighting the remarkable potential of MOX sensors in the agri-food sector, particularly for freshness evaluation, contaminant detection, and the prevention and identification of food fraud and adulteration.

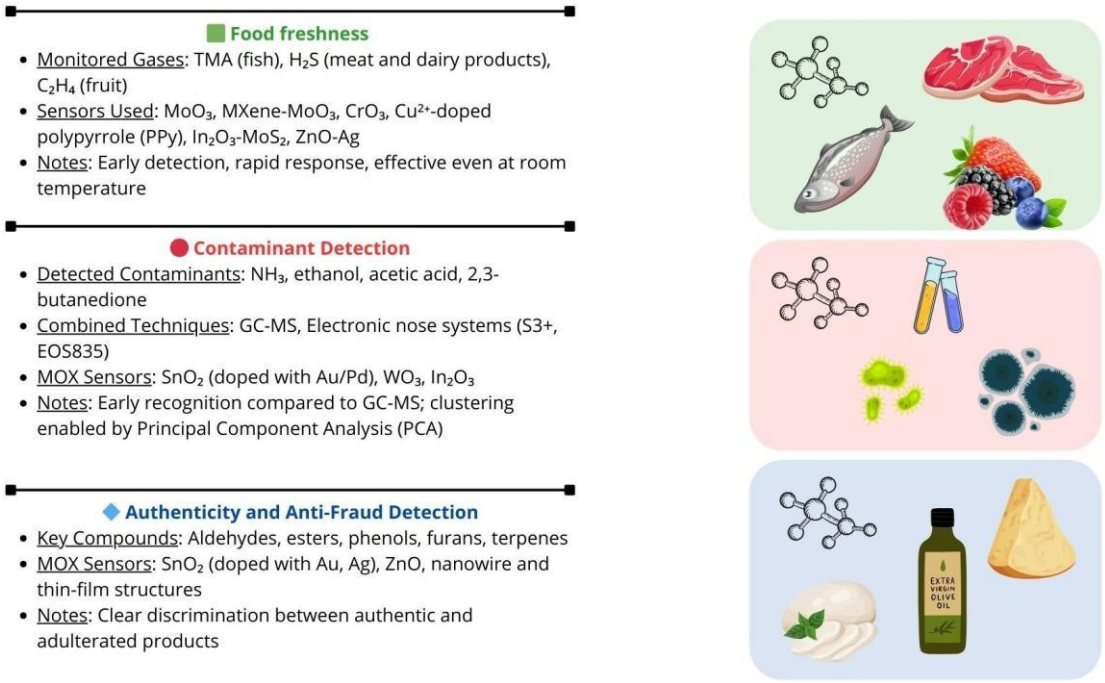


**Figure 3.** Graphical overview highlights the key role that MOX sensors can play in the agri-food sector.

## 2.5 MOX Sensors for Environmental Monitoring

Metal oxide sensors also represent a rapidly evolving technology for real-time environmental monitoring, with targeted applications for detecting atmospheric pollutants such as carbon monoxide (CO), nitrogen dioxide ($NO_2$), and ozone ($O_3$). Compared with traditional methods, they offer more compact, low-cost solutions suitable for distributed systems. Nonetheless, intrinsic challenges remain low chemical selectivity, signal drift over time, and sensitivity to environmental conditions [20]. To ensure metrological reliability, MOX sensors are often complemented by established reference techniques for VOC identification/quantification and by dynamic olfactometry (UNI EN 13725:2004) for sensory assessment of odor intensity, especially in industrial contexts [6]. In numerous studies, GC–MS and olfactometric data have been integrated with MOX sensor responses to improve calibration and the characterization of odor profiles; emerging spectroscopic techniques (UV–vis, FTIR) provide additional validation tools. Integrating these measurements with advanced data-analysis algorithms is fostering the development of increasingly accurate and "intelligent" monitoring systems [21].

### 2.5.1 Carbon Monoxide Detection: Challenges and Advances in MOX Sensors

Carbon monoxide (CO) is a colorless, odorless, and highly toxic gas that binds to hemoglobin with a much higher affinity than oxygen, leading to hypoxia and severe health effects. It is produced by the incomplete combustion of fossil fuels and originates from both natural and anthropogenic

sources, including vehicular traffic, heating systems, and industrial processes. Its detection requires highly sensitive and selective sensors capable of providing rapid responses in residential, urban, and industrial environments [22].

Among n-type semiconductors, $SnO_2$, $TiO_2$, and ZnO are the most extensively investigated, along with $In_2O_3$, $CeO_2$, and $WO_3$, which have also attracted attention for their performance potential. $SnO_2$ is widely employed due to its high sensitivity, which can be further enhanced by doping with Cu, Pd, or Pt, promoting oxygen adsorption and accelerating response dynamics. The use of nanostructures (nanowires, nanoparticles, thin films) optimizes surface activity and reaction kinetics; for instance, nanowires with diameters of about 60 nm and thin films of approximately 2–6 nm exhibit excellent performance at 300–325 °C. The addition of PdO or Au nanoparticles improves sensitivity and response time, while Ca modification or heterostructure formation (e.g., ZnO coupled with other oxides) enhances linearity and selectivity at low CO concentrations.

Hybrid approaches have shown additional improvements: CuO–$SnO_2$ composites enriched with graphene and Ag nanoparticles display higher sensitivity to 100 ppm CO at 400 °C compared with pure $SnO_2$. In the case of $TiO_2$, electrospun nanofibers and hollow hemispherical structures exhibit optimal responses at low concentrations and moderate temperatures due to their high porosity. MEMS-based sensors with integrated Mo micro-heaters and active $TiO_2$ layers achieve high sensitivity around 500 °C, while the integration of multi-walled carbon nanotubes (MWCNTs) enhances response up to sevenfold, with fast reaction times (4 s at 50 ppm) and excellent stability.

For ZnO and its derivatives, Al-doped films exhibit optimal performance near 400 °C, with faster responses for thinner layers. Al nanoparticles show high sensitivity in the 0–80 ppm range even at 300 °C. Doping with Cu, Pd, In, or Ga further improves sensitivity and selectivity depending on concentration and operating temperature, while coupling with $CeO_2$ maximizes response at high concentrations (up to 10,000 ppm at 380 °C) with fast response and recovery times.

Among p-type semiconductors, $Co_3O_4$, NiO, and CuO demonstrate rapid responses at low CO concentrations. Although generally less sensitive than n-type materials, $Co_3O_4$ is widely used thanks to its high surface-to-volume ratio. Multimetallic doping (e.g., AuPdPt–CoO) improves selectivity, while n–p heterojunctions (e.g., $SnO_2$–$Co_3O_4$) achieve optimal performance at 1–10 ppm around 350 °C. NiO supported on activated carbon benefits from increased surface area, and CuO nanowires obtained by thermal oxidation exhibit stability even under humid conditions. $CeO_2$–CuO composites (1:1) show enhanced sensitivity compared with individual oxides, in some cases even at room temperature.

Recent advancements in nanostructured and hybrid materials, combined with targeted doping and multiphase architectures, are enabling the development of MOX-based CO sensors with improved sensitivity, selectivity, response speed, and adaptability across a wide range of operating conditions [23].

### 2.5.2 MOX and FET Sensors for Nitrogen Dioxide Detection

Nitrogen dioxide ($NO_2$) is a major air pollutant, harmful to respiratory health and involved in smog and acid-rain formation; principal sources include traffic, industrial processes, and combustion. Although it lacks a distinctive odor at low concentrations, $NO_2$ can influence odor perception in polluted environments through secondary reactions (e.g., with $O_3$) that generate pungent compounds such as acrolein [24].

Reference quantification of $NO_2$ in monitoring networks relies on chemiluminescence: NO reacts with $O_3$ to produce light proportional to concentration; $NO_2$ is first catalytically reduced to NO, enabling highly sensitive and precise indirect measurements. To increase spatial coverage and temporal resolution, such systems can be complemented by low-cost, easily deployable MOX sensors, provided appropriate calibration strategies are adopted [25]. Field calibration (under real conditions) has been shown to outperform laboratory calibration. Materials such as $TiO_2$, $SnO_2$, and ZnO exhibit improved performance via dopants (e.g., V or Ca on $SnO_2$) and nanostructured architectures (nanowires, mesoporous films) that enhance adsorption; however, environmental variability necessitates robust calibration algorithms and, at times, hydrophobic materials for greater operational stability [26].

Beyond $SnO_2$ doping, modifying ZnO with self-assembled monolayers (SAMs) has proven effective for increasing sensitivity and selectivity toward $NO_2$. Organic molecules such as THMA and dodecanethiol (DT) improve performance: three configurations have been tested (pristine ZnO nanowires; SAM-coated nanowires; nanowires coated with ZnO nanoparticles functionalized with SAMs). Measurements at 0.2 V and 190 °C (temperature determined by TGA, stable up to ~225 °C) show a twofold increase in $\Delta R/R$ with THMA–ZnO nanoparticles relative to pristine nanowires, attributable to modulation of the depletion-region width induced by THMA ligands bound to nanoparticle surfaces [27]. XPS and FTIR analyses confirm the formation of Zn–S (DT) and N–Zn (THMA) bonds and the presence of functional groups; functionalization increases baseline conductivity and $NO_2$ sensitivity without evidence of poisoning, opening prospects for high-efficiency, low-power devices [24].

In parallel, FET sensors have been compared with MOX for $NO_2$ detection. Thanks to lower operating temperatures and reduced power consumption, FETs offer advantages in energy-constrained scenarios. In particular, $In_2O_3$ films modified with hydroxyl groups exhibit superior performance at low temperatures (~100 °C). DRIFTS measurements indicate that $NO_2$ initially adsorbs as nitrite ($NO_2^-$) and, with increasing temperature, converts to nitrate ($NO_3^-$); maximum efficiency is observed when the nitrite species predominates. These devices combine low power (~1.03 mW) with high responses (~2460% at 500 ppb), making them a promising alternative where high sensitivity and low power are required [28].

### 2.5.3 Tropospheric Ozone Detection with MOX Sensors

Tropospheric ozone ($O_3$) is a secondary pollutant harmful to health and ecosystems. Reference monitoring techniques (chemiluminescence and/or UV spectrophotometry) are accurate but costly and impractical for large-scale networks, spurring interest in innovative low-cost solutions. Commercial MOX sensors (e.g., MiCS-2610/2614, $O_3$ Sens 3000, Oz-47, SP-61) and $WO_3$-based prototypes have been evaluated under various operating conditions. These devices, typically operating at 300–400 °C, exhibit ppb-level sensitivity but show strong dependencies on temperature/humidity and temporal drift (up to ~30 ppb over 150 days). Response times range from 5–10 min (MiCS-2610 and $WO_3$-IMN2P) to ~90 min for other models; calibration curves are often sigmoidal, with some prototypes showing more linear behavior.

Experimental networks in Spain, Italy, and Austria have underscored the importance of continuous calibration and accurate conversion from electrical resistance to concentration. Urban-environment comparisons using different methodologies (laboratory calibration, field calibration, and the EASE approach) show that field or EASE calibrations correlate better with reference instruments ($R^2 \approx 0.93$–$0.96$) than laboratory calibration alone ($R^2 \approx 0.82$). Persistent issues include inter-device variability, fragility of certain chips, and low temperatures (<0 °C), which can alter thermal cycling. In summary, MOX sensors are effective for $O_3$ detection but require frequent calibration and environmental compensation.

### 2.5.4 Detection of Environmental VOCs with MOX Sensors and Electronic Noses

Odor analysis in environmental contexts has traditionally been performed using olfactometric tests with trained panelists, capable of providing reliable measurements of odor intensity and quality. As a complementary approach, calibrated sensor systems (including MOX) enable continuous, real-time monitoring, contributing to a more complete characterization of emitting environments. MOX sensors

have been widely studied for VOC monitoring, including methane ($CH_4$) and hydrogen sulphide ($H_2S$).

Methane is a greenhouse gas with a global warming potential 25–34 times higher than $CO_2$ over 100 years; it originates from natural sources (wetlands) and anthropogenic activities (agriculture, waste). In livestock farming, enteric fermentation of ruminants is a primary source, making the development of effective measurement techniques crucial. In addition to traditional methods (respiration chambers, masks/portable devices, $SF_6$ tracers, instrumented boluses), chemoresistive MOX sensors for $CH_4$ have shown limits of detection down to 5 ppm at 210–220 °C, with response/recovery times of ~250 s; porous, rough surfaces (AFM/SEM) improve adsorption, and CoO-based configurations have shown stability for at least six months [29; 30; 31].

For $H_2S$—a toxic gas with impacts on health and ecosystems—sensor performance depends on morphology, composition, and operating conditions [32]. CuO microspheres enriched with $CuFe_2O_4$ nanoparticles provide advantageous porous surfaces; an operating optimum (~240 °C) balances sensitivity and timing (response 31 s, recovery 40 s). Mesoporous materials such as $Co_3O_4$ nanorod chains treated at 600 °C show high efficiency, with response/recovery (46 s/24 s for 1–100 ppm) and good selectivity [33]. In parallel, MOF-type materials (e.g., $Zr(TBAPy)_5(TCPP)$) have demonstrated potential for optical sensing of $H_2S$: FTIR shifts in N–H and C=N bands and fluorescence changes proportional to concentration indicate specific interactions with $S^{2-}$. In general, microstructure (active sites, specific surface area, heterophase interactions) is decisive for sensitivity, selectivity, and response dynamics [34]. A critical aspect remains the operational stability of MOX sensors: prolonged exposure to reducing gases (such as $H_2S$) can cause aging and performance degradation; future development directions include surface functionalization and hybrid architectures to improve selectivity and resistance to poisoning [35]. Figure 4 summarizes the contents of this section, emphasizing the importance of MOX sensors in environmental applications, with reference to monitoring volatile compounds.

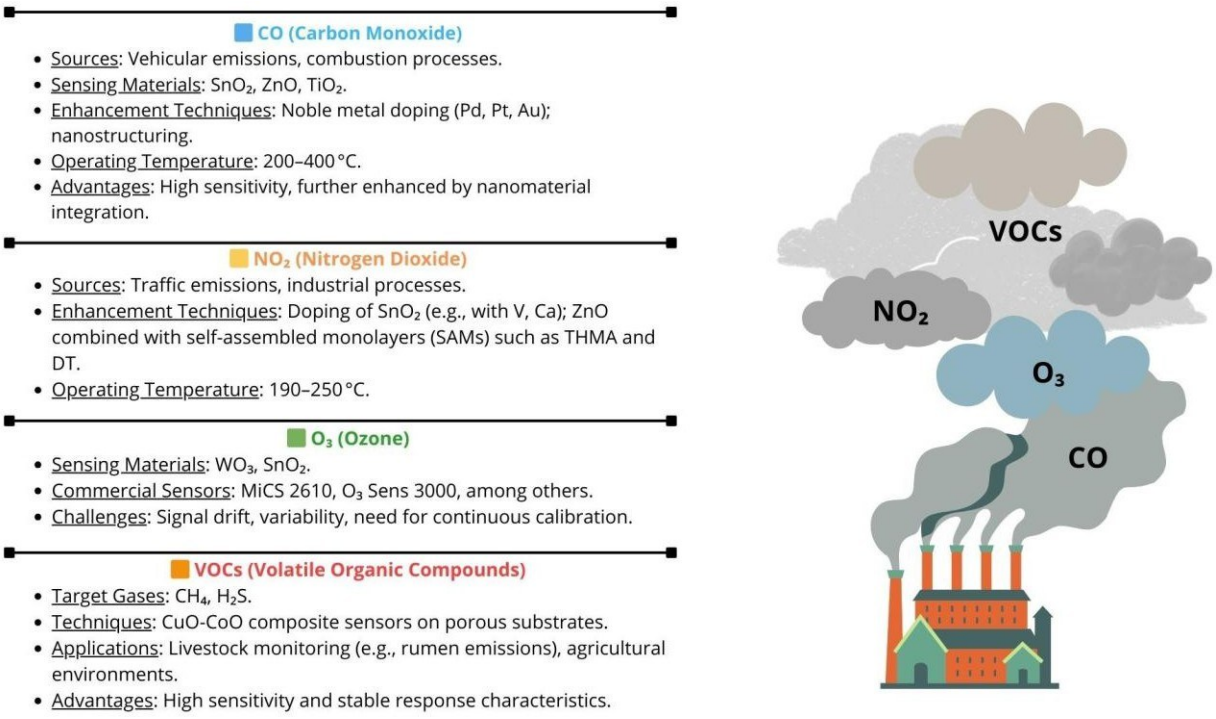


**Figure 4.** Volatile compounds targeted for monitoring by MOX sensors.

## 2.6 Biomedical Applications of MOX Sensors: Breath Analysis for Disease Diagnosis

Metal-oxide (MOX) sensors, originally developed for agri-food and environmental monitoring, are increasingly finding application in the medical field, particularly in the analysis of exhaled breath. The so-called *breathomics* aims to identify endogenous volatile organic compounds (VOCs) associated with pathological conditions such as infections, metabolic disorders, or neoplasms [36]. Interest in MOX sensors stems from their low cost, compactness, and real-time measurement capability. The main challenge is the extremely low concentration of breath biomarkers (ppb–ppt), which imposes stringent requirements in terms of sensitivity and selectivity [37]. For this reason, MOX sensors are often employed as rapid screening tools, integrated with high-resolution analytical techniques for target identification and confirmation. Spectroscopic methods (FTIR, Raman, NMR) can provide further interpretative support [38]. The integration of sensor platforms with machine learning and pattern recognition algorithms is enabling the development of non-invasive, rapid, and potentially scalable diagnostic devices in clinical settings [39].

### 2.6.1 MOX Sensors for Acetone as a Breath Biomarker

Acetone in exhaled air is considered a potential biomarker for diabetes monitoring, as its concentration correlates with metabolic status [40]. In healthy individuals, typical values are in the

ppm range but can increase significantly under ketosis; the exact range, however, depends on individual and methodological factors. In MOX sensors, the detection mechanism is based on the chemisorption of surface oxygen: interaction with acetone modulates semiconductor conductivity and thus electrical resistance. Sensitivity is critically dependent on operating temperature and material composition [41].

- $SnO_2$ is one of the most widely used materials; composites with NiO or graphene oxide enhance the response and lower the operating temperature. Ternary nanocomposites have shown rapid responses in the 0.25–30 ppm range around 200 °C [42].
- $TiO_2$ in pure form is poorly sensitive to VOCs, but heterojunctions ($TiO_2/Ag_2V_4O_{11}$, $TiO_2$–$Fe_2O_3$, $TiO_2$–$SnO_2$) improve selectivity, stability, and response times (up to ~15 s) [43].
- $WO_3$ (n-type with catalytic activity) achieves sub-ppm limits of detection; decoration with Au or Pt nanoparticles enables ppb-level detection at ~410 °C [44].
- $Fe_2O_3$ typically requires high temperatures, but sol–gel processes and doping (e.g., gadolinium) have enabled ~1 ppm detection at ~200 °C with good stability [45].
- $In_2O_3$ nanowires offer very rapid responses (1–7 s) and good selectivity, although the impact of humidity—typical of breath—must be carefully managed [46].
- CuO (p-type) shows intrinsically low sensitivity, but performance can be improved with $Cu_2O$–CuO composites decorated with Ag: responses from sub-ppb up to 1000 ppm have been demonstrated at ~350 °C, albeit still at relatively high temperatures for portable applications [47].

Dedicated breath-analysis prototypes have also been presented: compact multi-gas devices, ketone-measurement tools with pre-concentration/humidity management modules, and ultrasensitive heterojunction sensors (e.g., p-$Rh_2O_3$–n-ZnO) tested in simulated diabetic breath scenarios. Most of these systems are still undergoing laboratory or clinical validation.

### 2.6.2 Exhaled Ammonia: Sensors and E-Nose for Clinical Monitoring

The presence of ammonia in exhaled air is linked to systemic accumulation due to impaired urea excretion; $NH_3$ and $NH_4^+$ cross the blood–lung barrier and become detectable in breath, making them useful for patient monitoring, particularly in haemodialysis [48]. Highly sensitive instrumental techniques (PTR-MS, SIFT-MS, PAS, SAW, QCM) are available but costly and complex. In parallel, devices based on conductive nanomaterials (polyaniline nanofibers, polymer nanojunctions,

polypyrrole nanowires) and MOX sensors are showing promising performance [49; 50]. Examples include nanoporous semiconductor polymer sensors (e.g., PTB7) with a range of 50–8000 ppb, ~30 s response times, and humidity management; PANI nanojunctions with gold electrodes and anti-humidity filters; and doped MOX sensors (e.g., Si-doped $MoO_3$) with high selectivity and stability under high humidity [51; 52]. In studies on dialysis patients, commercial MOX arrays (TGS/MQ) enabled classification of samples with accuracies up to ~88%, as well as monitoring of $NH_3$ reduction post-treatment [53]. Portable prototypes have also been proposed, such as Si-doped $WO_3$ films and porous-film QCM devices, with LODs <20 ppb at ~350 °C. E-nose systems using quartz crystals coated with synthetic peptides have demonstrated the ability to recognize volatile biomarkers (uremia-related amines) correlated with uremic status [54].

### 2.6.3 Detection of Colorectal Cancer via Exhaled VOCs and MOX Sensors

For colorectal cancer, analysis of exhaled VOCs represents a non-invasive strategy based on the identification of biomarkers (aldehydes, ketones, hydrocarbons) linked to oxidative stress and tumor-related metabolic pathways [55]. MOX sensors have been developed using various semiconducting oxides ($SnO_2$, $TiO_2$, $WO_3$, $Nb_2O_5$, $V_2O_5$), often decorated with Au nanoparticles to enhance sensitivity, and typically operating between 350 and 450 °C. An example is the multi-sensor device *SCENT B2*, which combines four elements with complementary sensitivities; comparison of VOC profiles from pre- and post-surgical samples showed a significant reduction in sensor response after tumor removal. Multivariate analysis (PCA) and ROC curves highlighted high discriminative ability (AUC > 0.9) [56]. Studies on exhaled breath using high-temperature MOX (200–400 °C), combined with machine learning algorithms (e.g., C4.5), have reported ~77% accuracy, ~63% sensitivity, and ~84% specificity. Comparative analyses indicate particularly strong performance for Au-decorated $SnO_2$ and $TiO_2$, with sensitivity up to ~80% and specificity ~70% at ~450 °C, underscoring the importance of optimizing sensor materials and architecture. Once refined and clinically validated, these devices could be integrated into non-invasive screening pathways [57].

Figure 5 provides a graphical synthesis of the concepts discussed in this section, highlighting the central role of MOX sensors in the medical field, owing to their ability to detect or prevent diseases through the analysis of volatile compounds emitted by the human body.

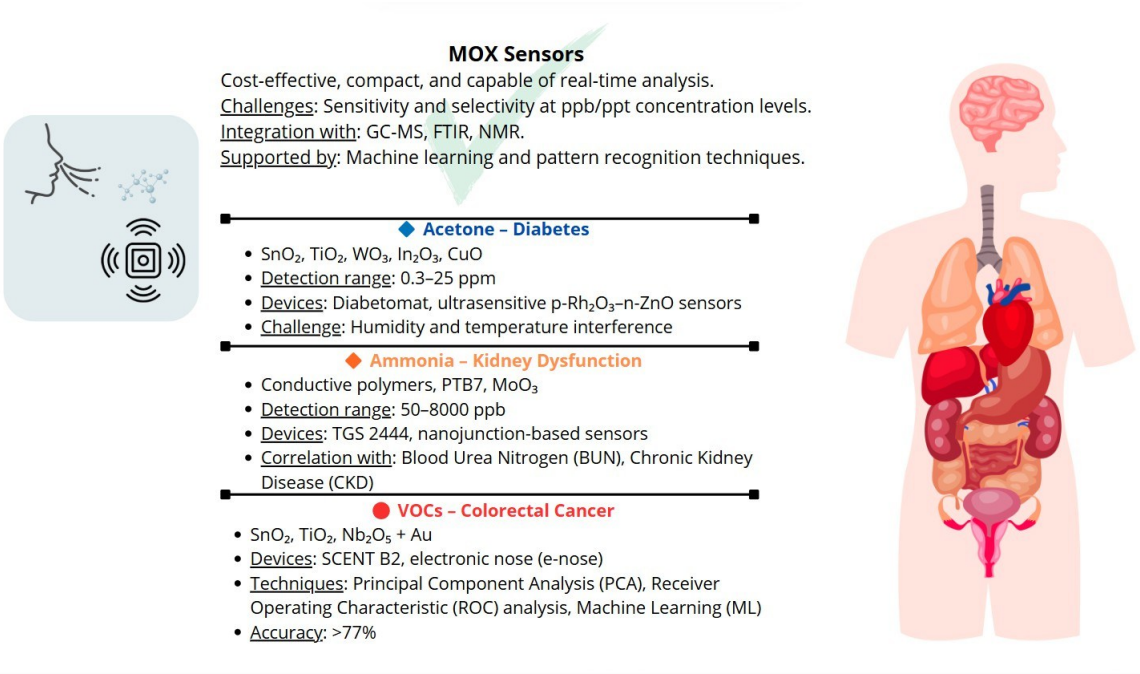


**Figure 5.** Graphical overview highlighting the key role that MOX sensors can play in the medical field.

## 2.7 Integration with IoT, Edge AI, and Operational Considerations

Modern systems combine local (edge) acquisition with analysis performed on embedded devices (microcontrollers/SoCs) or in the cloud. Edge AI reduces latency and dependence on connectivity, whereas the cloud facilitates model updates, federated learning, and multi-plant management. The choice depends on constraints related to power, bandwidth, privacy, and response time criticality.

Data quality is crucial: standardized sampling protocols, reference materials, and calibration routines (standard gases or certified samples) are required. The metrology of sensor data involves control charts for baseline and noise, repeatability/reproducibility tests, robustness studies (controlled variations of T/RH), and inter-calibration plan across instruments.

In IoT solutions, cybersecurity is a baseline requirement: data encryption, device authentication, signed updates, and segregation of industrial networks. Data governance (ownership, retention, audit trail) must be defined in compliance with regulatory and contractual supply chain requirements.

The most promising trajectories include: (i) high-surface-area nanostructures (nanowires, nanosheets, aerogels) to maximize gas–solid interactions; (ii) n–p heterojunctions and core–shell architectures to modulate internal barriers; (iii) catalytic doping and metallic decoration to lower activation energies; (iv) MOF/zeolite interfaces to selectively filter and pre-concentrate VOCs.

The use of multi-parametric modulations (temperature, polarization, light/UV for photocatalysis) and dynamic signature spectra increases discriminant information. Integration with on-chip micro-chromatography or selective membranes can provide a lightweight physical pre-separator.

Hybrid models (physics-informed and data-driven) promise greater interpretability and robustness. Techniques such as domain adaptation, transfer learning, and incremental learning address drift and domain shifts. Explainability (SHAP, saliency on dynamic features) facilitates auditing and regulatory acceptance.

The convergence of microfabrication, low-cost packaging, and ultra-low-power electronics enables portable, edge-ready devices. Simplified user interfaces (mobile apps, traffic-light indicators) could support prosumer use cases (rapid freshness verification at home), while maintaining a confirmation channel with reference methods when required. In the perspective of integration with traditional analytical methods, MOX sensors can bridge the gap between the need for rigorous controls and the demand for rapid, widespread, and sustainable solutions, thereby contributing to food chain quality, safety, and transparency [58].

## 2.8 Comparison of MOX, Electrochemical, and Optical Sensors: Performance and Applications

Compared to electrochemical sensors, known for their high sensitivity and selectivity but limited by shorter lifespan and higher susceptibility to operational conditions, MOX sensors provide superior stability [59].

In the agri-food sector, this feature allows rapid and low-cost assessment of freshness, ripening, and product quality, as an alternative to optical systems which, although accurate, are more complex and costly. In the environmental field, MOX sensors represent a reliable and low-cost solution for air quality monitoring and gas leak detection, demonstrating robustness even under variable operating conditions. In the medical domain, although optical sensors are often preferred for their accuracy and non-invasive operation, MOX sensors offer a more economically accessible alternative that is easily integrable into compact devices, making them promising for breath analysis and early diagnosis applications.

Overall, despite the specific strengths of electrochemical and optical technologies, MOX sensors stand out for their versatility, stability, and cost-effectiveness, establishing themselves as a cross-cutting solution with broad application prospects in all three domains considered [21].

## 2.9 BIBLIOGRAPHY


1. Poeta, E.; Núñez-Carmona, E.; Sberveglieri, V. A Review: Applications of MOX Sensors from Air Quality Monitoring to Biomedical Diagnosis and Agro-Food Quality Control. J. Sens. Actuator Netw. 2025, 14, 50. https://doi.org/10.3390/jsan14030050
2. Poeta, E.; Liboà, A.; Mistrali, S.; Núñez-Carmona, E.; Sberveglieri, V. Nanotechnology and E-Sensing for Food Chain Quality and Safety. Sensors 2023, 23, 8429. https://doi.org/10.3390/s23208429
3. Bayda, S.; Adeel, M.; Tuccinardi, T.; Cordani, M.; Rizzolio, F. The History of Nanoscience and Nanotechnology: From Chemical–Physical Applications to Nanomedicine. Molecules 2020, 25, 112.
4. Comini, E.; Baratto, C.; Faglia, G.; Ferroni, M.; Vomiero, A.; Sberveglieri, G. Quasi-One Dimensional Metal Oxide Semiconductors: Preparation, Characterization and Application as Chemical Sensors. Prog. Mater. Sci. 2009, 54(1), 1–67. https://doi.org/10.1016/j.pmatsci.2008.06.003
5. Schütze, A.; Baur, T.; Leidinger, M.; Reimringer, W.; Jung, R.; Conrad, T.; Sauerwald, T. Highly Sensitive and Selective VOC Sensor Systems Based on Semiconductor Gas Sensors: How to? Environments 2017, 4, 20.
6. Khorramifar, A.; Karami, H.; Lvova, L.; Kolouri, A.; Łazuka, E.; Piłat-Rożek, M.; Łagód, G.; Ramos, J.; Lozano, J.; Kaveh, M.; et al. Environmental Engineering Applications of Electronic Nose Systems Based on MOX Gas Sensors. Sensors 2023, 23, 5716.
7. Firooz, A.A.; Mahjoub, A.R.; Khodadadi, A.A. Highly Sensitive CO and Ethanol Nanoflower-like $SnO_2$ Sensor among Various Morphologies Obtained by Using Single and Mixed Ionic Surfactant Templates. Sens. Actuators B Chem. 2009, 141, 89–96.
8. Ponzoni, A.; Comini, E.; Concina, I.; Ferroni, M.; Falasconi, M.; Gobbi, E.; Sberveglieri, V.; Sberveglieri, G. Nanostructured Metal Oxide Gas Sensors: A Survey of Applications Carried Out at SENSOR Lab, Brescia (Italy) in the Security and Food Quality Fields. Sensors 2012, 12, 17023–17045.
9. Girmatsion, M.; Tang, X.; Zhang, Q.; Li, P. Progress in Machine Learning-Supported Electronic Nose and Hyperspectral Imaging Technologies for Food Safety Assessment: A Review. Food Res. Int. 2025, 209, 116285. https://doi.org/10.1016/j.foodres.2025.116285
10. Kim, H.J.; Lee, J.H. Highly Sensitive and Selective Gas Sensors Using p-Type Oxide Semiconductors: Overview. Sens. Actuators B Chem. 2014, 192, 607–627.

11. Wanniarachchi, P.C.; Kumarasinghe, K.G.U.; Jayathilake, C. Recent Advancements in Chemosensors for the Detection of Food Spoilage. Food Chem. 2024, 436, 137733.
12. Park, J.-C.; Yuk, Y.; Lee, S. Recent Trends in Gas Sensors for Food Spoilage Monitoring. J. Sens. Sci. Technol. 2024, 33, 412–418.
13. Wang, Z.; Ma, W.; Wei, J.; Lan, K.; Yan, S.; Chen, R.; Qin, G. Ultrasensitive Flexible Olfactory Receptor-Derived Peptide Sensor for Trimethylamine Detection by the Bending Connection Method. ACS Sens. 2022, 7, 3513–3520.
14. Chung, J.H.; Cho, Y.-H.; Hwang, J.; Lee, S.H.; Lee, S.; Park, S.-H.; Sohn, S.; Cho, D.; Lee, K.; Shim, Y.-S. Heterostructures of $SnO_2$-Decorated $Cr_2O_3$ Nanorods for Highly Sensitive $H_2S$ Detection. J. Sens. Sci. Technol. 2024, 33, 40–47.
15. Wen, Z.; Zhu, L.; Li, Y.; Zhang, Z.; Ye, Z. Mesoporous $Co_3O_4$ Nanoneedle Arrays for High-Performance Gas Sensor. Sens. Actuators B Chem. 2014, 203, 873–879.
16. Canhoto, O.; Magan, N. Electronic Nose Technology for the Detection of Microbial and Chemical Contamination of Potable Water. Sens. Actuators B Chem. 2005, 106, 3–6.
17. Ventura-Aguilar, R.I.; Lucas-Bautista, J.A.; Arevalo-Galarza, M.L.; Bosquez-Molina, E. Volatile Organic Compounds as a Diagnostic Tool for Detecting Microbial Contamination in Fresh Agricultural Products: Mechanism of Action and Analytical Techniques. Processes 2024, 12, 1555.
18. Carmona, E.N.; Sberveglieri, V.; Pulvirenti, A. Detection of Microorganisms in Water and Different Food Matrix by Electronic Nose. In Proc. 2013 Seventh International Conference on Sensing Technology (ICST), Wellington, New Zealand, 3–5 December 2013; pp. 699–703.
19. Wang, C.; Yin, L.; Zhang, L.; Xiang, D.; Gao, R. Metal Oxide Gas Sensors: Sensitivity and Influencing Factors. Sensors 2010, 10, 2088–2106.
20. Rodriguez-Aguilar, M.; Diaz de Leon-Martinez, L.; Gorocica-Rosete, P.; Padilla, R.P.; Thirion-Romero, I.; Ornelas-Rebolledo, O.; Flores-Ramirez, R. Identification of Breath-Prints for the COPD Detection Associated with Smoking and Household Air Pollution by Electronic Nose. Respir. Med. 2020, 163, 105901.
21. Isaac, N.A.; Pikaar, I.; Biskos, G. Metal Oxide Semiconducting Nanomaterials for Air Quality Gas Sensors: Operating Principles, Performance, and Synthesis Techniques. Mikrochim. Acta 2022, 189, 196.
22. Varon, J.; Marik, P.E.; Fromm, R.E., Jr.; Gueler, A. Carbon Monoxide Poisoning: A Review for Clinicians. J. Emerg. Med. 1999, 17, 87–93.

23. Nandy, T.; Coutu, R.A., Jr.; Ababei, C. Carbon Monoxide Sensing Technologies for Next-Generation Cyber-Physical Systems. Sensors 2018, 18, 3443.
24. Jung, G.; Shin, H.; Jeon, S.W.; Lim, Y.H.; Hong, S.; Kim, D.H.; Lee, J.H. Transducer-Aware Hydroxy-Rich-Surface Indium Oxide Gas Sensor for Low-Power and High-Sensitivity $NO_2$ Gas Sensing. ACS Appl. Mater. Interfaces 2023, 15, 22651–22661.
25. Tian, Y.; Wang, K.K.; Yang, G.P.; Li, P.F.; Liu, C.Y.; Ingeniero, R.C.O.; Bange, H.W. Continuous Chemiluminescence Measurements of Dissolved Nitric Oxide (NO) and Nitrogen Dioxide ($NO_2$) in the Ocean Surface Layer of the East China Sea. Environ. Sci. Technol. 2021, 55, 3668–3675.
26. Fazio, E.; Spadaro, S.; Corsaro, C.; Neri, G.; Leonardi, S.G.; Neri, F.; Lavanya, N.; Sekar, C.; Donato, N.; Neri, G. Metal-Oxide-Based Nanomaterials: Synthesis, Characterization and Their Applications in Electrical and Electrochemical Sensors. Sensors 2021, 21, 2494.
27. Waclawik, E.R.; Chang, J.; Ponzoni, A.; Concina, I.; Zappa, D.; Comini, E.; Motta, N.; Faglia, G.; Sberveglieri, G. Functionalised Zinc Oxide Nanowire Gas Sensors: Enhanced $NO_2$ Gas Sensor Response by Chemical Modification of Nanowire Surfaces. Beilstein J. Nanotechnol. 2012, 3, 368–377.
28. Spirito, P. Elettronica Digitale; McGraw-Hill Libri Italia SRL: Milano, Italy, 2006; ISBN 978-88-386-6323-9.
29. Chesler, P.; Hornoiu, C.; Anastasescu, M.; Calderon-Moreno, J.M.; Gheorghe, M.; Gartner, M. Cobalt- and Copper-Based Chemiresistors for Low Concentration Methane Detection, a Comparison Study. Gels 2022, 8, 721.
30. Rydosz, A. The Use of Copper Oxide Thin Films in Gas-Sensing Applications. Coatings 2018, 8, 425.
31. Kong, Y.; Teather, R.M.; Forster, R.J. Biodiversity and Composition of Methanogenic Populations in the Rumen of Cows Fed Alfalfa Hay or Triticale Straw. FEMS Microbiol. Ecol. 2013, 84, 302–315.
32. Aroca, A.; Gotor, C.; Bassham, D.C. Hydrogen Sulfide: From a Toxic Molecule to a Key Molecule of Cell Life. Antioxidants 2020, 9, 621.
33. Quang, P.L.; Cuong, N.D.; Hoa, T.T.; Long, H.T.; Hung, C.M.; Le, D.T.T.; Hieu, N.V. Simple Post-Synthesis of Mesoporous p-Type $Co_3O_4$ Nanochains for Enhanced $H_2S$ Gas Sensing Performance. Sens. Actuators B Chem. 2018, 270, 158–166.
34. Guo, L.; Wang, M.; Cao, D. A Novel Zr-MOF as Fluorescence Turn-On Probe for Real-Time Detecting $H_2S$ Gas and Fingerprint Identification. Small 2018, 14, 1703822.

35. Jo, S.B.; Kim, H.J.; Ahn, J.H.; Hwang, B.W.; Huh, J.S.; Ragupathy, D.; Lee, S.C.; Kim, J.C. Effects of Thin-Film Thickness on Sensing Properties of $SnO_2$-Based Gas Sensors for the Detection of $H_2S$ Gas at ppm Levels. J. Nanosci. Nanotechnol. 2020, 20, 7169–7174.
36. Heranjal, S.; Maciel, M.; Kamalapally, S.N.R.; Ramrakhiani, I.; Schulz, E.; Cao, S.; Liu, X.; Relich, R.F.; Wek, R.; Woollam, M.; et al. Establishing Healthy Breath Baselines with Tin Oxide Sensors: Fundamental Building Blocks for Noninvasive Health Monitoring. Mil. Med. 2024, 189(Suppl. S3), 221–229.
37. Glockler, J.; Jaeschke, C.; Padilla, M.; Mitrovics, J.; Mizaikoff, B. Ultratrace eNose Sensing of VOCs toward Breath Analysis Applications Utilizing an eNose-Based Analyzer. ACS Meas. Sci. Au 2024, 4, 184–187.
38. Santos, F.; Magalhães, S.; Henriques, M.C.; Fardilha, M.; Nunes, A. Spectroscopic Features of Cancer Cells: FTIR Spectroscopy as a Tool for Early Diagnosis. Curr. Metabolomics 2018, 6, 103–111.
39. Derveaux, E.; Van Brussel, T.; VanWeyenbergh, J.; Lievens, Y.; De Neve, W.; Derua, R.; Dhaene, T.; De Preter, K.; Bockstal, M.; Bosteels, C.; et al. NMR-Metabolomics Reveals a Metabolic Shift after Surgical Resection of Non-Small Cell Lung Cancer. Cancers 2023, 15, 2127.
40. Deng, C.; Zhang, J.; Yu, X.; Zhang, W.; Zhang, X. Determination of Acetone in Human Breath by Gas Chromatography–Mass Spectrometry and Solid-Phase Microextraction with on-Fiber Derivatization. J. Chromatogr. B 2004, 810, 269–275.
41. Righettoni, M.; Tricoli, A.; Pratsinis, S.E. Si:$WO_3$ Sensors for Highly Selective Detection of Acetone for Easy Diagnosis of Diabetes by Breath Analysis. Anal. Chem. 2010, 82, 3581–3587.
42. Chen, Y.; Cao, Y. Ultrasensitive and Low Detection Limit of Acetone Gas Sensor Based on ZnO/$SnO_2$ Thick Films. RSC Adv. 2020, 10, 35958–35965.
43. Lou, Z.; Li, F.; Deng, J.; Wang, L.; Zhang, T. Branch-like Hierarchical Heterostructure (α-$Fe_2O_3$/$TiO_2$): A Novel Sensing Material for Trimethylamine Gas Sensor. ACS Appl. Mater. Interfaces 2013, 5, 12310–12316.
44. Munoz-Bolanos, J.D.; Rodriguez-Paez, J.E. $WO_3$ Mono-Nanocrystals: Synthesis, Characterization and Evaluation of Their Electrical Behavior in Oxygen and Acetone Atmospheres. Mater. Sci. Eng. B 2021, 274, 115472.
45. Zahmouli, N.; Hjiri, M.; Leonardi, S.G.; El Mir, L.; Neri, G.; Iannazzo, D.; Espro, C.; Aida, M.S. High Performance Gd-Doped γ-$Fe_2O_3$ Based Acetone Sensor. Mater. Sci. Semicond. Process. 2020, 116, 105154.

46. Kohli, N.; Hastir, A.; Kumari, M.; Singh, R.C. Hydrothermally Synthesized Heterostructures of $In_2O_3$/MWCNT as Acetone Gas Sensor. Sens. Actuators A Phys. 2020, 314, 112240.
47. Wang, W.; Zhang, Y.; Zhang, J.; Li, G.; Leng, D.; Gao, Y.; Gao, J.; Lu, H.; Li, X. Metal–Organic Framework-Derived $Cu_2O$–CuO Octahedrons for Sensitive and Selective Detection of ppb-Level $NO_2$ at Room Temperature. Sens. Actuators B Chem. 2021, 328, 129045.
48. Krishnan, S.T.; Devadhasan, J.P.; Kim, S. Recent Analytical Approaches to Detect Exhaled Breath Ammonia with Special Reference to Renal Patients. Anal. Bioanal. Chem. 2017, 409, 21–31.
49. Anderson, J.C.; Lamm, W.J.E.; Hlastala, M.P. Measuring Airway Exchange of Endogenous Acetone Using a Single-Exhalation Breathing Maneuver. J. Appl. Physiol. 2006, 100, 880–889.
50. Statheropoulos, M.; Agapiou, A.; Georgiadou, A. Analysis of Expired Air of Fasting Male Monks at Mount Athos. J. Chromatogr. B 2006, 832, 274–279.
51. Chen, C.C.; Hsieh, J.C.; Chao, C.H.; Yang, W.S.; Cheng, H.T.; Chan, C.K.; Lu, C.J.; Meng, H.F.; Zan, H.W. Correlation between Breath Ammonia and Blood Urea Nitrogen Levels in Chronic Kidney Disease and Dialysis Patients. J. Breath Res. 2020, 14, 036002.
52. Jayasree, T.; Bobby, M.; Muttan, S. Sensors for Detecting Ammonia from the Exhaled Breath of Renal Disorder Patients. Sensor Lett. 2015, 13, 1003–1008.
53. Jayasree, T.; Bobby, M.; Muttan, S. Sensor Data Classification for Renal Dysfunction Patients Using Support Vector Machine. J. Med. Biol. Eng. 2015, 35, 759–764.
54. Marek, G.; Dobrzański, B.; Oniszczuk, T.; Combrzyński, M.; Ćwikła, D.; Rusinek, R. Detection and Differentiation of Volatile Compound Profiles in Roasted Coffee Arabica Beans from Different Countries Using an Electronic Nose and GC-MS. Sensors 2020, 20, 2124.
55. Dekker, E.; Tanis, P.J.; Vleugels, J.L.A.; Kasi, P.M.; Wallace, M.B. Colorectal Cancer. Lancet 2019, 394, 1467–1480.
56. Astolfi, M.; Rispoli, G.; Anania, G.; Artioli, E.; Nevoso, V.; Zonta, G.; Malagù, C. Tin, Titanium, Tantalum, Vanadium and Niobium Oxide-Based Sensors to Detect Colorectal Cancer Exhalations in Blood Samples. Molecules 2021, 26, 466.
57. Bax, C.; Robbiani, S.; Zannin, E.; Capelli, L.; Ratti, C.; Bonetti, S.; Novelli, L.; Raimondi, F.; Di Marco, F.; Dellacà, R.L. An Experimental Apparatus for E-Nose Breath Analysis in Respiratory Failure Patients. Diagnostics 2022, 12, 776.

58. Gouiza, N.; Jebari, H.; Reklaoui, K. Integration of IoT-Enabled Technologies and Artificial Intelligence in Diverse Domains: Recent Advancements and Future Trends. J. Theor. Appl. Inf. Technol. 2024, 102(5), Published 15 March 2024.
59. Khan, M.A.H.; Rao, M.V.; Li, Q. Recent Advances in Electrochemical Sensors for Detecting Toxic Gases: $NO_2$, $SO_2$ and $H_2S$. Sensors 2019, 19, 905.

# 3.

# QUALITY MONITORING OF TABLE GRAPES STORED IN CONTROLLED ATMOSPHERE USING AN S3 + MOS NANOSENSOR DEVICE

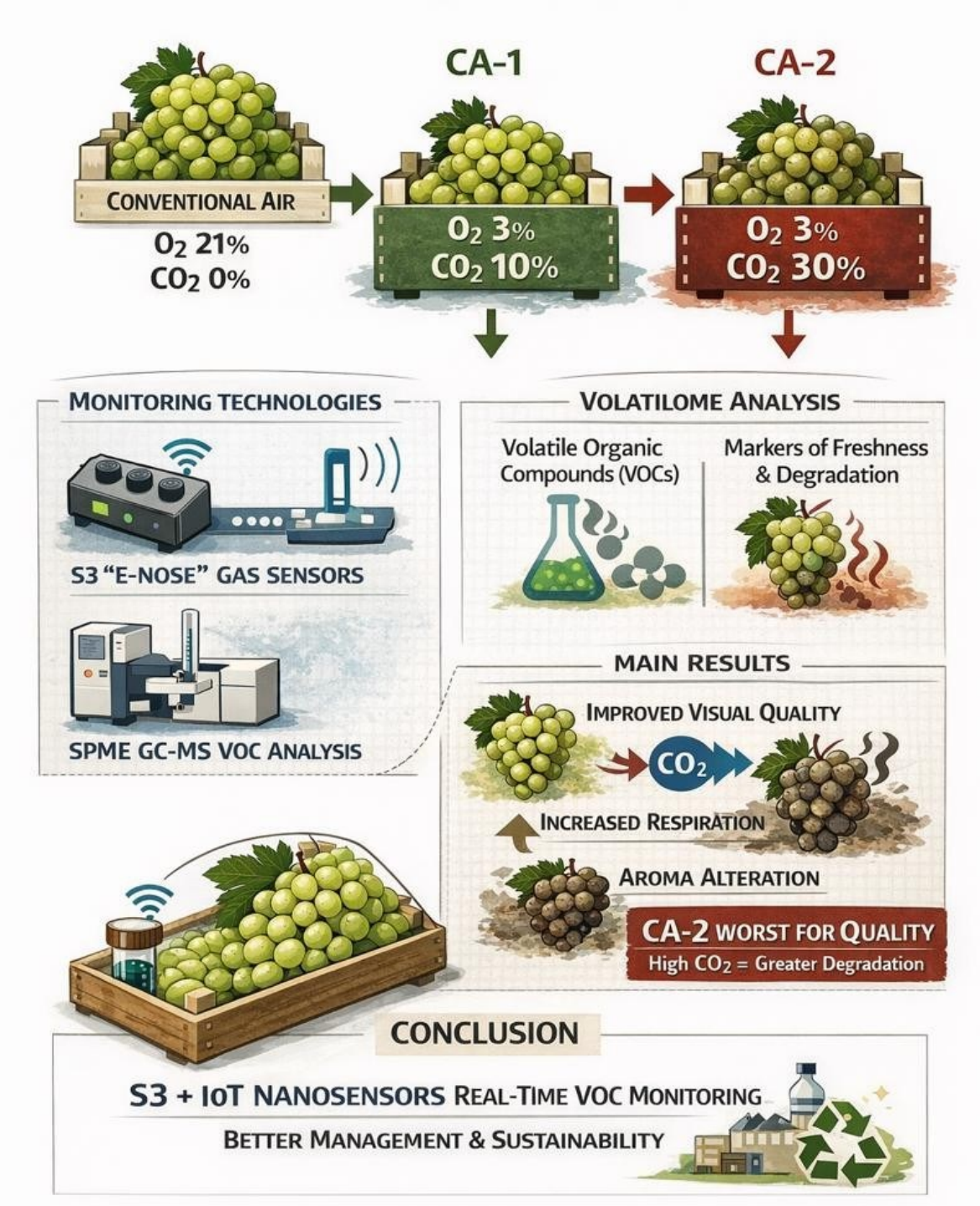

## 3.1 INTRODUCTION

Table grapes (*Vitis vinifera* L.) are among the most widely consumed and appreciated fruits worldwide, owing to their versatility, nutritional benefits, and the broad diversity of varieties and aromas [1]. Traditional preservation through sulphur dioxide fumigation combined with refrigeration helps maintain quality but entails risks for both food safety and the environment [2]. This has stimulated the search for safer alternative solutions [3].

A well-established approach to prolong the postharvest life of table grapes is the use of modified (MA) or controlled atmospheres (CA), which regulate the concentrations of oxygen ($O_2$) and carbon dioxide ($CO_2$). These methods, which reduce $O_2$ levels and/or increase $CO_2$ levels, avoid the use of synthetic chemicals and do not leave toxic residues on the product. Furthermore, thanks to their simplicity and cost-effectiveness, they have been widely adopted at the commercial scale [4].

Maintaining an appropriate $O_2/CO_2$ balance reduces fruit respiration and slows down metabolic processes, while also limiting microbial growth by interfering with cellular metabolism [4]. It is well established that high $CO_2$ concentrations ($\geq$ 15 kPa) delay softening and senescence and help control fungal development during grape storage [5; 6; 7; 8; 9; 10]. However, concentrations above 20 kPa may induce undesirable fermentation and sensory alterations, associated with ethanol and acetaldehyde accumulation [11]. Moreover, suboptimal storage conditions can stimulate the activity of key enzymes such as polyphenol oxidase (PPO) and peroxidase (PDO), responsible for enzymatic browning. Susceptibility to this phenomenon varies according to cultivar: some varieties are more resistant, while others are more prone to accelerated degradation [12].

Since aroma is a key determinant of consumer acceptance, monitoring volatile organic compounds (VOCs) released during storage under modified atmospheres is essential. Changes in VOC profiles, in terms of increases or decreases in emitted molecules, represent reliable indicators of freshness status or the onset of spoilage processes, and are therefore valuable for assessing product quality and shelf life [13; 14; 15].

Traditionally, VOC analysis in fresh fruit has relied on solid-phase microextraction coupled with gas chromatography–mass spectrometry (SPME-GC-MS), a technique that provides detailed molecular identification but is complex, destructive, expensive, and unsuitable for rapid monitoring. In recent years, the development of innovative, miniaturized, and low-cost sensors—particularly metal oxide semiconductor (MOS) sensors—has paved the way for new tools in food quality monitoring. The electronic nose, based on arrays of MOS sensors, enables rapid and non-destructive detection of volatile emissions, providing timely information on product freshness and storage status [16; 17].

In this context, SPME-GC-MS enables a comprehensive chemical characterization of volatile organic compounds (VOCs), while the S3+ device, based on MOS sensors, provides a global and comparative assessment of the volatile profiles of the same samples, allowing their differentiation without the need to identify individual compounds. The system can detect variations in emissions relative to a reference sample, offering an early indication of potential changes in storage conditions.

This study explores the innovative use of the S3+ system for monitoring table grapes during storage and assesses its reliability through parallel analyses using SPME-GC-MS, which serves as a reference method. The latter provided detailed chemical information useful for validating the effectiveness of the S3+ as an early warning tool.

The large-scale implementation of this technology could enable real-time and non-invasive monitoring of grapes throughout storage, representing a rapid, sustainable, and cost-effective alternative to conventional methods. Such an approach would support a more efficient supply chain management, allowing timely interventions in the regulation of storage atmospheres, optimization of market availability for international and off-season distribution, and contributing to waste reduction and lower environmental impact [18].

## 3.2 MATERIALS AND METHODS

### 3.2.1 Plant Material and Storage Conditions

Table grapes (*Vitis vinifera* L., cv. Italia) were provided by a farm located in Foggia (Southern Italy). Vineyards were cultivated under uniform agronomic conditions with standardized practices, and clusters were harvested at full maturity (total soluble solids of approximately 16 °Brix). Immediately after harvest, samples were transported to the postharvest laboratory of the Institute of Sciences of Food Production of the National Research Council (ISPA-CNR).

Clusters were selected for the absence of defects or disease symptoms and then randomly divided into three groups corresponding to different storage treatments. Two controlled atmosphere (CA) mixtures were applied by varying $CO_2$ concentration (10 or 30 kPa) in combination with 3 kPa $O_2$ in nitrogen. The two treatments were designated as:

- CA-1: 3.0/10.0 kPa ($O_2$/$CO_2$)
- CA-2: 3.0/30.0 kPa ($O_2$/$CO_2$)

As a control (Ctrl), samples stored in air were used. All samples were kept at 2 ± 1.0 °C. CA-1 and CA-2 treatments were carried out using Milano 2 equipment, equipped with independent cells (Fruit Control Equipment srl, Locate di Triulzi, Italy).

For each treatment (CA-1, CA-2, and Ctrl), 16 samples were prepared (4 replicates × 4 storage times), each consisting of approximately 1 kg of grapes (3 clusters of 350–400 g) placed in PET trays (model CL1/135, Carton Pack, Rutigliano, Italy).

Analyses were performed at harvest (0 days) and after 10, 20, 30, and 40 days of refrigerated storage. At each sampling time, qualitative parameters, sensory descriptors, and volatile organic compounds (VOCs) were evaluated using SPME-GC-MS and the innovative S3+ device, based on customized IoT nanosensors (Figure 1).

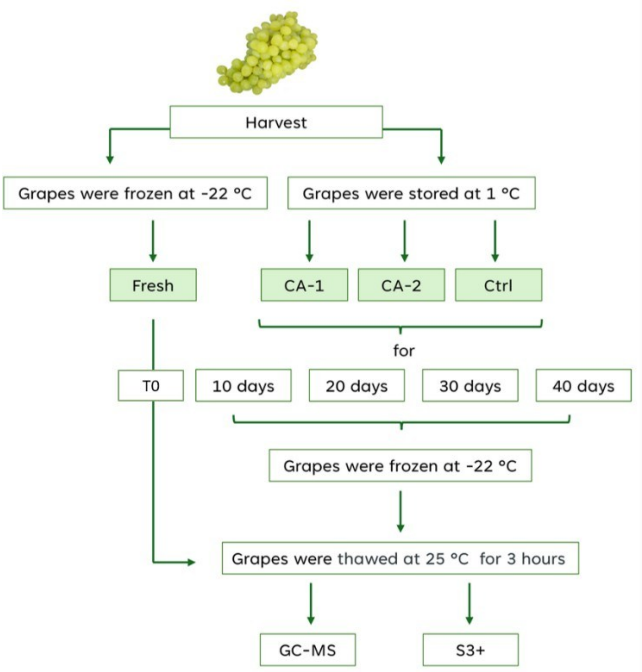


**Figure 1**. Schematic representation of the experimental design for the analysis of volatile organic compounds.

### 3.2.2 Chemicals and Reagents

For enzymatic activity assays, polyvinylpyrrolidone and monosodium phosphate monohydrate were purchased from Sigma Aldrich (Milan, Italy); disodium phosphate heptahydrate and hydrogen peroxide from Honeywell Fluka (New Jersey, USA). Chlorogenic acid was provided by Alfa Aesar Co. Inc., while 2-mercaptoethanol (99% purity) was purchased from Alfa Aesar (New Jersey, USA). Finally, helium, carbon dioxide, and nitrogen (99.99% purity) were supplied by Sapio s.r.l. (Bari, Italy).

### 3.2.3 Quality and Sensory Attributes of Table Grapes Evaluated at Harvest and During Storage

#### 3.2.3.1 Respiration Rate, Sensory Analysis, Relative Water Content, Decay Incidence, and Image Analysis

The respiration rate of table grape clusters was measured at harvest and at each sampling time using a closed system, as reported by Cefola et al. (2018) [19]. For each treatment and replicate (n = 4), approximately 400 g of fruit were removed from CA chambers and held for up to 24 h at 2 °C. Samples were then placed in sealed 3.6 L plastic jars (one per replicate), allowing $CO_2$ accumulation until 0.1 kPa (standard $CO_2$ concentration). The time required to reach this value was determined by measuring $CO_2$ at regular intervals with a gas chromatograph (p200 microGC, Agilent, Santa Clara, CA, USA) equipped with a dual column and thermal conductivity detector [20]. The respiration rate was expressed as mg $CO_2$ $kg^{-1}$ $h^{-1}$.

The relative water content (RWC) of the rachis was measured on fresh and stored samples using rachis portions of approximately 1 cm (total 2.5 g per replicate), cut with a knife [19]. Weights were determined as fresh weight (Fw), after 24 h of rehydration (Rw) in distilled water at room temperature, and after drying (Dw) at 65 °C until constant weight. RWC was calculated as a percentage using the following formula [21]:

$$RWC\ (\%) = (Fw - Dw)/(Rw - Dw) \times 100$$

Sensory analysis of table grapes was carried out by a selected panel of seven assessors (four women and three men), using descriptors reported by Cefola et al. (2018) [19]. Visual quality (VQ) was assessed on fresh and stored clusters using a 5–1 scale (5 = excellent; 4 = good; 3 = acceptable, sensory limit; 2 = poor; 1 = very poor).

For each treatment and sampling day, decay incidence was visually evaluated and assigned a sensory score on a 1–5 scale, where: 1 = no decay; 2 = slight decay, product still marketable, < 2% affected; 3 = moderate decay, product usable but not marketable, < 5% affected; 4 = moderately severe decay, < 15% affected; 5 = severe decay, product not usable [22].

The incidence of mold was calculated according to the formula proposed by Youssef and Roberto (2014) [23]:

$$\text{Mold incidence (\%)} = (\text{Number of decayed clusters} / \text{Total number of clusters}) \times 100$$

Colorimetric parameters of grape clusters were measured through image analysis. The acquisition system included an RGB digital camera AP3200TPGE (JAI Ltd., Yokohama, Japan), with spatial resolution of 3.2 MP at 2 fps and 24-bit/pixel color depth, equipped with a 12 mm focal length F1.8 lens (KOWA Lens mod. LM12NC3 1/2), providing a field of view of 35 × 30 cm. The camera was placed inside a photographic box HPB60D (HAVOX, Vendôme, France), equipped with two LED light sources (60 diodes each). A reference color target (X-Rite ColorChecker Passport, 24 patches) was placed within the camera field of view.

Images were processed with Matlab® R2021b (MathWorks Inc., Natick, MA, USA). Following Gonzalez et al. (2004) [24], raw images were segmented from the background to create binary images, removing unwanted edges and extracting RGB components (red, green, blue). RGB data were then converted into L*, a*, b* color space and used to calculate deltaE, according to Pathare et al. (2013) [25].

### 3.2.3.2 Polyphenol Oxidase (PPO) and Peroxidase (POD)

PPO and POD enzymatic activity was determined following the method described by Palumbo et al. (2024) [26]. Briefly, table grape berries were cut into small pieces, and, for each replicate, 10 g of sample were homogenized for 1 min on ice with 20 mL of chilled phosphate buffer (0.05 M, pH 6.2) containing 30 g $L^{-1}$ polyvinylpyrrolidone (PVPP). The mixture was filtered through two layers of Miracloth and centrifuged at 15,000 × g for 15 min at 4 °C. The supernatant was collected and kept on ice until analysis (within 5 h).

For PPO assay, enzymatic activity was determined using 15 mM chlorogenic acid in 0.05 M potassium phosphate buffer (pH 6.2), monitoring substrate oxidation at 410 nm for 2 min with a spectrophotometer (UV-1800, Shimadzu, Kyoto, Japan). One unit of PPO activity was defined as an absorbance change (Abs) of 0.001 per minute per gram of fresh weight under the described conditions.

POD activity was determined in the supernatant using 15 mM chlorogenic acid as reducing substrate in a reaction mixture containing 0.1 M potassium phosphate buffer (pH 5.0) and 30 mM $H_2O_2$. Chlorogenic acid oxidation was monitored by absorbance increase at 470 nm for 2 min. Similarly, one unit of POD activity was defined as an absorbance change of 0.001 per minute per gram of fresh weight under the specified conditions.

### 3.2.4 Volatile Organic Compounds (VOCs)

Samples were taken from the freezer (−22 °C), and three berries without pedicels (5 g each) were placed in sterile containers at room temperature (25 °C) for 3 h to allow volatile release and equilibration between gas and solid phases. For each sample, duplicate values were obtained in separate containers to ensure statistical validity.

A SPME DVB/CAR/PDMS 50/30 µm fibre (Supelco Co., Bellefonte, PA, USA) was exposed to the headspace at 25 °C for 10 min to adsorb VOCs. Separation of extracted compounds was carried out using a GC 2020 gas chromatograph (Shimadzu, Kyoto, Japan) coupled to an MS-QP2020 mass spectrometer (Shimadzu, Kyoto, Japan). The SPME fiber was thermally desorbed in the GC injector in splitless mode for 6 min at 240 °C. A MEGA-5MS column (25 m × 0.25 mm × 0.25 µm, Agilent Technologies, Santa Clara, CA, USA) was used for separation.

The mass spectrometer operated in EI (Electron Ionization) mode at 70 eV, with ion source maintained at 240 °C. Data acquisition was performed in TIC (Total Ion Current) mode with a scan range of 35–500 m/z and scan time of 0.3 s. Hydrogen (99.99% purity, GENius PF500, FullTech Instruments Srl, Rome, Italy) was used as carrier gas under the following conditions: 35.7 kPa, flow 2.2 mL/min, linear velocity 87.4 cm/s, purge flow 4.0 mL/min. Detector temperature was set at 240 °C.

The GC oven program was as follows: initial temperature 40 °C for 3 min, ramp 4 °C/min to 120 °C, then 7 °C/min to 220 °C, total run 40 min. Peak integration was performed automatically based on peak area, considering at least 70 chromatographic peaks with an integrated signal area ≥ 500 arbitrary units (a.u), corresponding to the summed mass spectral ion intensities. Additional integration parameters included: slope 100/min, peak width 2 s, drift rate 0/min, doubling time 1000 min, without smoothing.

Peak identification was carried out using Nist11, Nist11b, and FFNSC2 libraries, assigning compounds based on semi-quantitative analysis with a similarity index ≥ 90% as the main criterion. Quantification of VOCs was expressed as relative abundance (percentage of GC area) and reported as mean value ± standard deviation (SD).

### 3.2.5 Analysis with MOX Sensors

Following the same procedure as GC-MS analysis, 5 g of table grape berries were thawed at 25 °C for 3 h prior to analysis with the S3+ device. Samples were placed in polypropylene (PP) containers, with two openings in the lid for insertion of suction tubes.

### 3.2.5.1 Calibration of MOX Sensor Arrays

The S3+ system and its sensor arrays used in this study were developed in collaboration with Nano Sensor Systems Srl, a spin-off of the University of Brescia (Italy). The device is equipped with an array of metal oxide (MOX) sensors, fabricated with specialized materials and designed for the recognition of specific target compounds [27].

Calibration of the S3+ MOX sensor array followed a structured procedure to ensure stability, reproducibility, and accuracy in detecting volatile organic compounds (VOCs). Initially, each sensor underwent high-temperature annealing (500–800 °C, for 1–10 h) to stabilize the sensitive layer and remove potential contaminants that could interfere with sensor response. Subsequently, sensors were subjected to an aging period in continuous filtered air flow to reduce baseline resistance variability and ensure stable operating conditions before experimental use [28].

Calibration was performed in a controlled chamber with a gas flow regulation system, allowing exposure of sensors to mixtures of VOCs at known concentrations. Uniform distribution of gaseous compounds across sensors was ensured by a mass flow controller.

The electronic board played a crucial role in the calibration process, regulating sensor operating conditions, monitoring real-time changes in electrical resistance, and controlling temperature settings. Resistance signals were transmitted to a cloud platform for continuous validation of sensor responses [29].

The S3+ device includes a dedicated sensing chamber, a fluid-dynamic system for uniform distribution of volatile compounds, and an electronic control unit. The apparatus housed six custom-designed MOX sensors, based on $SnO_2$, $SnO_2$/Pd, and $SnO_2$/Au, arranged in a steel chamber maintained at 500 °C (Table 1), a condition ensuring high environmental differentiation capability [18].

**Table 1.** Description of the setup for the different sensing elements.

| SENSOR | DOPING | WORKING TEMPERATURE ( °C) |
|---|---|---|
| **MOX sensor** | $SnO_2$ | 500 °C |
| **MOX sensor** | $SnO_2$ + Pd | 500 °C |
| **MOX sensor** | $SnO_2$ + Au | 500 °C |

The chamber dimensions were 11 × 6.5 × 1.3 cm, and the sensors were selected based on their performance. MOX sensors responded to volatile compounds through variations in electrical resistance, which affected conductivity [30].

The fluidic circuit included a pump, connecting tubes, a solenoid valve, and an activated carbon cylinder for air filtration. The solenoid valve regulated the pump flow, with a maximum flow rate of 250 $cm^3$/min (standard).

The electronic board detected resistance variations, controlled sensor temperature—a critical parameter for volatile detection—and transmitted data to the S3+ web application, thereby demonstrating the IoT functionality of the system [31].

#### 3.2.5.2 S3+ Device Setup

The sample was connected to two activated carbon filters: one for air purification in the headspace and the other connected to the S3+ device. Each analysis lasted a total of 13 minutes, divided into three phases: 100 s for sensor stabilization, 200 s for sample measurement, and 500 s for sensor recovery.

For each sample, 10 replicates were performed, analyzing the sensor outputs, in particular electrical resistance, normalized to the initial acquisition value ($R_0$). For each sensor, the difference between the initial resistance value and the minimum value recorded during analysis was calculated. Subsequently, the $R/R_0$ parameter and its standard deviation were determined across the 10 replicates. The data collected from the sensors were transmitted to the Microsoft Azure platform, equipped with two web tools: a management portal and a mixture classification service. Sensor outputs were processed and interpreted through multivariate statistical analysis.

#### 3.2.5.3 Post-run Analysis

Linear Discriminant Analysis (LDA) is a statistical method commonly used in pattern recognition and machine learning to identify a linear combination of variables that optimally discriminates between two or more classes of events [32]. In this study, LDA was applied using MOX sensor data as predictive variables and different gas classes as target variables.

### 3.2.6 Statistical Analysis

To evaluate the effect of storage atmosphere (CA-1, CA-2, and control) and storage time on the measured parameters, data were subjected to two-way analysis of variance (ANOVA); means were

separated using Tukey's test at $P < 0.05$ (5% significance level), employing the StatGraphics Centurion XVI.I software (Stat Point Technologies, Inc., Warrenton, VA, USA).

For each storage time, a one-way ANOVA was also performed to determine the effect of storage conditions on the qualitative characteristics considered.

Finally, a selection of VOCs from stored table grapes, together with respiration rate, visual quality score, and decay incidence, was analyzed through principal component analysis (PCA) to establish relationships among the studied parameters.

## 3.3 RESULTS AND DISCUSSION

### 3.3.1 Qualitative and Sensory Parameters of Table Grapes Stored under Controlled Atmosphere

To better understand the effects of controlled atmosphere (CA) storage on table grapes, several qualitative parameters were evaluated, including visual quality (VQ), enzymatic activity, and respiration rate. Visual quality is a key indicator of freshness and commercial appeal, as external appearance directly influences consumer choice. Enzymatic activity and respiration rate, in turn, reflect the metabolic status of the fruit, determining ripening and decay processes as well as the onset of color alterations.

Controlled atmosphere conditions, characterized by low oxygen levels and high $CO_2$ concentrations (CA-1 or CA-2), contributed to improving the visual quality of grapes by limiting oxidation and berry browning phenomena and reducing mold development.

Specifically, VQ progressively decreased in all samples during storage, but values remained consistently higher in grapes stored under CA-1, followed by CA-2, and lowest in controls (Figure 2A). The VQ scores assigned by the sensory panel were based on the observation of clusters and rachis.

To complement sensory evaluation, a comparative instrumental analysis was performed, based on the measurement of berry browning (color parameter b*) and relative water content (RWC) (Figure 2C–D).

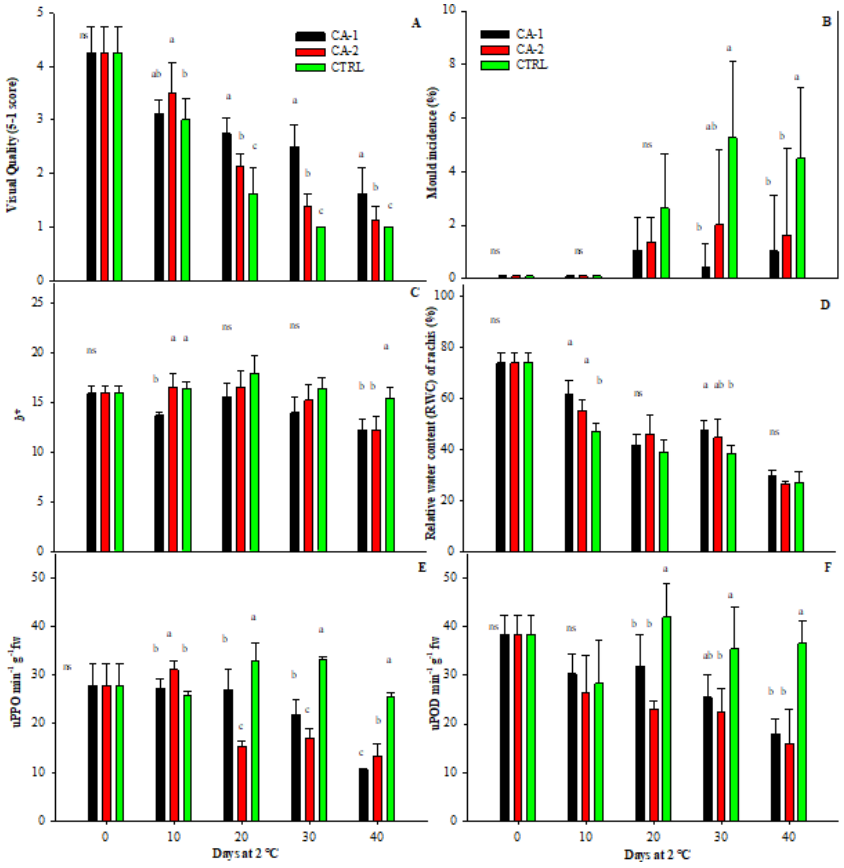


**Figure 2.** Effects of controlled atmosphere storage (CA-1: 3/10 $O_2/CO_2$%, CA-2: 3/30 $O_2/CO_2$%; CTRL: storage in air) on: A) visual quality, B) decay incidence, C) b* value, D) relative water content (RWC) of the rachis, E) PPO activity, and F) POD activity of Vitis vinifera L. cv. Italia table grapes during the storage period. Bars represent standard deviations. Means marked with different letters within the same storage time are significantly different according to Tukey's test ($P \leq 0.05$).

With respect to the b* parameter, significantly higher values were measured at the end of storage in the Ctrl samples compared with those stored under CA, indicating the development of browning in the control berries. This trend was further confirmed by the behavior of PPO and POD, the two main enzymes involved in oxidative processes, which showed higher activity throughout the storage period in Ctrl samples compared with those stored under CA (Figure 2E–F).

During storage, both CA conditions maintained the relative water content (RWC) of the rachis at values like those of fresh grapes (Figure 2D). In contrast, a marked reduction in RWC was observed in the Ctrl samples, in agreement with previous reports [19; 33].

Moreover, the high $CO_2$ concentration in CA conditions delayed mold development compared with Ctrl samples (Figure 2B). These results suggest a positive effect of elevated $CO_2$ in controlling decay, as already documented in the literature [11; 34; 35; 36]. Similarly, Crisosto et al. (2002b) [37]

observed that treatment with 10 kPa $CO_2$ in combination with 3, 6, or 12 kPa $O_2$ in the Red Globe cultivar limited the development of *Botrytis* decay during 12 weeks of cold storage.

On the other hand, although low $O_2$ and high $CO_2$ CA conditions improved the visual appearance of table grapes, a negative effect was observed on respiration rate and volatile profile. While Ctrl samples did not show significant variations during storage, grapes stored under CA-1 and CA-2 exhibited a marked increase in respiration rate, reaching a peak of approximately 6 and 12 mL $CO_2$ $kg^{-1}$ $h^{-1}$, respectively, after 20 days. Subsequently, a decrease in respiration rate was observed in both CA treatments (Figure 3).

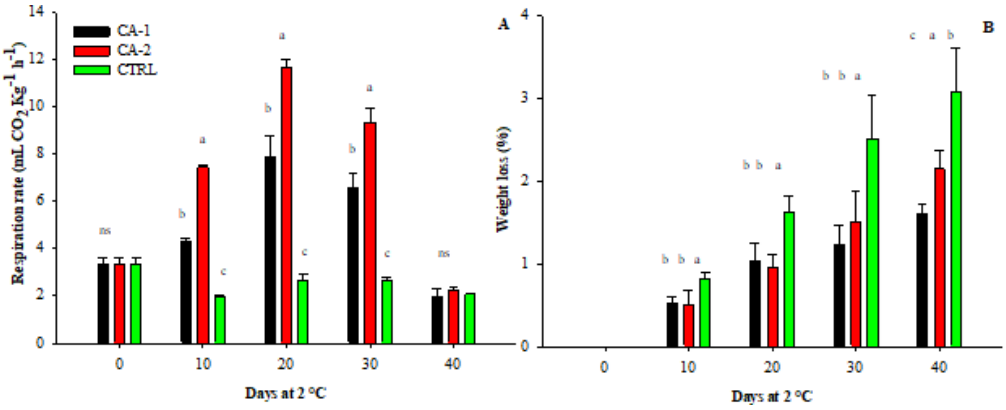


**Figure 3**. Effects of controlled atmosphere storage (CA-1: 3/10 $O_2$/$CO_2$%; CA-2: 3/30 $O_2$/$CO_2$%; CTRL: storage in air) on: A) respiration rate and B) weight loss of *Vitis vinifera* L. cv. Italia table grapes during the storage period. Bars represent standard deviations. Means marked with different letters within the same storage time are significantly different according to Tukey's test ($P \leq 0.05$).

A similar trend was reported by Cefola et al. (2018) [19] in *Italia* table grapes stored under modified atmosphere with high $CO_2$ concentrations (20–30%), a condition that confirmed the stress state induced by the gas. In our case, this effect was already detected with the application of 10% $CO_2$ under low $O_2$ concentrations, under nearly constant gas conditions. The increase in respiration rate indeed represents a physiological response of damaged grapes, leading to the onset of fermentative metabolism with negative repercussions on both sensory and overall product quality [11].

These results confirm that the application of high $CO_2$ concentrations (≥ 10%) under low-oxygen conditions in *Italia* table grapes can cause physiological damage due to $CO_2$-mediated inhibition of several Krebs cycle enzymes, including succinate dehydrogenase. This may result in the activation of anaerobic respiration or the accumulation of succinic acid, potentially toxic to cells [20; 38]. The subsequent in-depth analysis of volatile organic compounds (VOCs) confirmed this hypothesis, as described below. Regarding weight loss (Figure 3B), a significantly higher increase was observed in

Ctrl samples compared with CA-stored grapes, a phenomenon attributable to senescence development in samples stored in air [20].

### 3.3.2 VOCs Detected in Table Grapes Stored under Controlled Atmosphere

The regulation and optimization of $O_2$ and $CO_2$ levels in controlled atmosphere storage allow the preservation of the aromatic profiles of table grapes, maintaining freshness for longer without the use of chemical preservatives. VOCs play a crucial role in defining grape aroma quality.

In our samples subjected to different storage conditions, GC-MS analysis identified 113 volatile compounds, of which 33 metabolites were consistently detected across all samples. These belonged to different chemical classes, including aldehydes, alcohols, alkanes, alkenes, carboxylic acids, ketones, terpenes, and ethers, each contributing specifically to the perceived aroma and sensory profile [39]. Alkanes were the most abundant group, followed by alcohols, in line with the typical volatile composition of grapes [40]. In the *Italia* cultivar, characterized by a neutral aromatic nature, the presence of terpenes was limited, as typically observed in non-muscat compared to aromatic or muscat varieties [41].

In agreement with our findings, some of the same volatile compounds were identified and quantified by Yang et al. (2011) [42] and Kaya et al. (2022) [43] using chemical standards. The most representative compounds were subjected to two-way ANOVA, which showed significant effects of storage conditions (CA-1, CA-2, or control), time, and their interactions on most molecules (including ethanol, hexanal, 1-hexanol, 2,4-dimethyl-1-decene, D-limonene, anethole, 4-methyl-benzaldehyde, 2,6,6-trimethyl-octane, 2-butyl-1-octanol, 2-isopropyl-5-methyl-1-heptanol, 3,8-dimethyl-undecane, pentadecane). However, after 40 days of storage, most compounds did not show significant differences, confirming the variability of volatile profiles over time.

The evolution of VOCs under CA conditions is shown in Figure 4. Some compounds exhibited specific trends: for instance, ethanol markedly increased in CA-2 samples up to 30 days, indicating a higher predisposition to fermentative metabolism; conversely, other compounds (e.g., 2-butyl-1-octanol, 3,8-dimethyl-undecane, 4-methyl-benzaldehyde) maintained relatively stable levels. Other volatiles, such as D-limonene and pentadecane, showed pronounced variations under specific conditions (Ctrl and CA-1, respectively), suggesting differences in metabolic processes or selective volatilization, although not statistically significant due to variability among replicates.

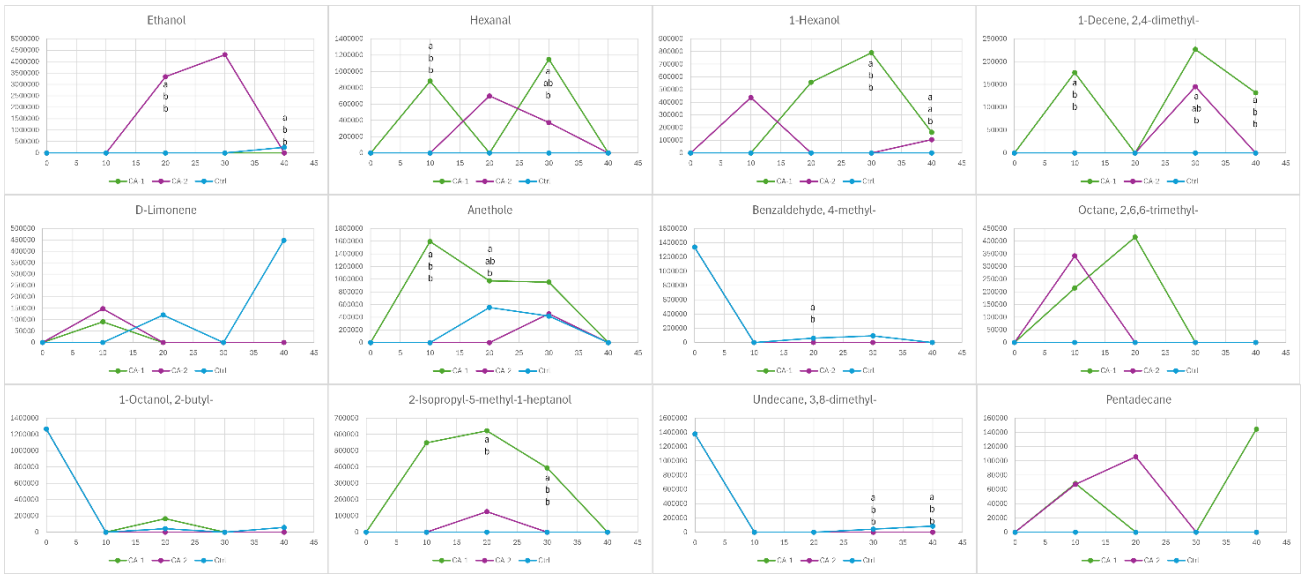


**Figure 4.** Trends of positive and negative markers in table grapes stored under different atmospheric conditions: CA-1 (3% $O_2$ – 10% $CO_2$); CA (3% $O_2$ – 30% $CO_2$), CTRL (20% $O_2$ – 0% $CO_2$).

The concentration of hexanal, 1-hexanol, 2,4-dimethyl-1-decene, anethole, and 2-isopropyl-5-methyl-1-heptanol was generally higher in CA-1 samples, with fluctuating trends attributable to differences among replicates. Overall, comparison of volatile profiles suggests that the CA-2 condition was the least favorable, showing the greatest presence of senescence and fermentation markers (particularly ethanol), followed by the control, whereas CA-1 ensured the best preservation by reducing degradation and maintaining greater stability of volatile compounds.

### 3.3.3 Relationship between VOCs and Qualitative Parameters

Datasets comprising a representative selection of VOCs, respiration rate, and two sensory parameters (visual quality score and mold incidence) were collected at harvest and after 10, 20, 30, and 40 days of cold storage, both in air and under the two controlled atmosphere conditions and were subjected to principal component analysis (PCA).

Application of PCA to the final dataset explained 65.3% of the total variance, with the first three components (PC1, PC2, PC3) accounting for 31.4%, 21%, and 13%, respectively. The score plot of the first three components (Figure 5) clearly discriminated between fresh samples at harvest and those stored in air (Ctrl), CA-1, and CA-2. The plot highlighted the impact of different treatments on VOC evolution during storage, showing how the applied gas mixture influenced product quality.

The sample distribution indicated:

- Ctrl samples clustered on the left side of the plot;

- CA-1 and CA-2 samples separated into distinct clusters, with subgroups according to storage time (e.g., CA-1_10, CA-2_30);
- Fresh samples (FRESH) positioned as outliers compared to the others.

CA-1 and CA-2 samples were more closely associated with VOCs such as hexanal and ethanol, whereas Ctrl samples showed lower values for these volatiles.

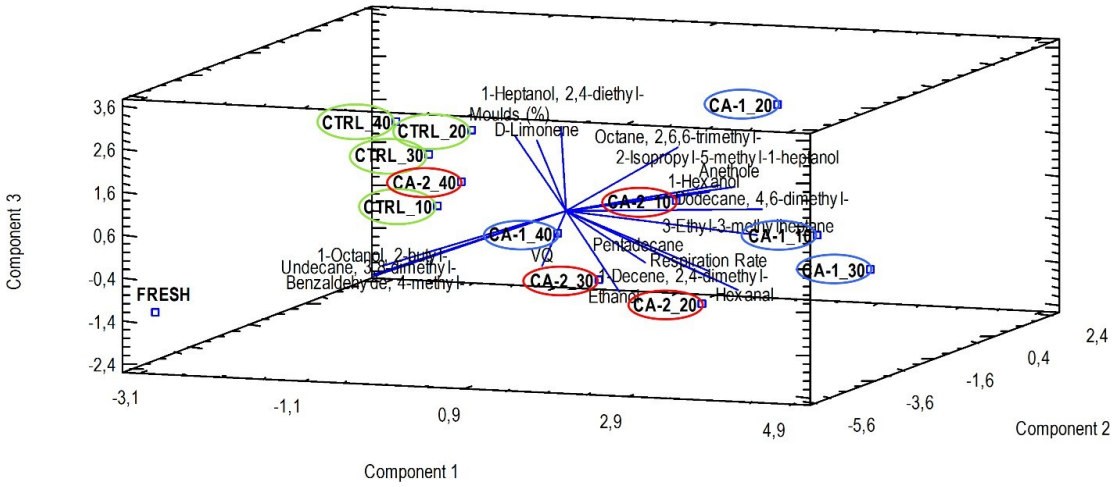


**Figure 5.** PCA plots of table grapes analyzed at harvest (Fresh, 0 d) and after 10, 20, 30, and 40 days of storage at 5 °C in: air (control, CTRL_10, CTRL_20, CTRL_30, CTRL_40), controlled atmosphere with 3% $O_2$ / 10% $CO_2$ (CA-1_10, CA-1_20, CA-1_30, CA-1_40), and controlled atmosphere with 3% $O_2$ / 30% $CO_2$ (CA-2_10, CA-2_20, CA-2_30, CA-2_40).

The plot suggests differences in physiological responses and VOC composition among treatments during storage, with CA-stored grapes showing more pronounced metabolic changes. Grapes stored in air (Ctrl) were positively correlated with mold incidence as a physical parameter, highlighting the positive effect of CA in delaying the onset of decay. Consequently, visual quality (VQ) was positioned opposite to mold percentage, instead showing a positive correlation with CA-stored samples (both conditions).

Although the cold chain slows down metabolic processes, including respiration rate and enzymatic reactions, grapes continue to respire and gradually ripen, leading to senescence and deterioration. Specifically, respiration rate, ethanol, pentadecane, and 2,4-dimethyl-1-decene were correlated with CA-2 samples, confirming the development of fermentative metabolism under stressful storage conditions. Ethanol, produced through alcoholic fermentation of sugars by yeasts, is a clear indicator of ongoing fermentative or degradative processes. Ethanol and 1-hexanol are indeed characteristic compounds of grapes stored under high $CO_2$ concentrations [44]. An increase in ethanol has also been

reported during the storage of apples and strawberries in $CO_2$-rich atmospheres, following the activation of fermentative metabolism [19].

Phenylpropenes, such as anethole, are compounds found in fresh fruits including apples, strawberries, and grapes [45]. For table grape storage, anethole was found to be predominantly correlated with CA-1 samples. This compound is typically present during fruit ripening and reaches its maximum concentration at full maturity.

Therefore, selected volatile compounds can serve as alternative indicators to assess table grape quality. Some volatile metabolites, such as ethanol and 1-hexanol, may act as markers of suboptimal storage conditions (e.g., high $CO_2$ concentrations). Conversely, hexanal and anethole may represent potential freshness markers for *Italia* table grapes. Hexanal, in particular, is associated with herbaceous characteristics typical of many table grape cultivars and is considered a freshness indicator for cv. Italia, as it is one of the main contributors to the characteristic berry flavour and varies according to the ripening process [19].

### 3.3.4 Application of Customized IoT Nanosensors for Estimating Table Grape Quality

To further investigate the impact of controlled atmosphere (CA) storage on table grape quality, an innovative IoT system based on nanosensors was employed to monitor the volatilome, providing valuable insights into the chemical changes occurring during storage.

In Figure 6, the x-axis represents time (minutes), while the y-axis shows normalized resistance. The use of normalized parameters allows the analysis of a dimensionless dataset, characterized by a mean value equal to 0 and standardized variability of 1. This approach is particularly useful for comparing samples expressed in different units or scales, which would otherwise make the analysis less accurate [46].

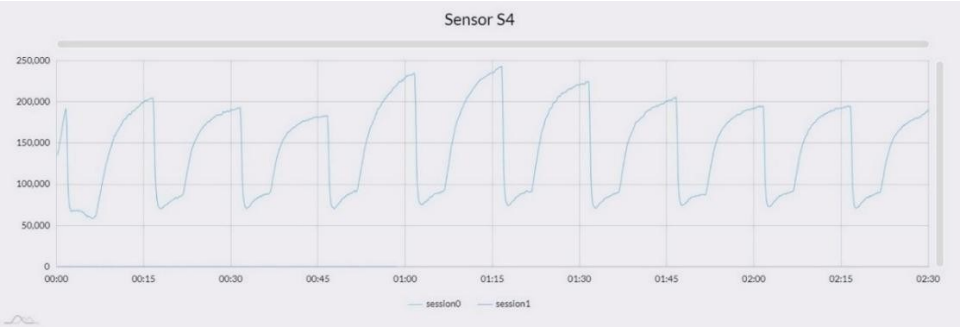


**Figure 6.** Graphical representation of the output from a single sensor, where the y-axis reports resistance (Ω) and the x-axis time (s).

The graph clearly shows how resistance starts at a high value and subsequently decreases. Sample analysis was divided into two phases. The first, dedicated to volatilome assessment, consisted of the contact between emitted volatile substances and the sensor, which caused a reduction in electrical resistance. The second phase, called recovery, involved the injection of filtered ambient air to return the sensor to its baseline value, reflecting its electrical resistance under standardized environmental conditions (humidity, temperature, and oxygen) [47].

In this study, the process included an initial stabilization phase of 100 s, followed by 200 s of sample analysis and 500 s of recovery, for a total duration of 13 minutes per analysis. Each sample was subjected to 10 replicates, for an overall analysis time of approximately 4 hours.

The quality and consumer acceptability of table grapes depend on several parameters, including aesthetic and aromatic aspects. The volatilome comprises the full set of volatile metabolites, as well as other volatile organic and inorganic compounds, originating from an organism, a super-organism, or an ecosystem. Although often considered a subset of the metabolome, the volatilome also includes exogenous compounds not generated by metabolic processes, such as environmental pollutants, thereby constituting a distinct entity.

In the specific case of grapes, the volatilome consists of several hundred VOCs with varying volatility and polarity, which may originate from raw materials or form during storage. The analysis performed with the S3+ device provided useful data to discriminate groups of samples stored under different conditions, based on the VOCs produced. During storage, chemical processes occurred that led to the release of VOCs, detected by the sensor array used in this trial. From a practical perspective, the results indicate that characterization of the grape volatilome requires at least three sensors with complementary sensitivities, capable of providing a reliable and discriminant analysis of volatile profiles.

To support the data obtained with GC-MS, a Linear Discriminant Analysis (LDA) was performed on the data collected with the S3+ system. The analysis (Figure 7) clearly shows that the red cluster, corresponding to fresh samples, is distinctly separated from all others. In the factorial plane, fresh samples were located near the CTRL and CA-1 samples, which were positioned very close to each other. This proximity suggests that grapes stored in air and in CA-1 shared a similar volatile composition, despite the different storage conditions. In contrast, CA-2 samples were significantly distant from both fresh samples and those stored in air or CA-1. This indicates that CA-2 was the least favorable condition among those tested, as it generated the greatest deviation from the profile of fresh grapes.

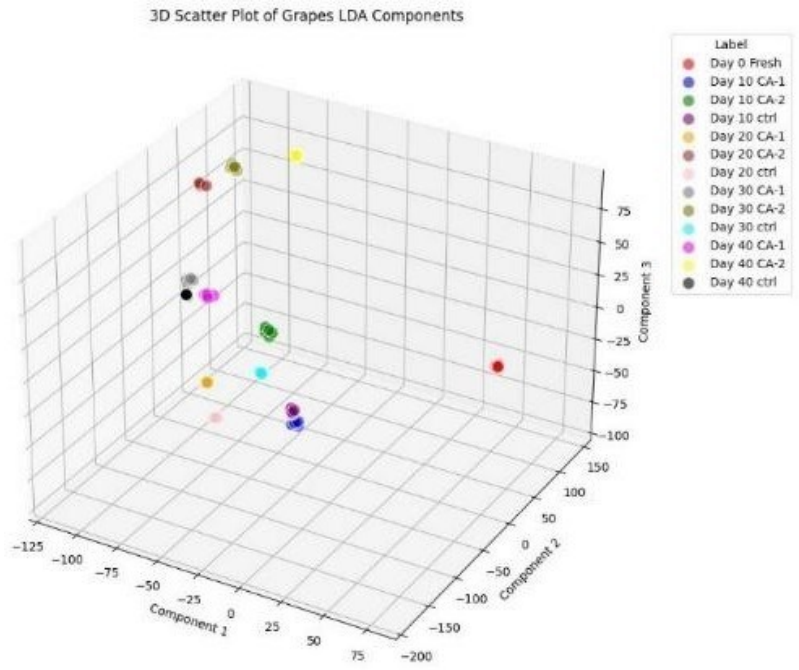


**Figure 7.** 3D representation by LDA of table grape samples stored under different conditions: controlled atmospheres (CA-1 and CA-2) and air (CTRL) at different storage intervals (10, 20, 30, and 40 days), including fresh samples for comparison.

The three MOX sensors in the S3+ device were neither analyzed individually nor averaged; instead, their combined signals were processed using a multivariate statistical approach to enhance pattern recognition capability. Each sensor exhibits different sensitivities to specific volatile organic compounds, thereby enabling a more comprehensive characterization of the grape volatilome.

Linear Discriminant Analysis (LDA) was applied to classify storage conditions by integrating the unique contributions of each sensor. Sensor responses were normalized to baseline resistance ($R/R_0$) and subsequently incorporated into the LDA model. This approach enabled the detection of subtle variations in VOC composition that individual sensors, when considered separately, would not have captured.

The LDA plot revealed a clear clustering of samples based on the combined sensor responses, allowing discrimination of both storage conditions and storage times. This method increased classification robustness, ensuring that no critical information was lost. The results demonstrate that the S3+ device can effectively detect variations in volatile profiles over time, distinguishing, for example, between grapes stored for 10 and 40 days. This ability to monitor storage duration underscores the effectiveness of the sensor array in evaluating postharvest quality and providing real-time information for controlled atmosphere storage management.

These findings are consistent with GC-MS results: the sum of the mean percentages of senescence- and fermentation-related molecules confirms that CA-2 (3/30 kPa $O_2/CO_2$) was the least favorable condition.

## 3.4 CONCLUSIONS

This study demonstrates that controlled atmospheres with high $CO_2$ concentrations and low $O_2$ levels improve the visual quality of table grapes and reduce mold development by preventing oxidative phenomena. However, such conditions also lead to an increased respiration rate and the production of undesirable volatile compounds, with negative consequences for freshness and aroma over time.

Statistical analysis revealed significant effects of storage conditions and time on volatile compounds, but most did not show significant differences after 40 days, indicating a certain instability of volatile profiles. Some markers, such as anethole and hexanal, were associated with CA-1 (3% $O_2$ / 10% $CO_2$) and may therefore be considered freshness indicators. Conversely, ethanol and other fermentation-related VOCs were associated with CA-2 (30% $CO_2$), identified as the least favorable condition.

Further studies are needed to optimize the $CO_2/O_2$ balance to improve storage strategies. The S3+ electronic nose confirmed the results obtained by GC-MS, proving to be an effective tool for grape quality monitoring, offering a non-destructive, rapid, and cost-effective method to prolong freshness, reduce waste, and enhance supply chain sustainability.

Large-scale application of these sensors throughout the distribution chain—from producers to consumers, including transport, international trade, and long-term storage for off-season demand—could help improve the final product quality. However, sensor calibration must be tailored to different cultivars and storage conditions, as a single universal model cannot be applied to all situations.

## 3.5 BIBLIOGRAPHY


1. Zhou, D.D.; Li, J.; Xiong, R.G.; Saimaiti, A.; Huang, S.Y.; Wu, S.X.; Yang, Z.J.; Shang, A.; Zhao, C.N.; Gan, R.Y.; Li, H.B. Bioactive Compounds, Health Benefits, and Food Applications of Grape. Foods 2022, 11(18), 2755. https://doi.org/10.3390/foods11182755
2. Suh, J.H.; Kim, H.J. Risk Assessment of Sulfur Dioxide Residue in Fruits and Vegetables: A Review. Food Control 2020, 113, 107170. https://doi.org/10.1016/j.foodcont.2020.107170
3. Soldateli, F.J.; Both, V.; Wendt, L.M.; Berghetti, M.R.P.; Batista, C.B.; Thewes, F.R.; Brackmann, A. Alternatives to $SO_2$ to Maintain Phenolic Compounds and Overall Quality of Ready-to-Eat Table Grapes during Long-Term Storage. N. Z. J. Crop Hortic. Sci. 2023, 1–21. https://doi.org/10.1080/01140671.2023.2221033

4. Palacios, I.; Moro, C.; Lozano, M.; D'Arrigo, M.; Guillamón, E.; García-Lafuente, A.; Villares, A. Use of Modified Atmosphere Packaging to Preserve Mushroom Quality during Storage. Recent Pat. Food Nutr. Agric. 2011, 3(3), 196–203. https://doi.org/10.2174/2212798411103030196
5. Maoz, I.; De Rosso, M.; Kaplunov, T.; Dalla Vedova, A.; Sela, N.; Flamini, R.; Lewinsohn, E.; Lichter, A. Metabolomic and Transcriptomic Changes Underlying Cold and Anaerobic Stresses after Storage of Table Grapes. Sci. Rep. 2019, 9, 2917. https://doi.org/10.1038/s41598-019-39253-8
6. Shahkoomahally, S.; Sarkhosh, A.; Richmond-Cosie, L.M.; Brecht, J.K. Physiological Responses and Quality Attributes of Muscadine Grape (Vitis rotundifolia Michx) to $CO_2$-Enriched Atmosphere Storage. Postharvest Biol. Technol. 2021, 173, 111428. https://doi.org/10.1016/j.postharvbio.2020.111428
7. Sanchez-Ballesta, M.T.; Alvarez, I.; Escribano, M.I.; Merodio, C.; Romero, I. Effect of High $CO_2$ Levels and Low Temperature on Stilbene Biosynthesis Pathway Gene Expression and Stilbenes Production in White, Red, and Black Table Grape Cultivars during Postharvest Storage. Plant Physiol. Biochem. 2020, 151, 334–341. https://doi.org/10.1016/j.plaphy.2020.03.049
8. Artés-Hernández, F.; Aguayo, E.; Artés, F. Alternative Atmosphere Treatments for Keeping Quality of 'Autumn Seedless' Table Grape during Long Term Cold Storage. Postharvest Biol. Technol. 2004, 31, 59–67. https://doi.org/10.1016/S0925-5214(03)00116-9
9. Crisosto, C.H.; Garner, D.; Crisosto, G. High Carbon Dioxide Atmospheres Affect Stored 'Thompson Seedless' Table Grapes. HortScience 2002, 37, 1074–1078. https://doi.org/10.21273/HORTSCI.37.7.1074
10. Soldateli, F.J.; Both, V.; Thewes, F.R.; Wendt, L.M.; Ludwig, V.; Rossato, F.P.; Thewes, F.R.; Batista, C.B.; Brackmann, A.; Wagner, R. Overall Quality, Phenolic Compounds, and Volatile Profile of 'BRS Isis' Seedless Table Grapes after Long-Term Storage: Effect of Ethanol and High $CO_2$. Sci. Hortic. 2023, 312, 111862. https://doi.org/10.1016/j.scienta.2023.111862
11. Cefola, M.; Pace, B. High $CO_2$-Modified Atmosphere to Preserve Sensory and Nutritional Quality of Organic Table Grape (cv. 'Italia') during Storage and Shelf-Life. Eur. J. Hortic. Sci. 2016, 81, 197–203. https://doi.org/10.17660/eJHS.2016/81.4.2
12. Sangeetha, S.; Sarada, D.V.L. Phenyl Derivative of Pyranocoumarin Precludes Fusarium oxysporum f.sp. lycopersici Infection in Lycopersicon esculentum via Induction of Enzymes

of the Phenylpropanoid Pathway. Appl. Biochem. Biotechnol. 2015, 175, 1168–1180. https://doi.org/10.1007/s12010-014-1285-4

13. Tiwari, S.; Kate, A.; Mohapatra, D.; Tripathi, M.K.; Ray, H.; Akuli, A.; Ghosh, A.; Modhera, B. Volatile Organic Compounds (VOCs): Biomarkers for Quality Management of Horticultural Commodities during Storage through E-Sensing. Trends Food Sci. Technol. 2020, 106, 417–433. https://doi.org/10.1016/j.tifs.2020.10.002
14. Mohapatra, D.; Kate, A.; Tiwari, S.; Tripathi, M.K.; Ray, H.; Akuli, A.; Ghosh, A.; Modhera, B. Volatile Organic Compounds (VOCs): Biomarkers for Quality Management of Horticultural Commodities during Storage through E-Sensing. Trends Food Sci. Technol. 2020, 106, 417–433. https://doi.org/10.1016/j.tifs.2020.10.002
15. Taiti, C.; Costa, C.; Menesatti, P.; et al. Use of Volatile Organic Compounds and Physicochemical Parameters for Monitoring the Post-Harvest Ripening of Imported Tropical Fruits. Eur. Food Res. Technol. 2015, 241, 91–102. https://doi.org/10.1007/s00217-015-2438-6
16. Galstyan, V.; Ponzoni, A.; Kholmanov, I.; Natile, M.M.; Comini, E.; Nematov, S.; Sberveglieri, G. [Article Title Missing in Source]. ACS Appl. Nano Mater. 2018, 1(12), 7098–7105. https://doi.org/10.1021/acsanm.8b01924
17. Di Stefano, V.; Avellone, G.; Bongiorno, D.; Cunsolo, V.; Muccilli, V.; Sforza, S.; Dossena, A.; Drahos, L.; Vékey, K. Applications of HPLC–MS for Food Analysis. J. Chromatogr. A 2012, 1259, 74–85. https://doi.org/10.1016/j.chroma.2012.04.023
18. Poeta, E.; Liboà, A.; Mistrali, S.; Núñez-Carmona, E.; Sberveglieri, V. Nanotechnology and E-Sensing for Food Chain Quality and Safety. Sensors 2023, 23, 8429. https://doi.org/10.3390/s23208429
19. Cefola, M.; Damascelli, A.; Lippolis, V.; Cervellieri, S.; Linsalata, V.; Logrieco, A.F.; Pace, B. Relationships among Volatile Metabolites, Quality and Sensory Parameters of 'Italia' Table Grapes Assessed during Cold Storage in Low or High $CO_2$ Modified Atmospheres. Postharvest Biol. Technol. 2018, 142, 124–134. https://doi.org/10.1016/j.postharvbio.2017.09.002
20. Kader, A.A. Postharvest Technology of Horticultural Crops, 3rd ed.; UC Publication 3311, University of California, Agriculture and Natural Resources, 2002.
21. Sanchez-Ballesta, M.T.; Jiménez, J.B.; Romero, I.; Orea, J.M.; Maldonado, R.; Ureña, Á.G.; Escribano, M.I.; Merodio, C. Effect of High $CO_2$ Pretreatment on Quality, Fungal Decay, and Molecular Regulation of Stilbene Phytoalexin Biosynthesis in Stored Table Grapes.

Postharvest Biol. Technol. 2006, 42(3), 209–216. https://doi.org/10.1016/j.postharvbio.2006.07.002

22. Cefola, M.; Pace, B.; Buttaro, D.; Santamaria, P.; Serio, F. Postharvest Evaluation of Soilless-Grown Table Grape during Storage in Modified Atmosphere. J. Sci. Food Agric. 2011, 91, 2153–2159. https://doi.org/10.1002/jsfa.4432
23. Youssef, K.; Roberto, S.R. Salt Strategies to Control Botrytis Mold of 'Benitaka' Table Grapes and to Maintain Fruit Quality during Storage. Postharvest Biol. Technol. 2014, 95, 95–102. https://doi.org/10.1016/j.postharvbio.2014.04.009
24. Gonzalez, R.C.; Woods, R.E.; Eddins, S.L. Digital Image Processing Using MATLAB; Pearson Prentice Hall, 2004. https://doi.org/10.1201/9781351228374
25. Pathare, P.B.; Opara, U.L.; Al-Said, F.A.J. Colour Measurement and Analysis in Fresh and Processed Foods: A Review. Food Bioprocess Technol. 2013, 6, 36–60. https://doi.org/10.1007/s11947-012-0867-9
26. Palumbo, M.; Cefola, M.; Pace, B.; Ricci, I.; Siano, F.; Amato, G.; Stocchero, M.; Cozzolino, R. Volatile Metabolites to Assess the Onset of Chilling Injury in Fresh-Cut Nectarines. Foods 2024, 13(7), 1047. https://doi.org/10.3390/foods13071047
27. Shunping, Z.; Changsheng, X.; Huayao, L.; Zikui, B.; Xianping, X.; Dawen, Z. A Reaction Model of Metal Oxide Gas Sensors and a Recognition Method by Pattern Matching. Sens. Actuators B Chem. 2009, 135, 552–559. https://doi.org/10.1016/j.snb.2008.10.021
28. Cai, G.; Man, K.; Zhang, X.; Wenjun, C.; Shaoming, W.; Jiandong, Y.; Hongwei, Z. Survey Network Design of Synchrotron in Heavy Ion Medical Machine in Lanzhou. High Power Laser Part. Beams 2014, 26, 015104. https://doi.org/10.3788/HPLPB201426.015104
29. Genzardi, D.; Núñez-Carmona, E.; Poeta, E.; Gai, F.; Caruso, I.; Fiorilla, E.; Schiavone, A.; Sberveglieri, V. Unraveling the Chicken Meat Volatilome with Nanostructured Sensors: Impact of Live and Dehydrated Insect Larvae Feeding. Sensors 2024, 24(15), 4921. https://doi.org/10.3390/s24154921
30. Genzardi, D.; Greco, G.; Núñez-Carmona, E.; Sberveglieri, V. Real Time Monitoring of Wine Vinegar Supply Chain through MOX Sensors. Sensors 2022, 22(16), 6247. https://doi.org/10.3390/s22166247
31. Masson, N.; Piedrahita, R.; Hannigan, M. Approach for Quantification of Metal Oxide Type Semiconductor Gas Sensors Used for Ambient Air Quality Monitoring. Sens. Actuators B Chem. 2015, 208, 339–345. https://doi.org/10.1016/j.snb.2014.11.032

32. Xanthopoulos, P.; Pardalos, P.M.; Trafalis, T.B. Linear Discriminant Analysis. In Robust Data Mining; SpringerBriefs in Optimization; Springer: New York, NY, USA, 2013; pp. 27–33. https://doi.org/10.1007/978-1-4419-9878-1_4
33. Rosales, R.; Fernandez-Caballero, C.; Romero, I.; Escribano, M.I.; Merodio, C.; Sanchez-Ballesta, M.T. Molecular Analysis of the Improvement in Rachis Quality by High $CO_2$ Levels in Table Grapes Stored at Low Temperature. Postharvest Biol. Technol. 2013, 77, 50–58. https://doi.org/10.1016/j.postharvbio.2012.10.009
34. Valero, D.; Valverde, J.M.; Martínez-Romero, D.; Guillén, F.; Castillo, S.; Serrano, M. The Combination of Modified Atmosphere Packaging with Eugenol or Thymol to Maintain Quality, Safety, and Functional Properties of Table Grapes. Postharvest Biol. Technol. 2006, 41(3), 317–327. https://doi.org/10.1016/j.postharvbio.2006.04.011
35. Teles, C.S.; Benedetti, B.C.; Gubler, W.D.; Crisosto, C.H. Prestorage Application of High Carbon Dioxide Combined with Controlled Atmosphere Storage as a Dual Approach to Control Botrytis cinerea in Organic 'Flame Seedless' and 'Crimson Seedless' Table Grapes. Postharvest Biol. Technol. 2014, 89, 32–39. https://doi.org/10.1016/j.postharvbio.2013.11.001
36. Liu, Y.-B. Controlled Atmosphere Treatment for Control of Grape Mealybug, Pseudococcus maritimus (Ehrhorn) (Hemiptera: Pseudococcidae), on Harvested Table Grapes. Postharvest Biol. Technol. 2013, 86, 113–117. https://doi.org/10.1016/j.postharvbio.2013.06.025
37. Crisosto, C.H.; Garner, D.; Crisosto, G. Carbon Dioxide-Enriched Atmospheres during Cold Storage Limit Losses from Botrytis but Accelerate Rachis Browning of 'Red Globe' Table Grapes. Postharvest Biol. Technol. 2002b, 26, 181–189. https://doi.org/10.1016/S0925-5214(02)00013-3
38. Kays, S.J. Postharvest Physiology and Handling of Perishable Plant Products, 1st ed.; Van Nostrand Reinhold: New York, NY, USA, 1991.
39. Garrido, J.; Borges, F. Wine and Grape Polyphenols—A Chemical Perspective. Food Res. Int. 2013, 54(2), 1844–1858. https://doi.org/10.1016/j.foodres.2013.08.002
40. González-Barreiro, C.; Rial-Otero, R.; Cancho-Grande, B.; Simal-Gándara, J. Wine Aroma Compounds in Grapes: A Critical Review. Crit. Rev. Food Sci. Nutr. 2015, 55(2), 202–218. https://doi.org/10.1080/10408398.2011.650336
41. Wu, Y.; Zhang, W.; Song, S.; Xu, W.; Zhang, C.; Ma, C.; Wang, L.; Wang, S. Evolution of Volatile Compounds during the Development of Muscat Grape 'Shine Muscat' (Vitis labrusca × V. vinifera). Food Chem. 2020, 309, 125778. https://doi.org/10.1016/j.foodchem.2019.125778

42. Yang, C.; Wang, Y.; Wu, B.; Fang, J.; Li, S. Volatile Compounds Evolution of Three Table Grapes with Different Flavour during and after Maturation. Food Chem. 2011, 128(4), 823–830. https://doi.org/10.1016/j.foodchem.2010.11.029
43. Kaya, O.; Incesu, M.; Ates, F.; Keskin, N.; Verdugo-Vásquez, N.; Gutiérrez-Gamboa, G. Study of Volatile Organic Compounds of Two Table Grapes (cv. Italia and Bronx Seedless) along Ripening in Vines Established in the Aegean Region (Turkey). Plants 2022, 11, 1935. https://doi.org/10.3390/plants11151935
44. Piazzolla, F.; Pati, S.; Amodio, M.L.; Colelli, G. Effect of Harvest Time on Table Grape Quality during On-Vine Storage. J. Sci. Food Agric. 2016, 96, 131–139. https://doi.org/10.1002/jsfa.7072
45. Atkinson, R.G. Phenylpropenes: Occurrence, Distribution, and Biosynthesis in Fruit. J. Agric. Food Chem. 2018, 66, 2259–2272. https://doi.org/10.1021/acs.jafc.6b04696
46. Greco, G.; Carmona, E.N.; Sberveglieri, G.; Genzardi, D.; Sberveglieri, V. A New Kind of Chemical Nanosensors for Discrimination of Espresso Coffee. Chemosensors 2022, 10(5), 186. https://doi.org/10.3390/chemosensors10050186
47. Wei, X.; Huang, Z.; Zhang, X.; Li, Q.; Lu, Z.; Shi, J.; Xu, Z. Monitoring the Microbial Community during Solid-State Acetic Acid Fermentation of Zhenjiang Aromatic Vinegar. Food Microbiol. 2011, 28(6), 1175–1181. https://doi.org/10.1016/j.fm.2011.03.011

# 4.

# UNRAVELING THE CHICKEN MEAT VOLATILOME WITH NANOSTRUCTURED SENSORS: IMPACT OF LIVE AND DEHYDRATED INSECT LARVAE FEEDING

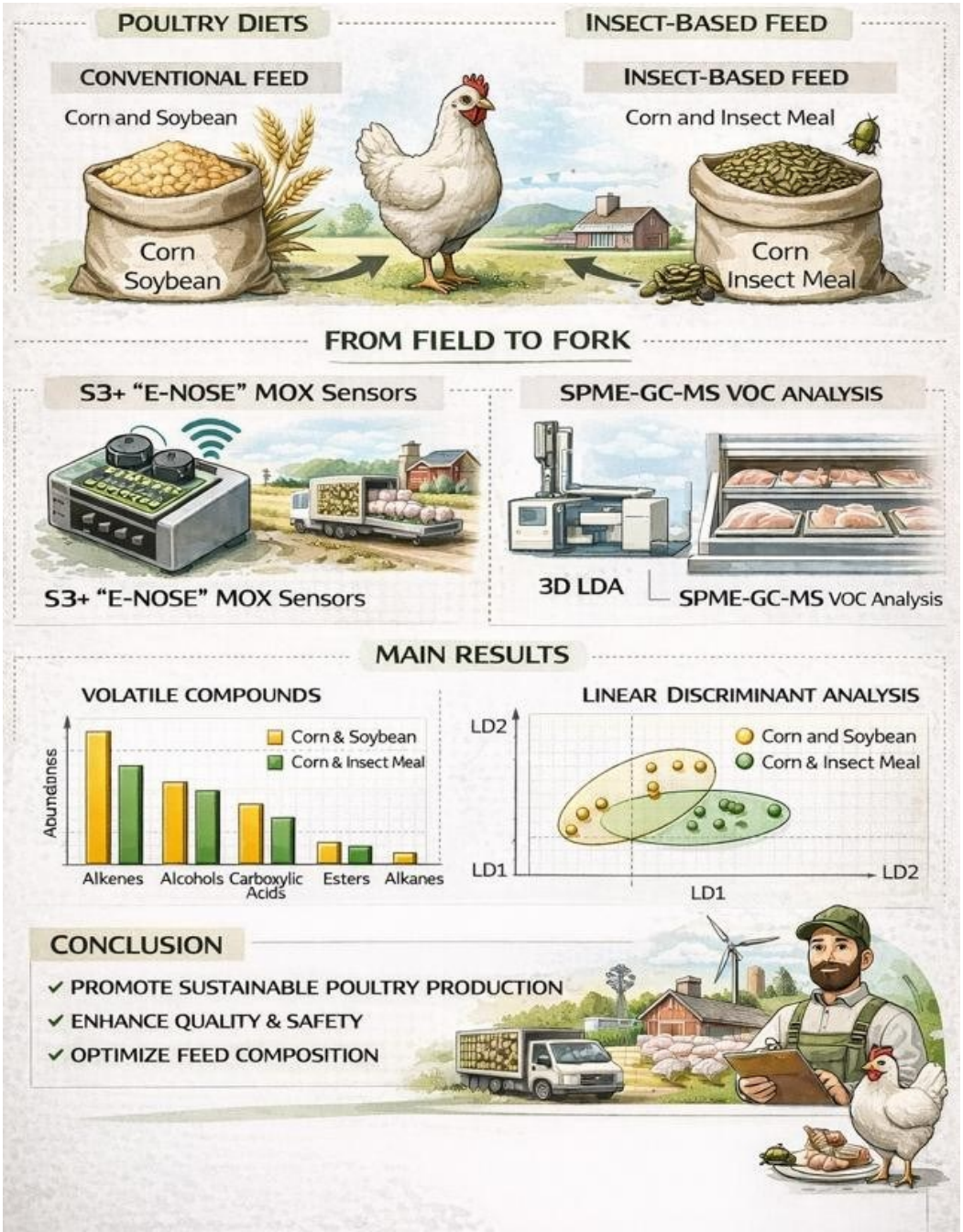

## 4.1 INTRODUCTION

Population growth, urbanization, and the expansion of the middle class have driven a significant increase in global food demand, especially for animal protein sources. In Europe, as in many other regions of the world, poultry meat consumption constitutes a substantial share of dietary protein intake and is deeply rooted in culinary traditions. Traditional production of protein-rich ingredients for animal feed, such as fishmeal, soy, and cereals, now requires further intensification in resource-use efficiency and integration with alternative sources [1; 2]. By 2030, it will be necessary to feed more than 9 billion people [3], in addition to the billions of animals reared annually for food or recreational purposes. At the same time, issues such as water and soil pollution from intensive livestock farming and deforestation driven by overgrazing contribute decisively to climate change and other negative environmental impacts.

In recent years, the link between agricultural practices, animal health, human health, and the environment has been more clearly recognized and formalized within the "One Health" paradigm, which encourages integrated solutions to contemporary challenges [4]. Within this framework, insect farming emerges as a tangible opportunity for addressing food security and protein availability issues. Insects are highly nutritious—rich in protein, lipids, and minerals—they can be reared on food waste and can be transformed into various forms: consumed whole, processed into meals or pastes, or incorporated into feeds or foods [5].

The use of insects in nutrition and animal husbandry offers numerous advantages: high feed conversion efficiency, the ability to convert organic waste into high-value proteins, and lower environmental impact. This approach aligns closely with principles of sustainability, circular economy, and resource optimization, making it a promising solution for poultry feed [6]. Insects are ubiquitous, reproduce rapidly, exhibit high growth and feed conversion rates, and require minimal resources throughout their lifecycle. Moreover, their use can bring benefits to the environment, human health, and socioeconomic conditions in many communities [7].

From a nutritional standpoint, insect meals present favorable amino acid profiles compared to conventional feeds, reducing the need for synthetic additives and production costs, with positive effects on poultry welfare—in terms of growth and development—and on meat quality [8]. From an environmental perspective, insects demand fewer resources and emit lower greenhouse gas quantities relative to conventional protein sources, thereby promoting more sustainable farming practices [9]. Additionally, the ability of insects to consume organic waste—such as food leftovers, compost, and manure—allows the transformation of low-value materials into quality proteins for feed production.

In light of this evidence, it is crucial to address the challenges posed by food security and the rising global demand for proteins. Insect meals offer a scalable and nutritionally dense solution complementary to conventional protein sources. On these foundations, our research examined chicken samples fed with different dietary regimes (traditional, sustainable, live larvae, and dried larvae) to identify related volatile patterns and characterize associated volatile organic compounds (VOCs).

For this purpose, both established analytical techniques, such as solid-phase microextraction coupled with gas chromatography–mass spectrometry (SPME-GC-MS), and advanced sensing approaches based on MOX sensor devices were employed. Although different in nature, these methodologies are complementary: SPME-GC-MS provides a detailed chemical characterization of volatile organic compounds (VOCs), allowing the identification and quantification of specific molecular classes (amines, aldehydes, alcohols, esters, ketones, etc.), while sensor-based systems enable a rapid, non-destructive, and cost-effective evaluation of complex aromatic profiles, offering an overall assessment of the sample's condition [10].

In this study, VOCs were investigated to assess the impact of different dietary formulations used in animal feeding. Variations in feed composition can influence the chemical properties and sensory traits of meat, leading to distinctive volatile patterns [11].

With the aim of combining environmental sustainability, animal welfare, production efficiency, and food safety, the research presented here adopts an integrated approach combining an innovative device (S3+) equipped with an array of six MOX sensors and SPME-GC-MS analysis. This strategy made it possible to highlight both the nutritional potential of insect-based flour as alternative protein sources and the capability of sensor technology to monitor the effects of diet and thermal processing (raw/cooked) on the volatile profile of poultry products.

Overall, the combination of reference analytical methods and innovative sensing technologies represents an effective decision-support tool for the agri-food industry, enhancing sustainability, quality, and safety within production systems, while promoting circular economy principles and reducing environmental impact.

## 4.2 MATERIALS AND METHODS

### 4.2.1 Animals, Management, and Diets

The in vivo trial was carried out at the poultry facility of the University of Turin (Italy) and followed experimental protocol no. 814715, approved by the University Bioethics Committee. All animals

were managed in accordance with European regulations on organic farming (Regulation EC No. 834/2007), maintaining uniform rearing and environmental conditions across groups.

On day 39 of life, chicks were individually wing-tagged and selected based on a live body weight (LW) average of 316.8 ± 1.4 g. A total of 192 subjects were allocated in the experimental facility, distributed among 18 pens (8 animals per pen; size: 2.0 × 3.2 m), with rice hull bedding and free access to an outdoor area of the same size.

Animals were divided into three groups, each comprising 6 pens (considered replicates). The control group (CONTROL) received a basal diet containing conventional ingredients such as soybean meals. The ST group received an experimental diet where soybean meal was fully replaced by alternative ingredients. Two additional experimental groups received the same basal diet as ST supplemented with *Hermetia illucens* larvae (Black Soldier Fly Larvae, BSFL), administered either in dehydrated (DL) or live (LL) form, at 5% of the expected daily dry matter (DM) intake. Actual feed intake was measured weekly, and the larvae allocation was adjusted to keep the 5% DM proportion constant.

The diets were formulated to be isonitrogenous and isoenergetic, following INRA nutritional values for chicken (metabolizable energy, AME 11.8–11.9 MJ/kg; crude protein 18.1%; ether extract 3.59–3.63%; crude fibre 3.28–4.80%). Details of the feeding regimens are reported in Fiorilla et al. (2024) [12]. Dehydrated larvae were supplied by Entomo Agroindustrial (Murcia, Spain), while live larvae were obtained from Inagro (Rumbeke-Beitem, Belgium), shipped weekly and maintained in diapause state, then reactivated before administration as per the procedure described by Bellezza Oddon et al. (2021) [13].

The trial lasted a total of 135 days, from 39 days until slaughter at 174 days. After a 12-hour fasting, chickens were stunned electrically following European regulations (Regulation EC No. 1099/2009 of 24 September 2009) [14]. The pectoralis major fillet of the right cranial side was weighed, vacuum-packed, and frozen at –20 °C.

For volatile profiling of poultry samples, two analytical methods were applied in parallel on the same sample: solid-phase microextraction coupled with gas chromatography–mass spectrometry (SPME-GC-MS) and electronic nose (E-nose) analysis via the S3+ device.

### 4.2.2 Sample Storage and Cooking

Samples were stored at –20 °C until analysis. For raw samples, thawing was performed overnight at 4 °C; cooked samples were immersed directly in hot water (85 °C) within glass containers. Vacuum-

packed cooking lasted 25 minutes, followed by cooling, sectioning, and insertion into analysis chambers.

To prevent contamination and formation of undesirable metabolites, all handling was conducted under sterile conditions, using sterilized materials, Bunsen burners or laminar flow hoods, and disinfected surfaces.

A total of 48 samples were analyzed across two slaughter sessions, each including the 4 dietary treatments:

- Conventional diet (CONTROL)
- Diet with live larvae (LL)
- Diet with dehydrated larvae (LD)
- Sustainable diet (ST)

For each treatment, 3 samples were analyzed as raw and 3 as cooked. Each sample underwent three replicate GC-MS analyses and ten measurements with the S3+ device, for a total of 624 analyses as shown in Table 1.

**Table 1.** Experimental design, sample allocation, and analytical replication for each dietary treatment.

| Group | Diet description | Supplementation | Pens (biological replicates) | Total animals | Analyzed samples | *Sample state | GC-MS replicates | S3+ measurements |
|---|---|---|---|---|---|---|---|---|
| CONTROL | Conventional basal diet (including soybean meal) | None | 6 | 48 | 6 | 3 raw + 3 cooked | 3 per sample | 10 per sample |
| ST | Experimental diet (soybean meal fully replaced) | None | 6 | 48 | 6 | 3 raw + 3 cooked | 3 per sample | 10 per sample |
| DL | ST diet + BSFL | Dried BSFL (5% DM) | 6 | 48 | 6 | 3 raw + 3 cooked | 3 per sample | 10 per sample |
| LL | ST diet + BSFL | Live BSFL (5% DM) | 6 | 48 | 6 | 3 raw + 3 cooked | 3 per sample | 10 per sample |
| Total | - | - | 18 | 192 | 24 | 12 raw + 12 cooked | - | - |

* For each treatment, six breast fillet samples were analyzed (three raw and three cooked). Three analytical replicates were performed per sample using SPME-GC-MS, and ten consecutive measurements were carried out using the S3+ electronic nose.

### 4.2.3 Sample Preparation for GC-MS

From each sample, 3 g were taken using corers and transferred into 20 mL chromatography vials with aluminum caps and PTFE/silicone septa. To ensure representativeness, each vial was filled with three aliquots from different sample points. After sealing, vials were held at 4 °C until analysis.

#### 4.2.3.1 GC-MS Analytical Conditions

The sampling and chromatographic analysis were carried out using the same GC-MS system employed for the study on table grapes described in Chapter 3 "Quality monitoring of table grapes stored in controlled atmosphere using an s3 + mos nanosensor device". The technical specifications of the SPME fiber, along with the operating conditions and instrumental parameters, are provided in detail in *Section 3.2.4.*

The oven program was: 40 °C for 1 min, ramp to 50 °C at 4.5 °C/min, then to 80 °C at 6.5 °C/min, and finally to 180 °C at 15 °C/min; total run 17 min; overall analysis time (including sampling) 107 min. Compound identification was based on Nist11, Nist11b, and FFNSC2 libraries. At least 70 peaks with area ≥ 500 AMU were considered. Integration was automated (slope 100/min, width 2 s, drift 0, doubling time 1000 min). Results were expressed as relative abundance (% of GC area, mean ± SD).

### 4.2.4 Sample Preparation for S3+

Residual samples (~6 g) were used for S3+ analyses. These were placed in polypropylene (PP) containers with perforated caps for insertion of aspiration tubes, then refrigerated until testing.

#### 4.2.4.1 Calibration of MOX Sensors

The S3+ device and sensor arrays were developed in collaboration with Nano Sensor Systems Srl (spin-off of the University of Brescia). The array comprises six MOX sensors based on $SnO_2$ and doped $SnO_2$ (Pd, Au), operating at 500 °C. Calibration included a high-temperature annealing phase (500–800 °C, 1–10 h) and subsequent aging in air to stabilize baseline resistance [15]. Validation was carried out in a standardized system with controlled flow chamber, mass flow controller, solenoid valves, and activated carbon filters.

#### 4.2.4.2 Configuration of the S3+ System

For S3+ analysis, samples were placed in a thermostatic bath at 30 °C, using a heating plate with thermal probe properly insulated to prevent water infiltration. Samples were connected to the

instrument and activated carbon filters via PP tubing sealed with Parafilm®. Two carbon filters were employed: one purifying the headspace air, the other directly connected to the S3+ device.

Each analysis lasted 13 minutes, divided into three phases: 100 s sensor stabilization, 200 s sample measurement, and 500 s recovery. Ten replicates were run per sample, for a total duration of about 130 minutes. A schematic of the experimental configuration is shown in Figure 1.

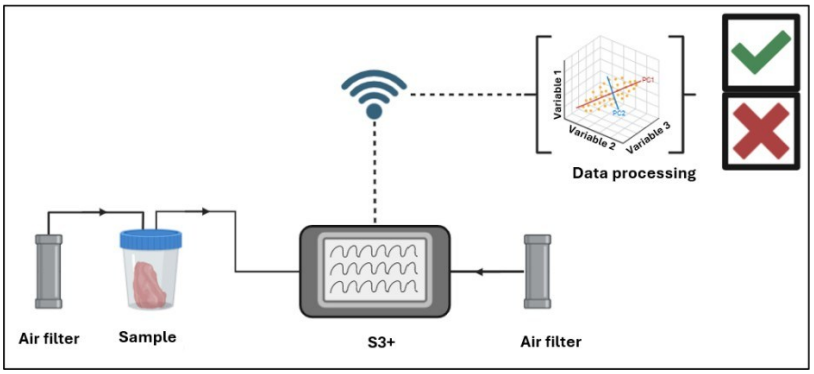


**Figure 1.** Representation of the S3+ setup.

During each replicate, the sensor output (Figure 2), expressed in terms of electrical resistance, was normalized to the initial value ($R_0$). For each sensor, the difference between the initial value and the minimum value recorded during the analysis was calculated. Subsequently, the $R/R_0$ parameter and the corresponding standard deviation were determined by considering all ten measurements for each sensor.

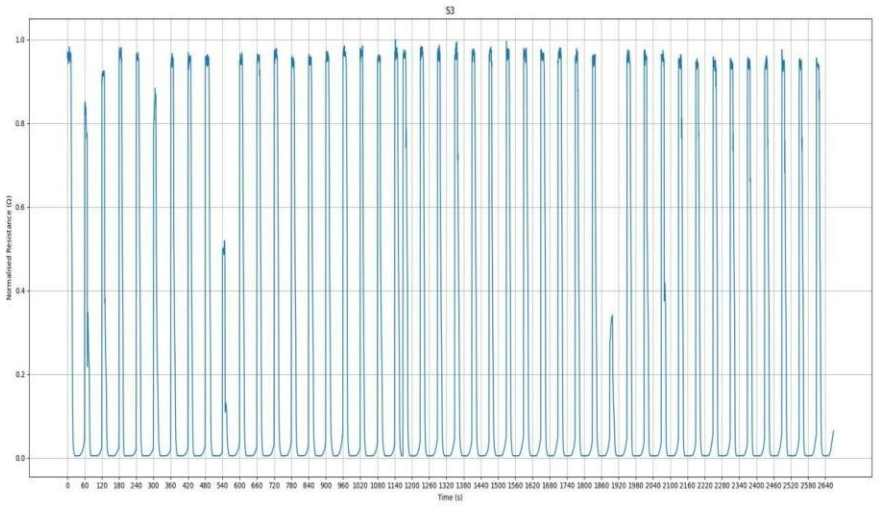


**Figure 2.** Graphical representation of the signal obtained from a single sensor.

The y-axis shows the resistance value (Ω), while the x-axis represents time (s). The data generated by the sensors were transmitted to the Microsoft Azure platform, which integrates

two web applications: a management portal and a mixture classification service. The interpretation of the acquired information was carried out using multivariate statistical analysis.

### 4.2.5 Post-Run Analysis

In this study, Linear Discriminant Analysis (LDA) was applied to reduce the dimensionality of the dataset, thereby facilitating the interpretation of the results without compromising the discriminant capability of the model (Table 2) [16; 17].

**Table 2.** Features extracted from the recorded tracks of each sensor.

| Features | Description |
|---|---|
| Sharpe Forward 25% | Variability index equivalent to the ratio between the mean and the standard deviation calculated from the beginning of the signal to 25% of it. |
| Sharpe Back 25% | Variability index equivalent to the ratio between the mean and the standard deviation calculated from the end of the signal to 25% of it. |
| Sharpe Forward 50% | Variability index equivalent to the ratio between the mean and the standard deviation calculated from the beginning of the signal to 50% of it. |
| Sharpe back 50% | Variability index equivalent to the ratio between the mean and the standard deviation calculated from the end of the signal to 50% of it. |
| Minimum derivative | Calculation of the minimum derivative of the function in the selected interval. |
| Maximum derivative | Calculation of the maximum derivative of the function in the selected interval. |
| Integral | Calculation of the integral of the function in the selected interval. |
| ΔR | Often called excursion range, this feature represents the difference between the maximum and minimum values observed in the time series. |
| Logarithm of sum | The sum of the natural of the signal. |
| Minimum | The minimum value observed in the time series. |
| Maximum | The maximum value observed in the time series. |

## 4.3 RESULTS AND DISCUSSION

### 4.3.1 Poultry Samples

In the present study, both raw and cooked poultry meat samples were analyzed, obtained from animals fed with different experimental diets (CONTROL, LL, LD, and ST). For the characterization of the volatile profile, both traditional and innovative analytical techniques were employed. It is well established that raw meat exhibits a mild aroma, generally lacking distinctive odor notes; however, it contains numerous aroma precursors that, upon heat treatment, give rise to volatile compounds responsible for the characteristic sensory attributes of cooked meat [18].

### 4.3.2 GC-MS Analysis Results

The SPME-GC-MS analysis enabled the identification of a wide spectrum of volatile compounds belonging to various chemical classes, including aldehydes, alcohols, ketones, alkanes, esters,

alkenes, carboxylic acids, and ethers. Among these, aldehydes, alcohols, alkenes, and carboxylic acids were the most abundant in both raw and cooked samples, regardless of the dietary treatment (Figure 3 A–B).

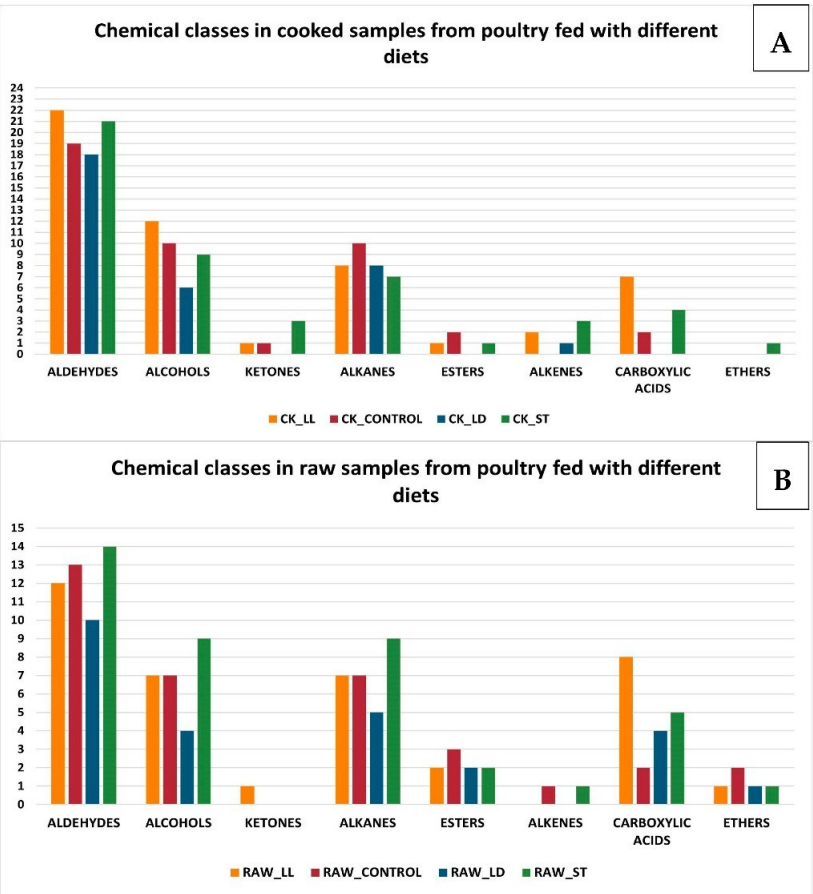


**Figure 3 (A, B).** Chemical classes in cooked and raw samples from poultry fed with different diets.

The comparison between raw and cooked meat revealed significant quantitative variations: in cooked samples, a general decrease in aldehydes, alcohols, and ketones was observed (with some exceptions related to specific diets), accompanied by an increase in esters, carboxylic acids, and ethers. Conversely, alkanes and alkenes showed nearly constant values [19].

These differences are mainly attributable to the chemical transformations induced by cooking, which include:

- Protein denaturation, leading to the formation of new volatile compounds;
- Lipid oxidation, which initially generates aldehydes, alcohols, and ketones, later converted into organic acids;
- Maillard reactions, occurring between amino acids and reducing sugars at high temperatures, resulting in a wide range of aromatic molecules;

- Strecker degradation, closely related to the Maillard reaction, responsible for the formation of aromatic aldehydes with low odor thresholds that play a key role in the sensory profile of meat.

From a chemical perspective, aldehydes, alcohols, and ketones tend to undergo further oxidation, producing carboxylic acids. Esters are formed through interactions between alcohols and acids, whereas ethers may originate from the condensation of alcohols under high-temperature conditions. Alkanes and alkenes, being relatively stable hydrocarbons, are less involved in heat-induced reactive processes.

A representative example is hexanal, an aliphatic aldehyde detected in all samples (Figure 4 A–B), which plays a crucial role in the aroma profile of cooked chicken due to its low odor threshold and its characteristic green, fresh note [20].

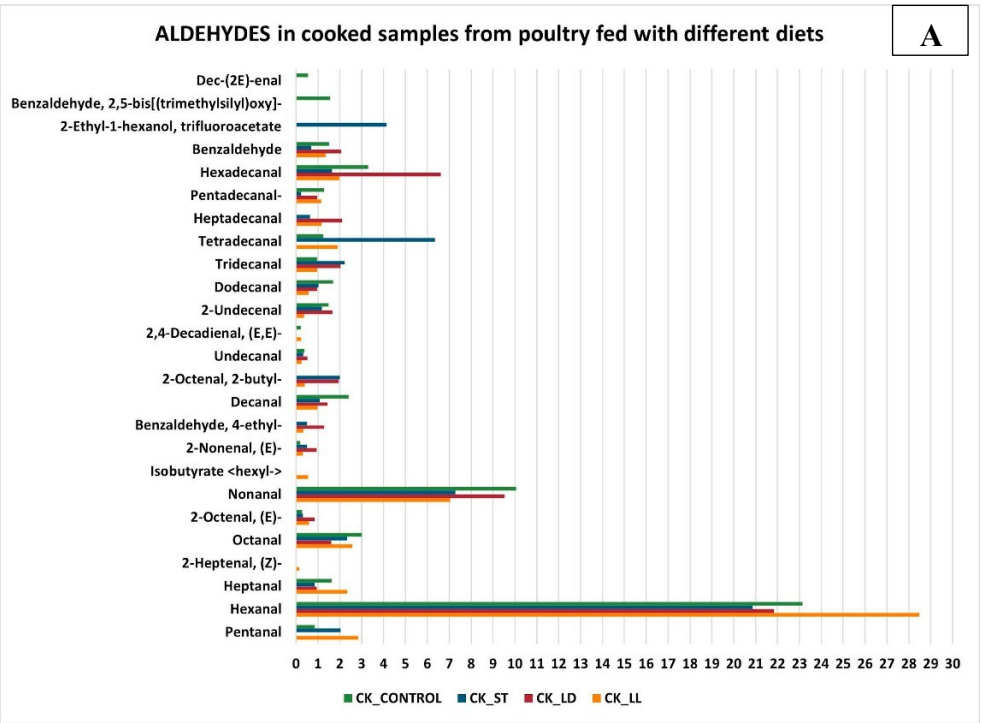

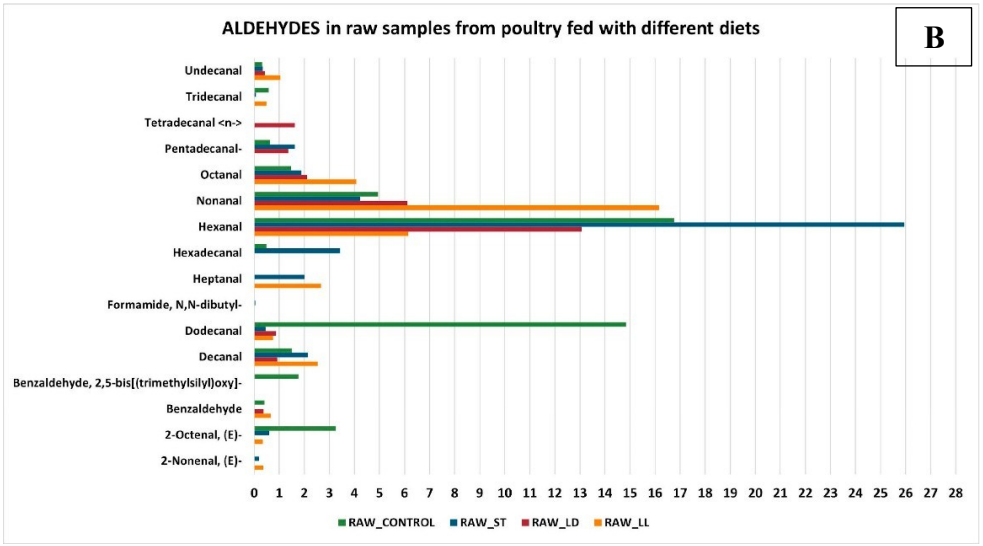


**Figure 4 (A, B).** Aldehydes in both cooked and raw samples.

Similarly, among alcohols (Figure 5 A–B), the most representative compound was 1-octen-3-ol, associated with mushroom-like notes, which can be considered an indicator of lipid oxidation [21].

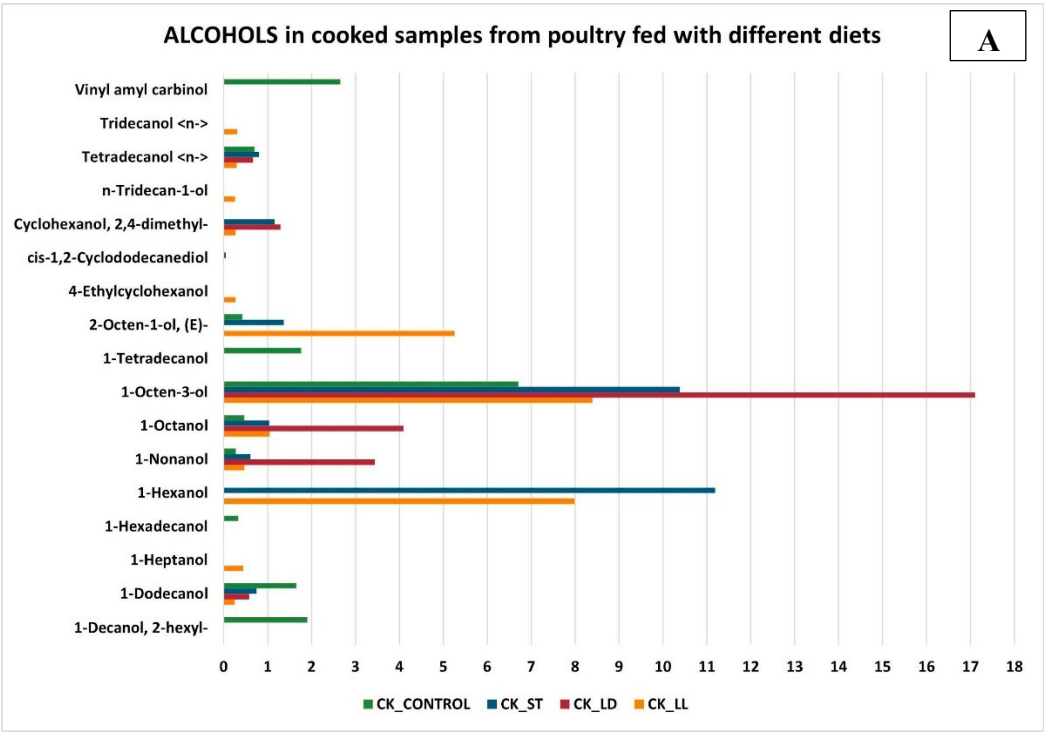

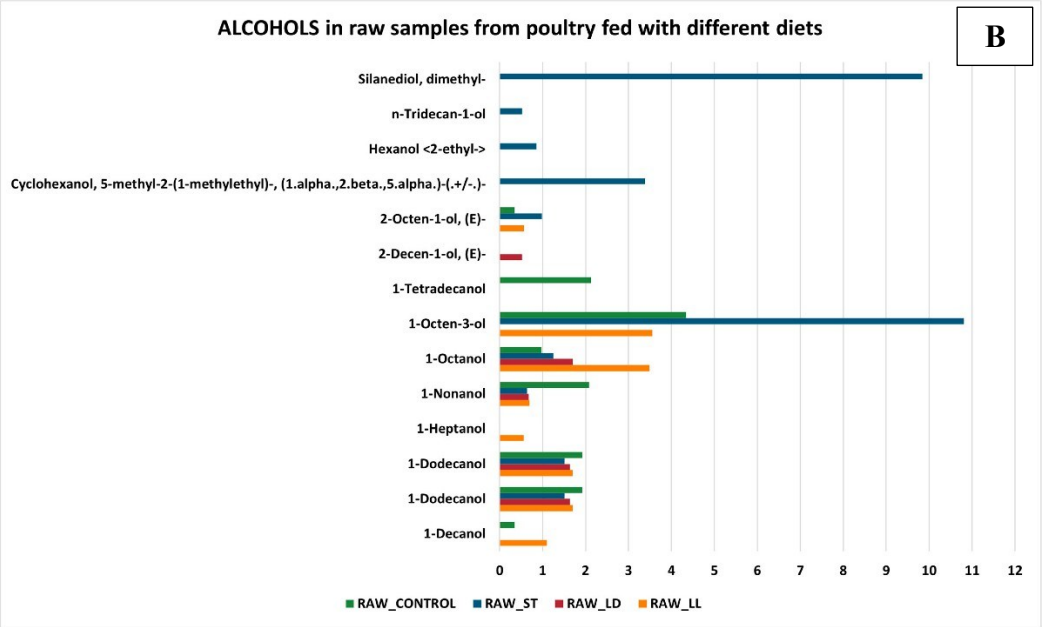


**Figure 5 (A, B).** Alcohols in both cooked and raw samples.

The analysis also revealed the presence of specific compounds associated with individual dietary regimens, suggesting that diet may selectively influence certain metabolic pathways and thus contribute to the diversification of the volatile profile [22]. Particular attention was given to carboxylic acids: while in cooked samples some of them (e.g., nonanoic acid and octanoic acid) appeared reduced due to oxidation, thermal degradation, and evaporation processes, in raw samples—particularly those from the LD diet—an increase was observed, likely related to enzymatic lipolysis occurring in the absence of heat treatment (Figure 6 A–B).

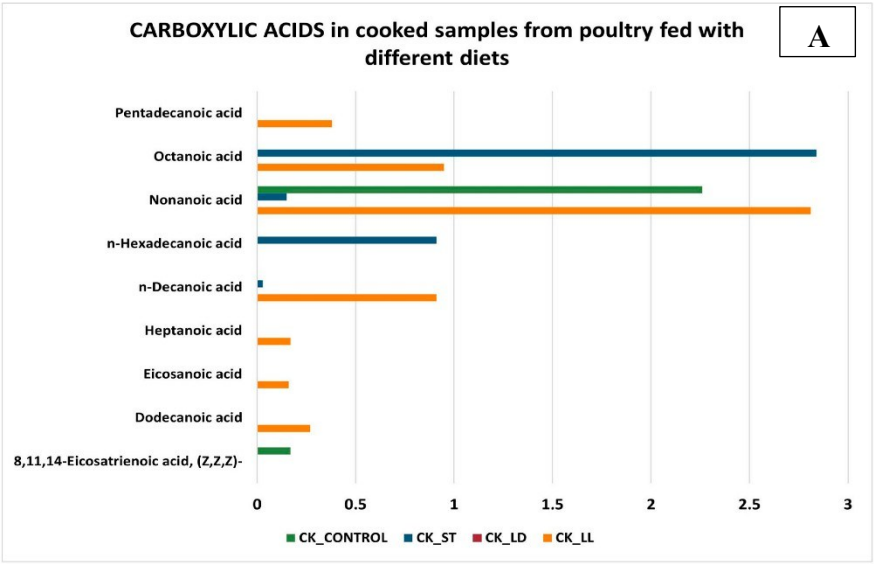

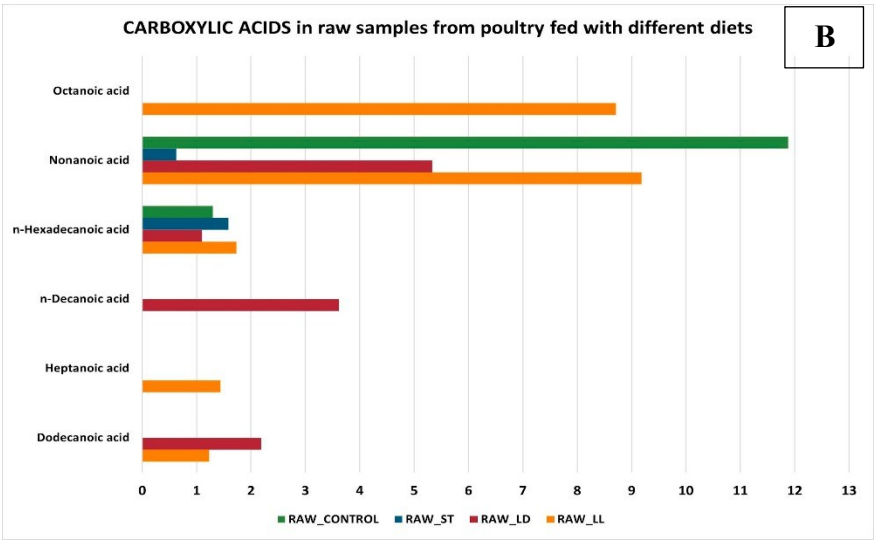


**Figure 6 (A, B).** Carboxylic acids in both cooked and raw samples.

Finally, although hydrocarbons such as alkanes and alkenes are not the primary contributors to aroma perception, they can nonetheless play a role in defining a complex and distinctive volatile profile, contributing to the overall organoleptic characteristics of poultry meat.

At the same time, esters, ethers, and ketones were detected in all types of samples analyzed, though in very low amounts, with an average abundance below 1%. This indicates that their overall impact on the meat's aromatic profile is limited. However, some ketones—particularly 2-heptanone, 3-octanone, and 2-nonanone—showed higher mean abundances in cooked samples from the ST group, reaching approximately 1.5%, 4.5%, and 2.3%, respectively. These compounds are of specific interest as they are associated with spoilage phenomena, being metabolic by-products of several microorganisms commonly involved in meat deterioration, including *Pseudomonas spp.*, *Carnobacterium spp.*, and *Enterobacteriaceae*.

### 4.3.3 Results of the S3+ Analysis

After performing GC–MS analysis to highlight differences in the volatile profiles of poultry samples, the S3+ sensor system was also applied to further investigate the olfactory fingerprints. The device proved effective in analyzing volatile compounds, enabling clear differentiation of samples based on dietary regimen. The collected data were processed using Linear Discriminant Analysis (LDA), a technique aimed at maximizing class separation while minimizing within-class variance. In this case, LDA was employed both as a dimensionality reduction method and as a graphical representation of differences among dietary groups (Figure 7).

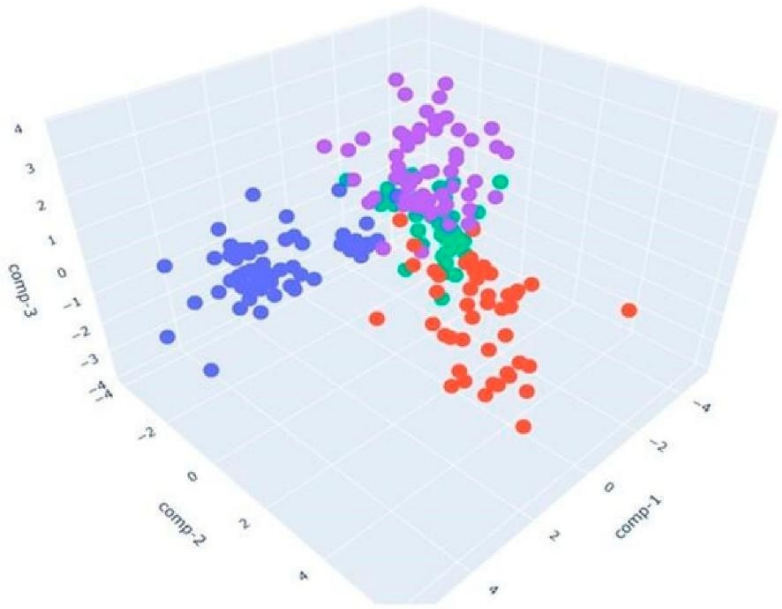


**Figure 7.** 3D LDA plot representing cooked samples from different dietary groups: CONTROL diet (blue points), ST (red points), LD diet (green points), and LL diet (purple points).

The resulting plot shows a clear distinction among the groups:

- Blue points represent the control samples (CK_CONTROL), clustered within a well-defined area, indicating a consistent olfactory profile.
- Red points correspond to samples from the sustainable diet group (CK_ST), positioned in a region clearly separated from the controls, confirming significant differences in volatile profiles associated with this diet.
- Green points represent samples from the diet containing dehydrated larvae (CK_LD), distributed mainly in the central area of the plot.
- Purple points identify samples from the live larvae diet group (CK_LL), located in a distinct region of the LDA space, suggesting a complex and characteristic volatilome associated with this feeding regimen.

The performance evaluation of the LDA model showed an accuracy of 86.53%, confirming the capability of the S3+ system to effectively discriminate samples based on diet.

Figure 8 presents the three-dimensional representation of the LDA analysis applied to raw chicken samples from different dietary treatments.

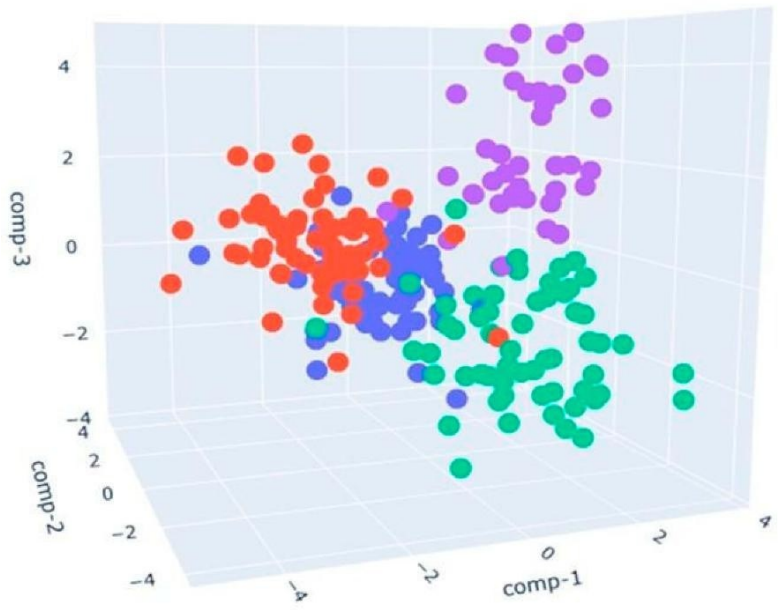


**Figure 8.** 3D LDA plot representing raw samples from different dietary groups: CONTROL diet (blue points), ST diet (red points), LD diet (green points), and LL diet (purple points).

The blue points represent control samples (RAW_CONTROL), mostly located in the central region of the plot. Red points, corresponding to samples from the sustainable diet (RAW_ST), are also concentrated near the center, partially overlapping with the control group. Green points, representing samples from the dehydrated larvae diet (RAW_LD), are mainly distributed in the lower-right portion of the plot. Finally, purple points, corresponding to samples from the live larvae diet (RAW_LL), are positioned in the upper-right area.

The distribution pattern shows that RAW_LD and RAW_LL samples (green and purple) exhibit good spatial separation from the other two groups (blue and red), indicating that the LDA successfully distinguished these samples based on the features identified by the S3+ system. Conversely, the control and sustainable diet samples display a high degree of overlap, suggesting very similar olfactory profiles. In this case, the LDA achieved a classification accuracy of 81.78%.

### 4.3.4 Confusion Matrix and ROC Curve

To evaluate the classifier's performance, the data obtained from the S3+ device were divided into a training set (80%) and a test set (20%). For raw samples, the test set consisted of 46 samples (20% of a total of 228), whereas for cooked samples, it included 42 samples (20% of a total of 209).

#### 4.3.4.1 Confusion Matrix

Figure 9 shows the confusion matrix for cooked samples, classified into four categories: COOKED_LD, COOKED_LL, COOKED_ST, and COOKED_CONTROL.

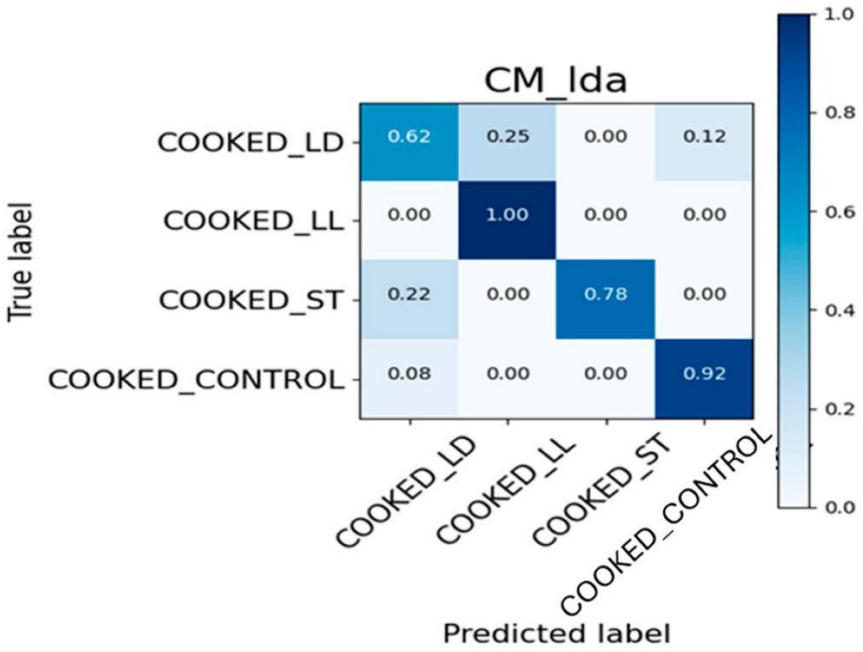


**Figure 9.** Confusion Matrix on cooked samples.

For the COOKED_LD class, the classifier correctly recognized 62% of the samples, while 25% were misclassified as COOKED_LL and 12% as COOKED_CONTROL, indicating some degree of overlap between categories.

The COOKED_LL class, on the other hand, showed 100% accuracy, with all samples correctly identified, confirming a high level of precision.

For the COOKED_ST class, the system achieved an accuracy of 78%; however, 22% of the samples were incorrectly classified as COOKED_LD.

Finally, the COOKED_CONTROL class showed an accuracy of 92%, with only 8% misclassified as COOKED_LD.

Figure 10 presents the confusion matrix results for raw samples, also divided into four categories: RAW_CONTROL, RAW_LD, RAW_ST, and RAW_LL.

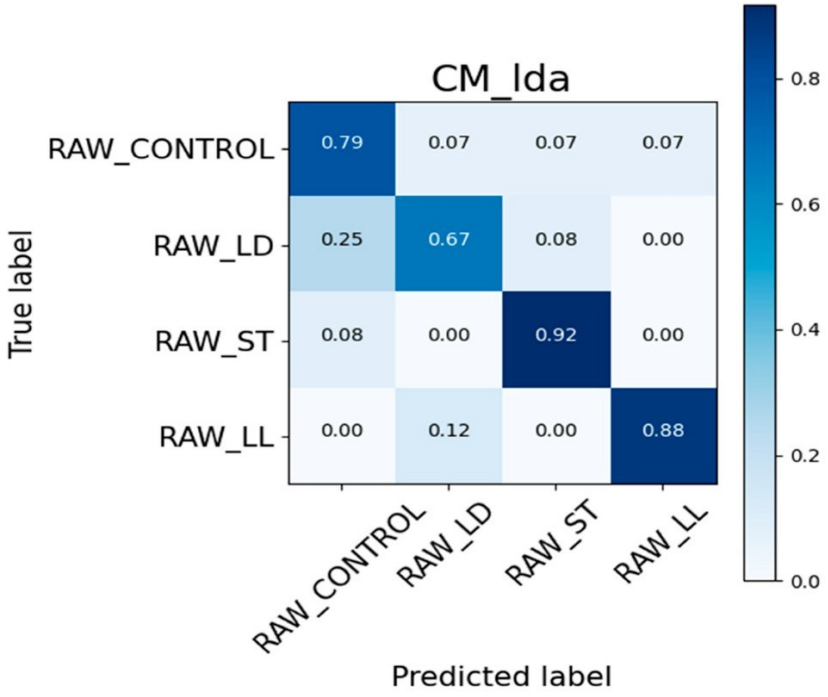


**Figure 10.** Confusion Matrix on raw samples.

The RAW_CONTROL class was correctly identified in 79% of the cases, with 7% of misclassifications distributed among RAW_LD, RAW_ST, and RAW_LL. The RAW_LD class showed lower accuracy (67%), with 25% of samples incorrectly classified as RAW_CONTROL and 8% as RAW_ST.

The RAW_ST class exhibited the best performance, with 92% of samples correctly identified and only 8% misclassified as RAW_CONTROL.

Finally, the RAW_LL class was correctly classified in 88% of the cases, with 12% of errors mainly toward RAW_LD.

Overall, the confusion matrix results demonstrate a good accuracy of the classifier, particularly for the RAW_ST and RAW_LL groups, while the RAW_LD samples showed a higher degree of confusion, especially with the control class.

### 4.3.4.2 ROC Curve

Figures 11 and 12 show the Receiver Operating Characteristic (ROC) curves for the different classes, along with the Area Under the Curve (AUC) values. The black dashed line represents the Random Classifier, i.e., a baseline model that produces aggregated predictions through an ensemble of decision trees trained using the bootstrap method and an additional degree of randomness in variable selection.

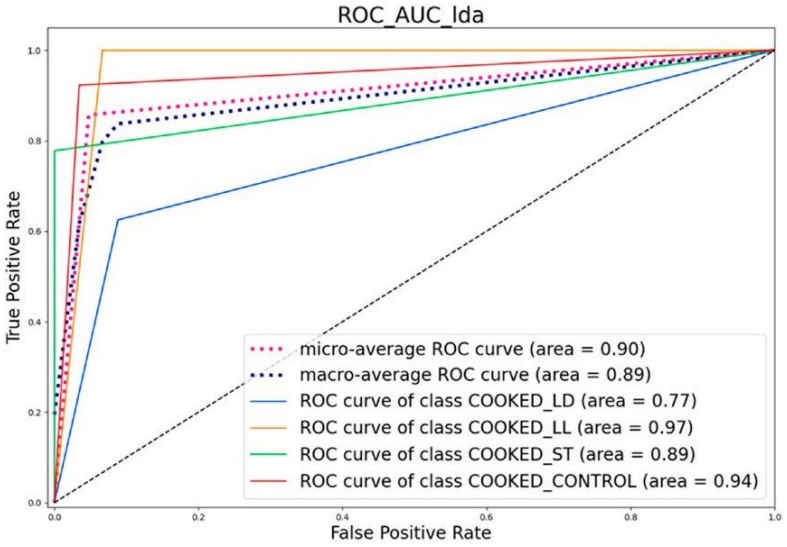


**Figure 11.** ROC Curve of cooked samples.

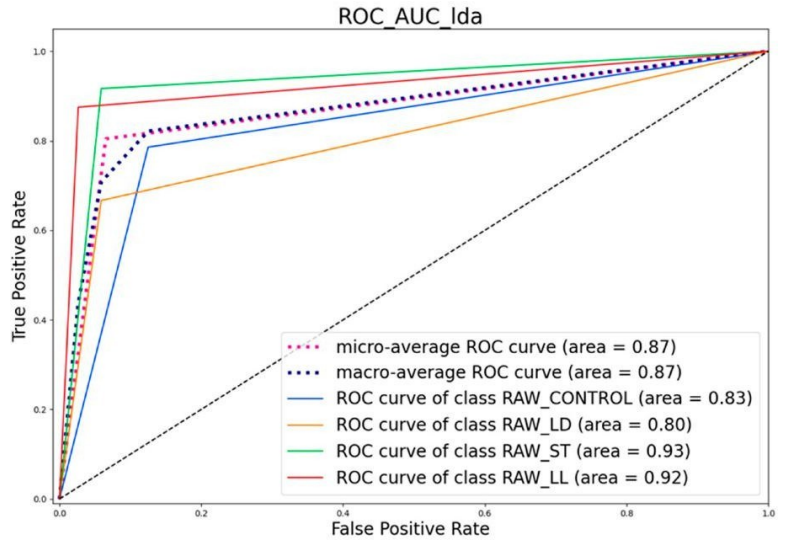


**Figure 12.** ROC Curve of raw samples.

The analysis of the ROC curves provided significant insights into the classifier's performance. For the cooked samples, the micro-average ROC curve showed an AUC value of 0.90, reflecting the model's average performance across all classes. Similarly, the macro-average curve, with an AUC of 0.89, confirmed a strong discriminative ability when classes were evaluated individually. Specifically:

- The COOKED_LD class exhibited an AUC of 0.77, indicating moderate performance, lower than the other categories;
- The COOKED_LL class achieved a very high AUC of 0.97, corresponding to excellent discrimination capability;

- The COOKED_ST class showed an AUC of 0.89, indicative of good performance;
- The COOKED_CONTROL class reached an AUC of 0.94, confirming outstanding classification accuracy.

Overall, for cooked samples, the classifier performed particularly well for the COOKED_LL and COOKED_CONTROL classes, while discrimination was less effective for COOKED_LD.

For raw samples, both the micro-average and macro-average ROC curves showed AUC values of 0.87, confirming a good overall discriminative capacity of the model. Specifically:

- The RAW_CONTROL class obtained an AUC of 0.83, corresponding to moderate performance;
- The RAW_LD class displayed a slightly lower value (AUC = 0.80), still within a moderate accuracy range;
- The RAW_ST class stood out with an AUC of 0.93, indicating excellent discriminative ability;
- The RAW_LL class achieved an AUC of 0.92, also reflecting very good performance.

The ROC curves for the raw samples thus confirm that the classifier performs best for RAW_ST and RAW_LL, while showing lower accuracy in distinguishing RAW_LD and RAW_CONTROL.

In summary, both confusion matrix and ROC curve analyses converge on the same conclusion: the model exhibits excellent precision for the COOKED_LL, COOKED_CONTROL, RAW_ST, and RAW_LL classes, while performance is less satisfactory for COOKED_LD and RAW_LD. These findings are crucial for understanding the model's strengths and identifying areas for improvement.

## 4.4 CONCLUSIONS

This study highlights the importance of exploring alternative feed sources for poultry intended for human consumption. The research focused on the volatile compound profiles of both raw and cooked chicken meat obtained from animals fed with different diets: traditional, sustainable, and diets supplemented with live or dehydrated larvae.

The analysis combined traditional analytical methods (GC–MS) with innovative sensor-based techniques (S3+), enabling not only the classification and quantification of volatile compounds but also the demonstration of the S3+ device's effectiveness as a standalone tool for discriminating between raw and cooked samples and among different dietary treatments.

The results suggest that the introduction of innovative insect-based feeds may represent a sustainable and potentially advantageous strategy to enhance the quality and resilience of poultry production systems, contributing to a more efficient and environmentally friendly supply chain.

Moreover, the application of Linear Discriminant Analysis (LDA) confirmed its usefulness as an advanced analytical approach for distinguishing complex gas mixtures, underscoring its relevance for both volatilome studies and the development of next-generation sensor technologies. In perspective, the implementation of continuous, non-destructive monitoring systems integrated with IoT technologies could enable real-time management of the entire production process, fostering innovative and high-impact applications in the agri-food sector.

## 4.5 BIBLIOGRAPHY


1. Van Huis, A.; Oonincx, D.G.A.B. The Environmental Sustainability of Insects as Food and Feed: A Review. Agron. Sustain. Dev. 2017, 37, 43.
2. Smetana, S.; Palanisamy, M.; Mathys, A.; Heinz, V. Sustainability of Insect Use for Feed and Food: Life Cycle Assessment Perspective. J. Clean. Prod. 2016, 137, 741–751.
3. Van Dijk, M.; Morley, T.; Rau, M.L.; Saghai, Y. A Meta-Analysis of Projected Global Food Demand and Population at Risk of Hunger for the Period 2010–2050. Nat. Food 2021, 2, 494–501. [PubMed]
4. Mackenzie, J.S.; Jeggo, M. The One Health Approach—Why Is It So Important? Trop. Med. Infect. Dis. 2019, 4, 88. [PubMed]
5. Sogari, G.; Amato, M.; Biasato, I.; Chiesa, S.; Gasco, L. The Potential Role of Insects as Feed: A Multi-Perspective Review. Animals 2019, 9, 119.
6. Yang, J.; Zhou, S.; Kuang, H.; Tang, C.; Song, J. Edible Insects as Ingredients in Food Products: Nutrition, Functional Properties, Allergenicity of Insect Proteins, and Processing Modifications. Crit. Rev. Food Sci. Nutr. 2023, 21, 1–23.
7. Akintan, O.; Gebremedhin, K.G.; Uyeh, D.D. Animal Feed Formulation—Connecting Technologies to Build a Resilient and Sustainable System. Animals 2024, 14, 1497. [PubMed]
8. Baéza, E.; Guillier, L.; Petracci, M. Review: Production Factors Affecting Poultry Carcass and Meat Quality Attributes. Animal 2022, 16 (Suppl. S1), 100331.
9. De Carvalho, N.M.; Madureira, A.R.; Pintado, M.E. The Potential of Insects as Food Sources—A Review. Crit. Rev. Food Sci. Nutr. 2020, 60, 3642–3652.

10. Abbatangelo, M.; Núnez-Carmona, E.; Sberveglieri, V.; Zappa, D.; Comini, E.; Sberveglieri, G. An Array of MOX Sensors and ANNs to Assess Grated Parmigiano Reggiano Cheese Packs' Compliance with CFPR Guidelines. Biosensors 2020, 10, 47.
11. Poeta, E.; Liboà, A.; Mistrali, S.; Núnez-Carmona, E.; Sberveglieri, V. Nanotechnology and E-Sensing for Food Chain Quality and Safety. Sensors 2023, 23, 8429.
12. Fiorilla, E.; Gariglio, M.; Martinez-Miro, S.; Rosique, C.; Madrid, J.; Montalban, A.; Biasato, I.; Bongiorno, V.; Cappone, E.E.; Soglia, D.; et al. Improving Sustainability in Autochthonous Slow-Growing Chicken Farming: Exploring New Frontiers through the Use of Alternative Dietary Proteins. J. Clean. Prod. 2024, 434, 140041.
13. Bellezza Oddon, S.; Biasato, I.; Imarisio, A.; Pipan, M.; Dekleva, D.; Colombino, E.; Capucchio, M.T.; Meneguz, M.; Bergagna, S.; Barbero, R.; et al. Black Soldier Fly and Yellow Mealworm Live Larvae for Broiler Chickens: Effects on Bird Performance and Health Status. J. Anim. Physiol. Anim. Nutr. 2021, 105, 10–18. [PubMed]
14. FAO. Commission Regulation (EU) No 142/2011 Laying Down Health Rules as Regards Animal By-Products and Derived Products Not Intended for Human Consumption. Available online: https://faolex.fao.org/docs/pdf/eur90989.pdf.
15. Guozhu, Z.; Changsheng, X.; Shunping, Z.; Jianwei, Z.; Tao, L.; Dawen, Z. Temperature-Programmed Technique Accompanied with High-Throughput Methodology for Rapidly Searching the Optimal Operating Temperature of MOX Gas Sensors. ACS Comb. Sci. 2014, 16, 459–465.
16. Sharma, A.; Paliwal, K.K. Linear Discriminant Analysis for the Small Sample Size Problem: An Overview. Int. J. Mach. Learn. Cybern. 2015, 6, 443–454.
17. Lin, W.; Wu, Z.; Lin, L.; Wen, A.; Li, J. An Ensemble Random Forest Algorithm for Insurance Big Data Analysis. IEEE Access 2017, 5, 16568–16575.
18. Flores, M. Chapter 13—The Eating Quality of Meat: III—Flavor. In Lawrie's Meat Science; Toldrá, F., Ed.; Woodhead Publishing: Sawston, UK, 2017; pp. 383–417.
19. Miglio, C.; Chiavaro, E.; Visconti, A.; Fogliano, V.; Pellegrini, N. Effects of Different Cooking Methods on Nutritional and Physicochemical Characteristics of Selected Vegetables. J. Agric. Food Chem. 2008, 56, 139–147. [PubMed]
20. Yaylayan, V.A. Recent Advances in the Chemistry of Strecker Degradation and Amadori Rearrangement: Implications to Aroma and Color Formation. Food Sci. Technol. Res. 2003, 9, 1–6.

21. Zhao, C.; Liu, Y.; Lai, S.; Cao, H.; Guan, Y.; San Cheang, W.; Liu, B.; Zhao, K.; Miao, S.; Riviere, C.; et al. Effects of Domestic Cooking Process on the Chemical and Biological Properties of Dietary Phytochemicals. Trends Food Sci. Technol. 2019, 85, 55–66.
22. Rickman, J.C.; Barrett, D.M.; Bruhn, C.M. Nutritional Comparison of Fresh, Frozen and Canned Fruits and Vegetables. Part 1. Vitamins C and B and Phenolic Compounds. J. Sci. Food Agric. 2007, 87, 930–944.

# 5.

# NANO-TAILORED TRIPLE GAS SENSOR FOR REAL-TIME MONITORING OF DOUGH PREPARATION IN KITCHEN MACHINES

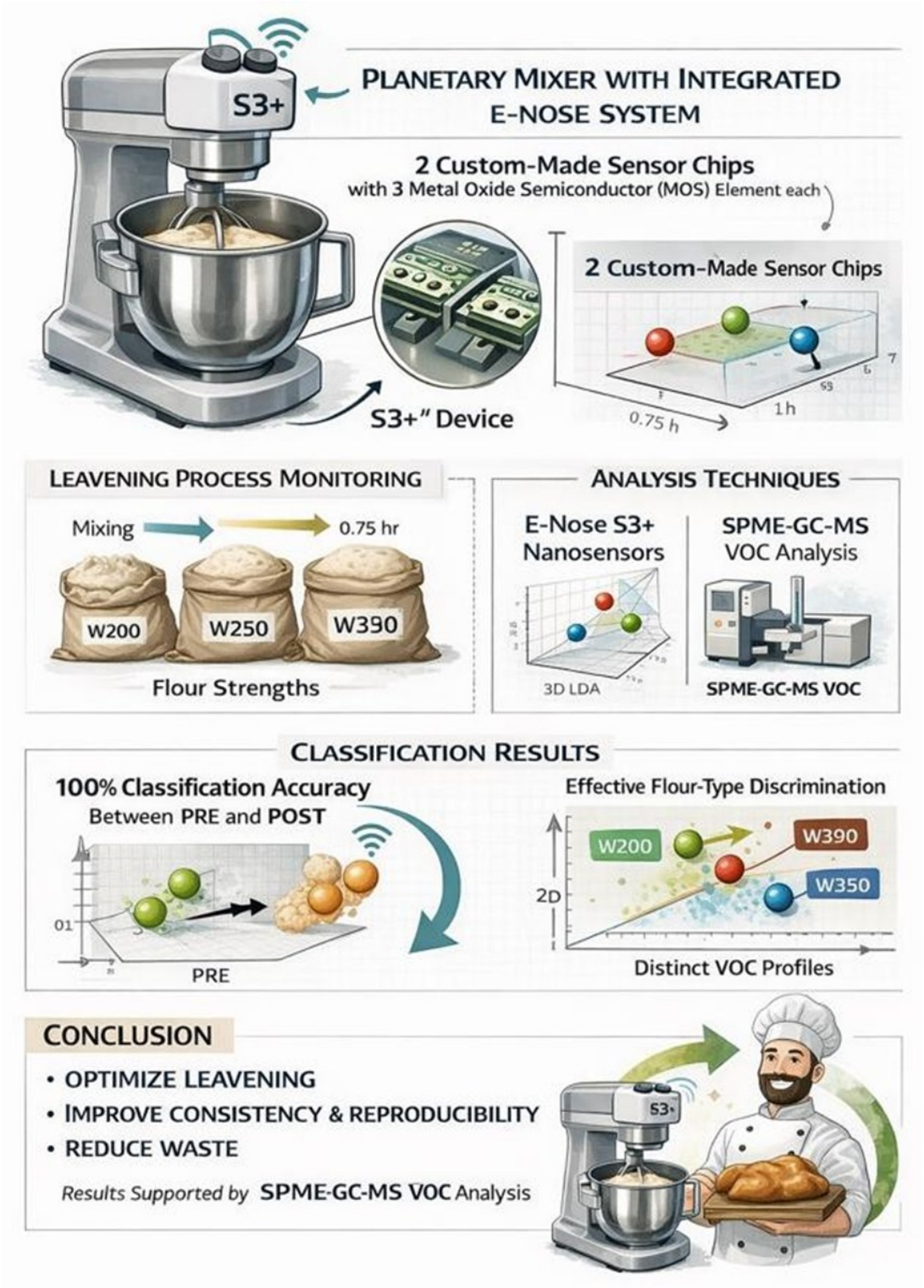

## 5.1 INTRODUCTION

In recent decades, technological progress—particularly in the fields of sensors, the Internet of Things (IoT), and artificial intelligence (AI)—has revolutionized food quality management [1], leading to the emergence of the *Food Processing 4.0* paradigm. This approach relies on the integration of robotics, smart sensors, AI, IoT, and Big Data into modern food production processes, with the aim of improving quality control, safety, production efficiency, and sustainability while reducing waste and optimizing resource use [2; 3; 4].

The implementation of IoT sensors in household appliances and industrial equipment—such as kitchen robots and ovens—enables real-time monitoring of critical parameters including temperature, humidity, volatile compound emissions, gas levels, and pH. This development has been driven by advances in nanotechnology and biotechnology, which have accelerated sensor miniaturization [5; 6].

The integration of sensors, IoT, AI, and machine learning techniques has become particularly relevant for real-time monitoring and optimization of leavening and fermentation processes [7; 8]. In bakery production, these phases are fundamental, as they determine the macroscopic structure of the final product and influence its appearance, texture, taste, and aroma [9; 10]. Leavening allows the dough to increase in volume, resulting in softness and a tender crumb—key attributes of high-quality bakery products [11]. This process is mainly driven by the activity of yeast or sourdough-based starters [12], which are responsible for fermentation that not only causes volume expansion but also contributes to the development of aroma, flavor, and sensory complexity [13].

During fermentation, yeasts metabolize flour sugars, producing carbon dioxide and alcohol [14]. Carbon dioxide induces dough expansion, while alcohol evaporates during baking, leaving behind a wide array of volatile organic compounds (VOCs)—including aldehydes, alcohols, esters, and organic acids—that define the characteristic aroma of fresh bread [15; 16]. VOC production is influenced by multiple factors, such as the type of leavening agent [17; 18], humidity conditions, fermentation time and temperature, and flour properties [19]. Among these, temperature and humidity play a crucial role in modulating fermentation kinetics and quality [20; 21].

Flour strength is a key parameter, as it affects gluten formation and, consequently, the dough's elasticity and extensibility [22]. The protein content—particularly glutenin and gliadin fractions—determines the flour's ability to develop a strong gluten network. The alveographic parameters *W* and

*P/L* provide a quantitative description of the dough's mechanical properties and its technological suitability.

Traditional methods for monitoring leavening, based on sensory observation (touch, sight, smell), are subjective and often inaccurate, leading to potential errors and quality loss [23]. These limitations have stimulated the development of objective, accurate, and non-invasive tools. Metal-oxide semiconductor (MOS) sensors, developed in the second half of the 20th century, are now widely used for food quality, safety, and traceability assessment due to their sensitivity, rapid response, and compatibility with digital technologies [24; 25]. Multi-sensor systems—or *electronic noses* (e-noses)—combined with machine learning algorithms have been employed to monitor VOCs in various applications, including fermentation and baking of dough-based products [26; 27].

The objective of this study is to evaluate the use of the S3+ device (Nano Sensor Systems S.r.l., Reggio Emilia, Italy), equipped with MOS nanosensors (e-nose), for real-time monitoring of dough leavening through VOC analysis. The innovative aspect lies in the integration of a miniaturized sensor array inside a planetary mixer, enabling continuous feedback and reducing the need for manual intervention. Using *Saccharomyces cerevisiae* as the leavening agent, the effects of flours with different strength indices (W200, W250, W390) on VOC profiles were studied over 1.5 h of fermentation, as well as during pre-leavening (PRE) and post-leavening (POST) phases.

To validate sensor-based data, SPME-GC-MS analyses were conducted on PRE and POST samples. The results demonstrate that sensor systems integrated with IoT and AI techniques represent a promising solution for process automation, requiring specialized expertise mainly during the initial training phase. Such systems provide a precise, non-destructive, and real-time method for leaving control, ensuring consistent quality, reducing waste, and enabling applicability in both artisanal and industrial baking contexts.

## 5.2 MATERIALS AND METHODS

### 5.2.1 Dough Preparation and Experimental Setup

Three different types of wheat flour, characterized by distinct strength values (W200, W250, and W390), were used for dough preparation. All ingredients were purchased from a local supplier. The recipe used for the experimental preparation of the doughs is reported in Table 1.

**Table 1.** Ingredients used for the preparation of dough samples with W200, W250, and W390 flours.

| Ingredients | Amount | Unit |
|---|---|---|
| Flour | 500 | g |
| Water | 300 | mL |
| Dry yeast | 7 | g |
| Salt | 10 | g |
| Sugar | 3 | g |

Flours with a protein content between 10 and 12% (10–12 g of protein per 100 g of flour) and a strength index (*W*) ranging from 220 to 300, with a *P/L* ratio ≤ 0.7, are classified as medium-strength flours, suitable for most bakery applications. Flours with a protein content higher than 12%, $W \geq 300$, and $P/L \leq 1$ are considered strong flours, particularly appropriate for products requiring a robust structure, such as bread and pizza. Conversely, flours with a protein content below 10%, *W* between 160 and 200, and $P/L \leq 0.6$ are categorized as weak flours, more suitable for the preparation of pastries and confectionery products.

For each dough sample, water, dehydrated *Saccharomyces cerevisiae* yeast, and sugar were first added to a Kenwood planetary mixer (Kenwood Ltd., Havant, UK; model KCL95.424SI) to initiate the mixing phase. Subsequently, the corresponding flour type and salt were incorporated, and mixing continued until a homogeneous dough was obtained. The doughs were then left to rise at room temperature (22 ± 1 °C) for 1.5 h. In this study, only ambient temperature was monitored; future developments could include the integration of sensors for humidity and mixing speed, which are also critical parameters affecting fermentation dynamics.

To analyze the volatile compounds released during leavening, two complementary techniques were employed: a custom-designed electronic nose (e-nose) based on metal oxide semiconductor (MOS) sensors, used for real-time monitoring of gaseous emissions, and solid-phase microextraction followed by gas chromatography–mass spectrometry (SPME-GC-MS), used for a detailed characterization of the volatile profile. The combined approach allowed the monitoring of both the overall evolution of the aroma profile and the identification of specific volatile compounds associated with dough fermentation. The experimental setup adopted for both techniques is illustrated in Figure 1.

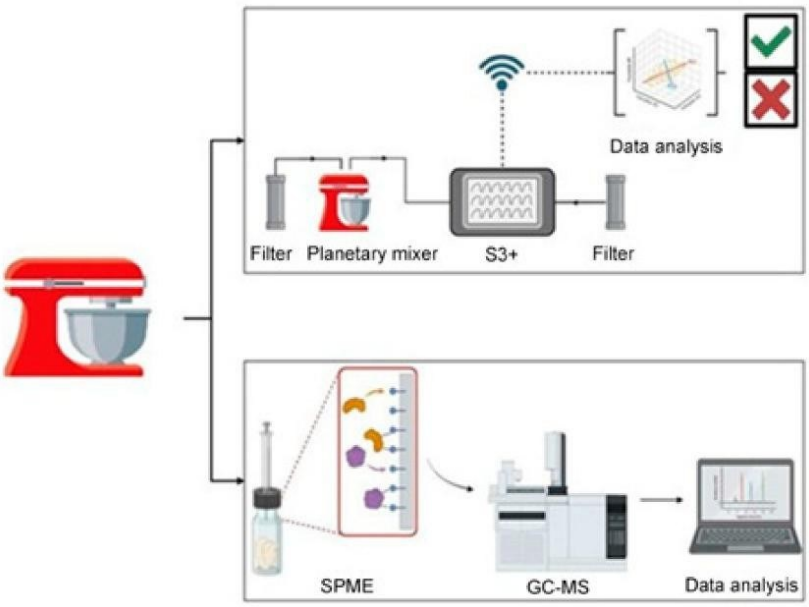


**Figure 1.** Schematic representation of the experimental setup used to monitor volatile compounds during dough leavening. The upper panel shows the real-time analysis performed with a custom-made electronic nose (e-nose) based on MOS gas sensors, enabling wireless data acquisition and classification of aroma profiles. The lower panel illustrates the complementary solid-phase microextraction followed by gas chromatography–mass spectrometry (SPME-GC-MS) approach.

### 5.2.2 S3+ Electronic Nose and Gas Sensor Technology

The S3+ device (designed by Nano Sensor Systems S.r.l., Reggio Emilia, Italy) was equipped with two sets of triple metal oxide semiconductor (MOS) sensors, specifically developed for the detection of volatile organic compounds (VOCs). Each set included sensors based on pure $SnO_2$ and $SnO_2$ doped with Au nanoparticles, to enhance selectivity and sensitivity. The sensors were housed inside a sealed stainless-steel sampling chamber, where air samples collected from the dough headspace were analyzed.

The core of the S3+ system consists of a sensor array chamber, a fluidic circuit, an electronic control system, and a data processing unit. The sensor chamber contains a total of six MOS sensors: two based on pure $SnO_2$, two on $SnO_2$ doped with Pd, and two on $SnO_2$ doped with Au, all operating at a working temperature of 500 °C (Table 2). The chamber dimensions (11 × 6.5 × 1.3 cm) were optimized to allow a controlled airflow across the sensing elements, thus ensuring consistent and reproducible exposure to the headspace samples.

**Table 2.** Working temperatures of MOS sensors with different dopants.

| Type of Sensor | Doping | Working Temperature (°C) |
|---|---|---|
| MOX sensor | $SnO_2$ | 500 |
| MOX sensor | $SnO_2$ + Pd | 500 |
| MOX sensor | $SnO_2$ + Au | 500 |

### 5.2.3 Sensor Integration with the Planetary Mixer

The S3+ device was connected to a planetary mixer via a polyurethane tube inserted through a custom-made opening in the machine's closure system (Figure 2). This configuration allowed the internal pump of the device to continuously draw the volatile compounds released from the dough throughout the entire leavening process and direct them into the sensor chamber. The integration of the sampling system enabled non-invasive and real-time monitoring of the aromatic evolution of the dough.

**Figure 2.** Details of the upper closure of the planetary mixer showing the perforated section used for gas sampling during VOC monitoring.

The integration of MOS sensors into kitchen appliances represents an initial step toward real-time food monitoring [28; 29]. Future developments will focus on the direct incorporation of sensors into the mixer's structure to improve response times, minimize sampling losses, and further optimize the automation of leavening monitoring.

The device's fluidic system includes a diaphragm pump (KNF Neuberger GmbH, Freiburg, Germany; model: NMP05B), a solenoid valve (Camozzi Group S.p.A., Brescia, Italy; model: K000-303-K11M), and a metal cylinder filled with activated carbon for ambient air filtration. This configuration ensures that only the sampled volatile compounds reach the sensors, preventing external

contamination. The inlet solenoid valve regulates the airflow—set to a maximum of 250 standard cubic centimeters per minute (sccm)—by controlling the sampling and purging phases.

The electronic control system continuously monitors and regulates sensor temperature, records resistance variations, and transmits real-time data via an IoT cloud platform. A dedicated algorithm processes the collected signals, extracting the main features for subsequent statistical analyses.

### 5.2.4 Sensor Calibration and Data Acquisition

Before analysis, the sensors underwent a multi-stage calibration process. An annealing phase (500–800 °C for 1–10 h) was performed to stabilize the sensitive layers, followed by an "aging" process in clean air to optimize baseline resistance.

Validation involved controlled exposure to gas mixtures containing ethanol, acetone, and other fermentation-related volatiles at known concentrations. Sensor responses were recorded and analyzed to construct reference curves. This calibration ensured signal reproducibility and minimized baseline drift during prolonged operation.

For each measurement, the S3+ device operated in 13-minute cycles: 100 s for sensor stabilization, 200 s for sample exposure, and 500 s for recovery. Each dough type was analyzed in triplicate, with 10 replicates per sample. Data were acquired at a frequency of 1 Hz and normalized with respect to the baseline resistance ($R/R_0$) to ensure comparability among sensors [30].

Before interpretation, raw signals were pre-processed to reduce noise and enhance comparability. Each response was initially normalized to the baseline resistance ($R_0$) to align the signals to a common value. A Savitzky–Golay filter was then applied to attenuate high-frequency noise while preserving signal trends. This preprocessing step was essential to minimize the effects of external variables such as temperature and humidity fluctuations, system noise, and residual odors from previous samples.

### 5.2.5 Gas Chromatography–Mass Spectrometry (GC–MS) Analysis

To validate the MOS sensor responses, volatile profiles were analyzed using solid-phase microextraction coupled with gas chromatography–mass spectrometry (SPME-GC-MS). Approximately 20 g of dough were transferred into sterile 120 mL glass jars perforated to allow insertion of the SPME fiber into the headspace. Extraction was performed using a DVB/CAR/PDMS fiber for 90 min at 30 °C.

Analytes were thermally desorbed and injected into a Shimadzu GCMS-QP2020 system (Shimadzu Corporation, Kyoto, Japan) equipped with a MEGA-5MS column (25 m × 0.25 mm × 0.25 μm). Hydrogen was used as the carrier gas at a flow rate of 2.2 mL/min. The oven temperature program was as follows: 40 °C (1 min), ramped at 4.5 °C/min to 50 °C, 6.5 °C/min to 80 °C, and finally 15 °C/min to 180 °C, for a total run time of 17 min.

Peak identification was carried out using three spectral libraries (Nist11, Nist11b, and FFNSC2), applying a similarity threshold > 90% for compound attribution. The results provided a detailed VOC profile released from the dough samples, allowing a direct comparison with the MOS sensor data.

### 5.2.6 Data Analysis and Statistical Processing

To distinguish between different flour types and leavening phases, multivariate statistical techniques were applied. Linear Discriminant Analysis (LDA) was performed using normalized sensor responses as input variables [31]. The goal of the model was to maximize variance between classes (PRE- and POST-leavening) while minimizing within-class variance.

Sensor response data, expressed as resistance variations, were transmitted to the Microsoft Azure cloud platform and subsequently processed. Figures 3A–C show the dynamic profiles of the three sensors composing the array: sensor 1 ($SnO_2$), sensor 2 ($SnO_2$ + Pd), and sensor 3 ($SnO_2$ + Au). This separation allowed a clearer visualization of the individual sensor behavior over time.

The pre-processed data were then analyzed through LDA, a technique capable of highlighting group separation by emphasizing inter-class differences and reducing intra-class variability. Statistical processing was carried out in MATLAB R2019b (MathWorks, Natick, MA, USA). To ensure consistency, raw responses were normalized to the initial value ($R_0$). For each sensor, the change between the initial resistance and the minimum value recorded during measurement was calculated. The $R/R_0$ ratio and corresponding standard deviation were computed across all 10 measurement cycles, with a maximum accepted uncertainty of 10%.

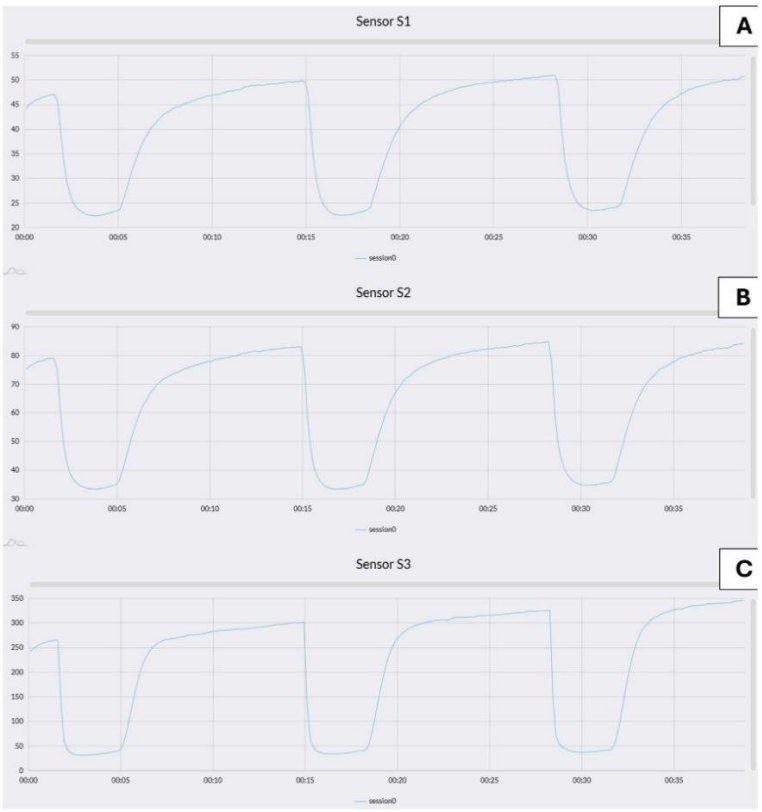


**Figure 3.** Response curves of the three sensing elements included in the MOS sensor array: (A) $SnO_2$ (sensor 1), (B) $SnO_2$ + Pd (sensor 2), and (C) $SnO_2$ + Au (sensor 3). Each graph shows the electrical resistance (Ω) on the y-axis as a function of time (s) on the x-axis. This curve represents the response to 100 ppm ethanol, a typical fermentation byproduct. The signal profiles illustrate the sensor behavior during exposure to clean air followed by ethanol, highlighting the sensitivity and dynamic response of each material.

Feature extraction from the sensor signals (Table 3) included parameters such as minimum and maximum derivative, integral of the response curve, peak response intensity (ΔR), and signal-to-noise ratio. A supervised feature selection process identified the most relevant variables for each sensor using a random forest classifier.

The selected features comprised: the meaning of the last 60 recorded values, the overall mean, the minimum response value, the integral of the signal (calculated using Simpson's rule), the difference between the mean of the first five and last five recorded values, the maximum response value, and ΔR (the difference between maximum and minimum resistance). These variables were used to enhance class discrimination, improving the model's performance in distinguishing between flour types and leavening stages.

**Table 3.** Overview of the extracted statistical and dynamic features used to characterize the sensor signals. LDA classification models were trained using leave-one-out cross-validation, and 2D/3D scatter plots were

generated to visualize group separation. These analyses demonstrated the effectiveness of the S3+ device in discriminating between dough types and leavening stages based on VOC profiles. To manage potential outliers, a threshold was set at three times the standard deviation (corresponding to a 99.7% confidence level).

| Features | Description |
|---|---|
| Sharpe Forward 25% | Variability index equivalent to the ratio between the mean and the standard deviation, calculated from the beginning of the signal to 25% of it. |
| Sharpe Back 25% | Variability index equivalent to the ratio between the mean and the standard deviation, calculated from the end of the signal to 25% of it. |
| Sharpe Forward 50% | Variability index equivalent to the ratio between the mean and the standard deviation, calculated from the beginning of the signal to 50% of it. |
| Sharpe Back 50% | Variability index equivalent to the ratio between the mean and the standard deviation, calculated from the end of the signal to 50% of it. |
| Minimum derivative | Calculation of the minimum derivative of the function in the selected interval. |
| Maximum derivative | Calculation of the maximum derivative of the function in the selected interval. |
| Integral | Calculation of the integral of the function in the selected interval. |
| ΔR | Often called excursion range, this feature represents the difference between the maximum and minimum values observed in the time series. |
| Logarithm of sum | The sum of the natural logarithm of the signal. |
| Minimum | The minimum value observed in the time series. |
| Maximum | The maximum value observed in the time series. |

## 5.3 RESULTS AND DISCUSSION

### 5.3.1 Evaluation of the Leavening Process through the Volatile Profiles of Different Doughs

Bakery products, characterized by a wide variety of types and regional variations, represent a key element in meeting diverse dietary preferences worldwide [32]. Product quality and consumer satisfaction largely depend on taste, aroma, and fragrance, which are strongly influenced by the leavening process—crucial to ensuring consistency in the final product. A mixture of more than 500 volatile organic compounds (VOCs), including alcohols, aldehydes, esters, fatty acids, ketones, lactones, phenols, and sulphur-containing compounds [33; 34], contributes to the formation of the aroma profile. These compounds originate both from the raw materials and as metabolic byproducts produced during leavening by microorganisms (e.g., yeasts and fungi) through catabolic processes such as glycolysis, proteolysis, and lipolysis [35].

Fermentation is therefore closely linked to the formation of volatile compounds, whose concentrations vary according to the stage of the process. As a result, the dough exhibits significant differences between the pre-leavening (PRE) phase—before fermentation—and the post-leavening (POST) phase, considered a critical stage for the development of sensory attributes [36]. Literature reports that the total amount of VOCs tends to progressively increase as leavening proceeds [37; 38]. An optimal fermentation time promotes gas retention and the expansion of the gluten network, improving dough elasticity and texture—key factors in achieving high-quality baked products.

In this study, the leavening time was set at 1.5 h, corresponding to the average duration used in household mixers. The results are consistent with those reported by Cao et al. (2020) [39], who observed that steamed breads fermented for 60–75 minutes exhibited higher specific volume and softer texture.

The leavening process is strongly influenced by environmental factors such as temperature, humidity, and the type and amount of leavening agent. In the present experimental setup, fermentation was carried out at room temperature (~22 °C) without active humidity regulation or heating. Despite these uncontrolled conditions, the system reliably monitored dough evolution through VOC analysis. The integration of the S3+ device with artificial intelligence algorithms enables assessment of the leavening state even in the absence of active environmental control. Properly trained machine learning models, based on large and heterogeneous datasets, can distinguish between fluctuations caused by external factors and real variations related to fermentation, thereby improving predictive robustness and assessment reliability.

A dynamic approach—based on the temporal evolution of volatile profiles rather than static PRE/POST measurements—further enhanced system reliability. Continuous VOC analysis enables real-time monitoring of the dough's chemical evolution: although absolute values may be affected by temperature and humidity, the shape and rate of change of the signal curves provide more robust information on the leavening state.

From a biological and compositional perspective, VOC production is closely linked to yeast (*Saccharomyces cerevisiae*) activity, which metabolizes dough sugars to produce ethanol and carbon dioxide through alcoholic fermentation [40]. This process not only contributes to the formation of the gluten structure but also leads to the synthesis of secondary aromatic compounds [41]. To ensure reproducibility and reduce testing time, commercial dehydrated yeast was used in the quantities specified by the recipe, depending on the flour type.

The quality of bakery products largely depends on the type of flour used [42]. Chemical, physical, and sensory properties—such as texture, volume, and aroma—are influenced by flour characteristics, with a direct impact on product recognizability and consumer acceptance [43]. Previous studies have shown that flour plays a more decisive role than other factors, such as fermentation temperature or starter origin, in determining acidity and overall bread characteristics [44]. Differences in flour composition involve not only starch but also proteins (gluten), non-starch polysaccharides, and lipids, which indirectly influence aroma development through their interactions with microbial fermentation processes [45; 46].

### 5.3.1.1 VOCs Analysis by MOS-Sensors (e-Nose)

To evaluate the capability of the S3+ device equipped with MOS gas sensors in discriminating dough samples based on their volatile organic compound (VOC) emission during fermentation, Linear Discriminant Analysis was employed. The analysis was performed both continuously over the entire leavening process and in discrete PRE and POST phases. In the continuous monitoring (2D LDA), doughs made from flours of different strength levels (W200, W250, and W390) were compared, while the 3D LDA models were applied to investigate the separation between PRE- and POST-leavening conditions within each flour type. The 2D LDA plot for the continuous analysis (Figure 4) demonstrates a clear separation among the three flour types during the leavening process. The clusters corresponding to CONTINUOUS_W200, CONTINUOUS_W250, and CONTINUOUS_W390 are distinctly located in separate regions of the LDA space, confirming the ability of the sensor array to differentiate between doughs of varying rheological properties based on their VOC emission dynamics over time. In particular, the W200 and W250 doughs form tightly clustered and non-overlapping groups, suggesting consistent and distinguishable VOC profiles over time. Notably, the CONTINUOUS_W390 cluster occupies a well-separated area in the LDA space, indicating that the sensor system is sensitive enough to detect differences in fermentation kinetics and metabolite release attributable to the increased gluten strength and higher gas-retention properties of stronger flours. These findings are consistent with previous studies indicating that flour strength significantly influences the release of VOCs during fermentation due to variations in water absorption, gluten network development, and sugar availability.

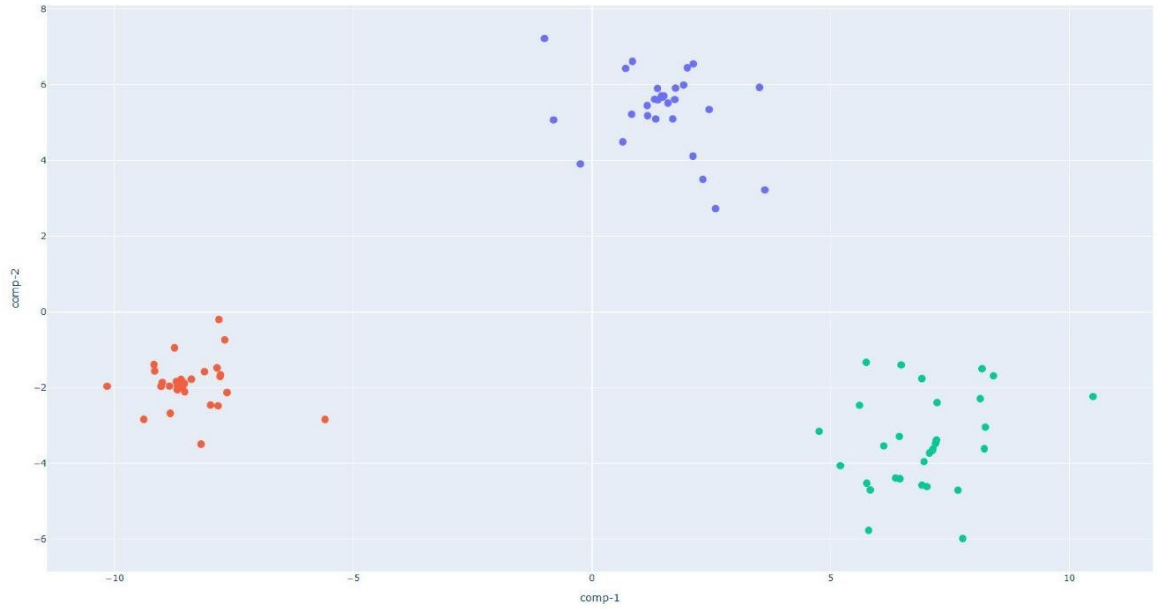


**Figure 4.** Two-dimensional Linear Discriminant Analysis (LDA) of continuously monitored dough samples during leavening, prepared with W200 (red), W250 (green), and W390 (blue) flours.

The 3D LDA analysis of PRE and POST conditions confirmed the discriminating power of the MOS sensor array in identifying the leavening progress within each flour type.

In the case of the W390 flour (Figure 5), the separation between PRE_W390 and POST_W390 is particularly evident along the first two discriminant components. The two groups form compact and distinct clusters, indicating significant differences in VOC composition before and after fermentation. This behavior reflects the high gas-retention capacity and slower fermentation kinetics of strong flours, leading to the development of well-defined metabolic profiles as fermentation progresses.

For the W250 flour (Figure 6), the separation is also clear, although the clusters appear slightly more dispersed compared to W390. The two phases remain non-overlapping, indicating a marked evolution of the volatile fingerprint during fermentation but with greater heterogeneity. This is consistent with the intermediate strength of this flour, which provides a good balance between elasticity and extensibility, resulting in adequate structural development but a less tightly controlled VOC dynamic compared to W390.

The W200 flour sample (Figure 7) shows the highest intra-class variance, with a wider distribution of PRE and POST clusters. This dispersion can be attributed to the intrinsic variability of weak flours, characterized by a lower gluten content and reduced gas-retention capacity. Such conditions lead to less uniform fermentation and a more variable VOC emission. Nonetheless, the distinction between the two phases remains evident. The higher heterogeneity aligns with previous literature reports, which describe weak flours as exhibiting a faster fermentation onset but a less stable leavening behavior, with VOC production particularly sensitive to environmental factors such as humidity and temperature [47].

The clusters observed in the LDA plots reflect differences in the overall composition of VOCs emitted during fermentation. Although MOS sensors are not compound-specific, they generate distinct response patterns depending on the concentration and mixture of volatile compounds. Processing these response patterns through LDA enables the spatial separation of flour types and leavening stages. Data obtained through GC-MS confirmed that variations in VOC classes—such as alkanes, alcohols, esters, and acids—contribute to this discrimination, thereby reinforcing the robustness of the sensor–LDA system in describing the complex aromatic evolution occurring during fermentation.

Overall, the 3D LDA results validate the sensitivity of the MOS-based e-nose system in detecting phase transitions (from PRE- to POST-leavening) and in discriminating between different flour types—not only based on their intrinsic chemical profiles but also through the temporal evolution of their VOC emissions. The combination of real-time monitoring and multivariate analysis confirms that electronic noses, when properly trained and integrated into household appliances, represent robust tools for quality control and process automation in the food industry. Moreover, the non-

invasive nature of the system enables continuous monitoring without compromising dough integrity—an essential feature for real-time applications in both domestic and industrial settings.

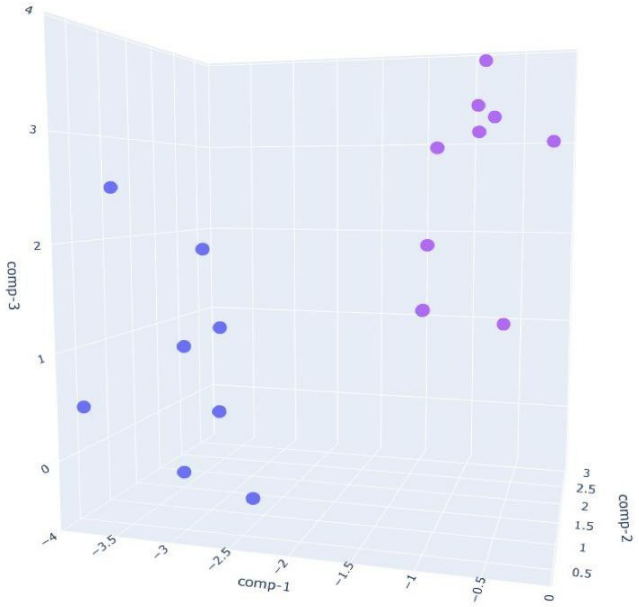


**Figure 5.** Three-dimensional Linear Discriminant Analysis (LDA) of dough samples prepared with W390 flour in PRE (purple)- and POST (blue)-leavening phases.

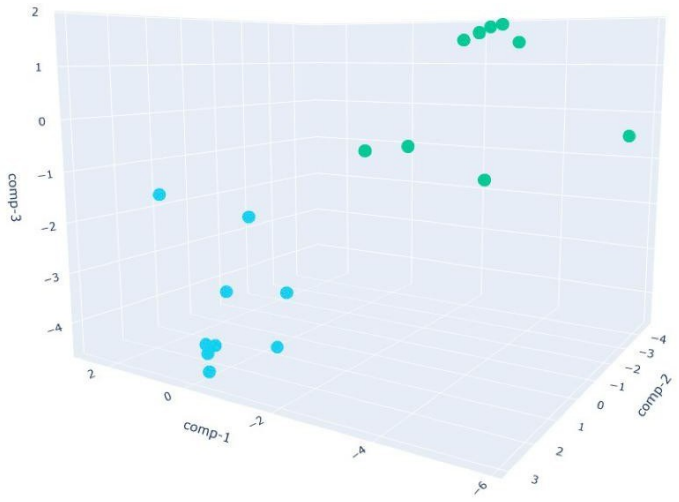


**Figure 6.** Three-dimensional Linear Discriminant Analysis (LDA) of dough samples prepared with W250 flour in PRE (cyan)- and POST (green)-leavening phases.

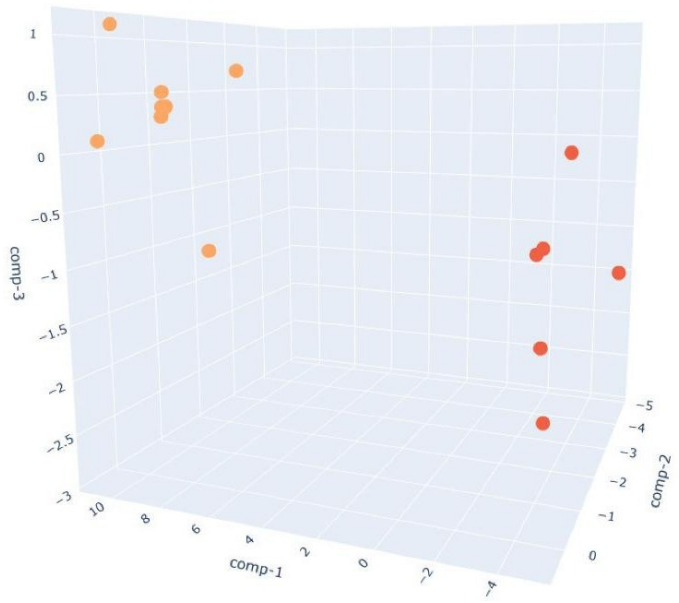


**Figure 7.** Three-dimensional Linear Discriminant Analysis (LDA) of dough samples prepared with W200 flour in PRE (orange)- and POST (red)-leavening phases. LDA clustering reflects VOC mixture variations; each cluster position correlates specific patterns of VOCs, as confirmed by the GC-MS analysis.

### 5.3.1.2 VOC Detection by SPME-GC-MS

In this study, the conventional SPME-GC-MS method was employed for the qualitative and quantitative analysis of the volatile profiles of three types of dough, prepared with flours of different strength levels, before and after leavening. This analysis enabled the determination of VOC concentrations and the identification of individual compounds, with the aim of providing a comparative assessment against the S3+ device.

Across all analyzed dough samples, a total of 108 different volatile compounds were identified, primarily belonging to the following chemical classes (in decreasing order of abundance): alkanes, alcohols, esters, carboxylic acids, alkenes, and aldehydes. Compounds such as ketones, ethers, amines, alkynes, and nitriles were detected only in trace amounts. Specifically, 72 VOCs were identified in the pre-leavening phase and 70 in the post-leavening phase, with 34 compounds common to both stages, 38 unique to the PRE phase, and 36 unique to the POST phase.

These results indicate that, while the total number of VOCs remained similar between the two conditions, significant qualitative differences were observed in their composition before and after leavening. Figure 8 illustrates the main chemical classes of VOCs detected in the three different doughs during the two analyzed phases.

Among the identified classes, alkanes (hydrocarbons) were the most abundant volatiles, representing the largest group compared to other chemical compounds. Notably, the number of alkanes remained constant in the PRE-leavening samples of W250 and in the POST-leavening samples of W250 and

W390. Conversely, the dough made with W390 flour exhibited alkanes only in the PRE phase, whereas the W200 dough showed a variable number of alkanes under both conditions (14, 17, and 12, respectively).

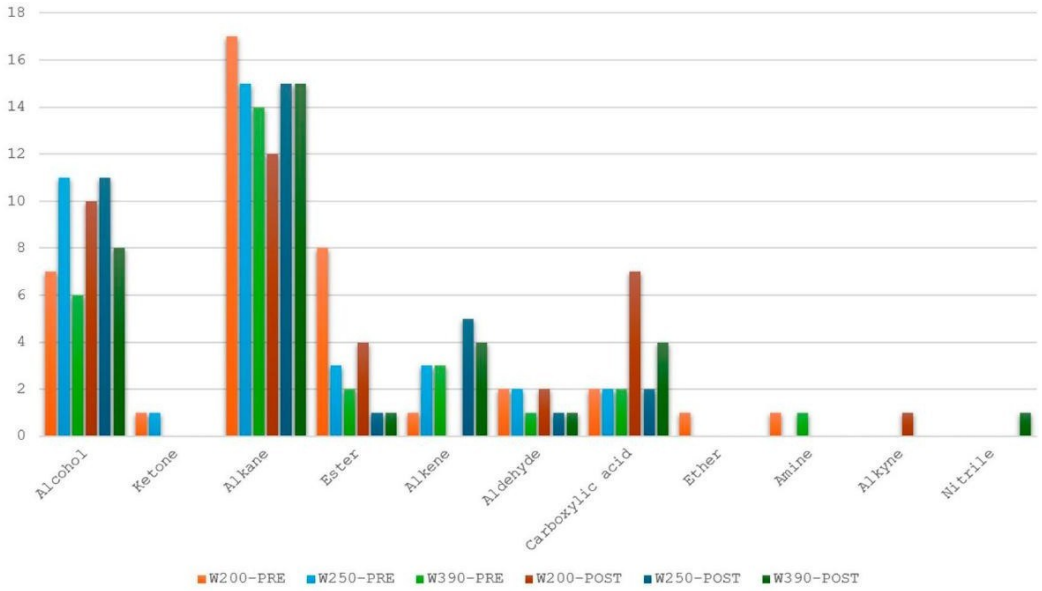


**Figure 8.** Number of compounds (y-axis) divided into chemical classes (x-axis) present in PRE- and POST-leavening doughs made with flours W200, W250, and W390.

Our results (Figures 9, 10, and 11) revealed significant differences not only between the pre- and post-leavening phases but also among the three types of dough analyzed (W200, W250, and W390). Specifically, several compounds were detected exclusively in one of the two phases or in specific flour types. For instance, in W200 samples, compounds such as 2,3,5-trimethyl-decane, 4-methyl-dodecane, and 2,6-dimethyl-octane were identified only in the PRE phase, whereas tetracosane was found exclusively in W390. Conversely, in the POST phase, 5,5-diethyl-heptadecane, 6-methyl-tridecane, and 5-butyl-nonane were detected in W200, 3-methyl-5-propyl-nonane in W250, and 3,8-dimethyl-decane and 7-methyl-heptadecane in W390, among others.

Some compounds, such as decane, were detected exclusively in the PRE phase across all analyzed conditions. The presence of decane only during the initial stage suggests that this compound originates from primary chemical reactions occurring before the onset of active fermentation; later, the chemical and enzymatic transformations characteristic of fermentation no longer favor its production or persistence.

The GC-MS data therefore confirms the ability to discriminate doughs based on both fermentation phase (PRE vs. POST) and flour strength, supporting the results obtained through e-nose analysis. It was observed that flour strength influences not only the structural properties of the dough but also its volatile composition, modulating fermentation dynamics and the formation of aromatic precursors.

In agreement with the literature, alkanes represent the most abundant chemical class detected during sourdough fermentation, followed by esters, alcohols, ketones, aldehydes, and sulphur compounds [48]. Hydrocarbons also constitute the most common volatiles in traditional cereal-based fermented foods, such as the Kurdish *Tarkhineh*—a product derived from bulgur and *doogh* [49; 50] and are generally predominant in the cereal raw materials themselves, formed mainly through decarboxylation and carbon–carbon bond cleavage of long-chain fatty acids.

Although alkanes exhibit high odor thresholds and contribute minimally to the direct aroma profile [51; 52], previous studies indicate that they may still influence the overall aromatic characteristics, particularly when combined with more odor-active compounds such as aldehydes, esters, and alcohols [53]. Therefore, while not considered primary sensory markers, hydrocarbons can indirectly modulate the final aroma of baked goods, acting as background components within a more complex volatile bouquet.

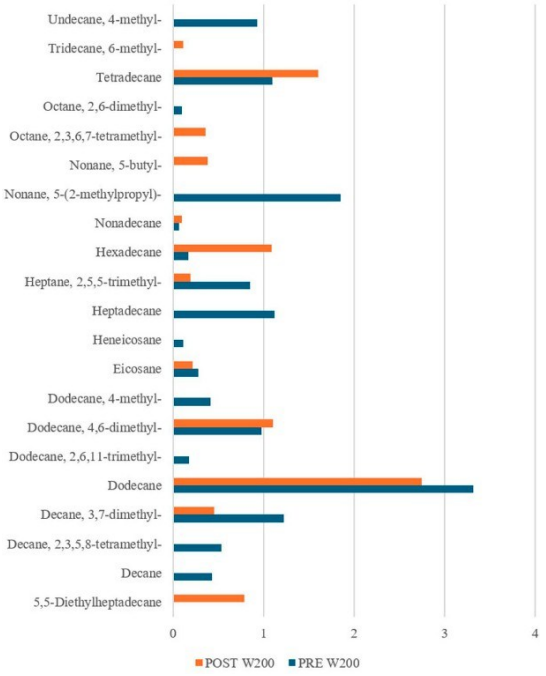


**Figure 9.** Alkane Compounds in dough samples made with flour of W200, PRE- (blue bars) and POST-leavening (orange bars).

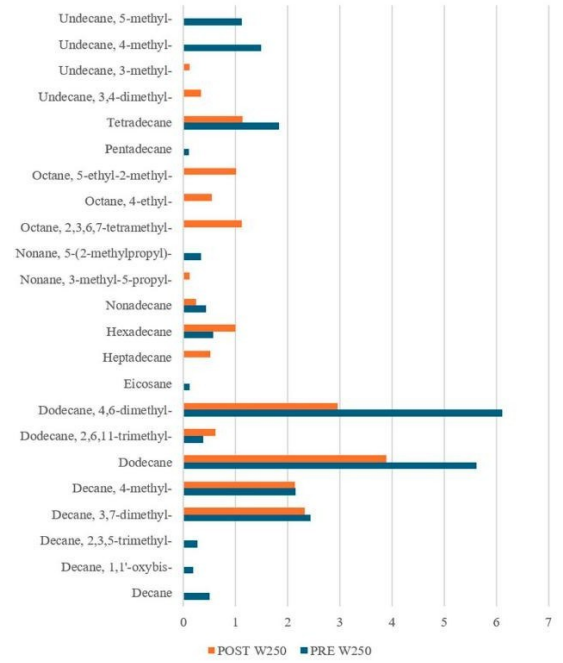


**Figure 10.** Alkane Compounds in dough samples made with flour of W250, PRE- (blue bars) and POST-leavening (orange bars).

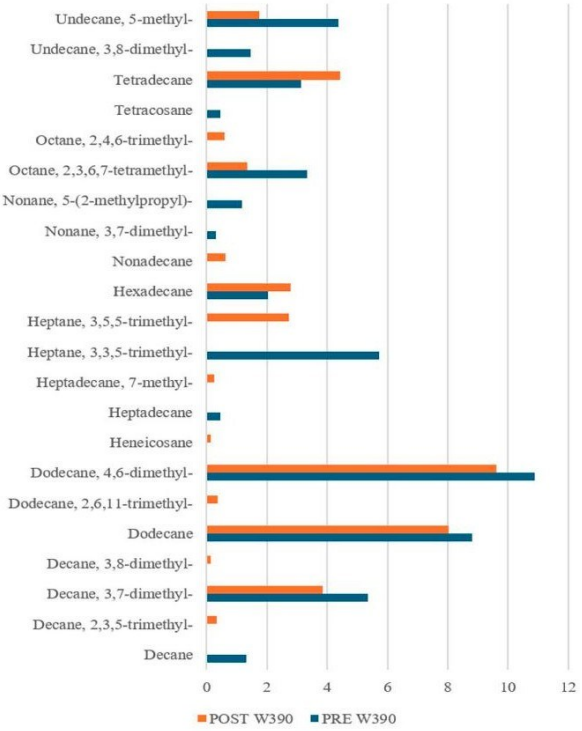


**Figure 11.** Alkane Compounds in dough samples made with flour of W390, PRE- (blue bars) and POST-leavening (orange bars).

Alcohols, aldehydes, ketones, and carboxylic acids are fermented metabolites derived from catabolic reactions such as deamination, decarboxylation, and transamination, and they play a crucial role in shaping the sensory characteristics of bakery products [54]. In our samples, alcohols

represented the second most abundant chemical class. An increase in the number of alcohols was observed between the PRE- and POST-leavening phases in doughs made with W200 and W390 flours, whereas no variation was detected for W250.

During fermentation, the yeast *Saccharomyces cerevisiae* degrades dough sugars and carbohydrates, primarily producing carbon dioxide ($CO_2$) and ethanol [55], which are responsible, respectively, for dough leavening and gluten network expansion [56]. Although ethanol is a volatile compound, its sensory impact is less pronounced compared to secondary aromatic molecules formed as byproducts. Nevertheless, it significantly contributes to the texture and porosity of the final product, as it evaporates during baking (boiling point ≈ 78 °C). In our samples, at the end of fermentation, ethanol concentration was higher than at the beginning for all three doughs (W200, W250, and W390).

Other alcohol compounds, such as 1-hexanol, 2-isopropyl-5-methyl-1-heptanol, and 1-dodecanol, 3,7,11-trimethyl, showed similar or lower concentrations in the POST phase, likely due to combined effects of microbial metabolism, volatilization, oxidation, or entrapment within the expanding gluten matrix. As reported in the literature [57], differential alcohol production may be linked to amino acid catabolism through the Ehrlich pathway, which leads to the formation of aldehydes or their corresponding alcohols. Fermentation temperature also affects the VOC profile: at 35 °C, an increase in aldehydes and esters and a relative decrease in alcohols were observed compared to fermentations conducted at 28 °C [58].

Like alkanes, certain alcohols were detected only under specific conditions. For example, 1-nonanol, 4,8-dimethyl was present in the PRE phase of W200 and W250 but not in W390; 1-nonanol and 2-decanol appeared in POST-W200; 1-undecanol in POST-W250; and 1-hexadecanol, 3,7,11,15-tetramethyl was detected exclusively in POST-W390. These alcohols generally contribute to fresh and fruity notes, except for the latter, which is associated with waxy and fatty nuances.

Regarding aldehydes, their presence was limited and slightly higher in PRE samples compared to POST, consistent with their conversion into alcohols and acids during fermentation [59]. Previous studies have confirmed the relative stability of aldehyde content in *S. cerevisiae*-based doughs [60]. The low concentrations observed are responsible for fresh and slightly grassy notes.

Ketones were detected at very low levels, present only in two PRE samples, except for 2,3-butanedione, which has been previously reported as a key fermentation metabolite. Acids showed low and constant levels before leaving but increased during the POST phase, except in the W250 dough. Eicosanoic acid was more abundant or exclusive in PRE samples, while stearic acid increased

in POST. These results are consistent with findings by Tasan (2003) [61], who reported that dough fermentation does not substantially alter fatty acid composition, which instead undergoes more significant changes after baking.

Finally, esters, while showing a numerical decrease after fermentation, exhibited selective increases in certain compounds (e.g., propyl octadecanoate, hexyl octyl sulphite), which were found at higher concentrations at the end of leavening. In agreement with literature reports, acids and esters tend to emerge mainly in the final stages of the process, contributing decisively to the aromatic differences between fermented and unfermented doughs.

## 5.4 CONCLUSIONS

In recent years, the food industry has increasingly embraced the Food Processing 4.0 paradigm, based on the integration of robotics, smart sensors, AI, IoT, and Big Data into production processes. In this context, the S3+ device, equipped with MOS nanosensors, proved to be highly effective for monitoring dough leavening. The system successfully discriminated against both fermentation stages (PRE vs. POST) and different flour types (W200, W250, W390), with LDA analysis confirming clear clustering of volatile profiles. Validation through GC-MS supported these findings, identifying over 100 volatile compounds and confirming the system's ability to detect key differences.

The integration of real-time monitoring with multivariate analysis demonstrates that electronic noses, once trained and embedded in kitchen appliances, can serve as intelligent tools for leavening control and quality assurance. Looking ahead, devices like S3+ could evolve into closed-loop systems, capable not only of monitoring but also of managing the process through integrated artificial intelligence modules and classification models. This would enable dynamic regulation of parameters such as time and temperature based on sensor feedback, ensuring consistent results, reducing waste, and supporting sustainable and reproducible baking, both in domestic and industrial contexts.

## 5.5 BIBLIOGRAPHY


1. Hassoun, A.; Jagtap, S.; Trollman, H.; Garcia-Garcia, G.; Abdullah, N.A.; Goksen, G.; Bader, F.; Ozogul, F.; Barba, F.J.; Cropotova, J.; et al. Food processing 4.0: Current and future developments spurred by the fourth industrial revolution. Food Control 2023, 145, 109507.
2. Huang, J.; Zhang, M.; Mujumdar, A.S.; Li, C. AI-based processing of future prepared foods: Progress and prospects. Int. Food Res. 2025, 201, 115675. [PubMed]
3. Da Costa, T.P.; Gillespie, J.; Cama-Moncunill, X.; Ward, S.; Condell, J.; Ramanathan, R.; Murphy, F. A systematic review of real-time monitoring technologies and its potential

application to reduce food loss and waste: Key elements of food supply chains and IoT technologies. Sustainability 2023, 15, 614.

4. Javaid, M.; Haleem, A.; Singh, R.P.; Rab, S.; Suman, R. Significance of sensors for Industry 4.0: Roles, capabilities, and applications. Sens. Int. 2021, 2, 100110.
5. Saeed, R.; Glamuzina, B.; Thi Tuyet Nga, M.; Zhao, F.; Zhang, X. Supervised learning-based artificial senses for non-destructive fish quality classification. Biosensors 2025, 13, 116770.
6. Alvarado, V.L.S.; Diaz, F.J.; Parra, L.; Lloret, J.; Aldana, C.; Saavedra, Y. Proposal for a gas sensor device to classify hydrobiological species and estimate non-refrigeration time. IEEE Sens. J. 2025, 23, in press.
7. Poeta, E.; Liboà, A.; Mistrali, S.; Núñez-Carmona, E.; Sberveglieri, V. Nanotechnology and e-sensing for food chain quality and safety. Sensors 2023, 23, 8429.
8. Krishna, K.G.; Parne, S.; Pothukanuri, N.; Kathirvelu, V.; Gandi, S.; Joshi, D. Nanostructured metal oxide semiconductor-based gas sensors: A comprehensive review. Sens. Actuators A Phys. 2022, 341, 113578.
9. Adamek, M.; Zvonkova, M.; Buresova, I.; Buran, M.; Sevcikova, V.; Sebestikova, R.; Adamkova, A.; Skowronkova, N.; Mlcek, J. Use of a thermodynamic sensor in monitoring fermentation processes in gluten-free dough proofing. Sensors 2023, 23, 534.
10. Toska, D.; Pulla, A.; Robustelli, S.; Fiamma, G. Leavening control system based on machine learning techniques. In Proceedings of the 7th World Forum on Internet of Things, New Orleans, LA, USA, 14 June–31 July 2021.
11. Skaf, A.; Nassar, G.; Lefebvre, F.; Nongaillard, B. A new acoustic technique to monitor bread dough during the fermentation phase. J. Food Eng. 2009, 93, 365–378.
12. Romano, A.; Toraldo, G.; Cavella, S.; Masi, P. Description of leavening of bread dough with mathematical modelling. J. Food Eng. 2007, 83, 142–148.
13. De Wijk, R.A.; Smeets, P.A.M.; Polet, I.A.; Holthuysen, N.T.E.; Zoon, J.; Vingerhoeds, M.H. Aroma effects on food choice task behavior and brain responses to bakery food product cues. Food Qual. Prefer. 2018, 68, 304–314.
14. Akbari, G.A.; Shehzad, A.; Khan, M.R.; Shabbir, M.A.; Amjid, M.R. Yeast, its types and role in fermentation during bread making process—A review. Pak. J. Food Sci. 2012, 22, 171–179.
15. Mesta-Corral, M.; Gomez-Garcia, R.; Balagurusamy, N.; Torres-Leon, C.; Hernandez-Almanza, A.Y. Technological and nutritional aspects of bread production: An overview of current status and future challenges. Foods 2024, 13, 2062.

16. Yang, Y.; Zhao, X.; Wang, R. Research progress on the formation mechanism and detection technology of bread flavor. J. Food Sci. 2022, 87, 3724–3736.
17. Sharma, R.; Garg, P.; Kumar, P.; Bhatia, S.K.; Kulshrestha, S. Microbial fermentation and its role in quality improvement of fermented foods. Fermentation 2020, 6, 106.
18. Liszkowska, W.; Berlowska, J. Yeast fermentation at low temperatures: Adaptation to changing environmental conditions and formation of volatile compounds. Molecules 2021, 26, 1035.
19. Petel, C.; Onno, B.; Prost, C. Sourdough volatile compounds and their contribution to bread: A review. Trends Food Sci. Technol. 2017, 59, 105–123.
20. Lai, H.; Lin, T. Bakery Products: Science and Technology; Bak. Prod. Sci. Technol.: 2006; 3, 65.
21. Chen, J.; Pu, D.; Cao, B.; Sun, B.; Zhang, Y. Effect of temperature and water addition ratio on the aroma release of yeast proteins. Foods 2025, 14, 1037. [PubMed]
22. Aplevicz, K.S.; Ogliari, P.J.; Sant'Anna, E.S. Influence of fermentation time on characteristics of sourdough bread. Braz. J. Pharm. Sci. 2013, 49, 233–239.
23. Khromeenkov, V.M. Technology of Long-Term Fermentation of Dough; Confectionery and Bakery Production: Mumbai, India, 2017; Volume 3, pp. 30–32.
24. Temieva, K.A.; Sheveleva, G.I.; Grigorieva, R.Z. The influence of baking methods on the quality of bakery products. In Food Innovations in Biotechnology: Materials of the VI International Scientific Conference of Students, Postgraduates and Young Scientists; A.Y. Prosekov, Ed.; Kemerovo State University: Kemerovo, Russia, 2018; Volume 2, pp. 274–275.
25. Makhoul, S.; Romano, A.; Cappellin, L.; Spano, G.; Capozzi, V.; Aprea, E.; Benozzi, E.; Mark, T.D.; Gasperi, F.; El Nakat, H.; et al. Volatile compound production during the bread-making process: Effect of flour, yeast and their interaction. Food Bioprocess Technol. 2015, 8, 1925–1937.
26. Tebben, L.; Shen, Y.; Li, Y. Improvers and functional ingredients in whole wheat bread: A review of their effects on dough properties and bread quality. Trends Food Sci. Technol. 2018, 81, 10–24.
27. Sberveglieri, V.; Bhandari, M.P.; Núñez Carmona, E.; Betto, G.; Sberveglieri, G. A novel MOS nanowire gas sensor device (S3) and GC-MS-based approach for the characterization of grated Parmigiano Reggiano cheese. Biosensors 2016, 6, 60.
28. Mariotti, R.; Núñez-Carmona, E.; Genzardi, D.; Pandolfi, S.; Sberveglieri, V.; Mousavi, S. Volatile olfactory profiles of Umbrian extra virgin olive oils and their discrimination through MOX chemical sensors. Sensors 2022, 22, 7164.

29. Genzardi, D.; Núñez Carmona, E.; Poeta, E.; Gai, F.; Caruso, I.; Fiorilla, E.; Schiavone, A.; Sberveglieri, V. Unraveling the chicken meat volatilome with nanostructured sensors: Impact of live and dehydrated insect larvae feeding. Sensors 2024, 24, 4921.
30. Sahner, K.; Schönauer, D.; Matam, M.; Post, M.; Moos, R. Selectivity enhancement of p-type semiconducting hydrocarbon sensors—The use of sol-precipitated nano-powders. Sens. Actuators B Chem. 2008, 130, 470–476.
31. Xanthopoulos, P.; Pardalos, P.M.; Trafalis, T.B. Linear Discriminant Analysis. In Robust Data Mining; SpringerBriefs in Optimization; Springer: New York, NY, USA, 2013.
32. Guiné, R.P.F. Textural properties of bakery products: A review of instrumental and sensory evaluation studies. Appl. Sci. 2022, 12, 8628.
33. Nicin, R.T.; Ozdemir, N.; Şimşek, O.; Con, A.H. Production of volatiles relation to bread aroma in flour-based fermentation with yeast. Food Chem. 2022, 378, 132125. [PubMed]
34. Pinu, F.R.; Villas-Boas, S.G. Rapid quantification of major volatile metabolites in fermented food and beverages using gas chromatography-mass spectrometry. Metabolites 2017, 7, 37.
35. Wang, B.; Xiao, L.; Chai, D.; Jiang, Y.; Wang, M.; Xu, X.; Li, C.; Dong, L. Metabolite analysis of wheat dough fermentation incorporated with buckwheat. Food Sci. Nutr. 2020, 8, 4242–4251.
36. Galoburda, R.; Straumite, E.; Sabovics, M.; Kruma, Z. Dynamics of volatile compounds in triticale bread with sourdough: From flour to bread. Foods 2020, 9, 1837.
37. Sabovics, M.; Straumite, E.; Galoburda, R. Detection of volatile compounds during wheat dough fermentation. Food Chem. 2017, 1, 93–99.
38. Wang, H.; Han, P.; Zhang, P.; Li, Y. Influence of yeast concentrations and fermentation durations on the physical properties of white bread. LWT-Food Sci. Technol. 2024, 19, 116063.
39. Cao, Y.; Zhang, H.; Yang, Z.; Zhang, M.; Guo, P.; Li, H. Influence of the fermentation time and potato pulp addition on the technological properties and volatile compounds of wheat dough and steamed bread. LWT-Food Sci. Technol. 2020, 128, 10937.
40. Zhang, G.; Sun, Y.; Sadiq, F.A.; Sakandar, H.A.; He, G. Evaluation of the effect of Saccharomyces cerevisiae on fermentation characteristics and volatile compounds of sourdough. J. Food Sci. Technol. 2018, 55, 2079–2086.
41. Troadec, R.; Regnault, S.; Nestora, S.; Jacolot, P.; Niquet Leridon, C.; Anton, P.M.; Jouquand, C. Effect of fermentation conditions of bread dough on the sensory and nutritional properties of French bread. Eur. Food Res. Technol. 2023, 249, 2749–2762.

42. Annett, L.E.; Spaner, D.; Wismer, W.V. Sensory profiles of bread made from paired samples of organic and conventionally grown wheat grain. J. Food Sci. 2007, 72, S254–S260. [PubMed]
43. Heinio, R.L. Sensory attributes of bakery products. In Bakery Products Science and Technology; Wiley-Blackwell: Hoboken, NJ, USA, 2014.
44. Salovaara, H.; Valjakka, T. The effect of fermentation temperature, flour type, and starter on the properties of sour wheat bread. Int. J. Food Sci. Technol. 1987, 22, 591–597.
45. Starr, G.; Petersen, M.A.; Jespersen, B.M.; Hansen, A.S. Variation of volatile compounds among wheat varieties and landraces. Food Chem. 2015, 174, 527–537.
46. Goesaert, H.; Brijs, K.; Veraverbeke, W.S.; Courtin, C.; Gebruers, K.; Delcour, J. Wheat flour constituents: How they impact bread quality and how to impact their functionality. Trends Food Sci. Technol. 2005, 16, 12–30.
47. Nor Qhairul Izzreen, M.N.; Petersen, M.A.; Hansen, Å.S. Volatile compounds in crumb of whole-meal wheat bread fermented with different yeast levels and fermentation temperatures. Cereal Chem. 2016, 93, 209–216.
48. Lutter, L.; Jõudu, I.; Andreson, H. Volatile organic compounds and their generation in sourdough. Agron. Res. 2023, 21, 504–536.
49. Mohammadi, N.; Ostovar, N. Chemical composition, fatty acid composition, volatile compounds of a traditional Kurdish fermented cereal food: Tarkhineh. Food Chem. Adv. 2023, 2, 100187.
50. Liu, J.; Li, S.; Zhang, A.; Zhao, W.; Liu, Y.; Zhang, Y. Volatile profiles of 13 foxtail millet commercial cultivars (Setaria italica Beauv.) from China. Cereal Chem. 2017, 94, 170–176.
51. Pizarro, F.; Franco, F. Volatile organic compounds at early stages of sourdough preparation via static headspace and GC/MS analysis. Curr. Res. Nutr. 2017, 5, 89–99.
52. Fan, H.; Zheng, X.; Ai, Z.; Liu, C.; Li, R.; Bian, K. Analysis of volatile aroma components from Mantou fermented by different starters. Food Process. Preserv. 2018, 42, 13627.
53. Hao, Y.; Wang, Z.; Zou, Y.; He, R.; Ju, X.; Yuan, J. Effect of static-state fermentation on volatile composition in rapeseed meal. J. Sci. Food Agric. 2020, 100, 2145–2152. [PubMed]
54. Cai, L.; Cao, M.; Cao, A.; Zhang, W. The effect of magnetic nanoparticles plus microwave thawing on the volatile flavor characteristics of largemouth bass (Micropterus salmoides) fillets. Food Bioprocess Technol. 2019, 12, 1340–1351.
55. Kieronczyk, A.; Skeie, S.; Olsen, K.; Langsrud, T. Metabolism of amino acids by resting cells of non-starter lactobacilli in relation to flavour development in cheese. Int. Dairy J. 2001, 11, 217–224.

56. Maicas, S. The role of yeasts in fermentation processes. Microorganisms 2020, 8, 1142.
57. Parapouli, M.; Vasileiadis, A.; Afendra, A.S.; Hatziloukas, E. Saccharomyces cerevisiae and its industrial applications. AIMS Microbiol. 2020, 6, 1–31.
58. Dzialo, M.C.; Park, R.; Steensels, J.; Lievens, B.; Verstrepen, K.J. Physiology, ecology and industrial applications of aroma formation in yeast. FEMS Microbiol. 2017, 1, 128.
59. Hansen, A.S.; Schieberle, P. Generation of aroma compounds during sourdough fermentation: Applied and fundamental aspects. Trends Food Sci. Technol. 2005, 16, 85–94.
60. Siepmann, F.B.; Sousa de Almeida, B.; Waszczynskyj, N.; Spier, M.R. Influence of temperature and of starter culture on biochemical characteristics and the aromatic compounds evolution on type II sourdough and wheat bread. LWT 2019, 108, 199–206.
61. Tasan, M. Fatty acid composition of traditional fermented and unfermented Turkish corn bread with the emphasis on trans fatty acids. Eur. Food Res. Technol. 2003, 217, 125–127.

# 6.

# MONITORING THE OLFACTORY EVOLUTION OF COLD-FERMENTED SOURDOUGH USING AN ELECTRONIC NOSE

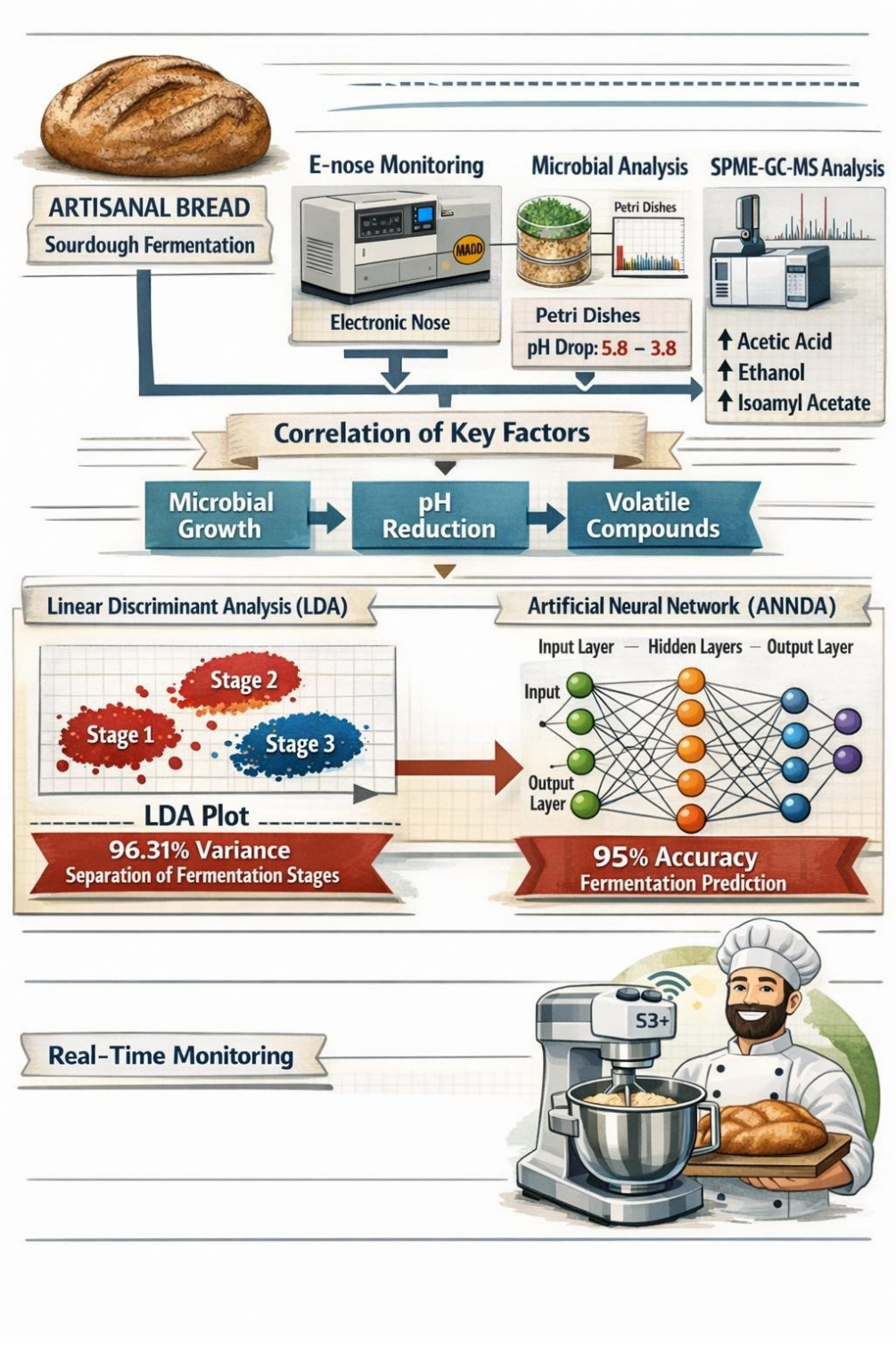

## 6.1 INTRODUCTION

As discussed in the previous chapter, fermentation represents a crucial stage in the production of baked goods, as it largely determines the structural, aromatic, and sensory characteristics of bread. Among the various types of fermentation, sourdough fermentation has attracted renewed scientific and industrial interest due to its complex microbial community and its ability to impart a distinctive aromatic profile, improved digestibility, and extended shelf life to the final product. In particular, cold fermentation is gaining attention as a slow process that enhances the development of complex aromas, reduces undesirable compounds such as FODMAPs and Phytic Acid, and promotes the formation of bioactive peptides with potential health benefits.

In this context, scientific research is increasingly moving toward multidisciplinary approaches that integrate microbiological, chemical, and engineering expertise to better understand and optimize fermentation dynamics. In continuity with the previous chapter, which explored the use of intelligent sensors and monitoring techniques based on the analysis of volatile compounds, this chapter focuses on the application of an electronic nose (E-nose) as an innovative tool for monitoring sourdough fermentation. Based on MOS sensor technology, the device enables real-time detection of volatile organic compounds (VOCs) released during the process, providing a rapid, non-invasive, and complementary analysis to conventional techniques such as SPME-GC-MS.

The integration of chemical, microbiological, and sensory data allows for a comprehensive understanding of the fermentation process, facilitating the identification of the optimal fermentation point and supporting the standardization and automation of quality control in baking. This approach represents a further step toward the Food Processing 4.0 paradigm, in which technological innovation is combined with the valorization of traditional practices to ensure high-quality, sustainable, and safe food products [1].

## 6.2 MATERIALS AND METHODS

To further investigate the specific characteristics of the samples, data obtained from the E-nose, gas chromatography, and microbiological analyses were compared. This integrated approach made it possible to assess the reliability and effectiveness of each technique in identifying chemical compounds and sensory attributes. The combination of the three methods provided a comprehensive understanding of the chemical and biological processes shaping the sensory properties of the samples, particularly regarding the formation and evolution of aromatic notes. Moreover, the integration of microbiological, chemical, and olfactory data clarified the interactions between microflora and volatile compounds during fermentation, highlighting their impact on the final aromatic profile. This

interdisciplinary strategy is applicable to several sectors—including breadmaking, fermented beverage production, and the broader food industry—where understanding sensory dynamics is fundamental to improving quality and standardization [2].

### 6.2.1 Experimental Design

All ingredients for dough preparation were provided by the artisanal bakery PanContigo S.L. (Badajoz, Spain). The formulation included a flour–water mixture (80%) inoculated with sourdough starter (20%, PIE). The flour–water mixture consisted of 50% flour and 50% water, using a blend of 25% whole meal flour and 25% high-protein flour, ensuring a balanced base suitable for fermentation.

The dough underwent cold fermentation at 5 °C. All samples were prepared using the same batch of sourdough and processed under identical conditions. Fermentations were conducted in parallel, and samples collected at 0 h served as the reference point for monitoring volatile compound evolution. To track fermentation progress, samples were collected for pH measurement, E-nose analysis, and microbiological evaluation. All analyses were performed under controlled laboratory conditions (20 ± 2 °C). E-nose measurements were conducted under a fume hood to avoid interference from external volatiles. Incubation temperatures were adjusted according to the analytical method: 25 °C for E-nose measurements, to simulate sensory conditions, and 37 °C for GC–MS, to promote volatile release. Since the study aimed to compare overall olfactory patterns rather than individual VOC behaviors, this temperature difference did not affect result validity.

For pH and microbiological analyses, at each fermentation time (0 h, 4 h, 20 h, and 24 h), 20 g samples were collected and analyzed in triplicate. For E-nose analysis, three 20 g samples per time point were analyzed, each undergoing six measurements—totaling 18 measurements per time point and 72 overall. E-nose data were randomly divided into two sets: 52 measurements for calibration and cross-validation, and 20 for external validation of the ANNDA model. For GC–MS analysis, at each selected time (0 h, 4 h, 8 h, 12 h, and 20 h), 20 g samples were taken from which three 2 g aliquots were placed in 20 mL vials equipped with PTFE/silicone septa.

### 6.2.2 Application of the Electronic Nose in the Evaluation of Artisanal Bread Quality

E-nose analysis provides an olfactory fingerprint representative of the volatile compounds emitted by the samples. This method excels in recognizing and differentiating aromatic features arising from the complex interactions among volatiles. The E-nose can detect a wide range of compounds responsible

for olfactory characteristics without requiring operator intervention, making it particularly suitable for rapid, repeatable, and non-invasive analyses.

The device used in this study was a custom-developed prototype, characterized by portability, energy efficiency, and Bluetooth connectivity through a dedicated mobile application. The system integrates five metal oxide semiconductor (MOS) sensors sourced from different manufacturers to ensure broad selectivity. The sensors feature a compact design combining analog and digital electronics, a micro-heating plate, and detection elements on a single chip. In addition to gas detection, the device includes auxiliary environmental sensors for measuring temperature, relative humidity, and atmospheric pressure [3].

A detailed description of the sensors employed is provided in Table 1.

**Table 1.** Sensors used for the E-nose device.

| Sensor | Production | Signals |
|---|---|---|
| BME680 | Bosch Sensortech Gmbh, Reutlingen, Germany | Temperature, Relative Humidity, Pressure, Resistance value (Ω) |
| SGP30 | Sensirion AG, Stafa, Switzerland | $CO_2$, TVOCs [1], $H_2$ (raw signal [2]), Ethanol (raw signal) |
| ZMOD4410 | Renesas Electronic Corporation, Tokyo, Japan | Ethanol (raw signal), resistance value (Ω), $CO_2$, TVOCs, IAQ [3] |
| CCS811 | ScioSense B.V., Eindhoven, The Netherlands | $CO_2$, TVOCs, resistance value |
| iAQ-Core | ScioSense, Eindhoven B.V., The Netherlands | $CO_2$ (ppm), TVOCs (ppb), and resistance value (Ω) |

[1] Total volatile organic compound. [2] Pre-processed signals from sensor resistance. [3] Indoor Air Quality.

The developed prototype features compact dimensions of 118 × 82 × 22.5 mm. The system is powered by a rechargeable lithium-ion battery (+3.7 VDC) and equipped with Bluetooth connectivity, enabling communication with a dedicated mobile application for device control and configuration. The architecture integrates a pump and a solenoid valve used for sampling the gaseous headspace of the analyzed specimens.

The total power consumption of the device is 684 mW, while the sensors provide a response time of approximately two seconds. Figure 1 shows an image of the prototype alongside the electronic board of the electronic nose.

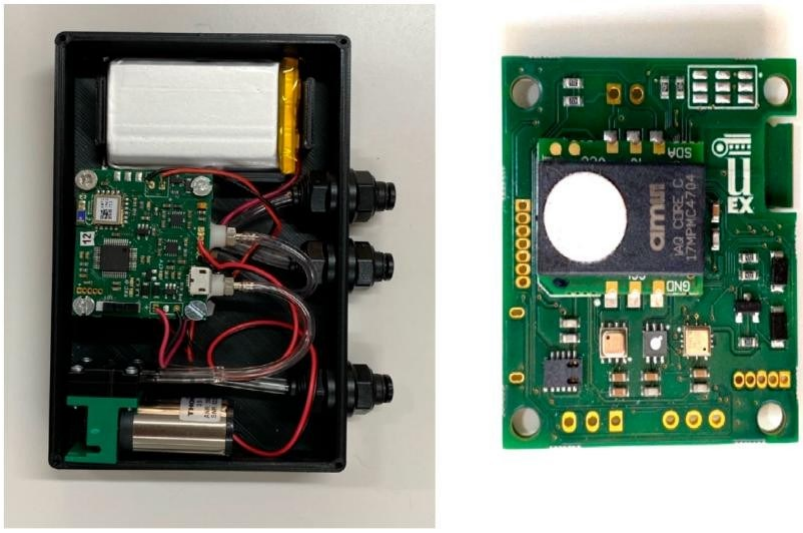

(a) (b)

**Figure 1.** (a) Photograph of the prototype and (b) electronic board of the E-nose (sensor layer).

The measurements performed with the electronic nose (E-nose) consisted of two main phases. The first was the desorption phase, lasting 60 s, during which the sensors were exposed exclusively to clean air. This step served as a reference baseline and ensured signal cleaning. The second was the adsorption phase, also lasting 60 s, in which the sensors analyzed the sample by drawing in its gaseous headspace. The transition between the two modes was managed by a solenoid valve, directly controlled by the microcontroller.

### 6.2.3 GC-MS parameters for the analysis of sourdough under cold fermentation

The volatile compounds of the dough samples were analyzed using gas chromatography coupled with mass spectrometry (GC-MS). Analyses were performed on an Agilent 6850 gas chromatograph coupled to a 5975C single-quadrupole mass spectrometer (Agilent Technologies, Santa Clara, CA, USA), equipped with a CombiPAL autosampler (CTC Analytics, Zwingen, Switzerland) for solid-phase microextraction (SPME) in headspace mode.

A total of 2.0 g of dough was weighed into 20 mL headspace vials, sealed with aluminum caps and PTFE/silicone septa (Agilent Technologies, Santa Clara, CA, USA). Extraction was performed under agitated and heated conditions using a PDMS/DVB fiber (65 µm, Supelco, Bellefonte, PA, USA). After 5 min pre-incubation at 37 °C with constant agitation at 250 rpm, the fiber was exposed to the headspace for 30 min and subsequently thermally desorbed in the injector for 10 min at 270 °C in splitless mode.

Separation of analytes was achieved using an Agilent HP-5 column (30 m × 250 µm × 0.25 µm, 5% phenyl-methyl-siloxane), with helium as carrier gas at a constant flow rate (36 cm/s). The injector

temperature was maintained at 270 °C, with a pressure of 6.75 psi. The total flow was 14.8 mL/min, with a purge flow of 10.8 mL/min starting at 1.00 min. The gas saver mode was activated at 20.0 mL/min after 2.00 min.

The oven temperature program was as follows: 35 °C for 10 min, ramped at 7 °C/min to 250 °C (held for 5 min), then at 10 °C/min to 270 °C, with a final temperature of 325 °C. The total run time was 45.71 min.

Mass spectra were acquired in full-scan mode (m/z 30–550), and volatile compounds were identified by comparison with the NIST library (NIST/EPA/NIH, Gaithersburg, MD, USA). All VOCs were tentatively identified, as no analytical standards were used for confirmation.

Peak areas were expressed as relative percentages, reflecting the composition of the volatile profile rather than absolute concentrations — an approach consistent with the global response of the E-nose.

### 6.2.4 Microbial groups and their role in aroma development

Each microbial group present in the dough contributes to the formation of specific aromatic compounds, thereby defining the final sensory profile of the product [4]. Understanding the evolution of microbial communities during fermentation is essential to optimize the production of desirable aroma compounds and to ensure consistent product quality [5].

The fermentation of sourdough is a complex process involving various microbial populations [6]. The main groups include:

- Mesophilic aerobes, active at moderate temperatures, responsible for producing volatile fatty acids and aldehydes associated with freshness and mild acidity [7].
- Psychrophilic aerobes, which at low temperatures synthesize alcohols and esters, contributing to sweet and fruity notes [8].
- Bacillus spp., capable of producing sulphur compounds that enrich the aroma with earthy and spicy nuances; their identification was facilitated using chromogenic agar [9].
- Yeasts, fundamental for ethanol and fruity ester production, key elements of bread's aromatic complexity [10]; their growth was promoted using PDA supplemented with chloramphenicol.
- Lactobacillus spp., responsible for lactic acid synthesis and for the characteristic fermentative notes [8].
- Acetic acid bacteria, which produce acetic acid, contributing sharp and sour sensory notes [10].

To isolate these microbial groups, selective culture media were employed: Plate Count Agar (PCA) for mesophilic and psychrophilic aerobic bacteria; HiCrome™ Bacillus Agar for *Bacillus spp.*; Potato Dextrose Agar (PDA) supplemented with chloramphenicol for yeasts; de Man, Rogosa and Sharpe (MRS) agar for *Lactobacillus spp.*; and Acetobacter Selective Agar (ABS) for acetic acid bacteria [11].

Samples were analyzed at 0, 4, 20, and 24 h, allowing the monitoring of microbial population dynamics and their correlation with the production of volatile compounds.

### 6.2.5 Statistical tools for data analysis and interpretation

Data acquired by the E-nose were processed using multivariate analysis with PLS_Toolbox 9.5 (Eigenvector Research Inc., Wenatchee, WA, USA) in MATLAB R2024b (The MathWorks Inc., Natick, MA, USA).

Characteristic values were extracted from the original signals by calculating the difference between Xmax (meaning the last five readings in clean air) and Xmin (meaning the last five readings in headspace). Before multivariate analysis, data were autoscaled (mean-centered and normalized to unit standard deviation) to ensure comparability among signals and to minimize the effects of sensor drift and environmental variability.

Two classification methods were employed:

- Linear Discriminant Analysis (LDA), which reduces data dimensionality while maximizing separation among predefined classes, assuming normal distribution and common covariance.
- Artificial Neural Network Discriminant Analysis (ANNDA) applied using a training set (70% of samples) and a test set (30%). The input layer included 16 neurons, corresponding to variables derived from the five MOS sensors (resistance, $CO_2$, ethanol, TVOC, and other signals). Model performance was evaluated through True Positive Rate (TPR), precision, and F1-score.

For GC-MS data, differences among sourdough samples were assessed using one-way ANOVA followed by Tukey's post hoc test. Statistical significance was set at $p < 0.05$. Results are expressed as mean ± standard deviation, and analyses were performed using IBM SPSS Statistics 20 (SPSS Inc., Chicago, IL, USA).

## 6.3 RESULTS AND DISCUSSION

### 6.3.1 Evaluation of sourdough characteristics using the E-nose

The plot shown in Figure 2 illustrates the results of a Linear Discriminant Analysis (LDA) applied to the olfactory evolution of the dough during fermentation.

The LDA model was constructed using only the 52 samples of the calibration set, with the aim of exploring class separation within the training data and visualizing the discriminant capability of the signals acquired by the E-nose.

This analysis therefore does not provide information on the model's generalization ability, which was instead assessed through an Artificial Neural Network Discriminant Analysis (ANNDA) trained on the same calibration set and validated on an independent test set (20 measurements).

The main axes represent the scores associated with the two most significant latent variables: LV1, explaining 96.31% of the variance (horizontal axis), and LV2, explaining 3.04% (vertical axis). The resulting scores reveal a clear separation among sourdough samples collected at different fermentation times: 0 h (red diamonds), 4 h (green squares), 20 h (blue triangles), and 24 h (light-blue inverted triangles).

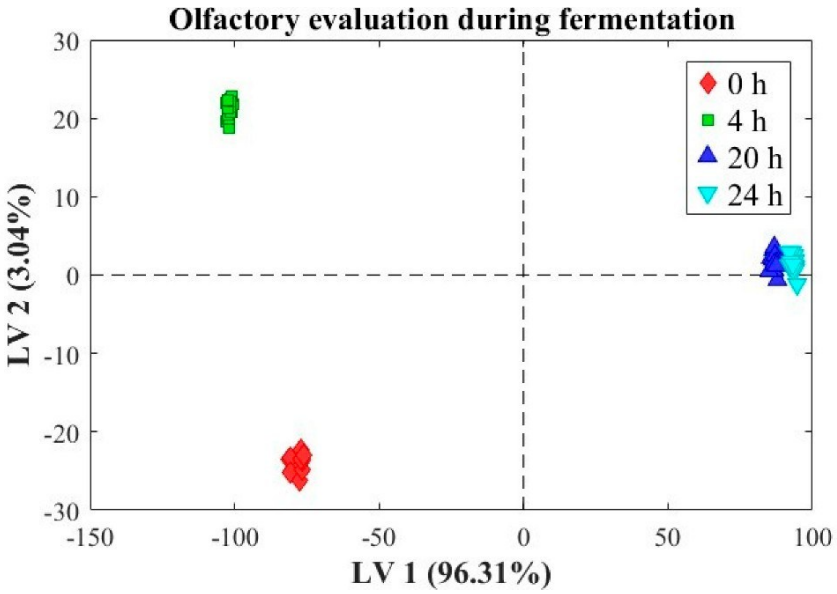


**Figure 2.** LDA of the olfactory evolution of dough fermentation.

The distribution of the data points along LV1 and LV2 reveals a clear temporal evolution of the olfactory profile, with a distinct separation between the initial observations (0 h) and those collected

at later stages (4, 20, and 24 h). In particular, the samples at 20 and 24 h exhibit strong similarity, clustering closely together in the latent variable space.

The LDA analysis thus highlights a progressive olfactory evolution throughout the dough fermentation process, characterized by an increasing temporal separation along LV1, which represents the main source of variation and explains almost the totality of the variance (96.31%).

The 0 h dataset is clearly separated from the others, showing negative scores on both LV1 and LV2. This indicates a markedly different initial olfactory profile, likely associated with the absence—or minimal presence—of volatile metabolites derived from microbial activity, as fermentation has not yet started. After 4 h, the samples shift significantly along both axes, reflecting the first substantial changes in volatile compounds, attributable to the early production of primary metabolites such as organic acids and alcohols by active microorganisms.

Samples collected at 20 and 24 h partially overlap, suggesting a strong similarity between the olfactory profiles at these stages. This indicates a stabilization in the production of typical fermentation volatiles—mainly esters and acids—and the achievement of a metabolic plateau. The stability observed in these later phases reflects an equilibrium among microbial populations and the metabolites produced, a key factor in defining the sensory quality of the final product.

In this study, the optimal fermentation point was defined as the time when the dough exhibited both stable olfactory profiles—evidenced by clustering in the E-nose signals—and a plateau in microbial dynamics and acidification. This equilibrium, observed starting at 20 h, was considered indicative of the technological completion of fermentation.

The plot therefore demonstrates that LDA is an effective tool to discriminate and monitor the olfactory evolution during dough fermentation. The results reveal a clear temporal progression of volatile profiles, with marked differentiation at early stages followed by stabilization, providing valuable insights for optimizing fermentation processes and improving the control of sensory properties in bakery production.

Subsequently, a discriminant analysis model based on Artificial Neural Networks (ANNDA) was developed using the variables extracted from the E-nose system, with the aim of classifying the samples into four fermentation stages (0 h, 4 h, 20 h, and 24 h).

To assess the robustness of the model beyond the training dataset, the data were divided into a calibration set (70%) and an independent validation set (30%). During the calibration phase, the model achieved 100% accuracy, correctly classifying all 52 samples (13 per class). The validation

phase, performed on the remaining 30% of the data (5 samples per class), produced the confusion matrix shown in Table 2.

**Table 2.** Confusion matrix of the ANNDA model on the 30% test set.

| True Class\Predicted Class | 0 h | 4 h | 20 h | 24 h | Unassigned |
|---|---|---|---|---|---|
| 0 h | 5 | 0 | 0 | 0 | 0 |
| 4 h | 0 | 5 | 0 | 0 | 0 |
| 20 h | 0 | 0 | 4 | 0 | 1 |
| 24 h | 0 | 0 | 0 | 5 | 0 |

The model maintained a high overall accuracy of 95%, with only one sample from the 20 h class misclassified. In this case, the error did not result in an incorrect class assignment but rather in an unclassified instance. This slight reduction in performance can be attributed to the strong similarity between the volatile profiles of the 20 h and 24 h samples, as already highlighted by the LDA analysis.

To provide a more comprehensive evaluation of the ANNDA model's performance, recall (TPR), precision (P), and F1-score indices were calculated for each fermentation stage based on the confusion matrix. The results are summarized in Table 3.

**Table 3.** Classification performance metrics of the ANNDA model based on the validation set. *TPR = true positive rate (recall); P = precision.*

| *Fermentation Stage* | *TPR (Recall)* | *Precision (P)* | *F1 Score* |
|---|---|---|---|
| 0 h | 1.00 | 1.00 | 1.00 |
| 4 h | 1.00 | 1.00 | 1.00 |
| 20 h | 0.80 | 1.00 | 0.89 |
| 24 h | 1.00 | 1.00 | 1.00 |

The values obtained indicate an excellent performance of the model across all classes, with a slightly lower recall observed at the 20 h fermentation stage.

The overall reliability of the classification is confirmed by F1-score values close to or equal to 1.00.

These findings support the use of electronic-nose systems combined with artificial intelligence models as powerful tools for olfactory discrimination and automated monitoring of fermentation processes.

The results are consistent with recent studies demonstrating the effectiveness of this approach in complex food matrices [11; 12] thereby confirming its applicability in both artisanal and industrial sourdough production.

## 6.3.2 GC-MS: VOCs detected in sourdough at different fermentation stages

The analysis of volatile organic compounds (VOCs) in dough samples collected at various fermentation times was carried out using gas chromatography–mass spectrometry (GC-MS). This approach enabled the identification of a wide range of compounds whose distribution and relative abundance varied throughout the process, as reported in Table 4.

**Table 4.** Volatile compounds measured (mean ± standard deviation, expressed as percentage of peak area for n = 3) during dough fermentation. Different lowercase letters indicate statistically significant differences according to the experimental treatment for each volatile compound (Tukey's test, $p < 0.05$).

| | | | | Peak Area (%) | | | | |
|---|---|---|---|---|---|---|---|---|
| **CAS Number** | **Volatile Compound** | **RT (min)** | **Odor Descriptors** | **0 h** | **4 h** | **8 h** | **12 h** | **20 h** |
| 64-17-5 | Ethanol | 1.63 | Vinous odor. Pungent taste. | 2.73 ± 0.53 $^{c}$ | 4.53 ± 1.63 $^{bc}$ | 6.32 ± 1.07 $^{b}$ | 7.79 ± 0.26 $^{b}$ | 11.95 ± 1.82 $^{a}$ |
| 141-78-6 | Ethyl Acetate | 2.34 | Fruity. Ethereal. Sweet. | 1.19 ± 0.52 $^{c}$ | 5.73 ± 2.34 $^{c}$ | 5.07 ± 0.93 $^{bc}$ | 9.81 ± 0.89 $^{ab}$ | 11.53 ± 2.79 $^{a}$ |
| 64-19-7 | Acetic acid | 2.84 | Acidic. Vinegary. Pungent. | nd | 2.17 ± 0.09 $^{b}$ | 5.87± 1.38 $^{ab}$ | 12.75 ± 2.05 $^{a}$ | 12.53 ± 2.25 $^{a}$ |
| 123-51-3 | 1-Butanol. 3-methyl- | 4.30 | Sweet. Alcoholic. Fruity. | 9.24 ± 0.48 $^{a}$ | 7.80 ± 1.10 $^{ab}$ | 6.65 ± 1.10 $^{b}$ | nd | 9.62 ± 0.52 $^{a}$ |
| 71-41-0 | 1-Pentanol | 5.43 | Sweet. Alcoholic. Herbal. | 4.27 ± 0.45 $^{b}$ | 3.91 ± 1.20 $^{b}$ | 5.15 ± 1.34 $^{ab}$ | 13.9 ± 2.73 $^{a}$ | 6.08 ± 2.07 $^{ab}$ |
| 513-85-9 | 2.3-Butanediol | 7.68 | Sweet. Creamy. Buttery. | nd | nd | nd | nd | 33.33 ± 4.7 $^{a}$ |
| 111-27-3 | 1-Hexanol | 11.47 | Fruity. Sweet. Herbal. | 5.31 ± 0.86 $^{b}$ | 5.95 ± 1.01 $^{b}$ | 5.73 ± 0.62 $^{b}$ | 10.37 ± 3.38 $^{a}$ | 5.94 ± 0.89 $^{b}$ |
| 123-92-2 | Isoamyl acetate | 12.02 | Banana. Fruity. Sweet. | nd | nd | nd | nd | 33.33 ± 6.58 $^{a}$ |
| 7785-26-4 | 1R-α-Pinene | 14.46 | Pine. Resinous. Herbal. | 22.95 ± 4.85 $^{a}$ | 5.97 ± 2.05 $^{b}$ | 4.40 ± 0.09 $^{b}$ | nd | nd |
| 1117-61-9 | 2-Hepten-1-ol. (E)- | 16.05 | Green. Herbal. Fruity. | nd | nd | nd | 33.33 ± 6.35 $^{a}$ | 30.33 ± 4.00 $^{a}$ |
| 18172-67-3 | L-β-pinene | 16.08 | Pine. Woody. Herbal. | 25.54 ± 5.36 $^{a}$ | 3.42 ± 0.71 $^{b}$ | nd | nd | nd |
| 111-70-6 | 1-Heptanol | 16.13 | Sweet. Herbal. Citrus. | nd | 6.17 ± 1.19 $^{b}$ | 10.58 ± 1.56 $^{ab}$ | 16.57 ± 3.99 $^{a}$ | 16.00 ± 2.60 $^{a}$ |
| 3391-86-4 | 1-Octen-3-ol | 16.41 | Earthy. Mushroom-like. Herbal. | 6.12 ± 1.19 $^{b}$ | 5.39 ± 1.26 $^{b}$ | 4.93 ± 0.54 $^{b}$ | 10.04 ± 2.46 $^{a}$ | 6.83 ± 1.27 $^{b}$ |
| 18172-67-3 | β-Pinene | 16.76 | Pine. Resinous. Herbal. | 25.78 ± 4.69 $^{a}$ | nd | 7.55 ± 1.17 $^{b}$ | nd | nd |
| 123-66-0 | Ethyl hexanoate | 17.11 | Fruity. Sweet. Floral. | nd | nd | nd | nd | 33.33 ± 5.86 $^{a}$ |

| CAS Number | Volatile Compound | RT (min) | Odor Descriptors | Peak Area (%) 0 h | 4 h | 8 h | 12 h | 20 h |
|---|---|---|---|---|---|---|---|---|
| 142-92-7 | Hexyl acetate | 17.54 | Fruity. Sweet. Apple-like. | nd | nd | nd | nd | 33.33 ± 5.07 [a] |
| 527-84-4 | o-Cymene | 17.76 | Citrus. Spicy. Herbal. | 33.33 ± 5.78 [a] | nd | nd | nd | nd |
| 5989-27-5 | Limonene | 17.89 | Citrus. Orange. Sweet. | 28.27 ± 4.92 [a] | 2.05 ± 1.52 [b] | 0.78 ± 0.11 [b] | 0.63 ± 0.27 [b] | 1.58 ± 0.62 [b] |
| 99-85-4 | γ-Terpinene | 18.78 | Spicy. Herbal. Citrus. | 31.46 ± 4.42 [a] | 1.87 ± 0.34 [b] | nd | nd | nd |
| 18409-17-1 | trans-2-Octenol | 19.09 | Fatty. Metallic. Fruity. | nd | nd | nd | nd | 33.33 ± 5.02 [a] |
| 464-48-2 | (-)-Alcanfor | 21.00 | Mentholated. Herbal. Camphoraceous. | 10.33 ± 1.54 [a] | 7.49 ± 0.51 [b] | 7.87 ± 1.35 [b] | 7.63 ± 1.79 [b] | nd |
| 10340-23-5 | cis-3-Nonen-1-Ol | 21.26 | Green. Fruity. Floral. | 2.53 ± 0.91 [b] | 4.19 ± 1.45 [ab] | 5.35 ± 0.77 [ab] | 11.27 ± 2.6 [a] | 9.98 ± 1.32 [ab] |
| 629-50-5 | Tridecane | 24.41 | Sweet. Waxy. Fatty. | 7.61 ± 2.19 [a] | 6.07 ± 1.10 [a] | 5.67 ± 0.88 [a] | 8.33 ± 1.94 [a] | 5.63 ± 0.46 [a] |

RT: retention time. CAS number and odor descriptors from PubChem (https://pubchem.ncbi.nlm.nih.gov/, accessed on 12 March 2025). nd: not detected. Different lowercase letters in the same row indicate statistically significant differences between fermentation times ($p < 0.05$, Tukey's HSD test).

Table 4 summarizes the evolution of volatile organic compounds (VOCs) at different fermentation times (0 h, 4 h, 8 h, 12 h, and 20 h), highlighting significant variations in their composition. These results demonstrate how fermentation dynamically modulates the aromatic profile of the dough, directly influencing the sensory properties of the final product [13].

In the initial phase (0–4 h), terpene compounds such as 1R-α-pinene (22.95%), L-β-pinene (25.54%), β-pinene (25.78%), o-pimene (33.33%), limonene (28.27%), and γ-terpinene (31.46%) predominated, contributing herbal, resinous, and citrus-like notes. At the same time, an increase in ethanol (from 2.73% at 0 h to 4.53% at 4 h) and the appearance of acetic acid (2.17% at 4 h) were observed, indicating the activation of yeasts and lactic acid bacteria and the onset of alcoholic and lactic fermentations.

During the intermediate stage (8 h), the production of ethanol (6.32%), acetic acid (5.87%), and 1-heptanol (10.58%) intensified, enriching the profile with alcoholic and green notes. The presence of 1-octen-3-ol (4.93%), a compound associated with earthy and mushroom-like aromas, was also detected, suggesting enzymatic lipid degradation [12].

In the final stages (12–20 h), concentrations of acetic acid (12.75% at 12 h; 12.53% at 20 h) and cis-3-nonen-1-ol (11.27% at 12 h; 9.98% at 20 h) reached their highest levels, accentuating acidic and grassy notes. Concurrently, an increase in fruity and sweet compounds such as ethyl acetate (from 1.19% at 0 h to 11.53% at 20 h) and isoamyl acetate (absent at 0 h, 33.33% at 20 h) was observed, consistent with the conversion of aldehydes into alcohols and esters during prolonged fermentation [14].

The progressive reduction of terpenes, such as β-pinene (from 25.78% at 0 h to undetected at 20 h) and limonene (from 28.27% at 0 h to 1.58% at 20 h), confirms their volatilization and the consequent attenuation of the bread's fresh aromatic notes [13].

The evolution of VOCs during sourdough fermentation directly affects the organoleptic characteristics of the product, modulating its aroma, flavor, and, indirectly, the perception of texture. Recent studies have shown that the presence of specific volatile compounds correlates with bread sensory quality and consumer acceptability [14].

Esters and alcohols, such as ethyl acetate (11.53% at 20 h) and isoamyl acetate (33.33% at 20 h), contribute fruity and sweet notes that enhance the bread's aromatic appeal [12]. A higher abundance of ethanol (11.95% at 20 h) and 1-pentanol (6.08% at 20 h) adds complexity to the alcoholic profile, evoking a sense of aromatic maturation. Conversely, elevated levels of acetic acid (12.53% at 20 h) and 1-octen-3-ol (6.83% at 20 h) impart acidic and earthy nuances, characteristic of artisanal baking, though excessive accumulation may generate undesirable notes.

The steady decline of terpenes such as limonene (from 28.27% at 0 h to 1.58% at 20 h) and β-pinene (from 25.78% at 0 h to undetected at 20 h) signals a loss of aromatic freshness in prolonged fermentations, with potential effects on final sensory perception [13].

From a technological standpoint, modulating fermentation time allows optimization of VOC production to enhance bread's sensory attributes. The findings suggest that balancing fruity, green, and acidic compounds is key to achieving a well-rounded aromatic profile. In this regard, future sensory studies will be crucial to correlate the identified compounds with consumer perception and to develop strategies aimed at improving fermentation processes in the baking sector.

A limitation of the present study is the absence of absolute quantification, which prevents direct comparison with human olfactory thresholds. Future work should therefore include internal standards for quantification and integrating sensory validation to confirm the perceptual impact of individual VOCs.

### 6.3.3 Microbial diversity and its role in sourdough fermentation dynamics

The microbial evolution of sourdough during fermentation at 5 °C is illustrated in Figure 3, which shows the temporal variations in the main microbial groups (expressed as $\log_{10}$ colony-forming units per gram, cfu/g) and the corresponding changes in pH. The monitored groups included total mesophilic aerobes (light blue line), yeasts (light green line), Lactobacillus spp. (yellow line), total psychrophilic aerobes (red line), and acetic acid bacteria (purple line), while pH is plotted on the right axis (dark blue line). Measurements were taken at four time points: at the start of fermentation (0 h), after 4 h, 20 h, and beyond 24 h.

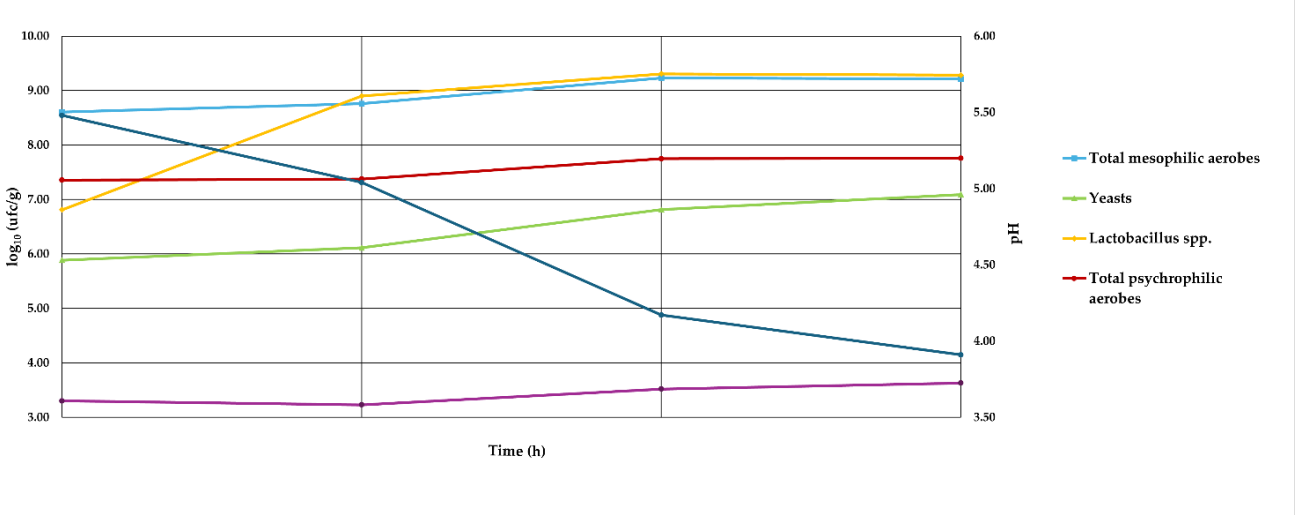


**Figure 3.** Microbial evaluation of sourdough during fermentation at 5 °C.

Regarding total mesophilic aerobes, the initial population (approximately 9 $\log_{10}$ cfu/g) showed a gradual decrease, dropping below 6 $\log_{10}$ cfu/g after 24 hours. This trend suggests that these microorganisms experience competition with other groups and that low-temperature fermentation conditions progressively become less favorable for their growth. In contrast, Lactobacillus spp. exhibited a marked increase, rising from about 8 $\log_{10}$ cfu/g to over 9 $\log_{10}$ cfu/g within 20 hours, before stabilizing. This behavior confirms the central role of these bacteria during the advanced stages of fermentation.

The yeast population increased slowly but steadily throughout the process, from approximately 6 $\log_{10}$ cfu/g to about 7.5 $\log_{10}$ cfu/g after 24 hours, demonstrating their adaptability to fermentative conditions and their contribution to volatile metabolite production. Total psychrophilic aerobes maintained a stable population (around 7 $\log_{10}$ cfu/g), indicating that the environmental conditions did not significantly affect their dynamics. Acetic acid bacteria, although initially present in small

numbers (around 3 $\log_{10}$ cfu/g), showed slight growth, reaching approximately 4 $\log_{10}$ cfu/g after 24 hours.

The system's pH decreased markedly, from about 5.8 to 3.8 after 24 hours, due to the production of organic acids — primarily lactic and acetic acids — by the dominant microorganisms, particularly Lactobacillus spp. and acetic acid bacteria. These results highlight the competitive dynamics among microbial groups and their ability to adapt to low-temperature fermentation conditions. The increase in Lactobacillus and yeast populations reflects their established role in producing acidic and aromatic compounds, whereas the decline in mesophilic aerobes can be attributed to system acidification, which limits the growth of acid-sensitive microorganisms. The stability of psychrophilic aerobes suggests that the favorable temperature does not create significant competition with other groups. Finally, the increase in yeast and acetic acid bacteria emphasizes the complementary nature of metabolic processes in shaping the characteristics of the fermented product.

Overall, fermentation at 5 °C promotes a balanced development of lactic acid bacteria and yeasts, contributing to pH control, which is a critical factor for the quality and safety of sourdough.

## 6.4 CONCLUSIONS

This study demonstrated the effectiveness of the electronic nose (E-nose) in rapidly and efficiently monitoring the olfactory evolution of dough during the different fermentation stages. Each phase was characterized by a distinctive volatile profile, closely correlated with changes in microbial populations, the overall composition of VOCs, and pH levels. Although these temporal associations are evident, further studies are needed to clarify the specific contributions of individual microbial groups to VOC production. In particular, the increase in yeast and lactic acid bacteria concentrations was temporally associated with the production of key compounds such as acetic acid and ethanol, both crucial for the sensory quality of bread.

The integration of traditional and advanced techniques — such as microbiological analyses and SPME-GC-MS — made it possible to deepen the understanding of microbial interactions and their impact on volatile profiles. It should be noted that the identification of VOCs was tentative, based solely on comparison with the NIST library and without confirmation using analytical standards.

The results suggest that the E-nose is a rapid and non-invasive tool for quality assessment, with significant potential for improving process control in artisanal breadmaking, ensuring consistency and optimization of fermentation. Although parallel trends were observed between microbials

evolution and VOC development, no direct statistical correlations were established in this study. Future work should include targeted analyses to further explore the relationships between microbial communities and aroma formation.

By adopting a multidisciplinary approach, this work confirms the value of the electronic nose as an innovative tool for the bakery industry, capable of real-time monitoring of microbiota changes that directly influence volatile profiles and, consequently, the sensory quality of bread prior to baking. The device thus represents promising support for process standardization and improvement, laying the groundwork for more effective and efficient quality control systems in the food industry.

## 6.5 BIBLIOGRAPHY


1. Šmidova, Z.; Rysova, J. Gluten-Free Bread and Bakery Products Technology. Foods 2022, 11, 480. [PubMed]
2. Longin, F.; Beck, H.; Gutler, H.; Heilig, W.; Kleinert, M.; Rapp, M.; Philipp, N.; Erban, A.; Brilhaus, D.; Mettler-Altmann, T. Aroma and Quality of Breads Baked from Old and Modern Wheat Varieties and Their Prediction from Genomic and Flour-Based Metabolite Profiles. Food Res. Int. 2020, 129, 108748.
3. Blaiotta, G.; Romano, R.; Trifuoggi, M.; Aponte, M.; Miro, A. Development of a Wet-Granulated Sourdough Multiple Starter for Direct Use. Foods 2022, 11, 1278. [PubMed]
4. Voidarou, C.; Antoniadou, M.; Rozos, G.; Tzora, A.; Skoufos, I.; Varzakas, T.; Lagiou, A.; Bezirtzoglou, E. Fermentative Foods: Microbiology, Biochemistry, Potential Human Health Benefits and Public Health Issues. Foods 2020, 10, 69.
5. De Vuyst, L.; Harth, H.; Van Kerrebroeck, S.; Leroy, F. Yeast Diversity of Sourdoughs and Associated Metabolic Properties and Functionalities. Int. J. Food Microbiol. 2016, 239, 26–34.
6. Boyaci Gunduz, B.C.P.; Agirman, R.; Gaglio, E.; Franciosi, N.; Francesca, L.; Settanni, H.; Erten, H. Evaluation of the Variations in Chemical and Microbiological Properties of the Sourdoughs Produced with Selected Lactic Acid Bacteria Strains during Fermentation. Food Chem. X 2022, 14, 100357.
7. Meuser, F.; Barber, B.; Fischer, G. Determination of the Microbial Activity of Dried Sourdoughs by Revitalization of Their Lactic Acid Bacteria and Yeasts. Food Control 1995, 6, 147–154.
8. Bender, D.; Fraberger, V.; Szepasvari, P.; D'Amico, S.; Tomoskozi, S.; Cavazzi, G.; Jager, H.; Domig, K.J.; Schoenlechner, R. Effects of Selected Lactobacilli on the Functional

Properties and Stability of Gluten-Free Sourdough Bread. Eur. Food Res. Technol. 2018, 244, 1037–1046. [PubMed]

9. Rocha, J.M.; Malcata, F.X. On the Microbiological Profile of Traditional Portuguese Sourdough. J. Food Prot. 1999, 62, 1416–1429.
10. Kim, D.-H.; Jeon, Y.-J.; Lee, Y.-M.; Lee, J.-Y.; Kim, K.-S.; Park, H.-D. Development of a Novel Selective Medium for the Isolation and Enumeration of Acetic Acid Bacteria from Various Foods. Food Control 2019, 106, 106717.
11. Abbatangelo, M.; Nunez-Carmona, E.; Sberveglieri, V.; Zappa, D.; Comini, E.; Sberveglieri, G. An Array of MOX Sensors and ANNs to Assess Grated Parmigiano Reggiano Cheese Packs' Compliance with CFPR Guidelines. Biosensors 2020, 10, 47. [PubMed]
12. Liboà, A.; Genzardi, D.; Nunez-Carmona, E.; Carabetta, S.; Di Sanzo, R.; Russo, M.; Sberveglieri, V. Different Diacetyl Perception Detected through MOX Sensors in Real-Time Analysis of Beer Samples. Chemosensors 2023, 11, 147.
13. Zhang, Y. The Potential of Wheat and Rye Sourdough Starter Cultures to Produce Functional and Nutritional Components during Sourdough Fermentation. Ph.D. Thesis, Massey University, Palmerston North, New Zealand, 2024. Available online: https://mro.massey.ac.nz/handle/10179/69819 (accessed on 10 April 2025).
14. Păucean, A.; Chiș, M.S.; Mureșan, V.; Șerban, L.R. In Vitro Carbohydrate Digestibility, Textural and Sensory Characteristics of Bread as Affected by Ancient Wheat Flour Type and Sourdough Fermentation Time. Food Chem. X 2024, 15, 100185.

# 7.

# MOX Sensors for Authenticity Assessment and Adulteration Detection in Extra Virgin Olive Oil (EVOO)

## 7.1 INTRODUCTION

Olive oil is a key component of the Mediterranean diet, globally appreciated for its nutritional value, distinctive sensory characteristics, and numerous health benefits [1]. Among the main European producing countries are Spain, Italy, and Greece, which together account for approximately 70% of global production. In Europe, the overall annual production of olive oil averages around 2 million tons, although it may fluctuate due to climatic conditions and agronomic factors [2].

In this study, three categories of olive oil were investigated: Extra Virgin Olive Oil (EVOO), Olive Oil (OO), and Olive Pomace Oil (POO). Volatile compounds were analyzed using gas chromatography–mass spectrometry (GC-MS) combined with headspace solid-phase microextraction (HS-SPME).

Among the various categories, EVOO represents the highest quality class. It is obtained exclusively through mechanical processes conducted at low temperatures, without the use of solvents or chemical treatments, thus preserving the phenolic fraction, fat-soluble vitamins (particularly vitamin E), and the volatile compounds responsible for its unique aromatic profile. These sensory and nutritional characteristics make EVOO highly valued not only from a gastronomic perspective but also in the prevention of various chronic and degenerative diseases [3].

Numerous scientific studies support its beneficial effects, including a reduced risk of cardiovascular diseases, anti-inflammatory properties, and modulation of oxidative responses, thanks to its high content of polyphenols and natural antioxidants [4,5]. Beyond its health-promoting properties, certification of origin and quality is a crucial aspect. Protected Designation of Origin (PDO) oils represent the most authentic expression of the link between product and territory [6]. The PDO certification guarantees compliance with strict specifications that regulate, among other aspects, the cultivars used, agronomic practices, harvesting methods, and processing techniques. These oils not only represent a cultural and gastronomic heritage but also play an important economic role for producing areas, contributing to the enhancement of local traditions and the protection of biodiversity. However, the prestige and high market value of PDO oils make them particularly vulnerable to fraud and adulteration [7,8]. Common fraudulent practices include blending with lower-quality oils, the addition of seed oils, or the use of oils from different harvest years or regions from those indicated on the label [9]. According to the International Olive Council (IOC), approximately 10% of olive oil traded globally shows non-compliance with label claims, with negative consequences for consumers,

who risk purchasing inferior products at unjustified prices, and for honest producers, who suffer in terms of reputation and economic return [10].

Considering these critical issues, it is essential to develop authentication methods that are rapid, reliable, and accessible, capable of supporting official controls and providing greater guarantees to consumers. A thorough understanding of the compounds present in EVOO makes it possible to detect alterations resulting from degradation processes, as well as potential fraudulent adulterations [11,12,13]. The identification of the aromatic characteristics of EVOO can be performed either through sensory evaluation (panel test) or by analyzing its volatile compounds. Although the panel test is an official method, it presents several disadvantages: it is costly and time-consuming, and its results may be influenced by subjective factors, such as the training and individual sensitivity of the panelists [14]. Among instrumental techniques, gas chromatography–mass spectrometry (GC-MS) combined with headspace solid-phase microextraction (HS-SPME) stands out for its high accuracy in the qualitative and quantitative analysis of the volatile fraction. This approach enables the acquisition of a detailed chemical fingerprint, useful for identifying cultivar, geographical origin, and potential adulterations. However, GC-MS also presents certain practical limitations, including complex sample preparation, lengthy analysis times, high equipment costs, and the requirement for highly specialized technical personnel [15,16].

In addition to chromatographic approaches, optical spectroscopic techniques have also been successfully applied to the detection of extra virgin olive oil adulteration. Laser-Induced Breakdown Spectroscopy (LIBS) and UV–Vis–NIR absorption spectroscopy have demonstrated high accuracy in discriminating EVOO from adulterated samples by exploiting elemental and molecular spectral information. While these laboratory-based techniques provide excellent predictive performance, they typically rely on complex instrumentation and are less suited for rapid or on-site screening applications [17].

In this context, the electronic nose (e-nose) emerges as an innovative and complementary tool, capable of providing rapid, non-destructive analyses that can potentially be applied directly in the field [18,19]. Its operation is based on an array of chemical sensors, in this case metal oxide (MOX) sensors, which are sensitive to the presence of volatile compounds [20]. When these molecules interact with the sensitive surface of the MOX sensors, variations in electrical conductivity occur, which are processed to generate a characteristic olfactory fingerprint of the sample. Among the main advantages of MOX sensors are their rapid response, robustness, potential for miniaturization, and ease of integration into automated systems. Moreover, the electronic nose does not require complex

pre-treatment steps and can provide real-time results. However, its main limitation lies in the inability to identify individual volatile compounds: the system is designed primarily for discrimination and classification tasks rather than for detailed chemical characterization [21].

The combined use of GC-MS and the electronic nose thus represent a promising approach for olive oil authentication, merging the analytical precision of GC-MS with the operational speed and flexibility of the electronic nose.

The main objectives of this study were to evaluate the discriminative capability of the electronic nose in classifying different types of olive oils (extra virgin olive oil, olive oil, and olive pomace oil), to compare the olfactory fingerprints generated by the MOX sensor system with the detailed chemical profiles obtained through GC-MS, and to explore the development of predictive models for rapid and non-destructive authentication of olive oils.

Protecting authenticity and enhancing the quality of olive oil, particularly those certified as PDO (Protected Designation of Origin), are strategic priorities for the agri-food industry and for consumer protection. The adoption of integrated analytical approaches, combining established techniques such as GC-MS with innovative tools like MOX sensor-based electronic noses, represents a decisive step toward a more modern, efficient, and sustainable control system, in line with market demands and current challenges related to food safety and transparency [22].

## 7.2 MATERIALS AND METHODS

In this study, three types of oils and their respective mixtures were analyzed: certified Protected Designation of Origin Extra Virgin Olive Oil (EVOO), Olive Oil (OO), and Olive Pomace Oil (POO). All samples were purchased from retail outlets in the large-scale distribution sector and stored at room temperature, ranging between 20 and 25 °C, outside of refrigeration. For each biological replicate, three independent measurements were performed for both gas chromatography–mass spectrometry (GC–MS) and e-nose analyses. Prior to analysis, the order of sample measurements was randomized using a computer-generated sequence to avoid systematic bias. In addition, the position of samples within the thermostatic bath and on the e-nose measurement platform was varied across replicates to minimize potential position effects.

### 7.2.1 Experimental Design

The study was conducted using two complementary approaches. The first involved the characterization of volatile organic compounds (VOCs) present in EVOO, OO, and POO samples through GC–MS combined with solid-phase microextraction (SPME). The second approach focused on analyzing the volatile fraction, or olfactory fingerprint, of both pure samples and their mixtures using a device equipped with MOX sensors.

### 7.2.2 Sample Preparation and Characterization of Oil Samples

A total of 30 samples were analyzed using the electronic nose (e-nose), including Extra Virgin Olive Oil (EVOO), Olive Pomace Oil (POO), Olive Oil (OO), and their respective mixtures prepared with adulteration percentages of 10%, 30%, and 50%. In addition, 9 pure oil samples (EVOO, POO, OO) were analyzed using the GC-MS technique. For the characterization of the volatilome, 50 mL of each pure sample was collected, transferred into glass containers, and subsequently analyzed using the electronic nose (e-nose). This volume was selected to ensure a stable and representative release of volatile compounds under dynamic headspace conditions and to maintain signal reproducibility over repeated acquisition cycles. Measurements were carried out in a thermostatic bath at 30 °C, a condition selected to promote the release of volatile compounds while minimizing oxidation or degradation processes in the sample (Figure 1).

**Figure 1.** Analysis of oil samples using an electronic nose.

In parallel, the same samples were analyzed using gas chromatography coupled with mass spectrometry (GC-MS), employing solid-phase microextraction (SPME) as the sampling technique. For this purpose, 20 mL of each sample were placed into sealed headspace vials, a volume optimized for the fixed vial geometry and liquid-to-headspace phase ratio required for reproducible HS-SPME analysis, sealed with caps featuring aluminum crimp tops and polyethylene-tetrafluoroethylene/silicone (PTFE/silicone) septa, ensuring tight sealing and preserving the integrity of the volatile profile.

The combined approach, integrating the rapid and non-destructive analysis of the e-nose with the detailed identification and quantification capabilities of GC-MS, allowed for a comprehensive and complementary characterization of the volatile fraction of each oil sample analyzed.
Several mixtures were subsequently prepared with the aim of evaluating the system's sensitivity in detecting potential adulterations or combinations of different oils.
Specifically:

- 50% mixtures: three samples, obtained by combining 50 mL of POO with 50 mL of EVOO DOP; 50 mL of OO with 50 mL of EVOO DOP; and 50 mL of OO with 50 mL of POO.
- 30% mixtures: two samples, one consisting of 30 mL of POO and 70 mL of EVOO DOP, and the other of 30 mL of POO and 70 mL of OO.
- 10% mixtures: two samples, one containing 10 mL of POO and 90 mL of EVOO DOP, and the other 10 mL of POO and 90 mL of OO.

This experimental approach was designed to assess the ability of metal oxide sensors to detect even minimal variations in composition, simulating real-world adulteration scenarios and evaluating the system's effectiveness in identifying fraud or quality alterations in olive oil. Table 1 provides a detailed description of the oil samples analyzed, including the number of replicates performed for each type.

**Table 1.** Schematic representation of the analyzed oil samples, indicating the number of replicates performed, the analytical techniques employed, and the total number of samples subjected to analysis.

| Sample | Replicate (R) | Techniques | Sample Number |
|---|---|---|---|
| EVOO (20 mL for GC-MS); EVVO (50 mL for e-nose) | R1 | GC-MS SPME; e-nose | 1 |
| EVOO (20 mL for GC-MS); EVVO (50 mL for e-nose) | R2 | GC-MS SPME; e-nose | 2 |
| EVOO (20 mL for GC-MS); EVVO (50 mL for e-nose) | R3 | GC-MS SPME; e-nose | 3 |
| POO (50 mL) | R1 | GC-MS SPME; e-nose | 4 |
| POO (50 mL) | R2 | GC-MS SPME; e-nose | 5 |
| POO (50 mL) | R3 | GC-MS SPME; e-nose | 6 |
| OO (50 mL) | R1 | GC-MS SPME; e-nose | 7 |
| OO (50 mL) | R2 | GC-MS SPME; e-nose | 8 |
| OO (50 mL) | R3 | GC-MS SPME; e-nose | 9 |
| 50% adulteration: (50 mL) EVOO + (50 mL) POO | R1 | e-nose | 10 |
| 50% adulteration: (50 mL) EVOO + (50 mL) POO | R2 | e-nose | 11 |
| 50% adulteration: (50 mL) EVOO + (50 mL) POO | R3 | e-nose | 12 |
| 50% adulteration: (50 mL) EVOO + (50 mL) OO | R1 | e-nose | 13 |
| 50% adulteration: (50 mL) EVOO + (50 mL) OO | R2 | e-nose | 14 |
| 50% adulteration: (50 mL) EVOO + (50 mL) OO | R3 | e-nose | 15 |
| 50% adulteration: (50 mL) POO + (50 mL) OO | R1 | e-nose | 16 |
| 50% adulteration: (50 mL) POO + (50 mL) OO | R2 | e-nose | 17 |
| 50% adulteration: (50 mL) POO + (50 mL) OO | R3 | e-nose | 18 |
| 30% adulteration: (70 mL) EVOO + (30 mL) OO | R1 | e-nose | 19 |
| 30% adulteration: (70 mL) EVOO + (30 mL) OO | R2 | e-nose | 20 |
| 30% adulteration: (70 mL) EVOO + (30 mL) OO | R3 | e-nose | 21 |
| 30% adulteration: (30 mL) POO + (70 mL) OO | R1 | e-nose | 22 |
| 30% adulteration: (30 mL) POO + (70 mL) OO | R2 | e-nose | 23 |
| 30% adulteration: (30 mL) POO + (70 mL) OO | R3 | e-nose | 24 |
| 10% adulteration: (10 mL) POO + (90 mL) EVVOO | R1 | e-nose | 25 |
| 10% adulteration: (10 mL) POO + (90 mL) EVVOO | R2 | e-nose | 26 |
| 10% adulteration: (10 mL) POO + (90 mL) EVVOO | R3 | e-nose | 27 |
| 10% adulteration: (10 mL) POO + (90 mL) OO | R1 | e-nose | 28 |
| 10% adulteration: (10 mL) POO + (90 mL) OO | R2 | e-nose | 29 |
| 10% adulteration: (10 mL) POO + (90 mL) OO | R3 | e-nose | 30 |

### 7.2.3 Volatile Organic Compounds (VOCs)

The analysis of volatile organic compounds (VOCs) was conducted using two complementary approaches: (i) identification by gas chromatography coupled with mass spectrometry (GC-MS) using solid-phase microextraction (SPME), and (ii) olfactory profiling through an electronic nose system based on metal oxide semiconductor (MOX) sensors.

For the GC-MS analysis, two grams of oil were placed in hermetically sealed headspace vials and incubated at 40 °C for 10 min. A DVB/C-WR/PDMS SPME fiber (Supelco, Bellefonte, PA, USA) was then introduced into the vial and exposed in the headspace (4 cm) for 30 min under agitation. Subsequently, thermal desorption of volatile compounds was performed in the injector port at 240 °C for 5 min. Compound identification was carried out using a gas chromatograph (model 7820A; Agilent Technologies, Santa Clara, CA, USA) coupled to a mass spectrometer (5977E MSD; Agilent Technologies, Santa Clara, CA, USA). The initial oven temperature was set at 40 °C for 10 min, increased to 200 °C at 3 °C/min (held for 3 min), and finally raised to 240 °C at 10 °C/min, maintained for 5 min. Separation was achieved using an HP-5MS capillary column (30 m × 0.25 mm × 0.25 µm; Agilent J&W, Santa Clara, CA, USA) with helium as the carrier gas at a constant flow of 1 mL/min. Injections were performed in splitless mode at 240 °C, with the transfer line maintained at 250 °C and the ion source at 230 °C. Electron ionization energy was set at 70 eV, and data acquisition was performed in scan mode from 30 m/z to 300 m/z. Qualitative analysis was based on the comparison of the obtained mass spectra with reference spectra available in the NIST Mass Spectral Search Program (v2.0; National Institute of Standards and Technology (NIST), Gaithersburg, MD, USA). This methodology enabled the identification of representative compounds present in the oils, including aldehydes, alcohols, acids, and esters, allowing a precise differentiation of volatilome composition across pomace, virgin, and extra virgin oils, as well as the detection of potential adulteration.

In parallel, a portable electronic nose system based on MOX sensors was employed. This compact device is designed for the rapid detection of volatile profiles by recording impedance changes in the sensing elements upon exposure to VOCs released by the samples. Analyses were conducted at 30 °C using a thermostatic bath, ensuring headspace generation without inducing thermal degradation of the oils. The system captured subtle variations in the volatile profiles, generating characteristic olfactory fingerprints that allowed reliable classification of the samples. The electronic nose integrates a multichannel MOX sensor with four resistive sensing elements, each displaying differential sensitivity to specific chemical families, including alcohols, aldehydes, ketones, and fatty acids. Operating at a controlled working temperature of approximately 400 °C, the sensor ensured stable and reproducible responses. The embedded system incorporates data acquisition electronics and wireless connectivity, facilitating its application as a portable and compact analytical tool. The recorded signals, based on impedance variations of each sensing element, provided unique olfactory patterns for each sample, enabling a robust and non-destructive characterization of the oils.

### 7.2.4 Electronic Nose Set-Up

The printed circuit board (PCB) of the system integrates various electronic components, as shown in Figure 2. The board is powered via a USB port and a 3.7 V lithium battery. The battery voltage is regulated by a buck–boost converter, which stabilizes the output at 3.3 V, supplying most of the electronic components. In addition, a linear voltage regulator further reduces this voltage to 1.8 V to power the ENS160 sensor (ScioSense, Eindhoven, The Netherlands).

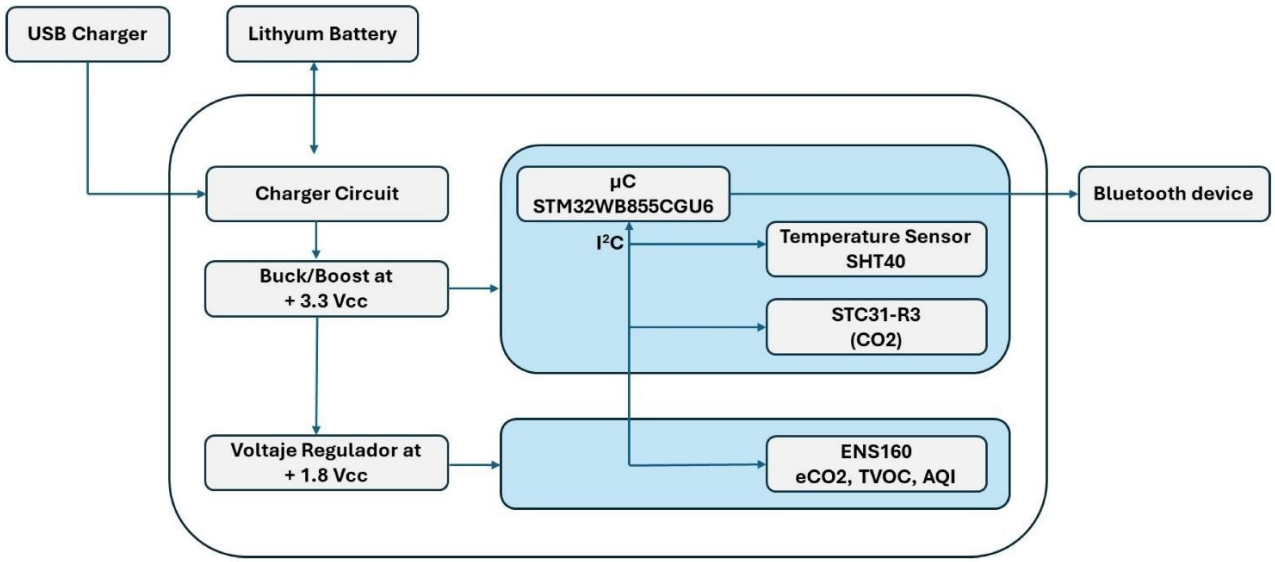


**Figure 2.** Block diagram of the device.

The data acquisition system is based on three different sensors, whose characteristics and measured signals are summarized in Table 2. The sensor outputs are transmitted via the I2C protocol to a 32-bit microcontroller (STM32WB55CGU6, STMicroelectronics, Geneva, Switzerland). This microcontroller manages both sensor communication and wireless data transmission via Bluetooth Low Energy (BLE) to external devices, such as smartphones, enabled by the integrated Arm Cortex-M0+ core (Arm Ltd., Cambridge, United Kingdom). Similar electronic nose architectures, combining low-power sensor interfaces, embedded microcontrollers, and wireless communication modules, have been successfully employed for the detection and discrimination of volatile organic compounds, as reported in the literature [23].

**Table 2.** Sensors used in the device.

| Sensor | Manufacturer | Type | Signal Measured |
|---|---|---|---|
| SHT40 | Sensirion | Temperature/ Humidity | Temperature (°C), Relative humidity (%) |
| ENS160 | Sensirion | MOX | $Eco_2$ (ppm), TVOCs (ppm), Air quality Index (AQI), Four resistive elements (Ohms) |
| STC31-R3 | Sensirion | $CO_2$ sensor | $CO_2$ (% vol) |
| | data | data | data |

The sensor array integrated in the portable e-nose comprises an ENS160 MOX gas sensor (TVOC/eCO2/AQI outputs) an SHT40 (temperature/relative humidity sensor; Sensirion AG, Stäfa, Switzerland), and an STC31-R3 (CO2 sensor; Sensirion AG, Stäfa, Switzerland) (see Table 2 for details).

Temperature and relative humidity were continuously recorded (SHT40) as quality-control/reference variables to confirm stable measurement conditions and were not included as input features in the PCA/ML models.

On one hand, Figure 3 (left) shows the layout of the printed circuit board (PCB), designed in a compact circular format with a diameter of 36.4 mm. The components have been strategically placed to maximize space efficiency. Among the key elements are a microcontroller, responsible for managing sensor communication and Bluetooth Low Energy (BLE) connectivity, and an RGB LED used to visually indicate air quality levels.

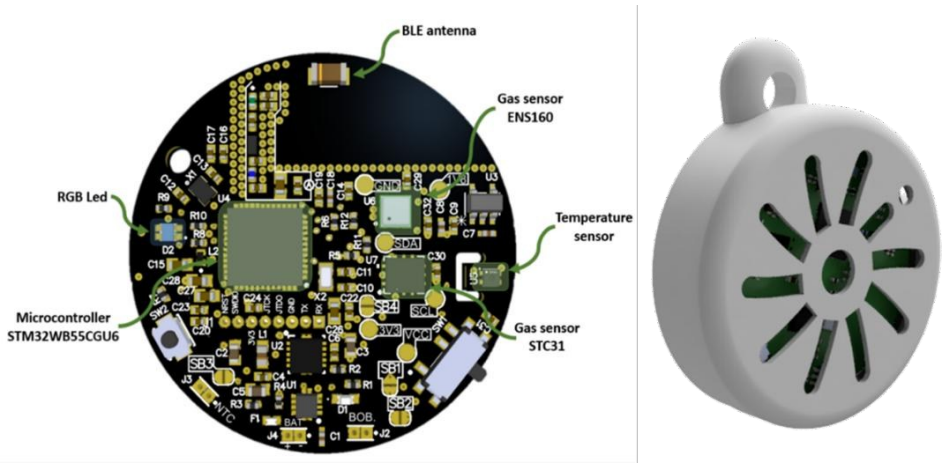


**Figure 3.** Electronic board (left) and case (right).

The sensing system includes three main sensors: the ENS160 gas sensor for air quality evaluation, the STC31 gas sensor for CO2 concentration measurement, and a dedicated temperature, along with a dedicated temperature and relative humidity sensor (SHT40). Communication between the sensors and the microcontroller is handled via the I2C protocol. A BLE antenna is also integrated to allow wireless data transmission to external devices such as smartphones.

Figure 3 (right) presents the external casing that encloses the PCB. This protective structure is designed with radial vents that enable air to circulate freely to the terminal sensors. The enclosure is optimized for portability and comfortable everyday use, ensuring that environmental measurements can be carried out reliably while the device is worn or transported.

## 7.3 RESULTS AND DISCUSSION

### 7.3.1 Characterization and Comparison of the Volatile Components of Pure Oils Using SPME-GC-MS

The analysis of the volatile profile of the three oils under investigation (EVOO, OO, POO), performed using gas chromatography–mass spectrometry (GC-MS) coupled with solid-phase microextraction (SPME), enabled the identification of 60 compounds. These were classified into seven main chemical groups: alkanes, alkenes, carboxylic acids, aldehydes, alcohols, ketones, and others (Table 3).

**Table 3.** Volatile compounds detected by GC–MS SPME for each oil. Each compound is presented in terms of abundance (a dimensional variable) represented the average of three biological replicas.

| | | | OO | EVOO | POO | |
|---|---|---|---|---|---|---|
| | | | Code: 25-L-CR051 | Code: 25-L-CR052 | Code: 25-L-CR050 | |
| RT | Volatile Compounds | CAS | Absolute Area | Absolute Area | Absolute Area | Description |
| 5.76 | Heptane | 142-82-5 | nd * | nd | $9.66 \times 10^5$ | Linear saturated hydrocarbon composed of a straight chain of seven carbon atoms fully saturated with hydrogen [24]. |
| 7.82 | n-Octane | 111-65-9 | $1.50 \times 10^7$ | $1.61 \times 10^7$ | $2.75 \times 10^6$ | Single chain of eight carbon atoms bonded to eighteen hydrogen atoms [24]. |
| 8.52 | Cyclohexane, 1,3-dimethyl-, cis- | 638-04-0 | nd | nd | $1.26 \times 10^6$ | Chemical compound; six-carbon cycloalkane with methyl groups at positions 1 and 3. Exists as two geometric isomers: cis and trans [25]. |
| 9.52 | Octene | 111-66-0 | $1.11 \times 10^6$ | $1.22 \times 10^6$ | nd | Linear alpha-olefin with double bond at position 1. Industrially produced from ethylene; used as comonomer in polyethylene and in hydroformylation to produce linear aldehydes [26]. |

| | | | | | | |
|---|---|---|---|---|---|---|
| 11.83 | Ethylcyclohexane | 1678-91-7 | nd | nd | $1.20 \times 10^6$ | Saturated hydrocarbon: ethyl group bound to a cyclohexane ring. Found in petroleum as a naphthene; produced by hydrogenation of ethylbenzene or hydrodeoxygenation of lignin [27]. |
| 12.20 | n-Nonane | 111-84-2 | nd | nd | $2.50 \times 10^5$ | Straight-chain alkane; colorless liquid with sharp odor. Volatile oil component and plant metabolite; insoluble in water. Found in various plant species [28]. |
| 12.34 | Acetic acid, ethyl ester, Ethyl acetate | 141-78-6 | $8.59 \times 10^6$ | $2.51 \times 10^6$ | $3.90 \times 10^5$ | Sweet-smelling, colorless, flammable ester of ethanol and acetic acid. Widely used as a solvent in paints, nail polish, decaffeination, perfumes, and wine; also used for insect collection [29]. |
| 12.82 | Acetic acid, hydroxy-(Glycolic acid) | 79-14-1 | $1.41 \times 10^7$ | $1.52 \times 10^7$ | $1.27 \times 10^7$ | Functions as a metabolite and keratolytic agent. Used in cosmetics and dermatology; safe up to 10% (pH $\geq$ 3.5) in consumer products [30]. |
| 13.79 | Pentanal | 110-62-3 | $9.87 \times 10^5$ | $1.06 \times 10^6$ | nd | Alkyl aldehyde; colorless volatile liquid with fruity, nutty odor. Produced via hydroformylation of butene; used in fragrance synthesis and as intermediate for plasticizers [31]. |
| 14.07 | butanal, 3-methyl | 590-86-3 | $8.20 \times 10^5$ | $9.58 \times 10^5$ | nd | Branched aldehyde with a methyl group at position 3; volatile compound found in olives. Acts as flavoring agent, plant metabolite, and product of yeast metabolism [32]. |
| 15.70 | Hexane, 1-methoxy-(Hexyl methyl ether) | 4747-07-3 | $1.57 \times 10^7$ | $1.76 \times 10^7$ | nd | Colorless liquid with characteristic odor. Contains a methyl group bonded to a hexane chain via oxygen; primarily used as a solvent [30]. |
| 16.70 | 3-buten-1-ol | 627-27-0 | $8.32 \times 10^5$ | $1.27 \times 10^6$ | nd | Organic compound belonging to the class of unsaturated alcohols. In the food sector, it can be detected as a volatile compound in certain vegetable oils [30]. |
| 17.85 | 3-pentanone | 96-22-0 | $3.56 \times 10^6$ | $1.89 \times 10^6$ | nd | Also known as diethyl ketone, is a simple symmetrical dialkyl ketone, with an odor like that of acetone [33]. |
| 17.95 | 3-methylbutanal | 590-86-3 | $1.03 \times 10^6$ | $8.49 \times 10^5$ | nd | Aldehyde, a colorless liquid and found in low concentrations in many types of food. Commercially it is used as a reagent to produce pharmaceuticals, perfumes and pesticides [34]. |
| 18.28 | Decane | 124-18-5 | $3.28 \times 10^6$ | $3.06 \times 10^6$ | $1.60 \times 10^6$ | Linear molecule of 10 carbons with a non-defined scent found in olive oil [30]. |
| 19.31 | 3-Ethyl-1,5-octadiene (c,t) | 105-54-4 | $3.72 \times 10^6$ | $6.72 \times 10^6$ | nd | 3-ethyl-1,5-octadiene is an alkadiene that is 1,5-octadiene substituted by an ethyl group at position 3. Has a non-defined scent [3]. |
| 19.55 | Methyl 3(Z)-Hexenyl Ether | 70220-06-3 | $8.87 \times 10^6$ | $7.83 \times 106$ | nd | Fragrance and flavoring agent with green, fruity, slightly floral scent; methyl ether of (Z)-3-hexen-1-ol; used in flavors, fragrances, and potentially in coatings [35]. |
| 20.18 | alfa-pinene | 80-56-0 | $4.41 \times 10^5$ | nd | nd | Bicyclic monoterpene, a volatile organic compound commonly found in essential oils from conifers and various aromatic plants. It exhibits anti-inflammatory, antimicrobial, antioxidant, and bronchodilator properties, making it useful in traditional and pharmaceutical applications [36]. |

| | | | | | | |
|---|---|---|---|---|---|---|
| 21.48 | Ethyl Butanoate | 105-54-4 | $1.03 \times 10^6$ | $3.34 \times 10^5$ | nd | It is soluble in propylene glycol, paraffin oil, and kerosene. It has a fruity odor and is a key ingredient used as a flavor enhancer in processed orange juices. It also occurs naturally in many fruits, albeit at lower concentrations [37]. |
| 22.42 | Butanoic acid, 2-methyl-, ethyl ester | 7452-79-1 | $1.73 \times 10^6$ | $3.44 \times 10^5$ | nd | Also known as ethyl 2-methylbutyrate. It is a fruity-scented volatile ester, used as a flavoring agent and naturally found in wines, strawberries, blueberries, apples and olive [38]. |
| 23.43 | Butanoic acid, 3-methyl-, ethyl ester | 108-64-5 | $4.33 \times 10^5$ | nd | nd | It has a fruity odor and flavor and is used in perfumery and as a food additive [39]. |
| 24.44 | Hexanal | 66-25-1 | $8.60 \times 10^6$ | $1.12 \times 10^7$ | $2.11 \times 10^6$ | Also called hexanaldehyde or caproaldehyde, it is an alkyl aldehyde. Its scent resembles freshly cut grass, with a powerful, penetrating characteristic fruity odor and taste. It occurs naturally and contributes to the flavor in green peas [40]. |
| 24.65 | 1-Propanol, 2-methyl- | 78-83-1 | $2.21 \times 10^6$ | $1.31 \times 10^6$ | nd | Also called isobutanol. It is produced by the carbonylation of propylene. Has ethereal, winey and cortex notes [41]. |
| 26.74 | Isoamyl acetate | 123-92-2 | $2.87 \times 10^6$ | $1.10 \times 10^6$ | nd | Colorless liquid, slightly soluble in water, highly soluble in organic solvents. Strong banana-like odor; used as food flavoring. Naturally from bananas or synthetically produced; also, a bee alarm pheromone [42]. |
| 27.20 | methyl laureate | 111-82-0 | $5.01 \times 10^5$ | $5.61 \times 10^5$ | nd | Fatty acid methyl ester of lauric acid; occurs in olive, fruits (e.g., grape, melon, pineapple), cheeses, wines, and spirits. Used as a flavoring agent; classified as a fatty acid ester [43]. |
| 27.44 | 2-pentenal | 623-36-9 | $6.24 \times 10^5$ | $6.81 \times 10^5$ | nd | Aldehyde found in cigarette smoke, virgin olive oil, and milk. It has a role as a plant metabolite [44]. |
| 28.72 | 1-Penten-3-ol | 616-25-1 | $1.66 \times 10^6$ | $1.80 \times 10^6$ | nd | Alcohol with pungent horseradish-like odor and tropical notes when diluted; used to enhance green, cucumber, melon, berry, and vegetable accords in fragrances [44]. |
| 30.33 | Dodecane | 112-40-3 | $3.50 \times 10^6$ | $2.26 \times 10^6$ | $1.29 \times 10^6$ | Linear branched molecule consisting of decane with 12 carbon atoms. It is a clear colorless liquid isolated from the essential oils of various plants including Zingiber officinale (ginger). It has a role as a plant metabolite is a natural product found in Erucaria microcarpa, with a balsamic scent found in olive oil [45]. |
| 30.50 | Heptanal | 111-71-7 | $1.28 \times 10^6$ | $1.67 \times 10^6$ | $3.60 \times 10^5$ | Aliphatic aldehyde; colorless liquid with strong fruity odor. Naturally found in ylang-ylang, clary sage, lemon, bitter orange oils, and in olives at low levels [46]. |
| 31.18 | Limonene | 138-86-3 | $8.53 \times 10^5$ | $9.85 \times 10^5$ | $7.20 \times 10^5$ | Limonene is a volatile hydrocarbon, a cycloolefin classified as a cyclic monoterpene, lemon-like odor that can be found in the rind of citrus fruits [47]. |
| 31.34 | Isoamyl alcohol | 123-51-3 | $1.12 \times 10^7$ | $3.88 \times 10^6$ | nd | Isomeric alcohol: natural ester used in banana oil and as flavoring, also present in black truffle aroma. By-product of cereal fermentation, found in alcoholic beverages; component of hornet alarm pheromone [48]. |

| | | | | | | |
|---|---|---|---|---|---|---|
| 32.55 | 2-hexenal | 505-57-7 | $4.98 \times 10^7$ | $3.06 \times 10^7$ | nd | 2-Hexenal is a chemical compound of the aldehyde group. Imparts fresh, green, and natural top note in fruity floral types. Apple, berry, and other fruit flavors. Also, citrus flavors, especially orange juice [41]. |
| 32.65 | 3,5-dimethyl-4-aza-4-heptene | 38836-40-7 | $8.56 \times 10^7$ | $1.32 \times 10^8$ | nd | Heterocyclic compound containing a nitrogen atom as part of a seven-membered ring, with two methyl groups attached to the carbon atoms at positions 3 and 5, and an ethyl group and a methyl group attached to the carbon at position 4 [48]. |
| 33.65 | 1-Pentanol | 71-41-0 | $7.32 \times 10^5$ | $2.58 \times 10^5$ | nd | It is an alcohol with five carbon atoms. Pungent, fermented, bready, yeasty, fusel, winey and solvent-like smell [41]. |
| 33.94 | Trans-β-Ocimene | 3779-61-1 | $6.83 \times 10^6$ | $7.88 \times 10^6$ | nd | β-Ocimene is trans-3,7-dimethyl-1,3,6-octatriene. Exists in two stereoisomeric forms, cis and trans, with respect to the central double bond. The ocimenes are often found naturally as mixtures of the various forms. Complex note, mainly herbal lavender with green citrus, metallic and mango nuances [49]. |
| 34.69 | Styrene (Ethenylbenzene) | 100-42-5 | $2.11 \times 10^6$ | $4.40 \times 10^5$ | nd | Aromatic hydrocarbon. The vinyl group attached to the aromatic ring is highly reactive, as the ring can delocalize charges and unpaired electrons to the ortho and para positions through various resonance forms [50]. |
| 35.04 | n-hexyl acetate | 142-92-7 | $1.15 \times 10^7$ | $1.32 \times 10^7$ | nd | Hexyl acetate is the acetate ester of hexan-1-ol. Green fruity note reminiscent of apple, pear [51]. |
| 36.11 | Octanal | 124-13-0 | $9.11 \times 10^5$ | $1.11 \times 10^6$ | nd | Colorless fragrant liquid with fruity odor; naturally in citrus and olive oils. Used in perfumes and as a flavoring in food industry [52]. |
| 36.21 | 3-hydroxy-2-butanone | 513-86-0 | $2.05 \times 10^6$ | $8.07 \times 10^5$ | nd | Chemical used in food flavoring and fragrances; intermediate in microbial butanediol cycle; also serves as an aroma carrier in flavors and essences [52]. |
| 36.74 | (E)-4,8-Dimethyl-1,3,7-nonatriene | 19945-61-0 | $5.27 \times 10^6$ | $5.85 \times 10^6$ | nd | Alkatriene consisting of 4,8-dimethylnonane having the three double bonds in the 1-, 3- and 7-positions [53]. |
| 37.41 | 3-Hexen-1-ol, acetate, (Z)- | 3681-71-8 | $9.39 \times 10^7$ | $1.34 \times 10^8$ | nd | Acetate ester from acetic acid and (Z)-hex-3-en-1-ol; metabolite with green, fruity aroma; found in tea, olive, and other plants [54]. |
| 38.13 | 2-Heptenal, (E)- | 18829-55-5 | $2.57 \times 10^6$ | $2.83 \times 10^6$ | nd | Monounsaturated fatty aldehyde with a green, fatty aroma; found mainly in pomelo peel, soybean oil, and pulses. Acts as a plant metabolite, food flavoring, and uremic toxin [19]. |
| 38.59 | 6-methyl-5-hepten-2-one | 110-93-0 | $1.08 \times 10^6$ | $1.09 \times 10^6$ | nd | Unsaturated methylated ketone; colorless liquid with citrus, fruity odor. Found as a mosquito attractant [55]. |
| 38.85 | 1-Hexanol | 111-27-3 | $3.40 \times 10^7$ | $2.91 \times 10^7$ | nd | It is an organic alcohol with a six-carbon chain. Smells pungent, ethereal, fuel oil, fruity and alcoholic, sweet with a green top note [56]. |
| 40.55 | 3-Hexen-1-ol, (Z)- | 928-96-1 | $7.56 \times 10^7$ | $8.07 \times 10^7$ | nd | Colorless oily liquid with intense grassy-green odor; produced by most plants as insect attractant. Key aroma compound in flavors and perfumes; used in fruit and vegetable notes [57]. |
| 41.29 | Nonanal | 124-19-6 | $9.32 \times 10^6$ | $1.37 \times 10^7$ | $9.78 \times 10^5$ | It is a formally saturated fatty aldehyde resulting from the reduction of the carboxyl group of nonanoic acid. Waxy, rose and orange peel [41]. |
| 41.50 | 2-Hexen-1-ol, (E)- | 928-95-0 | $1.59 \times 10^7$ | $8.83 \times 10^6$ | nd | Primary allylic alcohol derived from 2-hexene; acts as a plant metabolite. Classified as an alkenyl and allylic alcohol [58]. |
| 43.75 | Acetic acid | 64-19-7 | $3.29 \times 10^7$ | $6.51 \times 10^6$ | $6.72 \times 10^5$ | Colorless, acidic liquid; main component of vinegar. Widely used in food, chemical industry, and as acidity regulator. Central to metabolism (acetyl group) [59]. |

| | | | | | | |
|---|---|---|---|---|---|---|
| 43.75 | Acetic acid | 64-19-7 | $3.29 \times 10^7$ | $6.51 \times 10^6$ | $6.72 \times 10^5$ | vinegar. Widely used in food, chemical industry, and as acidity regulator. Central to metabolism (acetyl group) [59]. |
| 44.88 | trans,trans-2,4-heptadienal | 4313-03-5 | $1.40 \times 10^6$ | $1.02 \times 10^6$ | nd | Heptadienal with double bonds at positions 2 and 4 (E,E-isomer); used as a flavoring agent [60]. |
| 46.06 | α-copaene | 3856-25-5 | $2.30 \times 10^6$ | $1.68 \times 10^6$ | nd | It is an oily liquid hydrocarbon found in several plants that produce essential oils. Scents reminiscent of honey, spicy or woody notes [61]. |
| 47.59 | 2,3-Butanediol | 513-85-9 | $1.72 \times 10^6$ | $8.12 \times 10^5$ | nd | Organic compound; colorless vic-diol liquid. Occurs naturally in olive oil, cocoa butter, sweet corn, and rotten mussels. Used in plastics, pesticides, and GC carbonyl compound resolution [62]. |
| 47.73 | α-terpinolene | 586-62-9 | $7.31 \times 10^5$ | $7.29 \times 10^5$ | nd | Natural terpene found in lilac, sage, rosemary, nutmeg, conifers, olive, and tea tree oil. Colorless to pale yellow liquid with woody, citrus-like odor; slightly bitter at high concentrations [63]. |
| 47.93 | Benzaldehyde | 100-52-7 | $1.16 \times 10^6$ | $1.05 \times 10^6$ | $4.73 \times 10^5$ | Aromatic aldehyde; colorless volatile liquid with characteristic bitter almond odor. Naturally occurs in apricot, cherry, and almond seeds (as amygdalin precursor) [64]. |
| 48.17 | n-Octanol | 111-87-5 | $1.75 \times 10^6$ | $2.19 \times 10^6$ | nd | Eight-carbon alcohol; colorless liquid with characteristic odor. Hydrophobic and water-immiscible; used to determine partition coefficients of chemicals [64]. |
| 51.32 | Butanoic acid | 107-92-6 | $1.06 \times 10^6$ | $2.03 \times 10^5$ | nd | Carboxylic acid found esterified in natural fats and released during fat rancidification (e.g., in butter, aged cheeses, olive). Has a pungent odor at high concentration; contributes to characteristic aroma of fermented dairy at low levels. Formed via butyric fermentation of sugars and used in the synthesis of flavor and fragrance esters [65]. |
| 51.99 | Benzoic acid, methyl ester | 93-58-3 | $1.32 \times 10^6$ | $1.83 \times 10^6$ | nd | Methyl ester of benzoic acid; colorless liquid with pleasant floral odor. Found naturally in some plants; used in perfumes and as a scent marker in canine training. Poorly soluble in water, well soluble in organic solvents [66]. |
| 52.48 | (E)-2-Decenal | 3913-81-3 | $2.90 \times 10^6$ | $3.05 \times 10^6$ | nd | Oily aldehyde with strong waxy odor; occurs in coriander, meats, fruits, and various foods. Used as flavoring agent and also acts as pheromone [67]. |
| 56.09 | Farnesene | 502-61-4 | $7.92 \times 10^6$ | $1.04 \times 10^7$ | nd | Group of sesquiterpene isomers, including α- and β-farnesene; differ by double bond position. Found in green apple peel, cannabis, ginger, hop, and other plants. Acts as an insect alarm pheromone (e.g., aphids) and contributes to fruity, woody, and citrus aromas [68]. |
| 58.32 | Benzoic acid, 2-hydroxy-, methyl ester | 119-36-8 | $1.50 \times 10^6$ | $1.97 \times 10^6$ | nd | Also known as methyl salicylate; colorless liquid with characteristic odor. Found in wintergreen oil; used in flavors, fragrances, and as a counterirritant in topical medications [69]. |
| 61.44 | Benzenemethanol | 100-51-6 | $1.22 \times 10^6$ | $8.37 \times 10^5$ | nd | Aromatic alcohol; clear, colorless liquid with pleasant odor. Used as solvent, antioxidant, fragrance, and chemical intermediate; may cause irritation on contact [70]. |
| 62.78 | phenylethyl alcohol | 60-12-8 | $4.50 \times 10^6$ | $2.12 \times 10^6$ | nd | Aromatic alcohol with rose-like scent; naturally found in rose, peppermint, hyacinth, and orange blossom. Used in perfumes, soaps, and as antimicrobial agent; slightly soluble in water [71]. |

* nd = 'not detected', the compound was not detected in any of the three biological replicas or was found only in one of them.

The Extra Virgin Olive Oil (EVOO) samples exhibited a rich and complex aromatic profile, characterized by a high abundance of volatile compounds belonging to the C6 family, including

aldehydes (hexanal, E-2-hexenal), alcohols (1-hexanol, (Z)-3-hexen-1-ol), and their corresponding esters, such as (Z)-3-hexen-1-yl acetate. These compounds are primarily derived from the enzymatic lipoxygenase (LOX) pathway, which is activated during the processing of fresh and intact olives, converting polyunsaturated fatty acids into volatile metabolites with low odor thresholds. These molecules are responsible for the fresh, green, fruity, and herbaceous sensory notes that are typical of high-quality olive oils. Hexanal is one of the most abundant compounds in the volatile profile of EVOO and significantly contributes to green and freshly cut grass olfactory sensations, as widely reported in the literature [72,73,74]. E-2-hexenal, which is also frequently detected at high concentrations, is associated with a more intense and penetrating fruity aroma. According to García-Vico et al. (2017) [75], this compound is often the most abundant among the C6 volatile organic compounds (VOCs). C6 alcohols, such as 1-hexanol and (Z)-3-hexen-1-ol, also contribute to the aromatic profile by imparting sweet, floral, and slightly fruity notes. In particular, the latter serves as an important precursor of volatile esters such as (Z)-3-hexen-1-yl acetate, which imparts fresh and fruity aromatic nuances (e.g., tomato leaf, green banana), significantly enhancing the overall olfactory complexity of the oil [18]. Overall, aldehydes, alcohols, and their corresponding esters are the main contributors to the aromatic characteristics of EVOO, not only due to their abundance but also because of their low sensory threshold and high sensory impact (Figure 4). Their presence at high concentrations is commonly associated with high-quality raw material and a prompt, well-executed extraction process, thus representing reliable markers of the product's freshness and integrity [75,76,77].

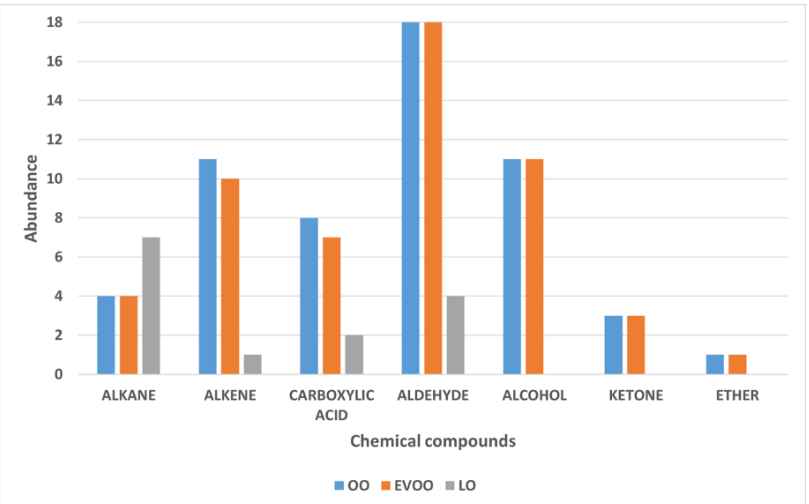


**Figure 4.** Chemical classes of Extra Virgin Olive Oil (EVOO), Virgin Olive Oil (OO), and Olive Pomace Oil (POO) samples analyzed by gas chromatography–mass spectrometry (GC–MS).

Although Virgin Olive Oil (OO) shares many volatile compounds with Extra Virgin Olive Oil (EVOO), it is characterized by a less intense and less complex aromatic profile, indicative of lower

commercial and sensory quality (Figure 5). The reduced presence of key volatile compounds in OO samples suggests a weakening or partial disruption of the main biosynthetic pathways. This is often associated with the use of lower-grade raw materials, longer storage times, or technological treatments such as refining [78].

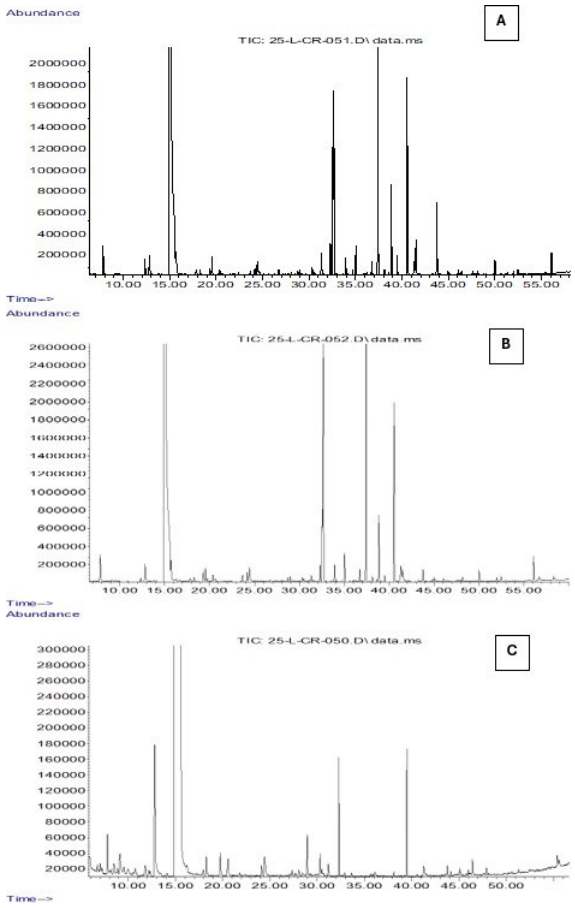


**Figure 5.** Total ion chromatograms (TICs) obtained by GC-MS analysis coupled with SPME of OO (A), EVOO (B), and POO (C) samples. The x-axis represents the retention time (min), while the y-axis indicates the relative abundance of the detected volatile compounds.

Principal Component Analysis (PCA) was applied to the volatile compound data obtained by gas chromatography–mass spectrometry (GC–MS) in order to investigate differences among the various types of olive oil analyzed. The resulting two-dimensional projection (Figure 6) shows that the first two principal components account for the total variability of the dataset: PC1 alone explains 82.2% of the variance, while PC2 accounts for 17.8%.

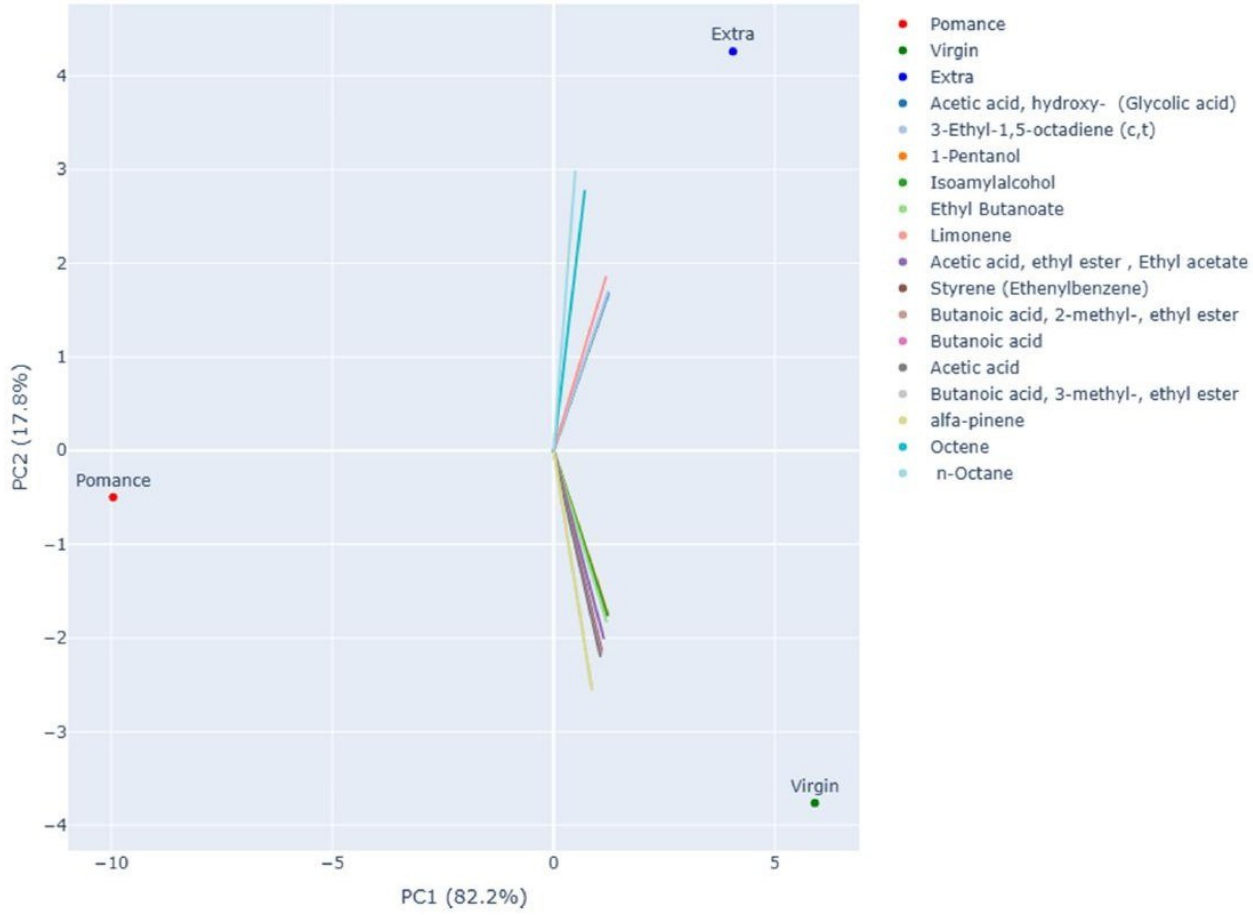


**Figure 6.** Interactive 2D PCA plot based on volatile compound data, displaying the 15 most influential loading vectors contributing to sample separation.

The distribution of the samples along PC1 highlights a clear separation between olive pomace oil and the other two groups. Pomace samples cluster at the far left of the plot, confirming a distinct aromatic profile characterized by the absence of key compounds and the presence of metabolites associated with oxidative and degradative processes.

The second principal component allows for a clear distinction between Extra Virgin Olive Oil (EVOO) and virgin olive oil (VOO). EVOO samples group in the upper right quadrant of the plot, suggesting a greater abundance of compounds derived from the enzymatic lipoxygenase (LOX) pathway, typically responsible for fresh and green sensory notes. Conversely, virgin olive oil samples are in the lower right quadrant, showing an intermediate profile—closer to EVOO than to olive pomace oil—but with quantitative differences in the concentration of the most representative volatiles.

The loading analysis supports these observations: alcohols (e.g., 1-pentanol, isoamyl alcohol), esters (ethyl butanoate, ethyl acetate, esters of butanoic acid), and terpenes (such as limonene and α-pinene)

are strongly associated with EVOO, contributing to its distinctive aromatic fingerprint. In contrast, short-chain acids (acetic acid, butanoic acid) and degradation-related molecules (octene, n-octane, styrene) appear more representative of pomace samples, and to a lesser extent of virgin olive oils. Overall, PCA effectively highlighted marked differences among the three olive oil categories, confirming that the volatile profile represents a reliable indicator of both product quality and preservation status.

### 7.3.2 Measurement Setup

The results obtained with GC-MS were compared with those acquired using the electronic nose, followed by a PCA to explore group separations and classification capabilities. Similar approaches are widely reported in the literature, where electronic noses, often combined with multivariate statistical tools, have been successfully applied to the discrimination of olive oils according to geographical origin, cultivar, and quality grade, yielding results comparable to those of consolidated analytical platforms such as GC-MS [17,18].

In the present study, measurements on olive oil samples were performed using a dynamic headspace configuration based on cyclic adsorption and desorption, specifically designed to capture the temporal evolution of volatile organic compounds (VOCs). The setup consisted of a cylindrical glass chamber with an internal volume of approximately 265 mL (75 mm diameter × 600 mm height). Pure and blended olive oil samples were introduced in fixed aliquots of 100 mL to ensure experimental reproducibility. The sensing unit was positioned directly above the headspace to maximize exposure to the emitted volatiles.

Each measurement session comprised 18 automated adsorption/desorption cycles. During the adsorption phase (60 s), the sensor was exposed to the headspace, allowing VOCs to accumulate on the sensing surface; during the subsequent desorption phase (60 s), the chamber was flushed with ambient air to restore baseline conditions and minimize hysteresis. This cyclic protocol enabled the acquisition of transient response dynamics while avoiding sensor saturation, a feature that distinguishes it from static headspace measurements commonly adopted in other e-nose studies.

The ENS160 gas sensor, integrated into a custom portable device, provided real-time TVOC measurements (ppb) over 18 consecutive cycles, generating robust time-series datasets for each sample. This acquisition strategy improved signal clarity and reproducibility and enabled advanced data processing approaches, including temporal pattern recognition and the training of machine learning models (e.g., neural networks). Compared with previous studies primarily based on steady-

state signals or averaged responses, the proposed cyclic approach provides greater analytical depth and supports the development of portable, cost-effective, and data-driven alternatives to conventional laboratory-based GC-MS analysis.

Figure 7 displays the temporal evolution of total volatile organic compounds (TVOCs) for three pure olive oil categories: extra virgin (V_Extra), virgin (V_Virgin), and pomace (V_pomace). The plotted curves represent the TVOC response over time during alternating adsorption and desorption phases. Extra virgin and virgin oils exhibit distinct and reproducible peak patterns, characterized by sharp rises during the adsorption phases followed by gradual descents in the desorption phases. Notably, extra virgin oil consistently produces the highest TVOC amplitudes, while virgin oil follows a slightly lower profile. In contrast, olive pomace oil shows a markedly flattened response, with minimal peak formation and subdued VOC release. This behavior reflects the reduced content of aroma-active volatiles in lower-quality oils, consistent with their known sensory degradation.

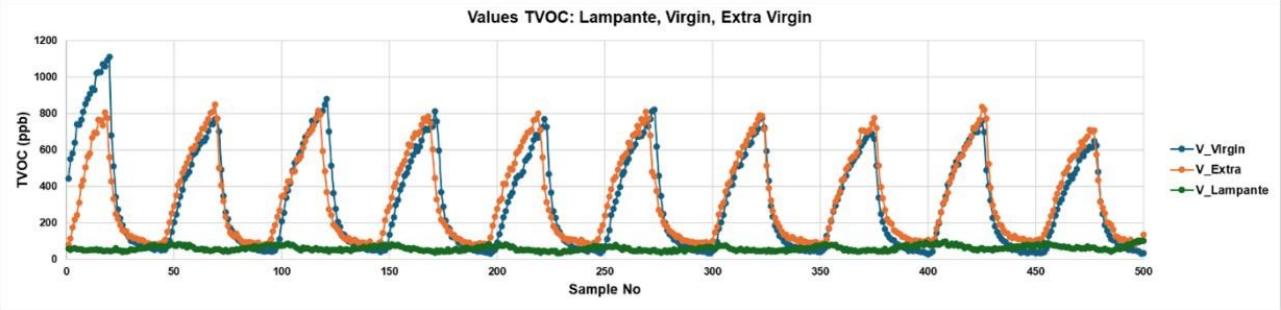


**Figure 7.** Temporal TVOC Response Profiles for Pure Olive Oil Samples: Extra Virgin, Virgin, and Pomace.

Figure 8 extends the analysis to blended samples created by mixing virgin olive oil with 10%, 30%, and 50% olive pomace oil. The cyclic TVOC patterns reveal a clear gradient in signal amplitude and dynamics associated with the degree of adulteration. The 10% blend (blue curve) maintains a peak structure like that of pure virgin oil but with slightly diminished intensities. As pomace content increases to 30% (orange curve) and 50% (green curve), the peaks become broader and less pronounced, indicating significant disruption of the volatile profile. These shifts in amplitude and temporal shape confirm the system's sensitivity to adulteration, even at low levels, and highlight the diagnostic potential of MOX sensor arrays for real-time detection of olive oil authenticity.

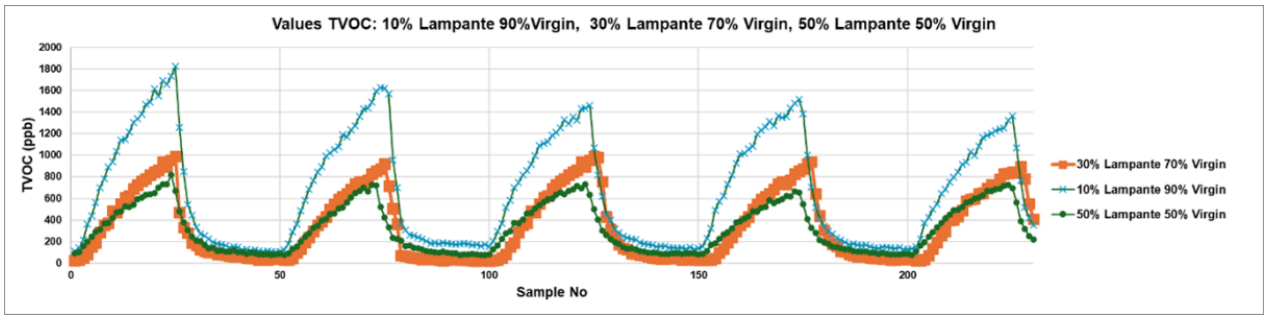


**Figure 8.** Temporal TVOC Response Profiles for Adulterated Olive Oils: Virgin Blends with 10%, 30%, and 50% Pomace.

### 7.3.3 Discrimination of Oil Samples Using a MOX Sensor-Based Device

The use of Principal Component Analysis (PCA) proved to be a particularly effective approach for exploring and visualizing the discriminative capability of the electronic nose based on MOX sensors in recognizing different types of oil and their mixtures. Initially, all available sensor outputs were considered; however, channels that added noise or did not improve discrimination/model performance were excluded from the final feature set to avoid unnecessary dimensionality. The plot shown (Figure 9) displays the projection of the data obtained from the electronic nose responses along the first principal components, which account for most of the variability within the dataset. This MOX sensor-based analysis was applied to samples of extra virgin olive oil, olive pomace oil, and virgin olive oil, with the aim of highlighting potential differences in the volatile compound profiles among the various oil types.

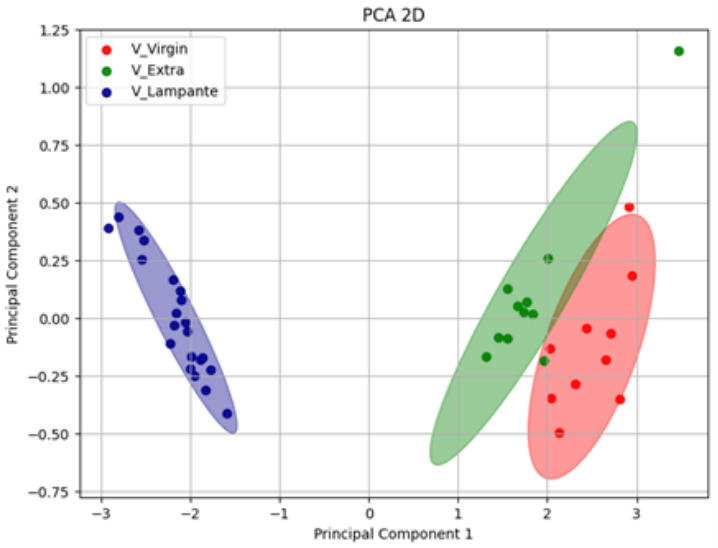


**Figure 9.** Three-dimensional Principal Component Analysis (PCA) showing the separation between extra virgin olive oil (green), olive pomace oil (blue), and virgin olive oil (red) samples.

To complement the two-dimensional projection, a three-dimensional PCA plot was also generated (Figure 10), offering a more detailed visualization of the clustering patterns among the oil samples. This 3D representation allows for a better assessment of the group separation and distribution in multidimensional space.

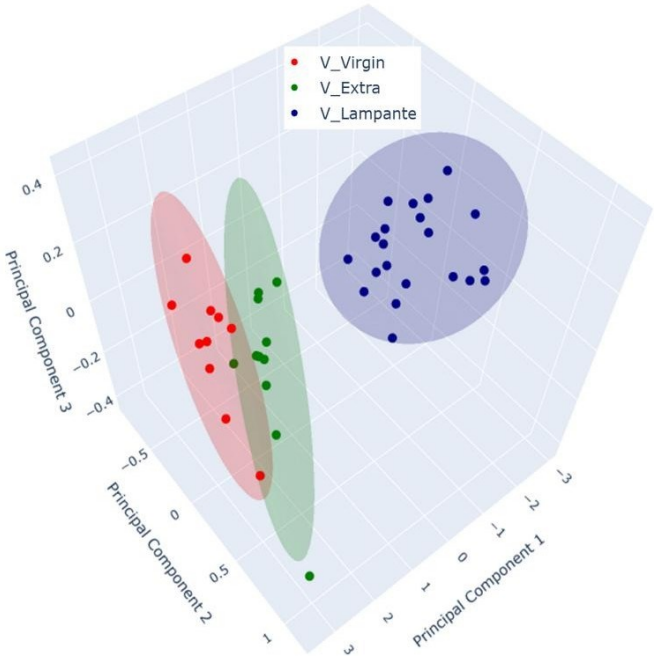


**Figure 10.** 3D Principal Component Analysis (PCA) of MOX sensor responses for olive oil classification.

In this case, Principal Components 1, 2 and 3 explain 97.32%, 2.25%, and 0.43% of the total variance, respectively, indicating that most of the variability in the dataset is captured by the first component alone. Despite the relatively low contribution of PC2 and PC3, their inclusion enhances the spatial perception of class separability and emphasizes subtle differences among samples, particularly within mixtures and borderline cases.

Together, both PCA plots (Figure 8 and Figure 9) illustrate the strong discriminative power of the MOX-based electronic nose in differentiating olive oil categories. The high variance explained by the first component in both the 2D and 3D analyses demonstrates the consistency and reliability of the sensor responses in capturing the key features that distinguish pomace, virgin, and extra virgin oils.

To further explore the potential of the MOX-based electronic nose to detect and classify adulterated olive oils, an additional Principal Component Analysis (PCA) was performed on a dataset including both pure samples and blends in various proportions. Figure 11 presents the two-dimensional PCA

projection, where each point corresponds to a sample measurement, and color-coded ellipses represent the different blend combinations and pure categories.

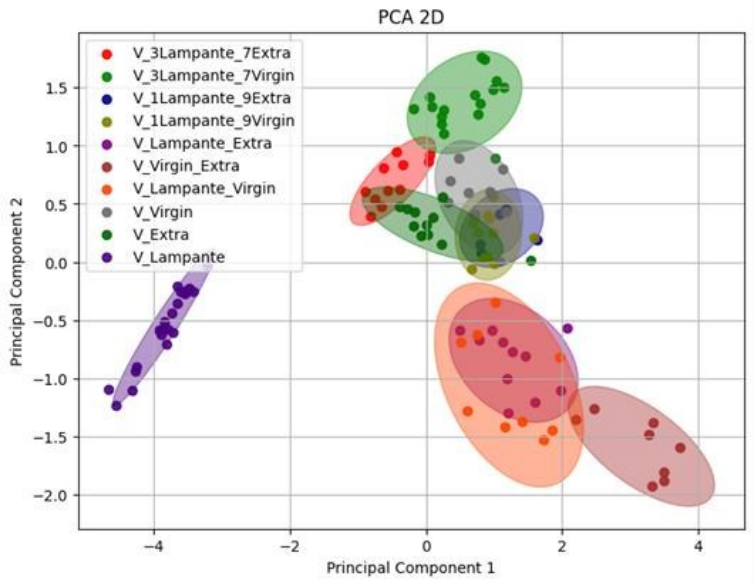


**Figure 11.** Two-dimensional Principal Component Analysis (PCA) demonstrating the separation between pure and blended oil samples in various proportions. Colors indicate the different combinations analyzed: blue for 10% olive pomace oil + 90% extra virgin olive oil, olive-green for 10% olive pomace oil + 90% virgin olive oil, red for 30% olive pomace oil + 70% extra virgin olive oil, light green for 30% olive pomace oil + 70% virgin olive oil, green for pure extra virgin olive oil, purple for pure olive pomace oil, brown for 50% olive pomace oil + 50% extra virgin olive oil, yellow for 50% olive pomace oil + 50% virgin olive oil, gray for pure virgin olive oil, and green for extra virgin olive oil.

The analysis reveals a well-defined separation between pure oils (extra virgin, virgin, and pomace) and their respective mixtures. The distribution of the samples in the PC1-PC2 plane reflects a gradient in volatile profile composition according to blend ratios. Notably, Principal Component 1 (PC1) explains 82.04% of the total variance, while PC2 accounts for 16.15%, providing a comprehensive representation of the variability within the dataset. The pure extra virgin olive oil samples (green) appear tightly grouped and are clearly distinct from both pomace (purple) and virgin oils (gray).

Blended samples form intermediate clusters depending on the ratio and type of oils used. For instance, the red cluster (30% pomace + 70% extra) and light green cluster (30% pomace + 70% virgin) are located closer to the extra virgin and virgin oil clusters, respectively. The blue and olive-green clusters (10% pomace + 90% extra / virgin) are more centrally positioned, while the light purple, orange, and brown clusters (50% blends) are placed further away from the pure groups, indicating greater

divergence in the volatile profiles. The confidence ellipses illustrate good internal consistency within each group and limited overlap, confirming the system's sensitivity to subtle changes in composition.

To provide a more nuanced visualization of these complex relationships, a three-dimensional PCA plot was constructed (Figure 12). The inclusion of Principal Component 3 (PC3), which accounts for 1.09% of the variance, enriches the interpretation by revealing spatial patterns and separations not evident in the 2D representation. The 3D plot maintains the separation among pure and blended oils, further reinforcing the electronic nose's capability to distinguish not only between different oil categories but also between subtle blend proportions.

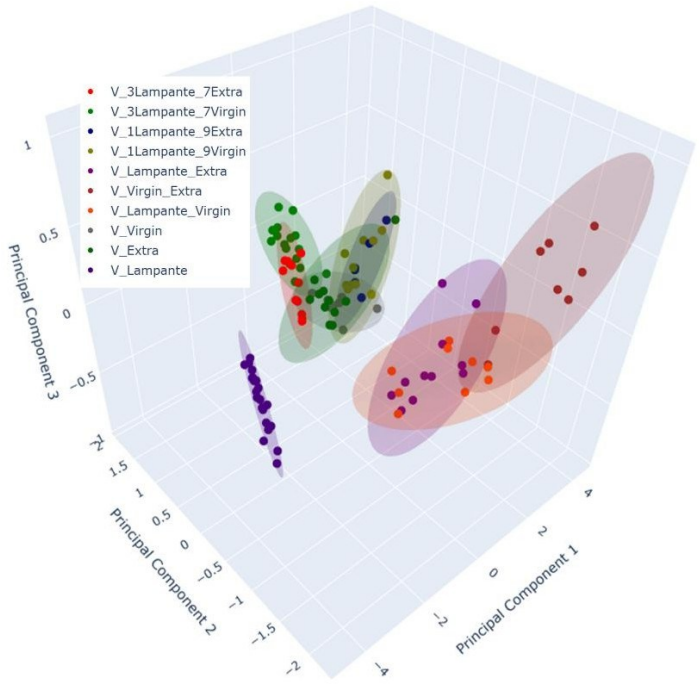


**Figure 12.** Three-dimensional Principal Component Analysis (PCA) demonstrates the separation between pure and blended oil samples in various proportions. Colors indicate the different combinations analyzed: blue for 10% olive pomace oil + 90% extra virgin olive oil, olive-green for 10% olive pomace oil + 90% virgin olive oil, red for 30% olive pomace oil + 70% extra virgin olive oil, light green for 30% olive pomace oil + 70% virgin olive oil, green for pure extra virgin olive oil, purple for pure olive pomace oil, brown for 50% olive pomace oil + 50% extra virgin olive oil, yellow for 50% olive pomace oil + 50% virgin olive oil, gray for pure virgin olive oil, and green for extra virgin olive oil.

### 7.3.4 Multilayer Perceptron Analysis

Figure 13 shows the confusion matrix obtained for the neuronal network model trained to classify olive oils into three categories: pomace, virgin, and extra virgin. The model achieved an overall

accuracy of 84.62%, with perfect classification of olive pomace oil, partial misclassification of extra virgin oils as virgin, and correct classification of virgin samples. These results suggest that while the model robustly identifies olive pomace oil, the classification between extra virgin and virgin oils is more challenging due to their compositional similarity.

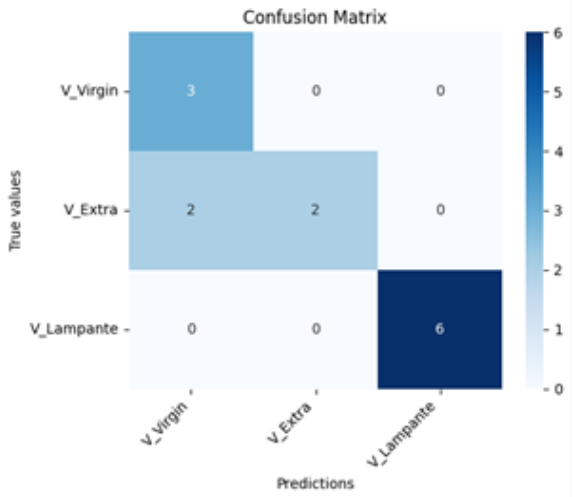


**Figure 13.** Confusion Matrix for Classification of Pure Olive Oil Categories: Virgin, Extra Virgin, and Pomace.

Figure 14 displays the evolution of loss and accuracy during training. As shown in the loss curve, both training and validation losses decrease significantly over the epoch, with the training loss reaching values near 0.2 after 500 epoch. In parallel, training and validation accuracy gradually increases, stabilizing above 90% in the final stages, confirming the convergence and generalization capability of the model.

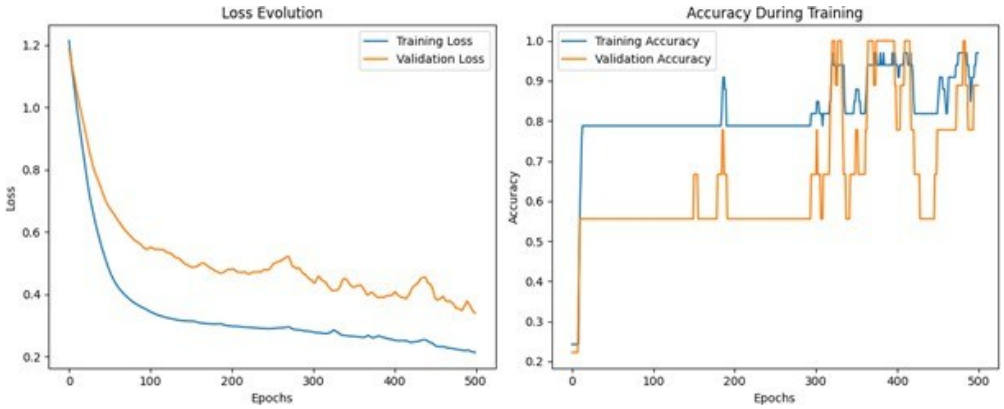


**Figure 14.** Neuronal network performance for classifying pure olive oils.

To further assess the similarity among the oil samples, Figure 15 presents the hierarchical clustering dendrogram. A clear separation between pomace and the other two categories is observed, supporting

the findings from PCA and classification results. Extra virgin and virgin oils form distinct subclusters, but with closer proximity, reflecting their overlapping volatile profile.

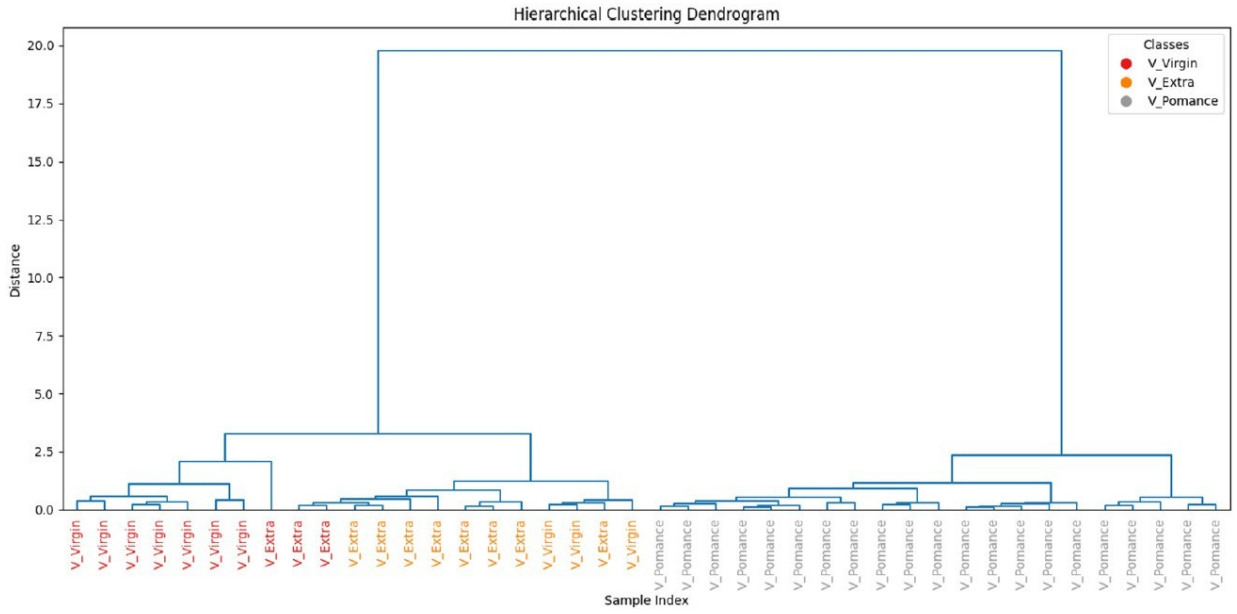


**Figure 15.** Hierarchical clustering of pure olive oil categories based on TVOC profiles.

Figure 16 and Figure 17 report the learned connection-weight matrices of the MLP. These matrices are provided for transparency as a qualitative visualization of the trained parameters. Because multilayer neural networks are non-linear and predictors may be correlated, individual weights are not directly interpretable as reliable feature importance. Therefore, we do not draw feature-importance conclusions from these plots, and model assessment is based on the classification performance reported in the Results.

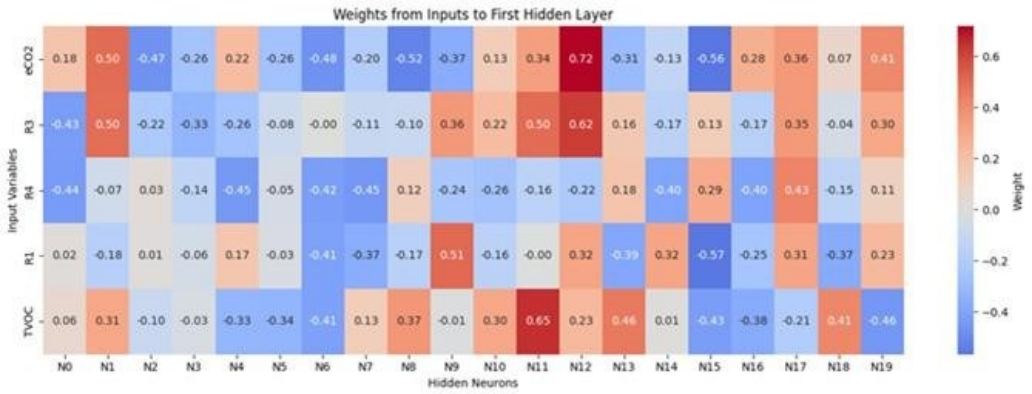


**Figure 16.** Connection weights from input variables to the first hidden layer neurons.

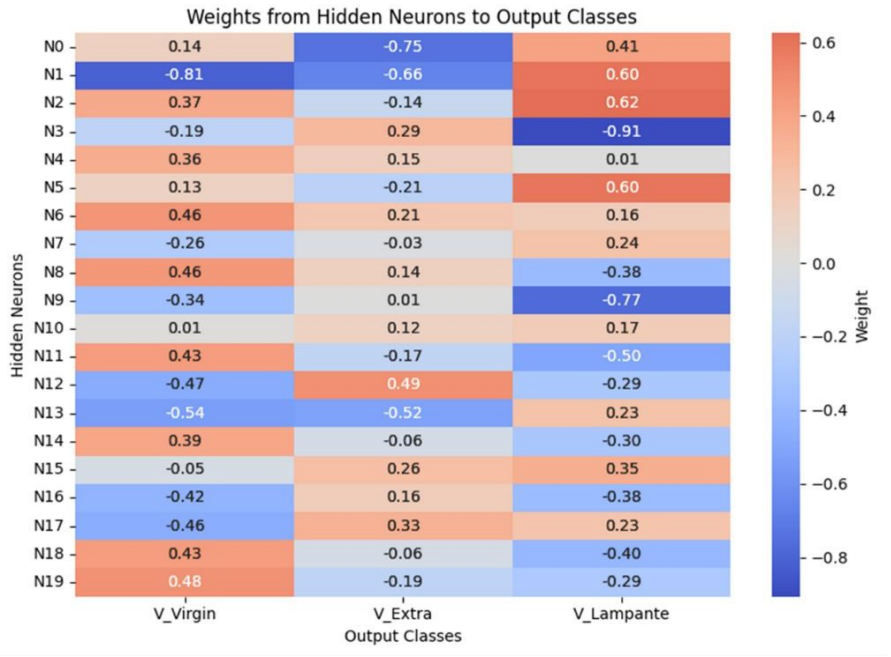


**Figure 17.** Connection weights from hidden layer neurons to output classes.

Figure 18 shows the confusion matrix corresponding to the classification of pure and adulterated olive oil samples using the MOX-based electronic nose. The model was trained with 500 epochs and includes 10 distinct classes: pure extra virgin, virgin, and olive pomace oil, as well as binary mixtures adulterated with 10%, 30%, and 50% olive pomace oil. The model achieved an overall accuracy of 77.14%, correctly classifying most pure samples (e.g., extra virgin and pomace) and several of the blended classes. Misclassification primarily occurred among blends with low pomace content (e.g., 10% or 30%), likely due to their similar volatile profiles.

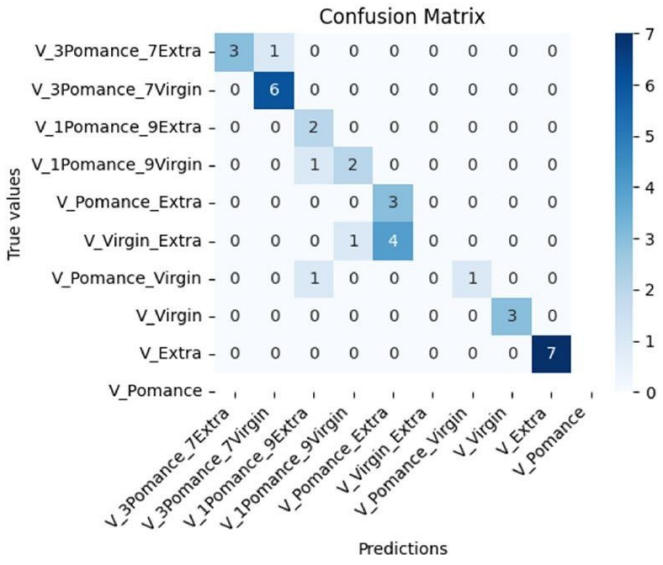


**Figure 18.** Confusion matrix for classification of pure and adulterated olive oils.

Although formal LOD/LOQ values are not directly applicable to this electronic-nose pattern-recognition method, the lowest adulteration level tested in this work was 10% (v/v), at which discrimination of pure oils was achieved under controlled conditions. Determining a formal limit of detection/quantification will require further experiments at levels below 10%, with greater replication and an explicit decision criterion.

Figure 19 displays the evolution of the training and validation loss (left) and accuracy (right) over the course of 500 training epochs. As observed, both training and validation loss steadily decrease with increasing epochs, while the accuracy curves show a gradual increase and stabilization beyond 400 epochs. The model converges with training accuracy close to 99% and validation accuracy stabilizing around 87% indicating good generalization performance despite the increased number of output classes.

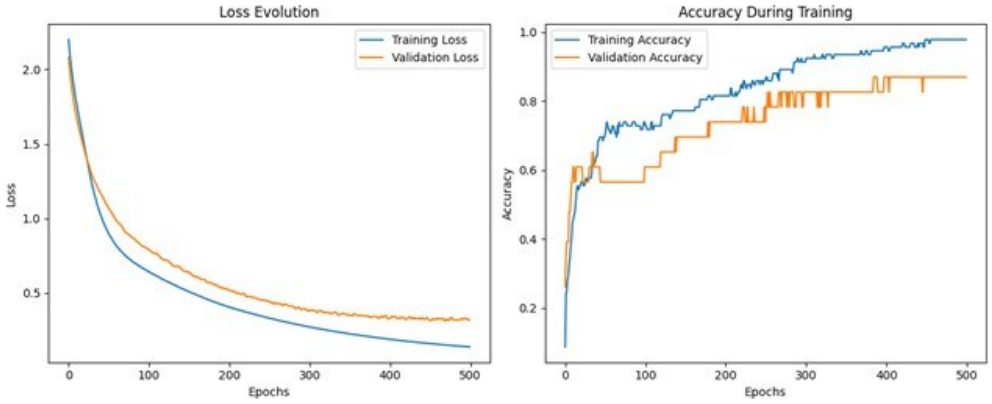


**Figure 19.** Training and validation performance of the neural network for olive oil adulteration detection.

To better understand sample similarities, Figure 20 shows a hierarchical clustering dendrogram generated from the learned features. The pure oil samples form well-defined and coherent clusters, while blended samples are grouped in intermediate positions, reflecting their compositional nature. Notably, mixtures with 50% pomace (such as V_Pomace_Extra and V_Pomace_Virgin) are positioned closer to the pomace cluster, suggesting that even moderate adulteration levels significantly alter the volatile profile.

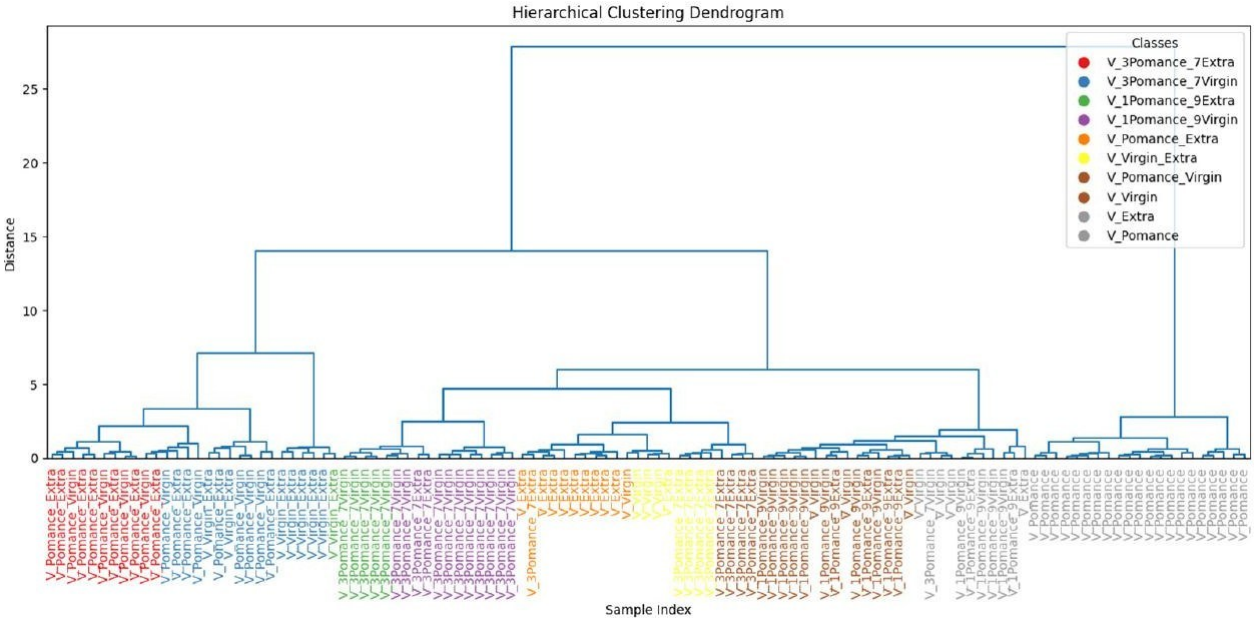


**Figure 20.** Hierarchical clustering of pure and adulterated olive oil samples based on sensor response.

Figure 21 and Figure 22 show the weight matrices of the fully connected layers in the extended model. They are included as a qualitative depiction of the learned parameterization and should be interpreted cautiously; they do not constitute a formal measure of variable importance. More rigorous interpretability analyses will be considered as future work to quantify input influence under controlled validation conditions.

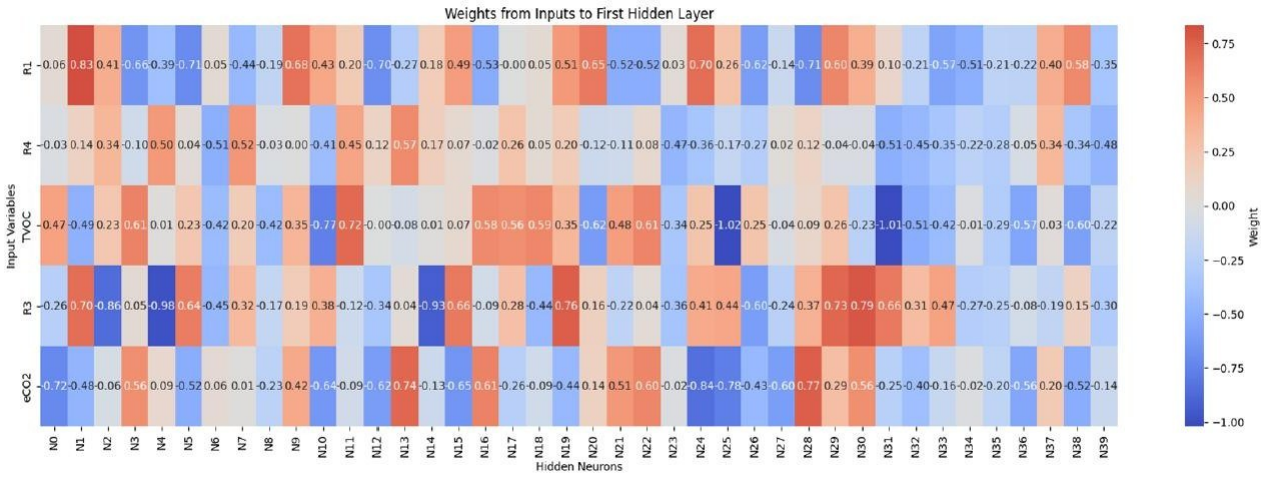


**Figure 21.** Synaptic weights from input features to neurons in the first hidden layer (deep network).

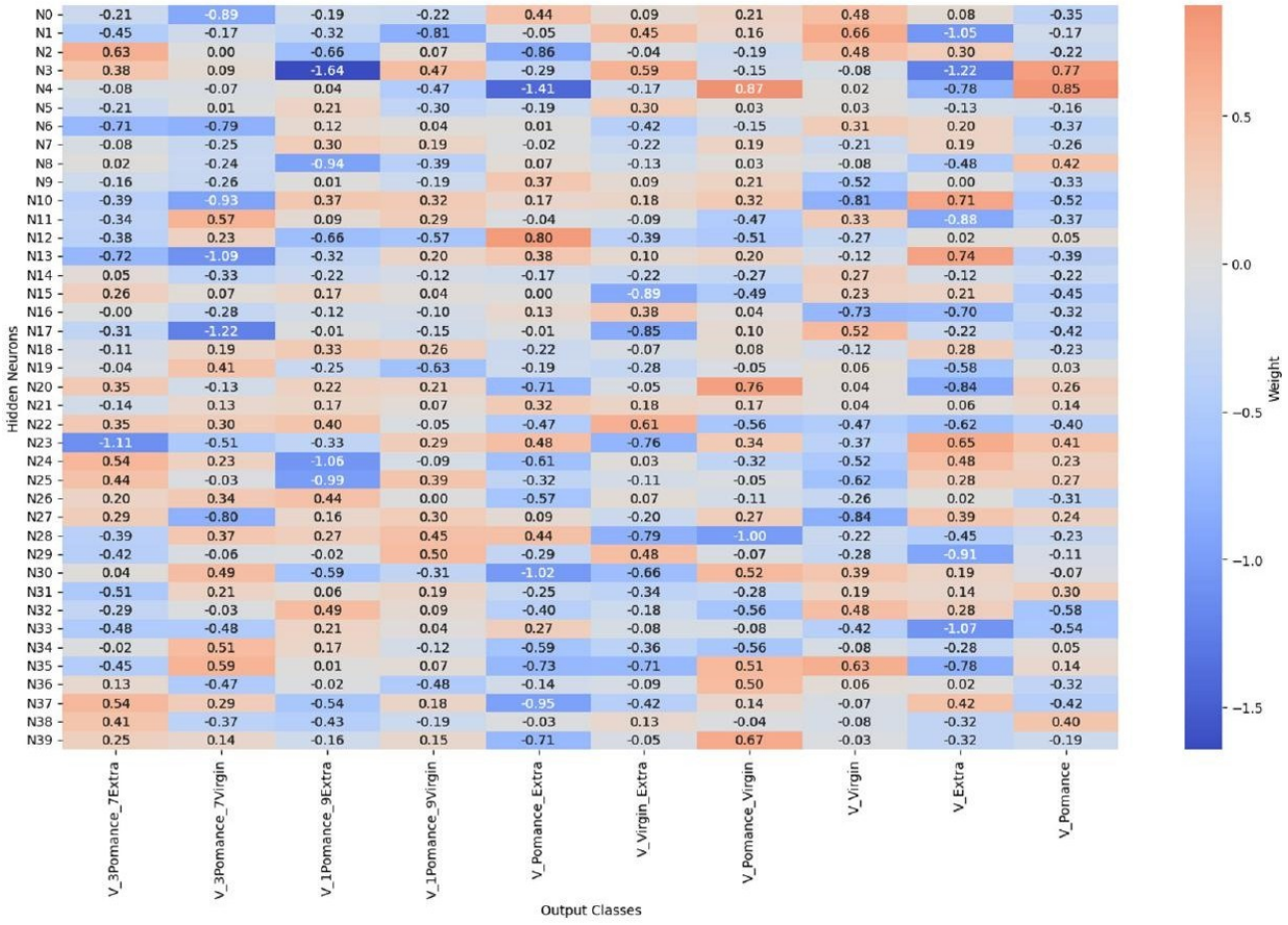


**Figure 22.** Synaptic weights from hidden neurons to output classes in extended olive oil classification.

## 7.4 CONCLUSIONS

The results obtained confirm the effectiveness of the electronic nose in distinguishing between different types of olive oil, demonstrating its ability to detect significant variations in volatile profiles. The comparison with GC-MS data revealed a clear correspondence between the olfactory fingerprints provided by the MOX-based sensor array and the chemical composition of the samples. GC-MS analysis indicated that differences among oil categories were mainly associated with variations in key classes of volatile compounds, such as aldehydes, alcohols, esters, and ketones, which are known to play a major role in defining olive oil aroma and quality and are sensitive to processing conditions and adulteration. These compound groups, rather than individual markers, contribute collectively to the recognition of oil authenticity and are effectively captured by the pattern-based response of the electronic nose. The integration of GC-MS with multivariate chemometric analysis, including PCA, therefore provides complementary information, combining detailed chemical insight with rapid discrimination capability. This integrated approach reinforces the potential of the MOX-based electronic nose as a fast, non-destructive screening tool for olive oil quality control and authenticity

assessment, particularly for certified products such as PDO olive oils. It is important to note that MOX sensors exhibit cross-sensitivity, meaning that their response is not specific to a single compound but reflects the combined effect of different VOC families (and may also be influenced by temperature and humidity). However, this behavior is consistent with the electronic-nose concept, which aims to mimic human olfaction: similarly to a sensory panel that perceives the global aroma profile rather than isolated compounds (as in chromatography), the e-nose captures an overall volatile fingerprint of the sample. Therefore, discrimination is not based on single-sensor selectivity, but on correlating multichannel signals and modeling them using multivariate methods (e.g., PCA) and machine-learning algorithms to extract robust patterns related to authenticity and adulteration.

Overall, the adoption of complementary analytical techniques represents a promising strategy to address current challenges in olive oil authentication, supporting the development of more efficient, sustainable, and transparent control systems. Future work will focus on expanding the dataset, refining predictive models, and implementing real-time and in-line monitoring solutions, with the aim of facilitating the integration of MOX-based sensing technologies into industrial production chains. Moreover, in future work, IoT integration of the system will require addressing practical implementation challenges: (i) ensuring robust data acquisition and transmission (e.g., BLE/Wi-Fi) by incorporating local storage and delayed retransmission in case of connectivity losses; (ii) optimizing power consumption through sleep modes and measurement duty-cycling (periodic sampling vs. continuous monitoring) to ensure sufficient autonomy; (iii) defining the model deployment strategy (on-device or near-edge ‘gateway’ inference vs. cloud inference), balancing latency, privacy, and cost; (iv) ensuring stable performance in real environments through temperature/humidity compensation, control of background VOCs, and drift/recalibration strategies; and (v) establishing traceability and maintenance of the model over time (model versioning and controlled model updates).

## 7.5 BIBLIOGRAPHY


1. Borzì, A.M.; Biondi, A.; Basile, F.; Luca, S.; Vicari, E.S.D.; Vacante, M. Olive oil effects on colorectal cancer. Nutrients 2019, 11, 32. [Google Scholar]
2. Tomé-Carneiro, J.; Crespo, M.C.; López de Las Hazas, M.C.; Visioli, F.; Dávalos, A. Olive oil consumption and its repercussions on lipid metabolism. Nutr. Rev. 2020, 78, 952–968. [Google Scholar]

3. Gorzynik-Debicka, M.; Przychodzen, P.; Cappello, F.; Kuban-Jankowska, A.; Marino Gammazza, A.; Knap, N.; Wozniak, M.; Gorska-Ponikowska, M. Potential health benefits of olive oil and plant polyphenols. Int. J. Mol. Sci. 2018, 19, 686. [Google Scholar]
4. Yubero-Serrano, E.M.; Lopez-Moreno, J.; Gomez-Delgado, F.; Lopez-Miranda, J. Extra virgin olive oil: More than a healthy fat. Eur. J. Clin. Nutr. 2019, 72, 8–17. [Google Scholar] [PubMed]
5. Salis, C.; Papageorgiou, L.; Papakonstantinou, E.; Hagidimitriou, M.; Vlachakis, D. Olive Oil Polyphenols in Neurodegenerative Pathologies. Adv. Exp. Med. Biol. 2020, 1195, 77–91. [Google Scholar]
6. Rusinek, R.; Kmiecik, D.; Gawrysiak-Witulska, M.; Malaga-Toboła, U.; Tabor, S.; Findura, P.; Siger, A.; Gancarz, M. Identification of the Olfactory Profile of Rapeseed Oil as a Function of Heating Time and Ratio of Volume and Surface Area of Contact with Oxygen Using an Electronic Nose. Sensors 2021, 21, 303. [Google Scholar]
7. Dias, C.; Mendes, L. Protected designation of origin (PDO), protected geographical indication (PGI) and traditional speciality guaranteed (TSG): A bibliometric analysis. Food Res. Int. 2018, 103, 492–508. [Google Scholar] [PubMed]
8. Lozano-Castellón, J.; López-Yerena, A.; Domínguez-López, I.; Siscart-Serra, A.; Fraga, N.; Sámano, S.; López-Sabater, C.; Lamuela-Raventós, R.M.; Vallverdú-Queralt, A.; Pérez, M. Extra virgin olive oil: A comprehensive review of efforts to ensure its authenticity, traceability, and safety. Compr. Rev. Food Sci. Food Saf. 2022, 21, 2639–2664. [Google Scholar] [PubMed]
9. Tarapoulouzi, M.; Agriopoulou, S.; Koidis, A.; Proestos, C.; El Enshasy, H.A.; Varzakas, T. Recent advances in analytical methods for the detection of olive oil oxidation status during storage along with chemometrics, authenticity and fraud studies. Biomolecules 2022, 12, 1180. [Google Scholar]
10. Zarezadeh, M.R.; Aboonajmi, M.; Ghasemi Varnamkhasti, M. Fraud detection and quality assessment of olive oil using ultrasound. Food Sci. Nutr. 2021, 9, 180–189. [Google Scholar] [PubMed]
11. Rocchi, R.; Mascini, M.; Faberi, A.; Sergi, M.; Compagnone, D.; Di Martino, V.; Carradori, S.; Pittia, P. Comparison of IRMS, GC-MS and E-nose data for the discrimination of saffron samples with different origin, process and age. Molecules 2019, 24, 4112. [Google Scholar]
12. Ziółkowska, A.; Wąsowicz, E.; Jeleń, H.H. Differentiation of wines according to grape variety and geographical origin based on volatiles profiling using SPME-MS and SPME-GC/MS methods. Food Chem. 2016, 213, 714–720. [Google Scholar]

13. Olmo-García, L.; Polari, J.J.; Li, X.; Bajoub, A.; Fernández-Gutiérrez, A.; Wang, S.C.; Carrasco-Pancorbo, A. Study of the minor fraction of virgin olive oil by a multi-class GC-MS approach: Comprehensive quantitative characterization and varietal discrimination potential. Food Res. Int. 2019, 125, 108649. [Google Scholar]
14. García-González, D.L.; Morales, M.T.; Aparicio, R. Olive and olive oil. In Handbook of Olive Oil: Analysis and Properties; Hui, Y.H., Ed.; John Wiley & Sons: Hoboken, NJ, USA, 2010; Chapter 43. [Google Scholar]
15. Sales, C.; Portolés, T.; Johnsen, L.G.; Danielsen, M.; Beltran, J. Classification of olive oil quality and organoleptic attributes by untargeted GC-MS and multivariate statistical analysis. Food Chem. 2019, 271, 488–496. [Google Scholar] [PubMed]
16. Aparicio-Ruiz, R.; García-González, D.L.; Morales, M.T.; Lobo-Prieto, A.; Romero, I. Comparison of two validated analytical methods for the determination of volatile compounds in extra virgin olive oil: GC-FID vs. GC-MS. Talanta 2018, 187, 133–141. [Google Scholar] [PubMed]
17. Nanou, E.; Bekogianni, M.; Stamatoukos, T.; Couris, S. Detection of Adulteration of Extra Virgin Olive Oil via Laser-Induced Breakdown Spectroscopy and Ultraviolet-Visible-Near-Infrared Absorption Spectroscopy: A Comparative Study. Foods 2025, 14, 321. [Google Scholar]
18. Poeta, E.; Núñez-Carmona, E.; Sberveglieri, V. A review: Applications of MOX sensors from air quality monitoring to biomedical diagnosis and agro-food quality control. J. Sens. Actuator Netw. 2025, 14, 50. [Google Scholar]
19. Poeta, E.; de Chiara, M.L.V.; Cefola, M.; Caruso, I.; Genzardi, D.; Núñez-Carmona, E.; Pace, B.; Palumbo, M.; Sberveglieri, V. Quality monitoring of table grapes stored in controlled atmosphere using an S3+ MOS nanosensor device. Postharvest Biol. Technol. 2025, 227, 113587. [Google Scholar]
20. Rusinek, R.; Siger, A.; Gawrysiak-Witulska, M.; Rokosik, E.; Malaga-Toboła, U.; Gancarz, M. Application of an electronic nose for determination of pre-pressing treatment of rapeseed based on the analysis of volatile compounds contained in pressed oil. Int. J. Food Sci. Technol. 2020, 55, 2161–2170. [Google Scholar]
21. Rusinek, R.; Jeleń, H.; Malaga-Toboła, U.; Molenda, M.; Gancarz, M. Influence of Changes in the Level of Volatile Compounds Emitted during Rapeseed Quality Degradation on the Reaction of MOS Type Sensor-Array. Sensors 2020, 20, 3135. [Google Scholar]

22. Mariotti, R.; Núñez-Carmona, E.; Genzardi, D.; Pandolfi, S.; Sberveglieri, V.; Mousavi, S. Volatile olfactory profiles of Umbrian extra virgin olive oils and their discrimination through MOX chemical sensors. Sensors 2022, 22, 7164. [Google Scholar]
23. Shooshtari, M.; Salehi, A. An electronic nose based on carbon nanotube–titanium dioxide hybrid nanostructures for detection and discrimination of volatile organic compounds. Sensors 2022, 22, 131418. [Google Scholar]
24. Kiritsakis, A.; Markakis, P. Olive oil: A review. Adv. Food Res. 1988, 31, 453–482. [Google Scholar]
25. Bulatović, S.; Ilić, M.; Šolević Knudsen, T.; Milić, J.; Pucarević, M.; Jovančićević, B.; Vrvić, M.M. Evaluation of potential human health risks from exposure to volatile organic compounds in contaminated urban groundwater in the Sava River aquifer, Belgrade, Serbia. Environ. Geochem. Health 2022, 44, 3451–3472. [Google Scholar] [PubMed]
26. Yang, J.; Wang, P.; Neumann, H.; Jackstell, R.; Beller, M. Industrially applied and relevant transformations of 1,3-butadiene using homogeneous catalysts. Ind. Chem. Mater. 2023, 1, 155–174. [Google Scholar]
27. Zhao, C.; He, J.; Lemonidou, A.A.; Li, X.; Lercher, J.A. Aqueous-phase hydrodeoxygenation of bio-derived phenols to cycloalkanes. J. Catal. 2011, 280, 8–16. [Google Scholar]
28. National Center for Biotechnology Information. Nonane—Compound Summary. PubChem Compound. Available online: https://pubchem.ncbi.nlm.nih.gov/compound/nonane.
29. Cilia, G.; Flaminio, S.; Quaranta, M. A novel and non-invasive method for DNA extraction from dry bee specimens. Sci. Rep. 2022, 12, 11679. [Google Scholar]
30. Fritz, K.; Salavastru, C.; Eren, S.; Tiplica, G.S. Einfluss von Diabetes auf ästhetische Eingriffe. Dermatologie 2025, 76, 15–20. [Google Scholar] [PubMed]
31. Siegel, H.; Eggersdorfer, M. Ketones. In Ullmann's Encyclopedia of Industrial Chemistry; Wiley-VCH: Weinheim, Germany, 2000. [Google Scholar]
32. Hernández, D.; Astudillo, C.A.; Fernández-Palacios, E.; Cataldo, F.; Tenreiro, C.; Gabriel, D. Evolution of physico-chemical parameters, microbial diversity and VOC emissions of olive oil mill waste exposed to ambient conditions in open reservoirs. Waste Manag. 2018, 79, 501–509. [Google Scholar]
33. The Good Scents Company. Flavor and Fragrance Information Catalog. The Good Scents Company Database 2009. Available online: http://www.thegoodscentscompany.com/data/rw1042361.html.

34. Cserháti, T.; Forgács, E. Flavor (flavour) compounds: Structures and characteristics. In Encyclopedia of Food Sciences and Nutrition, 2nd ed.; Elsevier Science: Amsterdam, The Netherlands, 2003; pp. 2509–2517. [Google Scholar]
35. Üçüncüoğlu, D.; Sivri-Özay, D. Geographical origin impact on volatile composition and some quality parameters of virgin olive oils extracted from the "Ayvalık" variety. Heliyon 2020, 6, e05011. [Google Scholar]
36. Wang, Y.; Hua, L.; Fu, Q.; Wu, C.; Zhang, C.; Li, H.; Xu, G.; Ni, Q.; Zhang, Y. Rapid identification of adulteration in extra virgin olive oil via dynamic headspace sampling and high-pressure photoionization time-of-flight mass spectrometry. J. Agric. Food Chem. 2022, 70, 6775–6784. [Google Scholar]
37. Boffa, L.; Binello, A.; Cravotto, G. Efficient capture of cannabis terpenes in olive oil during microwave-assisted cannabinoid decarboxylation. Molecules 2024, 29, 899. [Google Scholar]
38. Tseng, D.J.; Matthews, R.F.; Gregory, J.F., III; Wei, C.I.; Littell, R.C. Sorption of ethyl butyrate and octanal constituents of orange essence by polymeric adsorbents. J. Food Sci. 1993, 58, 801–804. [Google Scholar]
39. Chen, Z.; Ma, M.; Chen, X.; Peng, Z.; Liu, H.; Lu, J.; Wu, D. Characterization of volatile compound differences of Shaoxing Huangjiu aged for different years using GC-E-nose, GC–MS, and GC-IMS. Eur. Food Res. Technol. 2025, 251, 269–282. [Google Scholar]
40. The Good Scents Company. Ethyl Isovalerate. The Good Scents Company Database. Available online: http://www.thegoodscentscompany.com.
41. Gokbulut, I.; Karabulut, I. SPME–GC–MS detection of volatile compounds in apricot varieties. Food Chem. 2012, 132, 1098–1102. [Google Scholar]
42. Park, E.-R.; Lee, H.-J.; Kim, K.-S. Volatile flavor components in Bogyojosaeng and Suhong cultivars of strawberry (Fragaria ananassa Duch.). J. Food Sci. Nutr. 2000, 5, 119–125. [Google Scholar]
43. Boch, R.; Shearer, D.A.; Stone, B.C. Identification of isoamyl acetate as an active component in the sting pheromone of the honey bee. Nature 1962, 195, 1018–1020. [Google Scholar]
44. Gopalakrishnan, A.V.; Singh, P.K.; Krishnan, N.; Devadasan, V.; Gopinath, S.C.B.; Raman, P. Characterization of phytoconstituents of vital herbal oils by GC–MS and LC–MS/MS and their bioactivities. J. Food Sci. Technol. 2024, 61, 148–159. [Google Scholar]
45. Cui, Y.; Zhu, L.; Shang, H.; Xuan, X.; Lin, X. Effects of combined ε-polylysine and high hydrostatic pressure treatment on microbial qualities, physicochemical properties, taste, and volatile flavor profile of large yellow croaker (Larimichthys crocea). Food Bioprocess Technol. 2025, 18, 3610–3627. [Google Scholar]

46. Konoz, E.; Abbasi, A.; Paraster, H.; Moazeni, R.; Jalali-Heravi, M. Analysis of olive fruit essential oil: Application of gas chromatography–mass spectrometry combined with chemometrics. Int. J. Food Prop. 2015, 18, 316–331. [Google Scholar]
47. Burdock, G.A. Fenaroli's Handbook of Flavor Ingredients, 5th ed.; CRC Press: Boca Raton, FL, USA, 2005; ISBN 0-8493-3034-3. [Google Scholar]
48. Hirai, M.; Ota, Y.; Ito, M. Diversity in principal constituents of plants with a lemony scent and the predominance of citral. J. Nat. Med. 2022, 76, 254–258. [Google Scholar]
49. Wilson, C.; Davies, N.; Corkrey, R.; Wilson, A.J.; Mathews, A.M.; Westmore, G.C. ROC curve analysis links volatile organic compounds in potato foliage to thrips preference, cultivar and plant age. PLoS ONE 2017, 12, e0181831. [Google Scholar]
50. Thang, T.D.; Dai, D.O.; Hoi, T.M.; Ogunwande, I.A. Essential oils from five species of Annonaceae from Vietnam. Nat. Prod. Commun. 2013, 8, 1934578X1300800228. [Google Scholar]
51. Weissermel, K.; Arpe, H.-J.; Lindley, C.R. Industrial Organic Chemistry, 4th ed.; Wiley-VCH: Weinheim, Germany, 2003; pp. 341–344. ISBN 3-527-30578-5. [Google Scholar]
52. Gómez, E.; Ledbetter, C.A. Comparative study of the aromatic profiles of two different plum species: Prunus salicina Lindl. and Prunus simonii L. J. Sci. Food Agric. 1994, 65, 111–115. [Google Scholar]
53. Kohlpaintner, C.; Schulte, M.; Falbe, J.; Lappe, P.; Weber, J. Aldehydes, aliphatic. In Ullmann's Encyclopedia of Industrial Chemistry; Wiley-VCH: Weinheim, Germany, 2011. [Google Scholar]
54. Pham, D.L.; Ito, Y.; Yamasaki, M. Response of the oak ambrosia beetle Platypus quercivorus (Coleoptera: Platypodinae) to volatiles from fresh and dried leaves. Arthropod-Plant Interact. 2025, 19, 5. [Google Scholar]
55. Barta, T.; Monsempès, C.; Demondion, E.; Chatterjee, A.; Kostal, L.; Lucas, P. Stimulus duration encoding occurs early in the moth olfactory pathway. Commun. Biol. 2024, 7, 1252. [Google Scholar]
56. National Center for Biotechnology Information. 6-Methyl-5-hepten-2-one. PubChem. Available online: https://pubchem.ncbi.nlm.nih.gov/compound/6-Methyl-5-hepten-2-one.
57. Dourou, A.M.; Brizzolara, S.; Famiani, F.; Tonutti, P. Changes in volatile organic composition of olive oil extracted from cv. 'Leccino' fruit subjected to ethylene treatments at different ripening stages. J. Sci. Food Agric. 2021, 101, 3981–3986. [Google Scholar]

58. McRae, J.F.; Mainland, J.D.; Jaeger, S.R.; Adipietro, K.A.; Matsunami, H.; Newcomb, R.D. Genetic variation in the odorant receptor OR2J3 is associated with the ability to detect the "grassy" smelling odor, cis-3-hexen-1-ol. Chem. Senses 2012, 37, 585–593. [Google Scholar]
59. Adiani, V.; Ambolikar, R.; Gupta, S. Utilization of gamma irradiation for development of shelf-stable mint coriander sauce. J. Food Meas. Charact. 2025, 19, 328–340. [Google Scholar]
60. IUPAC. Nomenclature of Organic Chemistry: IUPAC Recommendations and Preferred Names 2013 (Blue Book); The Royal Society of Chemistry: Cambridge, UK, 2014; p. 745. ISBN 978-0-85404-182-4. [Google Scholar]
61. Raymer, R.; Jessa, S.M.; Cooper, W.J.; Olson, M.B. The effects of diatom polyunsaturated aldehydes on embryonic and larval zebrafish (Danio rerio). Ecotoxicology 2025, 34, 292–303. [Google Scholar]
62. Hieu, L.D.; Thang, T.D.; Hoi, T.M.; Ogunwande, I.A. Chemical composition of essential oils from four Vietnamese species of Piper (Piperaceae). J. Oleo Sci. 2014, 63, 211–217. [Google Scholar]
63. Dai, J.-Y.; Zhao, P.; Cheng, X.-L.; Xiu, Z.-L. Enhanced production of 2,3-butanediol from sugarcane molasses. Appl. Biochem. Biotechnol. 2015, 175, 3014–3024. [Google Scholar]
64. Bloch, D.R. Organic Chemistry Demystified; McGraw-Hill: New York, NY, USA, 2006; p. 359. ISBN 0-07-148710-7. [Google Scholar]
65. De Conti, A.; Tryndyak, V.; Koturbash, I.; Heidor, R.; Kuroiwa-Trzmielina, J.; Ong, T.P.; Beland, F.A.; Moreno, F.S.; Pogribny, I.P. The chemopreventive activity of the butyric acid prodrug tributyrin in experimental rat hepatocarcinogenesis is associated with p53 acetylation and activation of the p53 apoptotic signaling pathway. Carcinogenesis 2013, 34, 172–180. [Google Scholar] [PubMed]
66. Mostafa, S.; Wang, Y.; Zeng, W.; Jin, B. Floral scents and fruit aromas: Functions, compositions, biosynthesis, and regulation. Front. Plant Sci. 2022, 13, 860157. [Google Scholar] [PubMed]
67. Callaway, E. Soapy taste of coriander linked to genetic variants. Nature 2012, 486, 7. [Google Scholar]
68. Basu, S.; Clark, R.E.; Fu, Z.; Lee, B.W.; Crowder, D.W. Insect alarm pheromones in response to predators: Ecological trade-offs and molecular mechanisms. Insect Biochem. Mol. Biol. 2021, 128, 103514. [Google Scholar] [PubMed]

69. Zhao, L.; Pan, X.; Shi, J.; Ye, H.; Guan, H.; Guo, Y.; Zhong, J.-J. Formation of urocanic acid versus histamine from histidine in chub mackerel (Scomber japonicus) fillets as determined by a mixed-mode HPLC method. J. Food Compos. Anal. 2025, 142, 107431. [Google Scholar]
70. Shen, Y.; Bai, X.; Wang, J.; Zhou, X.; Meng, R.; Guo, N. Inhibitory effect of non-Saccharomyces Starmerella bacillaris CC-PT4 isolated from grape on MRSA growth and biofilm. Probiotics Antimicrob. Proteins 2025, 17, 227–239. [Google Scholar]
71. Gamal, M.; Awad, M.A.; Shadidizaji, A.; Ibrahim, M.A.; Ghoneim, M.A.; Warda, M. In vivo and in silico insights into the antidiabetic efficacy of EVOO and hydroxytyrosol in a rat model. J. Nutr. Biochem. 2025, 135, 109775. [Google Scholar] [PubMed]
72. Aprea, E.; Gasperi, F.; Betta, E.; Sani, G.; Cantini, C. Variability in volatile compounds from lipoxygenase pathway in extra virgin olive oils from Tuscan olive germplasm by quantitative SPME/GC-MS. J. Mass Spectrom. 2018, 53, 824–832. [Google Scholar]
73. Procida, G.; Cichelli, A.; Lagazio, C.; Conte, L.S. Relationships between volatile compounds and sensory characteristics in virgin olive oil by analytical and chemometric approaches. J. Sci. Food Agric. 2016, 96, 311–318. [Google Scholar]
74. Reboredo-Rodríguez, P.; González-Barreiro, C.; Cancho-Grande, B.; Simal-Gándara, J. Aroma biogenesis and distribution between olive pulps and seeds with identification of aroma trends among cultivars. Food Chem. 2013, 141, 637–643. [Google Scholar] [PubMed]
75. García-Vico, L.; Belaj, A.; Sánchez-Ortiz, A.; Martínez-Rivas, J.M.; Pérez, A.G.; Sanz, C. Volatile compound profiling by HS-SPME/GC-MS-FID of a core olive cultivar collection as a tool for aroma improvement of virgin olive oil. Molecules 2017, 22, 141. [Google Scholar] [PubMed]
76. Jimenez-Lopez, C.; Carpena, M.; Lourenço-Lopes, C.; Gallardo-Gomez, M.; Lorenzo, J.M.; Barba, F.J.; Pietro, M.A.; Simal-Gandara, J. Bioactive compounds and quality of extra virgin olive oil. Foods 2020, 9, 1014. [Google Scholar]
77. Garcia-Oliveira, P.; Jimenez-Lopez, C.; Lourenço-Lopes, C.; Chamorro, F.; Pereira, A.G.; Carrera-Casais, A.; Fraga-Corral, M.; Carpena, M.; Simal-Gandara, J.; Prieto, M.A. Evolution of flavors in extra virgin olive oil shelf-life. Antioxidants 2021, 10, 368. [Google Scholar] [PubMed]
78. Estruch, R.; Ros, E.; Salas-Salvadó, J.; Covas, M.I.; Corella, D.; Arós, F.; Gómez-Gracia, E.; Ruiz-Gutiérrez, V.; Fiol, M.; Lapetra, J.; et al. Primary prevention of cardiovascular disease with a Mediterranean diet supplemented with extra-virgin olive oil or nuts. N. Engl. J. Med. 2018, 378, e34. [Google Scholar]

# 8.
# FUTURE WORKS

Future developments of this research could focus on integrating additional sensing technologies to enhance the multidimensional characterization of food products. Combining olfactory sensing systems based on MOX sensors with optical or imaging sensors could provide complementary information, allowing simultaneous evaluation of both volatile profiles and visual attributes such as color, texture, and surface changes. This multimodal approach would enable a more comprehensive assessment of product quality, freshness, and shelf-life, mimicking more closely the human perception of food through multiple senses.

Although optical sensors and camera-based systems are powerful tools for visual inspection, they may sometimes overestimate certain parameters due to lighting or surface reflections. However, coupling these technologies with olfactory sensors could help mitigate this limitation, leading to more robust and reliable predictive models. Future work should therefore explore the development of hybrid sensing platforms and advanced data fusion strategies to fully exploit the synergistic potential of these complementary technologies.

# 9.

# GENERAL CONCLUSION

The research conducted during this Ph.D. aimed to develop and validate innovative approaches for monitoring the quality and freshness of food products, with a particular focus on bakery goods and fresh products. To this end, both traditional analytical techniques, such as gas chromatography coupled with mass spectrometry (GC–MS), and emerging technologies based on metal oxide (MOX) sensors were employed.

The use of GC–MS allowed for the accurate identification and quantification of volatile compounds responsible for the aromatic characteristics of the analyzed samples, providing a robust reference for the validation of innovative sensor systems. At the same time, MOX sensors proved to be promising tools for rapid, non-destructive, and potentially in-line analyses, capable of detecting variations in the volatile profile associated with product degradation or transformation processes.

The integration of machine learning methods enhanced the predictive capabilities of the models by identifying meaningful patterns within the sensor data, thereby enabling the automated classification or estimation of quality-related parameters. This data-driven approach demonstrated the potential of Electronic sensing systems to deliver timely and reliable information, representing a significant step toward the digitalization and automation of quality control in the food sector.

Overall, the results confirm that the combination of traditional analytical methods and innovative sensor technologies can provide a more comprehensive and complementary understanding of product quality. Although MOX-based systems cannot fully replace established laboratory techniques, they represent valuable tools for continuous monitoring and for use in industrial or field settings, where fast response and ease of operation are key requirements.

This research therefore highlights how the integration between reference chemical analyses and intelligent sensing technologies can open new perspectives for more sustainable, efficient, and accessible quality control, in line with the ongoing innovation and digital transformation of the agri-food industry.

Finanziato dall'Unione europea NextGenerationEU
Ministero dell'Università e della Ricerca
Italiadomani PIANO NAZIONALE DI RIPRESA E RESILIENZA
UNIMORE UNIVERSITÀ DEGLI STUDI DI MODENA E REGGIO EMILIA

Tesi di dottorato finanziata dall'Unione europea- Next Generation EU, Missione 4, componente 2 "Dalla Ricerca all'Impresa" - Investimento 3.3 "Introduzione di dottorati innovativi che rispondono ai fabbisogni di innovazione delle imprese e promuovono l'assunzione dei ricercatori dalle imprese".

# 10. ACKNOWLEDGMENTS

## 10.1 Institutional Acknowledgments

I would like to express my sincere gratitude to Prof. Fabio Licciardello, Coordinator of the PhD Program in Agri-food Science, Technology and Biotechnology, for his guidance, availability, and institutional support throughout my doctoral journey.

This PhD thesis was developed within the framework of several national and international research projects and was partially funded by the project "ON Foods—Research and Innovation Network on Food and Nutrition Sustainability, Safety, and Security—Working ON Foods" (Project code PE00000003), funded under the National Recovery and Resilience Plan (NRRP), Mission 4, Component 2, Investment 1.3, by the Italian Ministry of University and Research and supported by the European Union—NextGenerationEU.

I am deeply grateful to Nano Sensor Systems srl (NASYS) for the invaluable opportunity to work closely with MOX sensor technologies during my doctoral research. The collaboration with NASYS played a fundamental role in my scientific and technical training, allowing me to gain hands-on experience in the design, optimization, and application of electronic nose systems for agri-food quality assessment. I also thank the University of Modena and Reggio Emilia for stimulating scientific discussions and technical support that significantly contributed to the development of this work.

Part of this research was carried out within the NECA project (Development of new electronic nose prototypes and artificial intelligence-based neural network analysis for food quality monitoring), funded by the Regional Government of Extremadura and co-financed by the European Regional Development Fund (ERDF). I would like to thank PanContigo S.L. (Badajoz, Spain), the Scientific and Technological Research Center of Extremadura (CICYTEX) for their support and active participation

in the project. I also acknowledge the technical staff of CICYTEX–INTAEX and the School of Industrial Engineering of the University of Extremadura for their assistance with sample handling, laboratory analyses, and prototype development.

Finally, I gratefully acknowledge the financial support provided by the Poultrynsect project (H2020 ERA-NETs SUSFOOD2 and CORE Organic Cofund) and by the PRIMA program through the SUSTAvianFEED project, both supported by the European Union, which contributed to the completion of this doctoral research.

## 10.2 Personal Acknowledgments

Arrivare alla fine di un percorso di dottorato è un po' come concludere una lunga fermentazione: ci vuole tempo, pazienza, costanza, e soprattutto la giusta combinazione di ingredienti umani per ottenere un buon risultato. È un processo fatto di attese, tentativi, fallimenti e ripartenze, in cui nulla è immediato ma tutto, alla fine, trova il suo senso.

Per questo, il mio primo e più sentito ringraziamento va ai miei tutor, il Prof. Andrea Pulvirenti e la Dott.ssa Veronica Sberveglieri, per avermi insegnato molto più di quanto mi aspettassi. Non solo competenze scientifiche, rigore metodologico e professionalità, ma anche un modo di affrontare la ricerca — e le sue inevitabili difficoltà — con curiosità, equilibrio e determinazione. Grazie per avermi guidata con fiducia, per aver creduto nel mio lavoro e per avermi trasmesso non solo conoscenze, ma anche una visione più ampia della scienza e del ruolo che essa può avere. Questo insegnamento va ben oltre il dottorato e resterà con me nel tempo.

Un ringraziamento sincero e affettuoso va anche alla Dott.ssa Estefanía Núñez Carmona, che in laboratorio mi ha insegnato praticamente tutto. Con lei ho imparato che la scienza è fatta sì di dati, strumenti e risultati, ma anche di passione, collaborazione, pazienza e, perché no, di risate tra una misura e l'altra. Il suo supporto quotidiano, umano oltre che scientifico, ha reso il laboratorio un luogo di crescita, confronto e condivisione.

Un grazie speciale va ai miei amici e colleghi Dario, Dario (detto Paolo) e Giuseppe. Ognuno di loro, a modo suo, ha contribuito a rendere più leggera e più bella questa avventura, accompagnandomi tra esperimenti riusciti e falliti, pause caffè e momenti di sana follia che hanno spesso salvato le giornate più difficili. E un grazie particolare a Giuseppe, che da collega è diventato una delle persone più importanti della mia vita, trovando un posto speciale nel mio cuore e dimostrandomi quanto il dottorato possa regalare, oltre alla formazione scientifica, legami profondi e inaspettati.

Infine, un grazie immenso alla mia famiglia, la mia certezza più grande. Dirvi solo “grazie” o “vi voglio bene” non potrà mai bastare per esprimere tutto l’amore, il riconoscimento e la gratitudine che ho per voi. Siete stati il mio sostegno costante, la mia forza nei momenti di stanchezza, il mio rifugio quando tutto sembrava troppo. Perché, oltre a essere la mia famiglia, siete i miei migliori amici, la mia casa, il mio punto fermo. E a chi dice che la famiglia della Mulino Bianco non esiste… beh, esiste eccome: siamo noi ♡.

# 11.
# ANNEX

## 11.1Published Articles

**Poeta, E.**; Núñez-Carmona, E.; Sberveglieri, V.; Bernal, A.; Lozano, J.; Sánchez, R. MOX Sensors for Authenticity Assessment and Adulteration Detection in Extra Virgin Olive Oil (EVOO). Sensors **2026**, 26, 275. https://doi.org/10.3390/s26010275.

**Poeta, E.**; Núñez-Carmona, E.; Sberveglieri, V.; Lozano, J.; Sánchez, R. Monitoring the Olfactory Evolution of Cold-Fermented Sourdough Using an Electronic Nose. Chemosensors **2025**, 13, 187. https://doi.org/10.3390/chemosensors13050187.

**Poeta, E.**; Núñez-Carmona, E.; Sberveglieri, V. A Review: Applications of MOX Sensors from Air Quality Monitoring to Biomedical Diagnosis and Agro-Food Quality Control. J. Sens. ActuatorNetw. **2025**, 14, 50. https://doi.org/10.3390/jsan14030050.

Genzardi, D.; Caruso, I.; **Poeta, E.**; Sberveglieri, V.; Núñez Carmona, E. Nano-Tailored Triple Gas Sensor for Real-Time Monitoring of Dough Preparation in Kitchen Machines. Sensors **2025**, 25,2951. https://doi.org/10.3390/s25092951.

**Poeta, E.**; de Chiara, M.L.V.; Cefola, M.; Caruso, I.; Genzardi, D.; Núñez- Carmona, E.; Pace, B.; Palumbo, M.; Sberveglieri, V. Quality monitoring of table grapes stored in controlled atmosphere using an S3+MOS nanosensor device. Postharvest Biol. Technol. **2025**, 227, 113587. https://doi.org/10.1016/j.postharvbio.2025.113587.

Genzardi D, Núñez Carmona E, **Poeta E**, Gai F, Caruso I, Fiorilla E, Schiavone A, Sberveglieri V. Unraveling the Chicken Meat Volatilome with Nanostructured Sensors: Impact of Live and Dehydrated Insect Larvae Feeding. Sensors (Basel). **2024** Jul 29;24(15):4921. doi:10.3390/s24154921. PMID: 39123968; PMCID: PMC11314963.

**Poeta, E.**; Liboà, A.; Mistrali, S.; Núñez-Carmona, E.; Sberveglieri, V. Nanotechnology and E-Sensing for Food Chain Quality and Safety. Sensors **2023**, 23, 8429. https://doi.org/10.3390/s23208429.

## 11.2 Conferences and Courses

**04/02/2026 - 04/02/2026 Online**

**CNR (National Research Council of Italy) - Oral Presentation**

One-hour oral presentation entitled “Applications of MOX Sensors for Volatile Organic Compound Detection in the Agri-Food Sector”, focused on innovative sensing technologies for quality monitoring in agri-food systems.

**10/09/2025 - 12/09/2025 Teramo**

**29th Workshop on Developments in Italian PhD Research - Oral Presentation**

Oral presentation: “Applications of MOX Sensors for Volatile Organic Compound Detection in Agri-Food sector.”

**14/12/2024 – 14/12/2024**

**Participation in a television program focused on the promotion of research and innovation in Spain.**

**Link:** https://www.canalextremadura.es/a-la-carta/la-besana-en-verde/videos/extremadura-crea-narices-inteligentes

**18/09/2024 - 20/09/2024 Catania**

**28th Workshop on the Developments in the Italian PhD research - Poster Presentation Poster** presentation “Studying the effectiveness of controlled atmosphere to improve the shelf life of table grapes using innovative taylor made IoT nanosensors.”

**08/09/2024 - 12/09/2024 Rimini**

**22nd World Congress of Food Science and Technology - Oral Presentation**

International event in food science and technology with global experts and researchers. An oral presentation was delivered titled: "Nanotechnological Sensor Device to Support the Fruit Trading Market."

**25/07/2024 - 25/07/2024 Reggio Emilia**

**BIP UNIMORE - Two-hours lecture (Universities of Caen, Prague and Valencia)**

Title: “Sensors and Volatilome: in which way nanotechnology would support the agrifood systems”.

**25/06/2023 - 25/06/2023 Reggio Emilia**

**BIP UNIMORE - Two-hours lecture (Universities of Caen, Prague and Valencia)**

Support of Tradition and Geographical Identification of Foodstuffs (with a Focus on Olearic Products) - Why Python is Your Best Ally in Biological Data Analysis."

**12/11/2025 - 14/11/2025 Online**

**The 12th International Electronic Conference on Sensors and Applications - Conference Participation**

The event covered recent advances in innovative and sustainable sensor technologies and their applications

across multiple domains, including artificial intelligence–based sensing, electronic and physical sensors, sensor networks and IoT, smart cities, robotics and Industry 4.0, wearable sensors for healthcare, chemo- and biosensors, and smart agriculture sensors. The program included keynote lectures and thematic sessions focused on the design, development and real-world deployment of advanced, sustainable sensing systems for monitoring and decision support.

**12/11/2025 - 12/11/2025 Online CNR (National Research Council of Italy) - Webinar Participation** “Actinobacteria and MOX Gas Sensors: An Integrated Approach to Enhance Plant Tolerance to Drought and Salt Stress”, presenting a multidisciplinary strategy combining microbial inoculation and gas-sensing technologies for plant stress monitoring.

**27/05/2025 - 27/05/2025 Online**

**CNR (National Research Council of Italy) - Webinar Participation**

“Traceability of Extra Virgin Olive Oil: Genetic and Digital Tools for a Safe Value Chain”, focusing on the application of genetic and digital technologies to ensure traceability throughout the olive oil production chain, within the framework of the European project WATSON.

## 11.3 Achievements

- **March 20, 2025 - January 31, 2026 - Editorial Management – MDPI Journal, Special Issue: Development of Metal Oxide Gas Sensors: From Design and Synthesis to Real-World Applications.** Editorial management of the MDPI Journal, supporting manuscript evaluation, peer-review coordination, and editorial decision-making. Assisted in issue planning and journal promotion, ensuring scientific integrity, adherence to deadlines, and high-quality standards throughout the publication process
- **November 11, 2025 - "Premio Stanca" (2025**), awarded by the PhD Program in Agri- food Science, Technology and Biotechnology at the University of Modena and Reggio Emilia, in recognition of outstanding scientific productivity achieved during the doctoral training.
- **October 2025 – Cover article** of the *Journal of Sensor and Actuator Networks* (MDPI): *"Applications of MOX Sensors from Air Quality Monitoring to Biomedical Diagnosis and Agro-Food Quality Control"*.